THE UNIVERSITY OF QUEENSLAND

A U S T R A L I A

Small Natural Draft Dry Cooling Towers for Renewable Power Plants

Yuanshen Lu

Master of Engineering

A thesis submitted for the degree of Doctor of Philosophy at

The University of Queensland in 2014

School of Mechanical and Mining Engineering

Abstract

In thermal power plants using variety of heat sources, the redundant heat needs to be removed through cooling devices such as heat exchangers and cooling towers. Natural draft dry cooling towers (NDDCTs) feature no water loss and no parasitic power consumption during operation and are widely used in thermal power plants around the world, especially in arid areas. The Queensland Geothermal Energy Centre of Excellence (QGECE) is focusing on developing small- or medium-scale engineered geothermal system (EGS) geothermal and concentrated solar thermal (CST) power plants for Australia. The proposed renewable power plants are most likely to be located in arid remote areas where dry cooling is the only cost-effective option. These power plants may initially be introduced to supply remote communities away from the national grid. Such off-grid applications are expected to be relatively small reflecting the size of the demand. The aim of this Thesis project is to investigate whether natural draft dry cooling towers (NDDCTs) can be used for these small- or medium-scale renewable power plants.

Crosswind is the most common factor affecting the cooling performance of natural draft cooling towers. But current NDDCT design procedures do not take the crosswind effect into account. It is probably not a critical impediment for large towers as the negative influence of the crosswind is negligible when the draft heights are above 100 m. On the other hand, in small NDDCTs with total heights less than 30 m, the crosswind effect could be substantial.

A numerical study was carried out to investigate the thermal performance of the horizontally arranged heat exchangers in small NDDCTs under various crosswind conditions. In particular, a 15 m-high CFD NDDCT model was constructed and simulated to examine the crosswind actions in detail. It was found that at certain crosswind speeds the cooling tower performance can be considerably reduced. A very effective mitigation device, a tri-blade-like windbreak wall, has been found to dramatically improve the cooling performance of the small tower. The effect of the windbreak was sensitive to its orientation with respect to the crosswind direction.

An experimental study was conducted with a 1:12.5 scaled natural draft dry cooling tower model in the wind tunnel. The thermal performance of the scaled tower was measured with and without the windbreak wall. The experimental results verified the numerical predictions for the small tower cooling performance and the effectiveness of the windbreak wall.

The most important finding of this study is that the total heat transfer in a small natural draft cooling tower is a combination of the heat transfer by both natural convection and forced convection, with the contribution of the latter increasing at higher crosswind speeds. A simple correlation between

the heat transfer and the crosswind speed was proposed to estimate the crosswind-affected thermal performance of natural draft dry cooling towers at different sizes and with horizontal heat exchanger arrangements.

The study demonstrates the feasibility of utilising small natural draft dry cooling towers in renewable power plants. Crosswind could have a fatal effect on the performance of these towers without a proper design. However, by applying the mitigation method considered in the Thesis, crosswind can actually be converted to a beneficial effect for the cooling tower performance.

<u>Declaration by author</u>

This thesis is composed of my original work, and contains no material previously published or written by another person except where due reference has been made in the text. I have clearly stated the contribution by others to jointly-authored works that I have included in my thesis.

I have clearly stated the contribution of others to my thesis as a whole, including statistical assistance, survey design, data analysis, significant technical procedures, professional editorial advice, and any other original research work used or reported in my thesis. The content of my thesis is the result of work I have carried out since the commencement of my research higher degree candidature and does not include a substantial part of work that has been submitted to qualify for the award of any other degree or diploma in any university or other tertiary institution. I have clearly stated which parts of my thesis, if any, have been submitted to qualify for another award.

I acknowledge that an electronic copy of my thesis must be lodged with the University Library and, subject to the General Award Rules of The University of Queensland, immediately made available for research and study in accordance with the *Copyright Act 1968*.

I acknowledge that copyright of all material contained in my thesis resides with the copyright holder(s) of that material. Where appropriate I have obtained copyright permission from the copyright holder to reproduce material in this thesis.

Publications during candidature

Peer-reviewed papers

1. Y. Lu, Z. Guan, H. Gurgenci, Z. Zou, Windbreak walls reverse the negative effect of crosswind in short natural draft dry cooling towers into a performance enhancement. International Journal of Heat and Mass Transfer, 2013. 63(0): p. 162-170.

2. Yuanshen Lu, Zhiqiang Guan, Hal Gurgenci, Suoying He, The influence of windbreak wall orientation on the cooling performance of small natural draft dry cooling towers. International Journal of Heat and Mass Transfer, 2014. 79(0): p. 1059-1069.

3. Yuanshen Lu, Zhiqiang Guan, Hal Gurgenci, The performance analysis of inlet air pre-cooling for applications in small size natural draft dry cooling towers. Energy, 2014 (submitted).

4. Yuanshen Lu, Zhiqiang Guan, Hal Gurgenci, Kamel Hooman, Suoying He, Desikan Bharathan, Experimental study of crosswind effects on the performance of small cylindrical natural draft dry cooling towers. Energy Conversion and Management, 2014 (submitted)

Conference papers

1. Y. Lu, Z. Guan, and H. Gurgenci, CFD simulations on small natural draft dry cooling towers. In: P. A. Brandner and B. W. Pearce, Proceedings of the 18th Australasian Fluid Mechanics Conference. 18th Australasian Fluid Mechanics Conference, Launceston, Australia, (2012). 3-7 December 2012.

2. Lu, Yuanshen, Guan, Zhiqiang, Gurgenci, Hal and Zou, Zheng. Development of small natural draft dry cooling towers for geothermal power plants. In: Zhao Shun'an and Li Wuquan, Proceedings: The 15th IAHR Cooling Tower and Air-Cooled Heat Exchanger Conference & 2011 Annual Symposium of Industrial Cooling Tower Study Committee of CSEE Thermal Power Chapter. The 15th IAHR Cooling Tower and Air-Cooled Heat Exchanger Conference & 2011 Annual Symposium of Industrial Cooling Tower Study Committee of CSEE Thermal Power Chapter, Beijing, China, (308-316). 23 - 26 October 2011.

Conference abstracts

1. Yuanshen Lu, The natural convection in small cooling towers subjected to crosswind, the 8th Australian Natural Convection Workshop, the University of Sydney, Sydney, Australia, 16-17 December 2013.

<u>Publications included in this thesis</u>

Y. Lu, Z. Guan, H. Gurgenci, Z. Zou, Windbreak walls reverse the negative effect of crosswind in short natural draft dry cooling towers into a performance enhancement. INTERNATIONAL JOURNAL OF HEAT AND MASS TRANSFER, 2013. 63(0): p. 162-170– incorporated as Chapter 4.

Contributor	Statement of contribution
Author Y. Lu (Candidate)	Set up and conducted the modelling and simulations. Wrote the paper.
Author Z. Guan	Provided the numerical methodology and edited the paper.
Author H. Gurgenci	Provided the numerical methodology and edited the paper.
Author Z. Zou	Conducted the grid-independent check for the modelling.

Yuanshen Lu, Zhiqiang Guan, Hal Gurgenci, Suoying He, The influence of windbreak wall orientation on the cooling performance of small natural draft dry cooling towers. International Journal of Heat and Mass Transfer, 2014. 79(0): p. 1059-1069.

Contributor	Statement of contribution
Author Yuanshen Lu (Candidate)	Set up and conducted the modelling and simulations. Wrote the paper.
Author Zhiqiang Guan	Provided the numerical methodology and edited the paper.
Author Hal Gurgenci	Provided the numerical methodology and edited the paper.
Author Suoying He	Run part of simulations.

Yuanshen Lu, Zhiqiang Guan, Hal Gurgenci, Kamel Hooman, Suoying He, Desikan Bharathan, Experimental study of crosswind effects on the performance of small cylindrical natural draft dry cooling towers. Energy Conversion and Management, 2014 (submitted)

Contributor	Statement of contribution
Author Yuanshen Lu (Candidate)	Set up and conducted the modelling and simulations. Wrote the paper.
Author Zhiqiang Guan	Provided the numerical methodology and edited the paper.
Kamel Hooman	Edited the paper.
Author Hal Gurgenci	Provided the numerical methodology and edited the paper.
Author Suoying He	Run part of simulations.
Desikan Bharathan	Edited the paper.

Contributions by others to the thesis

No contributions by others

Statement of parts of the thesis submitted to qualify for the award of another degree

None

<u>Acknowledgements</u>

Keywords

natural draft dry cooling tower, crosswind effect, air-cooled heat exchanger, cooling enhancement, windbreak wall, scaled cooling tower model

Australian and New Zealand Standard Research Classifications (ANZSRC)

ANZSRC code: 091305, Energy Generation, Conversion and Storage Engineering, 60%

ANZSRC code: 091307, Numerical Modelling and Mechanical Characterisation, 40%

Fields of Research (FoR) Classification

FoR code: 0913, Mechanical Engineering, 100%

Table of Contents

List of Figures

List of Tables

List of Symbols and Abbreviations

A area (m^2)

A_a, A_{fr}, A_r air-side area, frontal area and fin-root area of heat exchangers, respectively (m^2)

A_c minimum area of free flow (m^2)

A_{cell} surface area of numerical cell (m^2)

a constant

b constant

C inertial resistance factor or discharge coefficient

C_1, $C_{1\varepsilon}$, C_2, $C_{3\varepsilon}$ constants in turbulence equations

c_p specific heat at constant pressure (J kg^{-1} K^{-1})

c_v specific heat at constant volume(J kg^{-1} K^{-1})

C_μ coefficient in turbulent viscosity

D tower diameter (m)

d diameters in the heat exchanger tube (m)

d_r fin-root diameter of finned tube (m)

E energy (J)

Eu Euler number

F source term in momentum equations (Pa)

Fr, Fr_D Froude number and densimetric Froude number, respectively

F_T temperature correction factor

f pressure drop coefficient

G_k, G_{kb} generation term of k due to mean velocity gradients and buoyancy, respectively

G_r Grashof number

G_ω, $G_{\omega b}$ generation term of ω due to mean velocity gradients and buoyancy, respectively

H tower height, elevation (m)

h convective heat transfer coefficient (W m^{-2} K^{-1})

$\hat{h}$ enthalpy (J/kg)

I turbulence intensity

K_r, K_{resist} pressure loss coefficient

K, K_e, K_t laminar, effective, and turbulent thermal conductivity, respectively (W m^{-1} K^{-1})

k turbulent kinetic energy (m^2 s^{-2}); thermal conductivity (W m^{-1} K^{-1})

m, $\dot{m}$ mass flow rate (kg s^{-1})

Nu Nusselt number

n	iteration number in CFD calculation
n_r	number of tube rows in a heat exchanger bundle
P	pressure (Pa)
Pr, Pr_t	laminar and turbulent Prandtl number, respectively
p_t, p_d	fin pitch and tube diagonal pitch, respectively (m)
Q, $\dot{Q}$	heat transfer rate (W)
q	heat flux (W m^{-2})
R	gas constant (J Kg^{-1} K^{-1})
Re, Re_t	Reynolds number and turbulence Reynolds number, respectively
S	modulus of the mean rate-of-strain tensor
S_ϕ	volumetric source term for variable quantity ϕ
S_X	standard deviation of sample X
s	coordinate of 1D system
T, Θ	temperature (K)
ΔT_{lm}	logarithmic mean temperature difference (K)
U, V, W	velocity components in x-, y-, and z- direction (m s^{-1})
V_c	numerical cell volume (m^3)
v	velocity scalar (m s^{-1})
W_M, W_Q	mechanical work, heat transferred, respectively (J)
X	sample data
x, y, z	Cartesian co-ordinates

Greek letters

α	permeability (m^2)
β	bulk thermal expansion coefficient (K^{-1}); benefit of pre-cooling
Γ_ϕ	diffusion coefficient for variable quantity ϕ
γ^*, γ	constants in dissipation terms of k and ω, respectively
δ	velocity ratio
ε	turbulent kinetic energy dissipation (m^2 s^{-3})
ε_X	fractional uncertainty of the sample X
η	heat transfer efficiency; relative performance
ℓ	latent heat (J kg^{-1})
μ, μ_e, μ_t	laminar, effective, and turbulent viscosity, respectively (kg m^{-1} s^{-1})

ρ, $\bar{\rho}$	density and mean density (kg m^{-3})
θ	angle (°)
σ_k, σ_ε, σ_ω	turbulent Prandtl number for k, ε, and ω, respectively
σ_ρ	constant in generation terms of k
σ_X	uncertainty of the sample X
ϕ	scalar quantity (u, v, w, T, k, ε...)
φ	relative humidity;
τ	scale ratio of cooling tower model
ω	turbulence energy specific dissipation rate (s^{-1})
ξ, ξ^*	constants in generation terms of ω
ψ	c_p/c_v
χ	humidity ratio

Vectors

$\vec{v}$	velocity

Subscripts

a, w	air side, liquid (water) side
c	minimum free flow area
cw	crosswind
e	effective
hx	heat exchanger
i, o	inside or inlet and outside or outlet
m	scaled model
N	pure natural convection
p	prototype
r	radiator
$resist$	resistant
t	tower
u	overall
x, y, z	Cartesian co-ordinates
0, ref	reference value

Chapter 1 Introduction

1.1. Motivations

About 90% of electric power today is generated in thermal power plants using Rankine cycles [1]. In a thermal power plant, no matter what heat sources is used, only a fraction of the heat inputs is converted into electricity and the redundant heat needs to be removed using devices such as condensers or heat exchangers [2]. The thermal power plant cooling systems are generally referred to as cooling towers of various types. The focus of this Thesis project is on dry cooling using natural draft in the context of small- to medium-scale renewable thermal power. Natural draft dry cooling towers (NDDCTs) feature no water losses and virtually no parasitic power consumption. They are therefore widely used in traditional fossil-fired thermal power plants around the world. NDDCTs are usually the highest buildings in a power plant. The basic principle for natural draft dry cooling tower is that the airflow across the heat exchanger bundles is driven by the buoyancy force caused by the density difference between the hot air inside and the cold air outside [3]. Unlike fan-forced mechanical cooling towers, the airflow in a NDDCT highly depends on the tower height [4]. In traditional thermal power plants with capacities more likely in the scale of hundreds or thousands of megawatts, the natural draft cooling towers are often over 100 m high with 70-90 m in base diameter.

The performance of the cooling towers is crucial to the efficiency of the entire power plant. It was observed that when the cooling tower systems operate at efficiencies lower than their design values, the power plant output may be reduced by as much as 4% [5]. In United States alone, the losses have been estimated to equal to about 0.3 GW of lost electricity or approximately $20 million lost revenue each year [6]. Thus it is very important to improve the cooling tower efficiency.

After the ambient temperature, crosswind is the most common environmental factor that affects the cooling performance of natural draft cooling towers, especially dry towers. Unfortunately, current design theories for NDDCT thermal performance estimation (e.g. [7]) do not take the crosswind effect into account.

Some experimental and numerical studies on natural draft dry and wet cooling towers subject to crosswinds revealed that the cooling performance decreases along with the increase of cross wind speed [3, 8-14]. All of these previous studies were conducted on large natural draft dry cooling towers with heights of more than 100 m for heat rejection rates exceeding 100 MW. In these large NDDCTs, cross winds could cause significant reductions in cooling performance [12], but even at

high crosswind speeds tall cooling towers would remain operational continuing to dump heat for the whole power plant system.

What is an annoyance for large thermal power plants could cause critical failure in small- to medium-scale renewable thermal power plants. Geothermal and solar thermal power plants are two types of renewable power generation alternatives, both using Rankine cycles. Australia enjoys one of the richest solar resources in the world, and it also holds substantial proven reserves of geothermal heat in the form of Enhanced Geothermal Systems (EGS). The challenge for the country is to find ways of utilising them efficiently. The Queensland Geothermal Energy Centre of Excellence (QGECE) is one of the major institutions in Australia dedicated in the research and development of EGS and solar thermal power plant technologies [15-17]. The Centre research programs aim development of small renewable thermal power plant applications for Australian remote communities. These are isolated districts with demand limited to a few megawatts and often much less. The low-maintenance natural draft dry cooling towers are the best option for their cooling systems as these plants will be located in arid areas far away from towns. However, these cooling towers do not need to be as big as those in large-scale coal-fired power plants. Instead, small NDDCTs are required. QGECE has proposed small NDDCTs with heights below 30 m. The towers are equipped with horizontally-arranged finned-tube heat exchanger bundles placed inside the towers above the air intake.

The cooling efficiency of small NDDCTs is a serious question as no precedence of application in renewable power plants has ever been seen. Especially the cross wind effect on their cooling performance might be much more significant than that on large towers with 100 m+ height. For example, by causing cold inflow or by disturbing the air flow at the outlet of tower, cross wind is known reduce the effective draft height for the tall towers used in large plants. This effect could be the cause of total failure with small cooling towers. Currently, most short cooling towers are mechanical draft type and they have less crosswind-associated problems than natural draft towers. Until very recently, there has been no publication related to crosswind effects on small natural draft dry cooling towers.

The following questions need to be answered to help designers of short cooling towers:

1. Can the existing methods for cooling tower design be transplanted directly into small tower design without any amendment? What is the minimum cooling tower height?
2. How significant is the influence of crosswind on the thermal performance of small cooling tower?
3. What are the mechanisms through which crosswinds affect the short cooling tower performance?

4. How should the current theories be revised to include the crosswind effect when design small NDDCTs?

5. What methods can be applied to reduce the negative cross wind effects?

1.2. Thesis objectives and scope

The general aims of this Thesis project are to determine the validity and effectiveness of the existing natural draft cooling tower design theories when they are applied to relatively short natural draft dry cooling towers for renewable power plants, especially in the consideration of crosswind effect; to determine the smallest cooling tower that can be built based on particular design conditions; and to develop a design method for small natural draft cooling towers taking the crosswind effect into account. These aims can be achieved by following the specific objectives below:

1. Identify the natural draft cooling tower size range that can be built at typical design conditions for small- to medium-scale renewable thermal power plants. These design conditions include the cooling water inlet temperature T_{wi}, the ambient air temperature T_{ai} and the total heat to be rejected Q. Without taking crosswind effect into account, this can be done by using the existing tower design theories. Explore possible benefits of evaporative cooling of the inlet air to improve the cooling tower performance for short towers.

2. Analyse the overall thermal performance of the NDDCTs identified above by CFD modelling with and without the effect of crosswind. Assess the difference in cooling performance based on the thermal efficiency variations at different crosswind and ambient conditions.

3. Propose the crosswind mitigation measures, specifically windbreak walls, and investigate the benefits of the windbreak walls on the cooling tower performance under crosswind conditions. Analyse different configurations (angles) of the windbreak walls and identify the optimized ones that lead to the best improvement of cooling tower heat dumping ability.

4. Validate the methodology used in the CFD analysis by carrying scaled natural draft dry cooling tower tests in a wind tunnel. Test the methods that can be used to prevent negative crosswind effects on small NDDCTs under windy conditions.

5. Propose corrections for the existing NDDCT design theories based on numerical and experimental results. The crosswind effect will be reflected in the corrections.

1.3. Thesis structure

The structure of this Thesis is organized on the basis of the detailed objectives of the study as followings.

Chapter 2 is a broad review of past literature on natural draft dry cooling tower technologies, design methods and crosswind effects.

Chapter 3 introduces a one-dimensional mathematical model for cooling performance estimation of the NDDCT. The model is used to scale down the NDDCT for small power plants and predict its cooling capacity under normal (non-crosswind) conditions. A case study on the conventional NDDCT equipped with the inlet air pre-cooling facilities is conducted finally.

Chapter 4 presents the CFD modelling investigation on the heat transfer performance of a 15m-high small NDDCT under different crosswind speeds. The mechanisms of wind effects are analysed in detail. A simple correlation of cooling tower heat transfer with the crosswind speed is proposed based on the CFD results, indicating that the total thermal performance of the cooling tower is a result of a combination of natural convection heat transfer and forced convection heat transfer. This combination causes a turn-around trend with the cooling tower performance first decreasing and then increasing with crosswind speed.

Chapter 5 proposes a windbreak wall design to prevent the negative crosswind effect and examines the effect of the wall orientation angles with respect to wind. Through more detailed analysis at different velocity ratios, the variation of the heat transfer rates across the heat exchanger area are examined and explained by considering the vortices in the air flow. The best windbreak wall orientation is identified. The results provide further assistance to designers who need to design relatively short natural draft dry cooling towers for renewable power plants.

Chapter 6 presents a wind tunnel experiment using a 1.2 m-tall natural draft dry cooling tower model. The experiment results are compared against the predictions of two 3D CFD models: a 15 m-high tower model and a 1.2 m-high tower model. Both experiment results and CFD findings are matched up with each other generally well. The total heat transfer rate and airflow velocity in scaled tower model experience the same decrease-turnaround trend along with the increase of crosswind speed as found in the CFD simulations. The air temperature distributions inside the cooling tower model indicate the existence of the local air circulation cells in the tower. The validation indicates that the methodology used in numerical modelling is reasonable. It is also found that CFD models may slightly overestimate the circulation of the airflow especially near the tower outlet.

Chapter 1

Chapter 2 Literature review

2.1 Cooling tower technology

In a thermal power generating cycle, heat is need to be discharged due to the energy transfer efficiency is limited well below hundred per cent by the laws of thermodynamics. The typical efficiency for fossil fired power plant is about 33% to 48% [12]. This means only a small part of the heat input of steam is converted into power, and the rest is dumped through heat removal devices, in most cases, cooling towers.

Cooling towers using the evaporation of water to remove waste heat and cool the working fluid are known as wet cooling towers. Cooling towers that uses ambient air to cool the closed-cycled working fluid are known as dry cooling towers. In addition to being wet or dry, cooling towers can be categorised by different ways [18]. By air-to-water flow they are catalogued into cross-flow towers and counter-flow towers. By heat transfer methods there are dry surface cooling towers and wet evaporative towers. And by air flow generation methods there are mechanical draft, natural draft and the hybrid type of both.

2.1.1. Mechanical draft

Mechanical draft cooling towers use fans to force the air to flow through heat exchangers. Depending on the location where fans are installed, they can be divided into forced mechanical draft and induced mechanical draft. Mechanical draft towers control cooling rates using fan diameter and fan speed. These towers are usually arranged in an in-line layout to form a rectangular bank, which contains several areas (each with their own fan) called cells.

It is well known that mechanical draft cooling towers are associated with recirculation and interference problems [19, 20]. Recirculation is directly related to the degradation of cooling tower performance. It can be measured as the ratio of the amount of exhaust air which re-enters the tower divided by the total amount of air going through the tower [20, 21]. Kröger [22] had investigated the effectiveness of mechanical draft cooling tower due to the warm-air recirculation through analytical, numerical and experimental methods, and found that the effectiveness drops by up to 16% in different conditions.

2.1.2. Natural draft cooling towers

In a natural draft cooling tower, warm air naturally rises due to the buoyancy force caused by the pressure difference between the inside and the outside of the tower due to the different of the warm air density inside and the ambient air density outside. The most common types of natural draft

towers are natural draft dry cooling towers (NDDCT) and natural draft wet cooling towers (NDWCT). For NDDCT, heat exchangers can be arranged horizontally inside the tower above the inlet or vertically in the periphery of the tower base (as shown in Figure. 2.1). Comparing to natural draft dry cooling towers, natural draft wet cooling tower delivers a better cooling performance but consumes a large amount of fresh water [23]. With increasing water costs, NDDCTs become more economic and may actually be the only option in some arid areas where water supply is extremely limited [24].

The fundamental equations of natural draft cooling towers are the draft and energy balance equations [3]:

$$\Delta P \approx (\rho_{ao} - \rho_{ai})g(H_t - H_{hx}) = (\sum K_{resistances})\frac{\bar{\rho}_a v^2}{2}$$

$$\qquad (2.1)$$

$$Q_a = Q_w = Q_{hx} \qquad (2.2)$$

where H_t is the tower height, H_{hx} is the mean elevation of heat exchanger bundles, and ρ is the mean density.

The pressure difference between tower inlet and outlet in this equation is proportional to the difference of densities and tower height, which has to be balanced by all terms of resistance to air flow. The dominant resistance is caused by heat exchangers whose coefficient is K_{hx} [3]. K_{hx} is a function of parameters of tubes and fins of heat exchanger as well as the speed of air flow.

Eq. (2.2) represents the equilibrium among the heat transferred by air, by water as well as by heat exchangers [3]. All these can be expressed as:

$$Q_a = m_a c_{pa}(T_{ao} - T_{ai})$$

$$Q_w = m_w c_{pw}(T_{wi} - T_{wo}) \qquad (2.3)$$

$$Q_{hx} = h_u A F_T \Delta T_{lm}$$

where m_a and m_w are the mass flow rates of air and water, respectively. h_u is the overall heat transfer coefficient based of the area of the cylindrical exchanger tube and it consists of the air side transfer coefficient h_a, the water side coefficient h_w, and the tube wall conductivity k [4]:

$$h_u = \frac{1}{A_a/(A_w h_a) + A_a \ln(r_o/r_i)/(2\pi k L) + 1/(h_w)} \qquad (2.4)$$

where A_a and A_w are heat transfer areas of air and water side, respectively. L is the effective length of water tube.

The heat transfer coefficients for both sides are related to not only the geometry of tube and fin but also the Reynolds number and Prandtl number for each side.

2.1.3. Heat exchanger arrangements in natural draft cooling towers

For practical reasons, in most towers the heat exchanger bundles are arranged either vertically around the circumference of the tower or horizontally in the inlet cross-section of the tower [12, 25] as shown in Figure. 2.1.

(a)   (b)   (c)
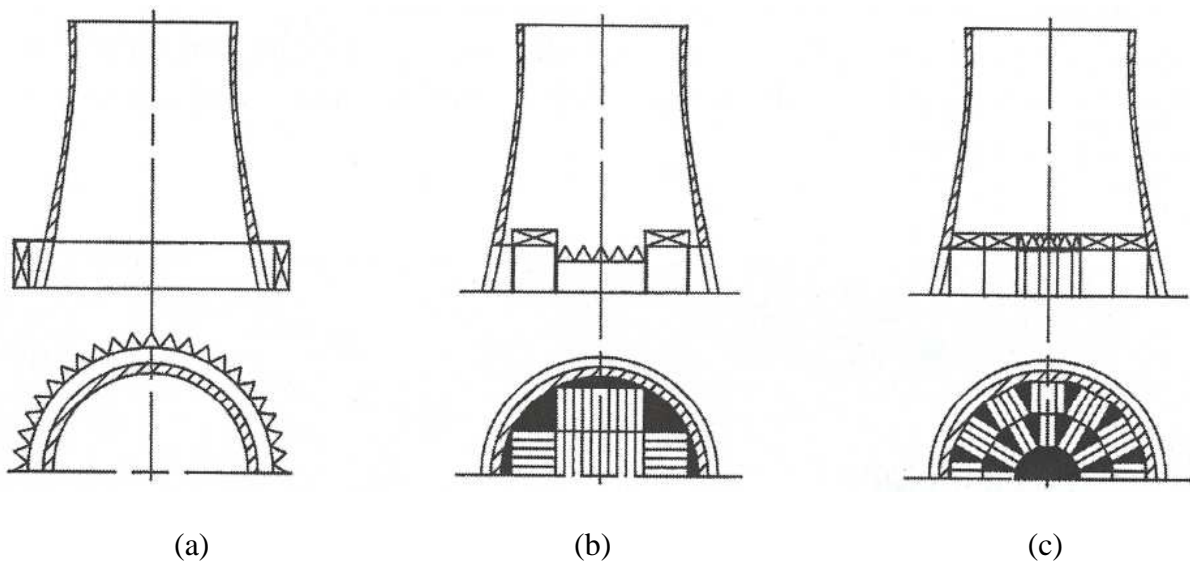
Figure 2.1. Heat exchanger bundle arrangements: (a) vertical circumferential; (b) horizontal rectangular; (c) horizontal radial [12].

The heat exchanger bundles are usually arranged in several forms: in flat pattern; deltas or A-frames which is indicated in Figure 2.2. A-frame configuration is composed of two heat exchanger bundles which are inclined at a certain angle θ with respect to each other [4]. The purpose of the arrangement is to maximize the heat exchanger area and save the tower cross-section area required [26]. The surface area facing oncoming air flow is referred to as frontal area A_{fr}, while the projection area of bundle on ground is called effective area A_e.
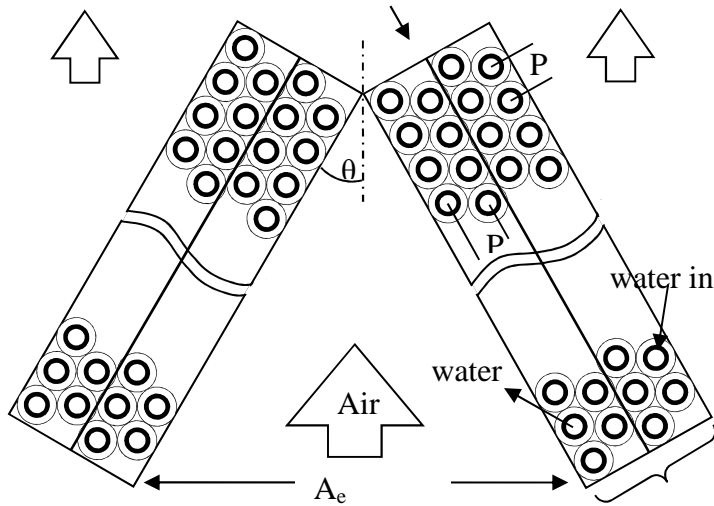
Figure 2.2. A-frame Heat exchanger bundle

2.1.4. Performance assessment of natural draft cooling tower

Currently, there is no an universal standard to evaluate the thermal performance of natural draft cooling tower [27]. However, practically several commonly used methods are used as stated in the following [28]:

Range

Range is defined as the difference between the cooling tower water inlet and outlet temperature. A high Range means that the cooling tower has been able to reduce the water temperature effectively, and is thus performing well.

$$\Delta T_{range} = T_{wi} - T_{wo} \qquad (2.5)$$

Approach

The definition of Approach is the difference between the cooling tower outlet water temperature and inlet air temperature. Generally speaking, the lower the Approach, the better performance the cooling tower has. Although, both Range and Approach should be monitored, the Approach is a better indicator of cooling tower performance.

$$\Delta T_{approach} = T_{wo} - T_{ai} \qquad (2.6)$$

Effectiveness

Effectiveness is the ratio between the Range and the ideal Range (difference between cooling water inlet temperature and air inlet temperature). It can be expressed as below [29]. The higher this ratio is, the higher the cooling tower Effectiveness is.

$$e_f = \frac{T_{range}}{T_{range} + T_{approach}}$$
(2.7)

2.2. Crosswind effects on large cooling towers

The performance of NDDCT is influenced by crosswind condition to a certain degree. The wind influence on the thermal performance of a dry-cooling tower can commonly be expressed in two methods. The first method uses the parameter of change in the Approach T_{app}, which is defined as the difference between the Approach in no crosswind condition and that subjected to cross wind condition [12], i.e.

$$\Delta T_{appr} = T_{appr}^N - T_{appr}^{cw}$$
(2.8)

The second method uses the cooling tower thermal effectiveness, η_Q, which is defined as the ratio of the heat dumping rate under crosswind condition–Q_{cw}, to the heat dumping rate under pure natural convection condition (no crosswind)–Q_N [30]

$$\eta_Q = \frac{Q_{cw}}{Q_N}$$
(2.9)

Both methods can assess the differences in effectiveness of cooling system under various crosswind conditions. However, for large natural draft cooling towers, the first method is preferred because the Approach temperature is a major parameter measured in operation of cooling towers.

Systematic studies on the crosswind influence on natural draft cooling towers date back to 1970s [31, 32]. The methods used in various studies in the past decades can be catalogued into three groups: field measurements, scaled model tests in laboratory and numerical analysis. Each of them has advantages and drawbacks.

Field measurement is the most direct way to investigate the cross wind effect; however, it is expensive and time consuming to obtain sufficient data due to the complexity of the environmental conditions and the difficulties of field instrumentation in large tower. And the measurement data are usually highly scattered and thus require to be presented statistically.

Scaled model tests in laboratory overcome the disadvantages associated with field measurements. With more sophisticated instruments, systematic theoretical analysis can be done on the crosswind

effect. But laboratory experiments require well designed models and testing facilities to repeat the similar conditions in real cooling towers, which is actually very difficult to achieve sometimes.

Numerical simulation offers the most economical alternative way for the crosswind study, especially on large cooling towers. It uses numerical way to solve the mathematic problems. The challenge is that the accuracy of the results directly relies on the quality of mathematical models. With the advances in both the CFD fundamentals and computing equipment, well-conducted numerical analysis delivers acceptable accuracy at much lower cost.

In most literatures, field measurements and modelling test in wind tunnel were also referred as to the experimental testing in cross wind effect research.

2.2.1. Experimental Testing

Most early researches on cross wind effect in natural draft cooling towers were conducted through the experimental testing or measurements on either real operating cooling tower systems (full scaled) or the scaled models in laboratory. In these tests, inlet and outlet water temperature, air temperature and velocity before and after heat exchanger bundles as well as at tower outlet are measured. The ambient conditions, such as dry-bulb air temperature distribution and three-dimensional wind velocity profile, were obtained through meteorological testing methods [33].

Du Preez and Kröger [33] had made a field measurement on the natural draft dry-cooling tower in Kendal power plant in South Africa. They used 7 chromel-alumel thermocouples and 12 anemometers to obtain the air temperature and velocity respectively in the positions 1.5m below heat exchanger and tower throat. The mean water temperatures were measured by thermocouples attached to the outer surface of the water tubes with sensing tips insulated from the atmosphere. The measurement took nearly 2 months. They obtained large number of data on the change of Approach at different cross wind speeds using the natural variation of the wind speeds at the site. Figure 2.3 shows the measurement results on a cooling tower with a design heat rejection capacity of 650 MW together with the empirical correlation and numerical prediction.
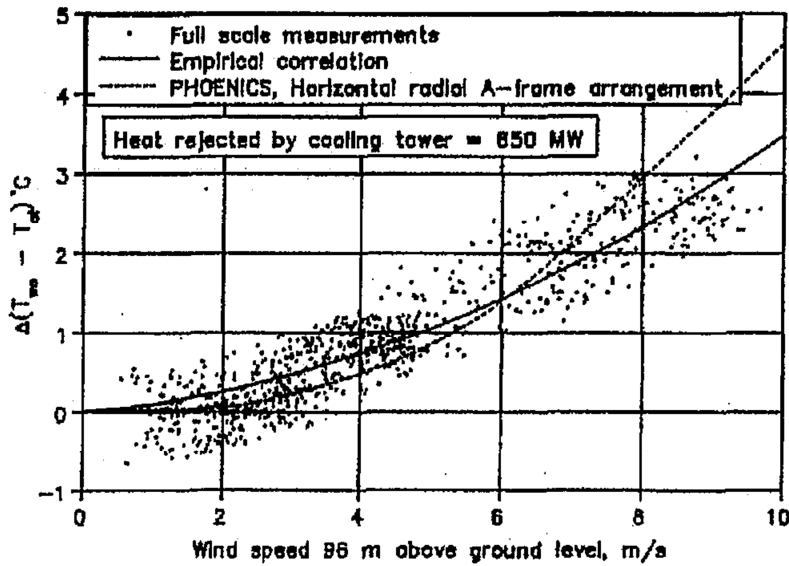
Figure 2.3. Measurement result on cooling tower with heat rejection capacity of 650 MW[33]

Wei *et al.* [8] conducted measurements both on a full scale tower in the field and on a wind tunnel model in laboratory for the purpose of finding out the mechanism of negative effects of wind on cooling efficiency of dry cooling towers. The full scale test measured the air flow velocity and temperature inside an in-service dry cooling tower with a height of 125 m, a base diameter of 108 m, and an outlet diameter of 65 m, using anemometers and temperature sensors controlled by remote devices.

(a)   (b)
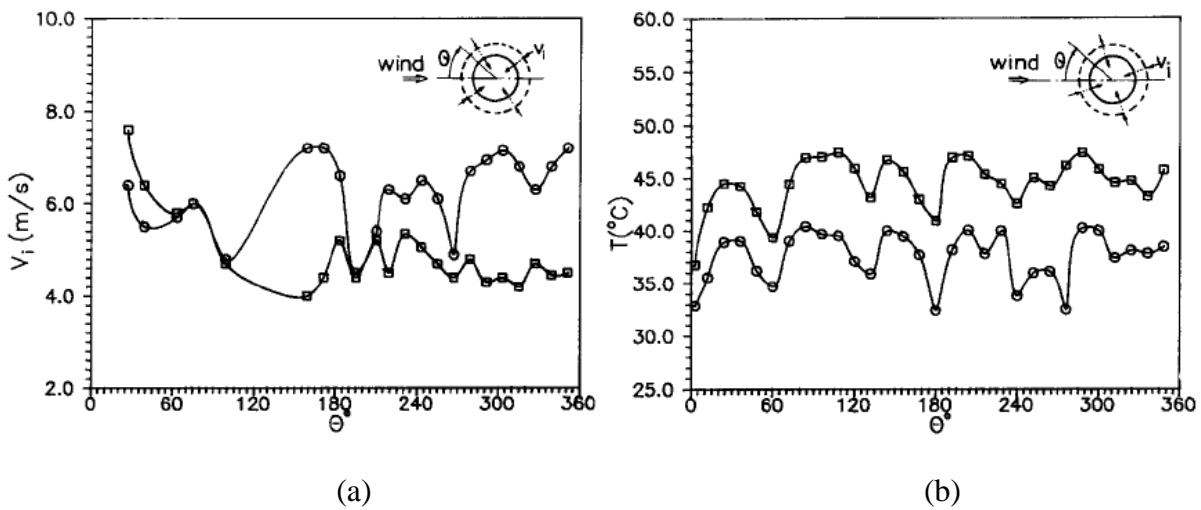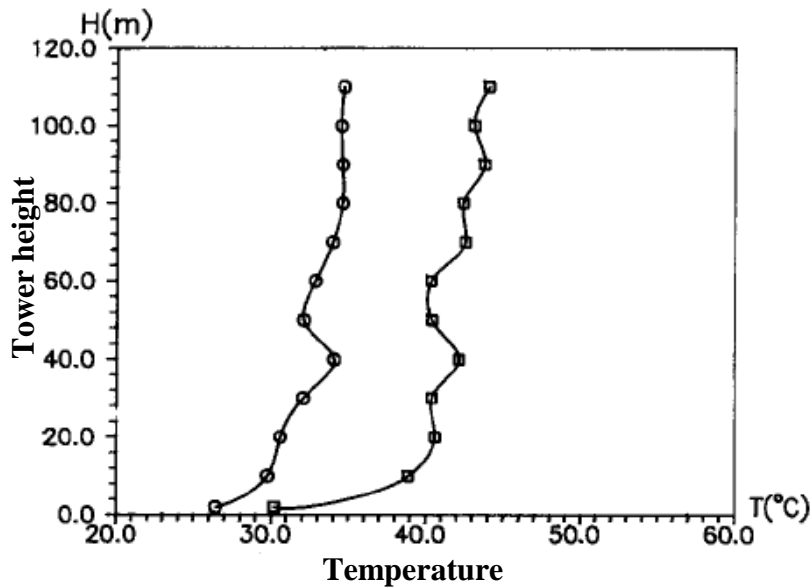
(c)

Figure 2.4 Distribution of (a) the mean draft speed V_i at the inlet, (b) mean temperature along the annular radiator inside the tower, and (c) mean temperature along the central axis of the tower, when wind speed ($\circ$) $V_w = 0$ m/s and ($\square$) $V_w = 6$ m/s. [8]

The distribution of the mean draft velocity $V_i(\theta)$ (Figure 2.4.a) as well as the mean temperature T (Figure 2.4.b) along the annular heat exchangers was measured at different cross wind speeds: $V_w=0$ m/s and $V_w=6$ m/s. θ is the angle between the wind direction and the measurement point in clockwise direction. The figures indicate that $V_i(\theta)$ decreased by around 20% at a large part of the annular heat exchangers at cross wind speed $V_w=6$ m/s, which results in the decrease of heat transfer of the cooling tower. The temperature distribution along the central line in the cooling tower has been measured at different wind speeds too, from which it is seen that, with the crosswind, the mean upward air flow rate decreases as the result of mean temperature increase.

In the wind tunnel testing, Wei $et\ al.$ [8] used a 1/200th scaled model with the same structure as the tower in field measurement is used. Plus, a 1/400th and a 1/800th scaled models were built for testing the effects of lateral wind on the internal flow at tower outlet and for the visualization study. These models were all constructed under the restriction of two similarity parameters: density Froude number and speed ratio while the Reynolds number similarity was not achieved.

The wind effect coefficient C_w was introduced to assess the influence of crosswind, which was defined as $C_w = (\Delta T_{cw} - \Delta T_0)/\Delta T_0$, where ΔT_{cw} and ΔT_0 were the range of the heat exchangers with and without crosswind respectively. The distribution of C_w along the annular heat exchanger inlet (Figure 2.5) indicates that the overall wind effect coefficient decreases by up to 8.85% under

windy condition. Here C_{wi} stands for the wind effect coefficient of the radiator segment No. i ($i = 1$-6).
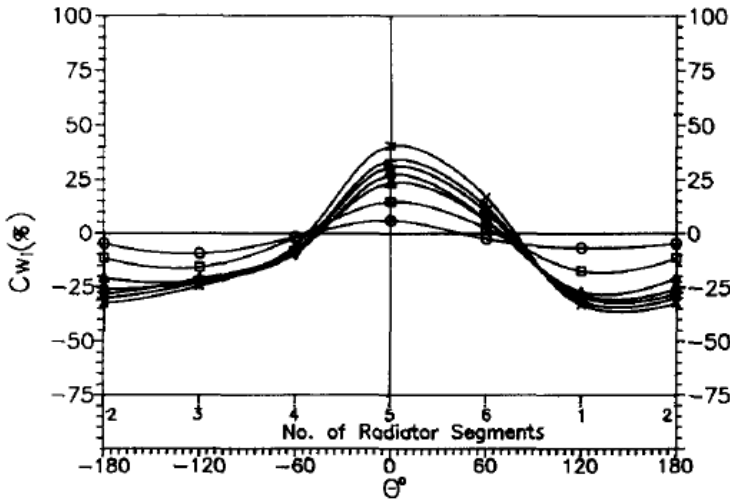
Figure 2.5. Wind effect coefficient C_{wi} (○) $V_w/V_i = 1.0$, $C_w = -3.28\%$; (□) $V_w/V_i = 2.0$, $C_w = -4.98\%$; (Δ) $V_w/V_i = 2.8$, $C_w = -7.95\%$; (◇) $V_w/V_i = 3.2$, $C_w = -8.85\%$; (☆) $V_w/V_i = 3.6$, $C_w = -8.57\%$; (+) $V_w/V_i = 4.0$, $C_w = -7.70\%$; (x) $V_w/V_i = 5.0$, $C_w = -6.47\%$ [8].

The visualization study on the 1/800th scaled tower model in [8] shows the hot air rising uniformly without cross wind. Some backflow is observed in the presence of cross wind and the backflow is measured to have lower temperature and occurs at the leeward part of the tower throat. The backflow is induced by the leading edge separation vortex and reduces the effective area of the tower outlet, which causes a lower heat dumping efficiency for the cooling tower.

In natural draft wet cooling towers, similar measurements were carried out by several researchers. Gao *et al.*[34] studied the variation of heat transfer performance of natural draft wet cooling towers under cross-wind conditions, by comparing the circulating water temperature difference *Δt*, defined as the difference of inlet water temperature and outlet water temperature, and cooling efficiency of tower *η*, defined as:

$$\eta = \frac{\Delta t}{t_{in} - t_{\lim}} \tag{2.10}$$

Where t_{in} is the water inlet temperature, and t_{lim} is the wet bulb temperature of inlet air.

Their experimental rig was mainly comprised of a 1:100 scaled cooling tower model, tow water tanks, water pumps, electric heater as well as testing devices, shown in Figure 2.6.
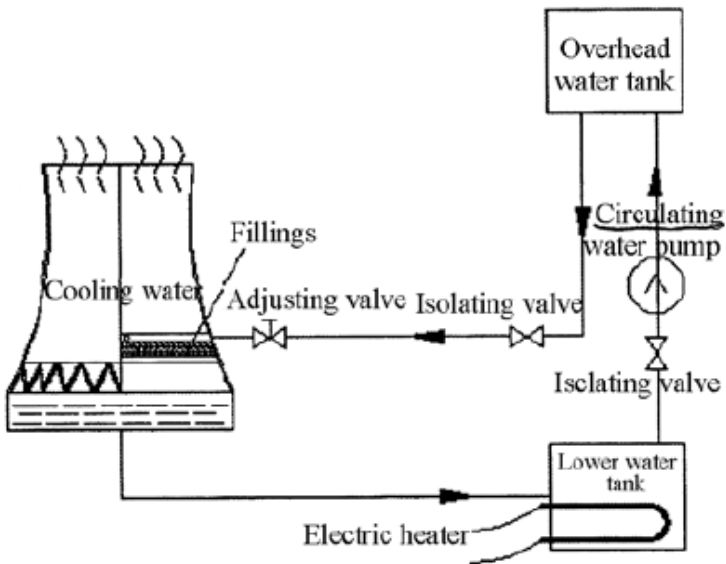
Figure 2.6. Schema of the experimental rig [34]

The scaled tower model is built under the similarity restriction only in the density Froude number Fr_d, which is expressed as:

$$Fr_d = \frac{v}{\sqrt{\frac{\Delta\rho}{\rho_i} gL}}$$

(2.11)

where $\Delta\rho$ is the density difference between inside and outside tower, and L is the characteristic dimension.

Figure 2.7 (b) shows that there exists a minimum value of Δt at the cross wind velocity of about 0.4m/s, and the wind speed is called the critical wind velocity point. This phenomenon also occurs in the cooling efficiency as shown in Figure 2.7 (a)
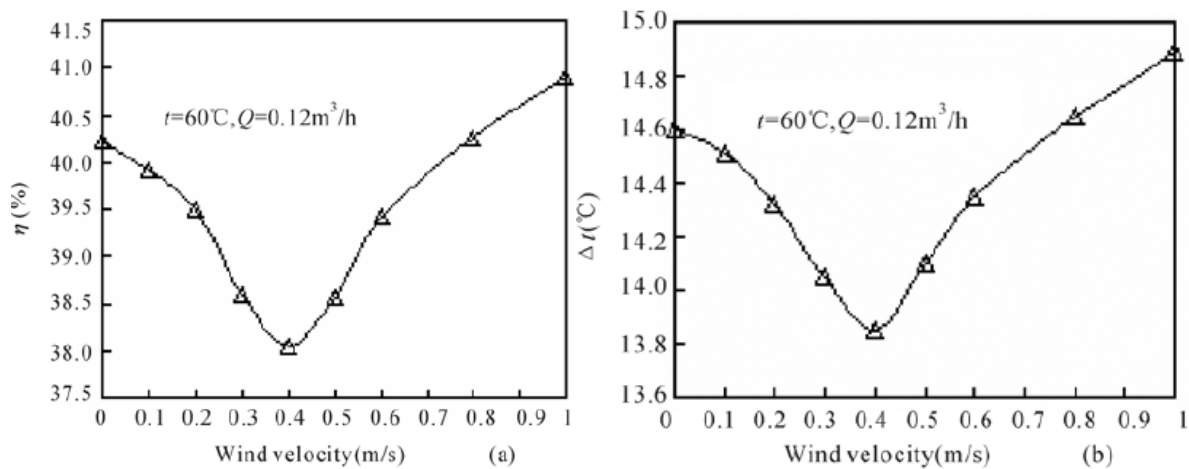
Figure 2.7. The correlation of cooling performance with wind velocity [34]

Gao et al. [34] concluded that the crosswind had a great influence on the circulating water temperature and the coefficient of efficiency, and the decreases were about 9.2% and 9.6%, respectively.

2.2.2. CFD studies on cross wind effect

In the last twenty years, numerical analysis has gradually become the most efficient method in studying the crosswind effect on natural draft cooling towers. As the result of advances in computational fluid dynamics (CFD) technology, both the accuracy and the computation speed have improved dramatically, making CFD simulation the first choice in cooling tower studies nowadays.

In CFD studies found in open literature, numerical models of cooling towers are set up with several approximations and simplifications. The variable fields are solved through a set of procedures. Although different models were used in different publications, some typical approaches are found:

1. Governing equations

In all general-purpose CFD codes widely used today, the discretised differential governing equations are solved which can be expressed in the general form [35]:

$$\nabla \cdot (\rho \boldsymbol{v} \phi - \Gamma_\phi \nabla \phi) = S_\phi \qquad (2.12)$$

where ρ is air density; $\boldsymbol{v}$ is air velocity vector; Γ_ϕ is the diffusion coefficient and S_ϕ is the source term. The scalar ϕ could be any quantity in U, V, W and T as well as k and ε, if k-ε model is used for turbulence. The k-ε model is based on model transport equations for the turbulence kinetic energy k and its dissipation rate ε [36]. The model transport equation for k is derived from the exact equation, while the model transport equation for ε was obtained using physical reasoning and bears little resemblance to its mathematically exact counterpart. The particular expressions of ϕ, S_ϕ and S_ϕ are shown in table below [37]:

Equation	ϕ	S_ϕ	Γ_ϕ
Continuity	1	0	0
x momentum	U	$-\frac{\partial p}{\partial x} + \frac{\partial}{\partial x}\left(\mu_{eff}\frac{\partial U}{\partial x}\right) + \frac{\partial}{\partial y}\left(\mu_{eff}\frac{\partial V}{\partial x}\right) + \frac{\partial}{\partial z}\left(\mu_{eff}\frac{\partial W}{\partial x}\right) + \frac{\Delta p_x A_c}{V_c}$	μ_{eff}
y momentum	V	$-\frac{\partial p}{\partial y} + \frac{\partial}{\partial x}\left(\mu_{eff}\frac{\partial U}{\partial y}\right) + \frac{\partial}{\partial y}\left(\mu_{eff}\frac{\partial V}{\partial y}\right) + \frac{\partial}{\partial z}\left(\mu_{eff}\frac{\partial W}{\partial y}\right) + g\left(\rho - \rho_{ref}\right) + \frac{\Delta p_y A_c}{V_c}$	μ_{eff}
z momentum	W	$-\frac{\partial p}{\partial z} + \frac{\partial}{\partial x}\left(\mu_{eff}\frac{\partial U}{\partial z}\right) + \frac{\partial}{\partial y}\left(\mu_{eff}\frac{\partial V}{\partial z}\right) + \frac{\partial}{\partial z}\left(\mu_{eff}\frac{\partial W}{\partial z}\right) + \frac{\Delta p_z A_c}{V_c}$	μ_{eff}
Energy	T	$\frac{1}{c_p}\left(\frac{q A_c}{V_c}\right)$	$\frac{\mu}{Pr} + \frac{\mu_t}{Pr_t}$
Turbulent energy	k	$G_k + G_b - \rho\varepsilon$	$\frac{\mu_{eff}}{\sigma_k}$
Energy dissipation	ε	$C_{1\varepsilon}\frac{\varepsilon}{k}(G_k + C_{3\varepsilon}G_b) - C_{2\varepsilon}\rho\frac{\varepsilon^2}{k}$	$\frac{\mu_{eff}}{\sigma_\varepsilon}$

where

$$G_k = \mu_{eff}\left\{2\left[\left(\frac{\partial U}{\partial x}\right)^2 + \left(\frac{\partial V}{\partial y}\right)^2 + \left(\frac{\partial W}{\partial z}\right)^2\right] + \left(\frac{\partial V}{\partial x} + \frac{\partial U}{\partial y}\right)^2 + \left(\frac{\partial V}{\partial z} + \frac{\partial W}{\partial y}\right)^2 + \left(\frac{\partial U}{\partial z} + \frac{\partial W}{\partial x}\right)^2\right\}$$

$$\mu_{eff} = \mu + \mu_t; \quad \mu_t = C_\mu\rho\frac{k^2}{\varepsilon}; \quad G_b = -g\frac{\mu_t}{\rho Pr_t}\frac{\partial\rho}{\partial y}; \quad C_{3\varepsilon} = \tanh\left(\frac{U_{pa}}{U_{pe}}\right)$$

$$C_{1\varepsilon} = 1.44; \quad C_{2\varepsilon} = 1.92; \quad C_\mu = 0.09; \quad \sigma_k = 1.0; \quad \sigma_\varepsilon = 1.3; \quad Pr = 0.71; Pr_t = 0.85$$

Figure 2.8. Three-dimensional governing equations parameters [37]

2. Boundary conditions

The computational domain of CFD model is cylindrical or cubic shaped in most publications, and the boundary conditions applied to the domain include followings [37]:

Velocity inlet boundary condition is applied at the surface where crosswind comes from define the the inlet airflow velocity. The *x*-direction component of velocity in the inlet flow is set to the crosswind speed with a particular profile, whereas the other components are set to 0. The ambient air temperature T_a is set to constant as described in the assumptions.

Pressure inlet boundary condition defines the air static pressure at inlet surfaces. This boundary replaces the velocity inlet boundary when there is no cross wind in consideration.

Pressure outlet boundary condition is defined for the static pressure of air at the domain boundary opposite to the inlet boundary. At pressure outlet boundary, the air velocity ans temperature are computed by codes while the pressure gradient in vertical direction and horizontal directions are equal to the atomospheric pressure lapse rate and 0 respectively.

Wall boundary condition used at the tower shell, the ground and the windbreak wall is set to no-slip with some particular values of roughness, corresponding to the physical property of real case. The velocity gradient at wall boundary is constantly 0, while the turbulence quantities k and ε are computed using the standard wall functions.

Radiator boundary is used to represent the heat exchangers. The boundary is considered a lumped face without thickness. The pressure drop through it is proportional to the dynamic head of airflow, namely:

$$\Delta P = \frac{1}{2} k_L \rho v^2 \tag{2.13}$$

where v is the velocity component perpendicular to the radiator surface. And the heat flux transferred between the hot circulating water in heat exchanger tubes and the air outside the heat exchanger is determined as

$$q = h(T_{he} - T_{ai}) \tag{2.14}$$

Where k_L and h, the pressure loss coefficient and heat transfer coefficient, are also the functions of the air velocity component in normal direction v: $k_L = f(v)$ and $h = f(v)$. T_{he} and T_{ai} are hot water temperature and the ambient air temperature (Reference temperature), respectively.

3. Solver

Since the governing equations are partial differential equations that cannot be solved directly, CFD codes use discretization to convert the continuous partial differential equations and appropriate boundary conditions into a discrete system of algebraic equations. In discretization process, a finite volume method with a segregated solver and implicit differencing scheme are used. Pressure and the velocity fields are calculated by mostly two segregated types of algorithms: semi-implicit method for pressure-linked equations (SIMPLE) algorithm or SIMPLE-Consistent algorithm (SIMPLEC), and then used to solve the energy equation [36]. The numerical domains are also segregated using unstructured mesh cells, and at least a second order upwind spacial discretization scheme are used to approximate the spatial derivatives at all interior grid points.

CFD studies are conducted for the effect of cross wind on both the dry and wet cooling towers as well as on the mechanical draft towers using both two-dimensional and three-dimensional models in the past decades.

Su et al.[38] numerically studied the fluid flow and temperature distribution in a dry-cooling tower under crosswind using the finite volume method (FVM). The model is three-dimensional Heller-type dry cooling tower with regular hexahedron shaped computational domain, as shown in Figure 2.9. The Boussinesq eddy-viscosity hypothesis for the incompressible air flow, as the fluid model, is used. Boundary conditions are also shown in Figure 2.9.
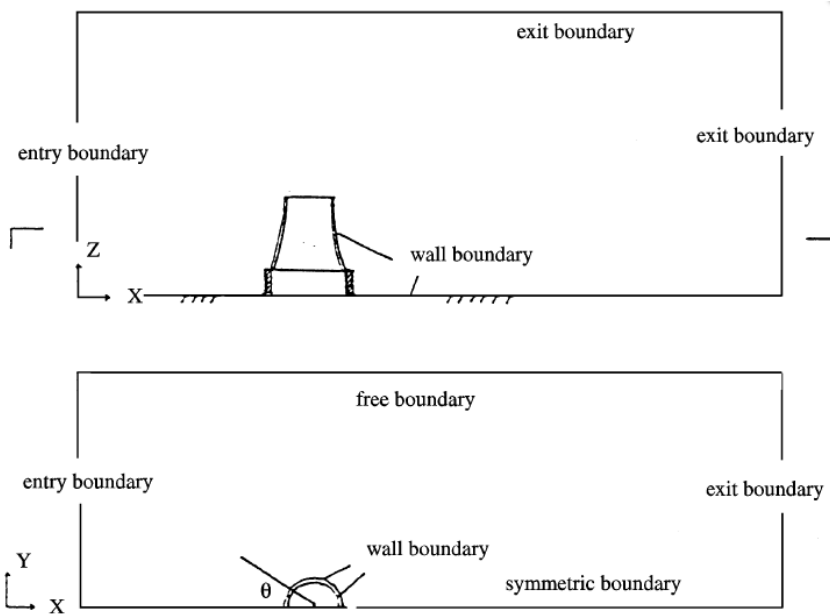
Figure 2.9. The cooling tower model and the boundary conditions [38]

They obtained the velocity vectors on the symmetric plane and horizontal plane at the middle elevation of the heat exchangers under cross wind speed 10 m/s (Figure 2.10.). It is seen that air flows through the windward part of heat exchangers and decreases in the leeward part. And at inside the cooling tower base, vortices are seen, which are caused by air flows passing through both the windward and leeward part of heat exchangers. The air entering through the lateral part of tower (90°-120°) nearly disappears due to the pressure difference between both sides of heat exchanger approaches zero because of the existence of cross wind, thus reduces the heat transfer significantly at this part of heat exchangers, which also can be seen in the Figure 2.11. Meanwhile at the top the cross wind plays somehow a role of 'wind lid' over the tower, which hinders the upward air flow through tower outlet.
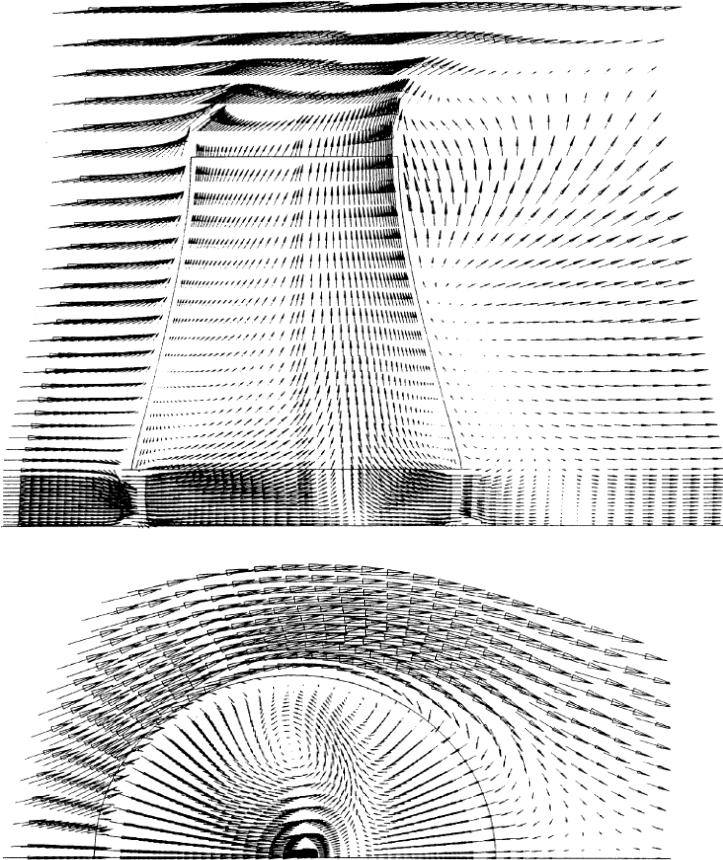
Figure 2.10. Computed natural draft dry cooling tower velocity field [38]
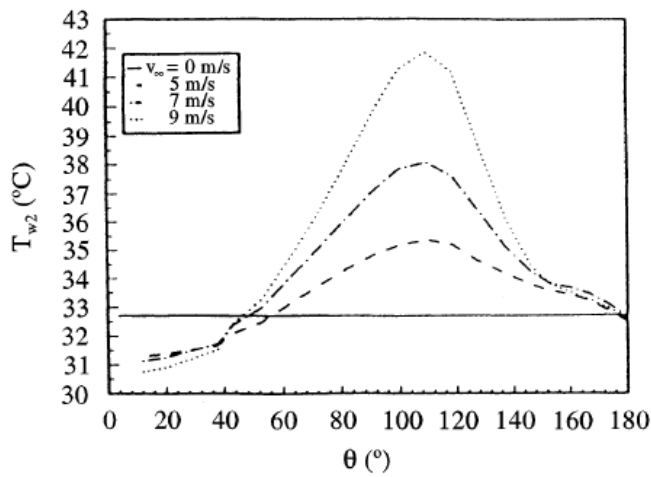
Figure 2.11. The effect of the cross-wind speed on the temperature of the cooling water [38]

The effect of cross-wind speed on the temperature of the cooling water is shown in Figure 2.12. The solid line denotes the results reported at no crosswind in various power stations from literature. The dashed lines are the numerical results obtained by Su *et al.* [38].
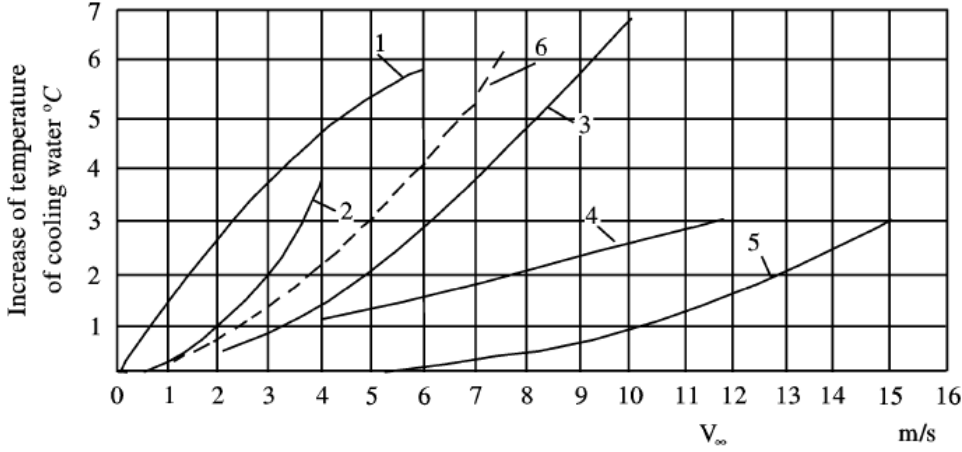
Figure 2.12. The influence of the cross wind speed on the water temperature at the exit of the radiator:(1) Lazdain PS of USSR, Q =265 MW; (2) Ibbenbueren PS of Germany Q =188 MW; (3) Kakalin PS of Hungary, Q =331 MW; (4) Grudfry PS of South Africa, No. 5, Q =331 MW; (5) Grudfry PS of South Africa, No. 6, Q =331 MW; (6) Datong PS Q =200 MW [38].

Bender *et al*. [10] presented a numerical study on a two-dimensional finite-volume model of the flow over a counter-flow wet cooling tower, whose geometry shape is hexahedron. The study predicted the flow pattern on a prototype cooling tower with the dimensions of 11.7 × 18.3 × 9.14m (height x width x length) with the tower inlet height of 2.59m. The 2.875 m-high protective wind wall located 1.875m in front of the cooling tower.

The numerical model calculates the flow field by solving discrete forms of the continuity and Navier-Stokes equations under specified boundary conditions:

$$\frac{\partial U_i}{\partial x_i} = 0 \tag{2.15}$$

$$U_j \frac{\partial U_i}{\partial x_j} = -\frac{1}{p}\frac{\partial P}{\partial x_i} + \frac{\partial}{\partial x_j}\left[\mu \frac{\partial U_i}{\partial x_j} + \mu_t \left(\frac{\partial U_i}{\partial x_j} + \frac{\partial U_j}{\partial x_i}\right) - \frac{2}{3}\delta_{ij}k\right] \tag{2.16}$$

The eddy viscosity model is calculated by:

$$\mu_t = C_\mu \frac{k^2}{\varepsilon} \tag{2.17}$$

where turbulence kinetic energy k and turbulence dissipation rate ε are computed by the transport equations defined by standard k-ε model. The discretised transport equations for each variable with in each control volume are solved in velocity-pressure based SIMPLEC algorithm.

In their study, the 2D model uses quadrilateral meshes with meshing size of 100 by 78 cells in the whole numerical domain. The boundary conditions for the tower wall are all no-slip wall boundaries, while for the fill zone inside the tower and tower inlet which contains the louvers the

porous media boundary is applied. The benefit of using porous media boundary condition is that no special treatments are needed near the wall with the porous wall model. The turbulence parameters can self-adjust through the increased fluid stresses created by the porous structure.

Bender *et al*. [10] studied the flow field for some typical velocities using this numerical code of cooling tower. The authors presented the velocity field for the cross wind condition (v = 9.0 m/s at z = 10 m) as well as predictions for both a solid and 10% porous protective wind wall.

(a)   (b)
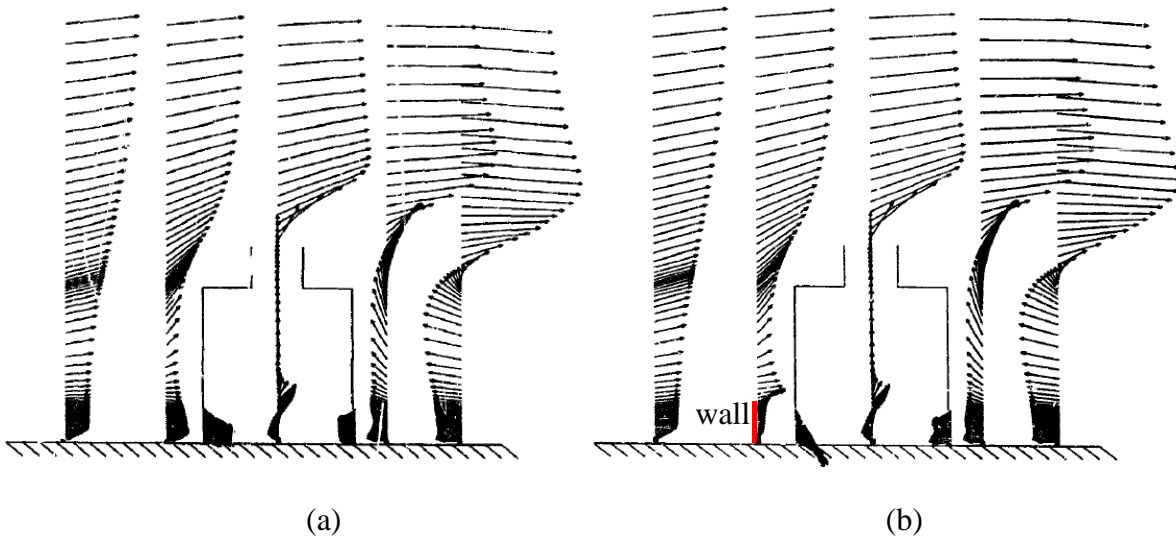
Figure 2.13. Air velocity vector field around cooling tower (a) without break wall; (b) with solid break wall [10]

Figure 2.13(a) shows a vector distribution under the design wind condition. The imbalance between the windward and leeward inlet flow rates is seen clearly. The air flow goes through the exhaust duct at top of the tower and turns quickly by the cross wind once leaving the duct. Figure 2.13(b) demonstrates the flow vectors over the cooling tower with the existence of solid break walls. The presence of the wall, the air velocity at the tower inlet in windward side decreases dramatically.

Bender *et al*. [10] have also compared the numerical results with their experimental data and found that the main difference between the two results is in the inlet velocity profile. The numerically predicted intake velocity profiles much more uniform than those measured experimentally, which may be due to the porous media model used in their analysis. The conclusion from their research is that the numerical prediction for the flow field over the cooling tower was generally realistic, and suggested to use more accurate turbulence model than standard k-ε, in order to better investigate the air flow over a cooling tower or any tall building.

Chapter 2

Demuren and Rodi [35] calculated the flow and temperature field of cooling towers using $61 \times 31 \times 32m$ three-dimensional numerical model which has the rectangular numerical grid. The governing equations for the steady-state, three-dimensional turbulent flow and temperature field are:

Momentum equations:

$$\rho U_j \frac{\partial U_i}{\partial x_j} = -\frac{\partial P}{\partial x_i} + \frac{\partial}{\partial x_j}\left(-\rho \overline{u_\iota u_j}\right) + g_i(\rho - \rho_\infty)$$ (2.18)

Temperature equation:

$$\rho U_j \frac{\partial T}{\partial x_j} = \frac{\partial}{\partial x_i}\left(-\rho \overline{u_\iota T'}\right)$$ (2.19)

The local density ρ here is considered a function of temperature as described in Bousinessq approximation. The terms $-\rho \overline{u_\iota u_j}$ and $-\rho \overline{u_\iota T'}$ are the turbulent stresses and the heat fluxes, respectively. The model assumes that the local state of turbulence is characterized by the turbulent kinetic energy k and by the rate of its dissipation ε, which are also referred to as the k-ε model in Figure 2.8.

The computational domain of the numerical model has the following boundaries conditions: inflow plane, outflow plane, three wind-tunnel walls at the top, the ground, a symmetry plane (only one half of the flow field is calculated), the surface wall of the cooling tower, and the circular exit plane of the tower. Particularly, the inflow plane located at the tower inlet with a uniform longitudinal velocity U and the uniform temperature T. This boundary condition treats the tower inlet as a constant source of energy providing upward air flow, avoiding the use of heat exchanger or radiator boundary. The benefit of this approximation is that the effect of cross wind on the tower inlet air flow is eliminated thus the calculation is simplified; however it sacrifices the veracity of the numerical model.

Duvenhage and Kröger [39] numerically investigated the effect of wind on fan performance and recirculation in a forced draught air-cooled cooling tower. A two-dimensional model, which included a horizontal heat exchanger arrangement and fans installed 3 meters under the heat exchangers, has been constructed. The heat exchanger bundles have a frontal area of 72.12 m^2 per bundle, with the thickness of 0.72 m.

The numerical model uses a body-fitted non-orthogonal coordinate system, and the mesh contains $28 \times 138 \times 98$ cells in the x-, y- and z-direction, respectively. The model is constructed with non-uniformly distributed mesh to obtain finer mesh around the heat exchanger and buoyant plume as

needed. The free atmospheric boundaries are placed far away from the heat exchanger so that the air flow is well developed ahead of it reaches the cooling tower as well as heat exchangers.

In this numerical model the pressure drop through the heat exchanger is modelled as a force applied on the air in the direction opposite to the air flow. The overall pressure drop through heat exchangers is the function of normal air flow velocity (Eq. (2.20)), which consists of two parts: the loss due to the finned tube bundles and the flow separating at the leading edge of the tube fins. The former is derived from the correlation for a six-row tube bundle with round finned tubes in a staggered tube layout proposed by Robinson-and-Briggs [40], while the latter follows from the correlation reported by Moore and Torrence [41].

$$\Delta p = \frac{1}{2}\rho_a V^2 (K_{he} + K_{i\theta}) = \frac{1}{2}\rho_a V^2 \left(928.837\{\frac{\rho_a V}{\mu_a}\}^{-0.316} + \{\frac{1}{sin\theta} - 1\}^2\right) \tag{2.20}$$

Where θ is the angle between the approach air flow direction and the heat exchanger bundles.

For the overall thermal characteristic parameter of heat exchanger, it is integrated into the numerical model by summing two parts, the air-side and the fluid-side heat transfer coefficient. The two coefficients form the overall heat transfer coefficient (Eq. (2.21)) which is also a function of the air mass flow rate. The air-side heat transfer coefficient is the function of the frontal velocity of the heat exchanger bundles according to the Briggs-and-Young correlation [42], while the fluid-side heat transfer coefficient, h_w, is assumed to be constant.

$$U = \frac{(\frac{v_{fr}^{0.681}}{108392.6053} + h_w/223.19)^{-1}}{36.06} \tag{2.21}$$

Two wind directions are taken into consideration: the cross wind and the wind that parallel to the vertical axis of heat exchanger. The cross-wind profile model [43] showed below (applied outside the cooling tower) is adopted:

$$v_{cw} = v_{cw_{ref}} (\frac{z}{z_{ref}})^b \tag{2.22}$$

This equation gives the distribution of atmospheric boundary layer. $v_{cw_{ref}}$ and z_{ref} are the reference values for wind velocity and altitude respectively. The exponent b was selected as 0.2 by the author.

In their study, the PHOENICS code was used to solve the discretised differential governing equations which can be expressed in the general form. The air was considered to be incompressible and its density was determined by the ideal gas law (Eq. (2.23)), while the buoyancy force of the air

was modelled by the Boussinesq model and was integrated in the body force term. The k-ε turbulent model was similar to the one presented by Bender *et al*. [10].

$$\rho = \frac{P}{RT} \tag{2.23}$$

Where R is the gas constant.

The temperature of inflow over the boundary is assumed to be constant, which equals to the ambient temperature. The zero gradient boundary conditions are set for the variables, U_x, U_y, U_z, k, ε and the pressure p at the atmospheric boundary and wall functions are used to treat near solid surfaces.

The investigation of wind influence on the heat exchanger performance is to evaluate the ratio of heat transferred with cross wind condition to that without cross wind:

$$\eta = \frac{Q_w}{Q_0} = \frac{T_{aow} - T_{aiw}}{T_{ao} - T_{ai}} \tag{2.24}$$

where T_{ao} is calculated with the overall heat transfer coefficient.

In Duvenhage and Kröger 's study [39], they found that when the cross wind velocity slightly increases, the heat transfer increases because of the weakening of plume recirculation compare to no crosswind condition. But as the speed of crosswind increases, the heat transfer effectiveness decreases due to strengthening of plume recirculation. The authors ascribed this phenomenon due to the factor that in windless conditions plume recirculation exists at both sides of the heat exchanger, and the low speed crosswind will prevent the formation of recirculation at one side of heat exchanger. The temperature distribution above the area of the heat exchanger at the reference speed of 3m/s is shown in Figure 2.15, which clearly indicates that some part of hot plume is draught back to the inlet of heat exchangers, causing degrading of heat transfer performance.
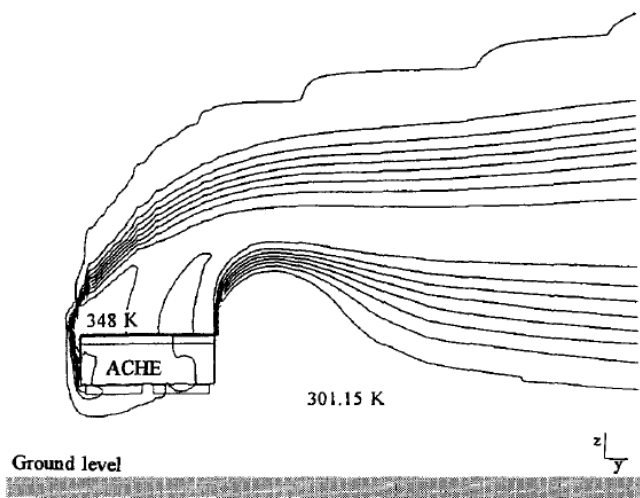
Figure 2.14. Temperature distribution for air flow at a longitudinal section of an ACHE bank in a longitudinal axis wind of 3.0 m/s. [39]

Al-Waked and Behnia [11, 14] numerically investigated the effect of cross-wind on the heat transfer performance of natural draft cooling towers with a commercial CFD code FLUENT. With the same method, an extended study on natural draft wet cooling tower and the effect of break wall on the improvement of thermal performance under windy conditions has been conducted by them later. In their studies, a three-dimensional CFD model was used for natural draft cooling tower with hyperbolic shape. The basic numerical simulation region is a cylindrical tower enclosed with a radius of 250m and a height of 260m enclosure.

Several assumptions have been adopted in order to simplify the model and calculation. The heat exchangers are arranged horizontally at cooling tower base covering the entire cross-section area of the inlet, and no A-frame arrangement is considered. All walls are adiabatic. The simulation was run in steady-state model. The air is essentially dry therefore was treated as an incompressible ideal gas. The external body force applied in momentum conservation equations included gravity and buoyancy force. The temperature throughout the numerical domain outside cooling tower is identical. The radiation heat transfer is negligible with respect to the overall heat transfer.

The governing equations for the single-phase incompressible turbulent flow used in their studies are similar to Eq. (2.12).

The CFD code used the finite-volume differencing scheme, the semi-implicit method for pressure-linked equations (SIMPLE) algorithm to calculate the pressure and velocity field. The computational domain contained 500, 000 unstructured mesh cells associated with second order upwind discretization scheme.

The flow and temperature field inside and outside the cooling tower without crosswind was investigated firstly. The air going through the cooling tower was driven by the natural convection. Throughout the inside cooling tower the velocity and temperature distributions are uniform.
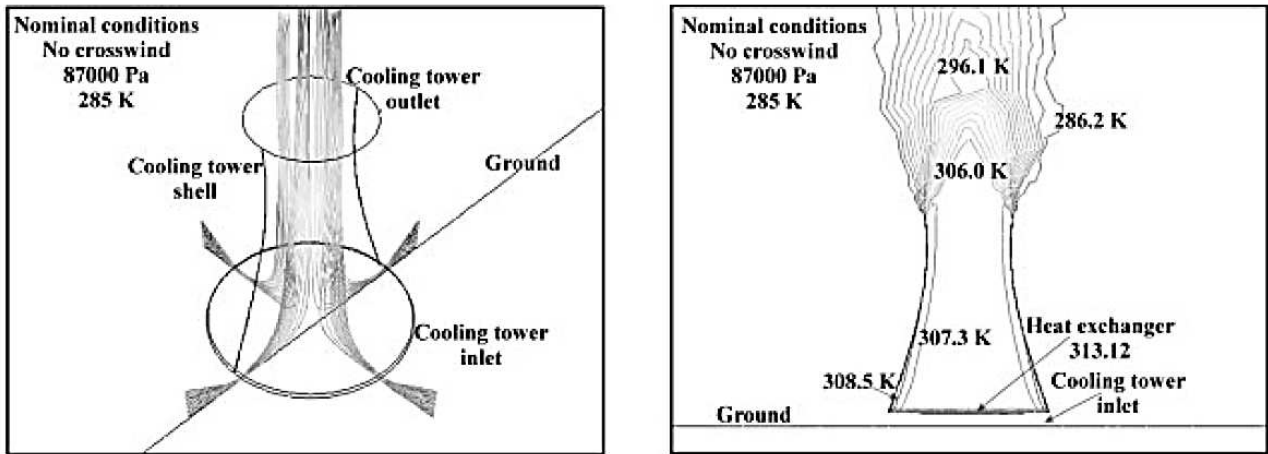
Figure 2.15. (a) The air flow path lines through the NDDCT and (b) temperature contours under no wind condition. [11]

The crosswind effect on the cooling performance of the NDDCT was investigated at different crosswind velocities [11]. The cross wind effect on the cooling performance was reflected by the change in Approach temperature $\Delta(T_{wo}-T_{ai})$. And the correlation between the approach temperature and crosswind velocity was obtained. This result was compared with the one obtained by Preez and Kröger [12], who had done both a series of tests and numerical analysis on an isothermal scale model of a circular natural draft dry-cooling tower, as shown in Figure 2.17.
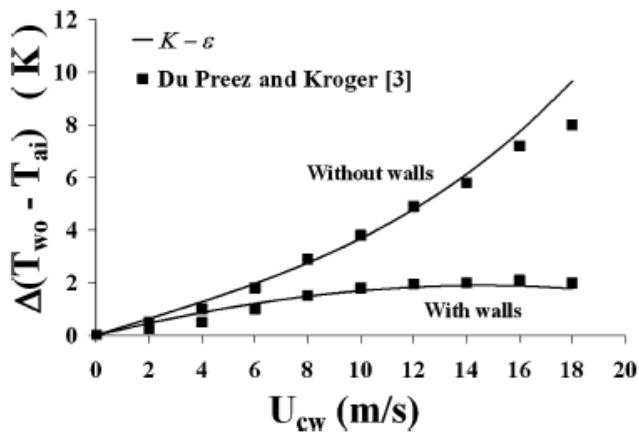
Figure 2.16. The change in Approach temperature at different cross wind speed with or without windbreak walls [11].

Both results are in good agreement and indicate that the increase of cross wind speed causes the increase of the Approach Temperature, which indicates that the outlet water temperature of the heat exchangers, T_{wo}, increases as the results of the increase of the crosswind velocity. It can be seen from the figure that the Approach Temperature increases nearly 4°C at crosswind speed of 10m/s, and increase about 8°C at the crosswind speed of 20m/s if no wind break walls are used. It can be

seen also from the figure, the windbreak walls are very effective on reducing the negative effect caused by crosswind.

Figure 2.17 illustrates the ambient air temperature around the NDDCT when the crosswind velocity is 5m/s. To compare with the case of no crosswind, a higher temperature occurs on the cooling tower windward side. As the air accelerates to the inlet of cooling tower, a lower static pressure zone below the heat exchangers occurs, causing the air temperature to increase on windward side.
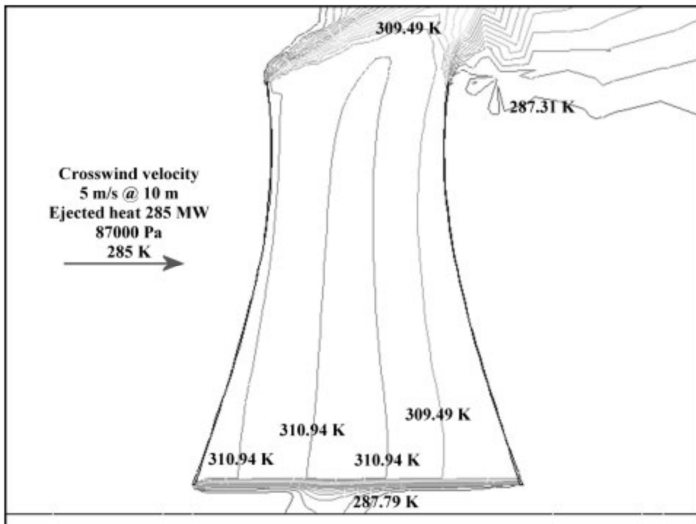
Figure 2.17. Air temperature inside and outside the NDDCT at a crosswind velocity of 5m/s. [11]

The air flow outside the cooling tower acts similar to the flow passing around a cylinder object. At the lateral side of cooling tower, air flow accelerates because of circumferential motion. As the result, the static pressure difference between outside and inside of tower decreases, causing a drop of intake air flow. The effect decreased when wind break wall was used at the peripheral of tower base.

2.3. Summary

Cooling towers are the important devices to dump the redundant heat from thermal power plants. Natural draft dry cooling towers (NDDCTs) feature no water loss and no parasitic power consumption during operation and thus are widely used. In a NDDCT, heat exchanger bundles are usually arranged either vertically around the circumference of the tower or horizontally in the inlet cross-section of the tower. Crosswind is a challenge for the cooling performance of NDDCTs. In the past decades, a variety of researches have been conducted on the crosswind effect on the cooling towers through field measurements, scaled model tests in laboratory or numerical simulations. These studies generally found that the heat dump capacity of is negatively affected by the crosswind.

Therefore, facilities that prevent the unfavourable crosswind effect are necessary in order to improve the cooling performance of the natural draft cooling towers under windy conditions.

Chapter 3 Analysis of NDDCTs for small renewable power plants

3.1. Introduction

The cooling system is an indispensable part in a thermal cycle of the steam turbine-based power generation, regardless of what heat source the power plant uses. The heat dump capacity of a cooling system directly affects the efficiency of the power conversion and consequently the rate of net electricity generation. In cooling systems, the heat is removed by either evaporation of hot water- wet cooling, or the air-cooled condensers or heat exchangers where hot working fluid is circulated in the closed loops- dry cooling. Cooling towers and/or mechanical fans are always used to accelerate the heat dissipation. The choice of different types of cooling for a given power plant depends mainly on the environmental condition under which the plant is built.

The natural draft dry cooling tower (NDDCT) with the surface heater exchangers is particularly favourable for the geothermal power plants and concentrated solar thermal (CST) power plants which are more likely located in arid regions, as no water and extra energy consumed during its operation. In this chapter the 1D mathematical model for cooling performance estimation of the NNDCT is analysed first. And then the model is used to design a NDDCT for small power plants and predict its cooling capability under normal conditions. A case study on the conventional NDDCT equipped with the inlet air pre-cooling facilities is conducted finally.

3.2. The analytical 1D model on the performance of NDDCT

The working principle of a typical natural draft dry cooling tower with surface heat exchangers can be summarized as simple as "buoyancy effect". Figure 3.1 shows the distribution of air temperatures in a typical model of NDDCTs equipped with horizontal heat exchangers that cover the whole cross-section area on top of the tower base. Six positions along with the streamline of air flow are numbered in the same way as that in [3].
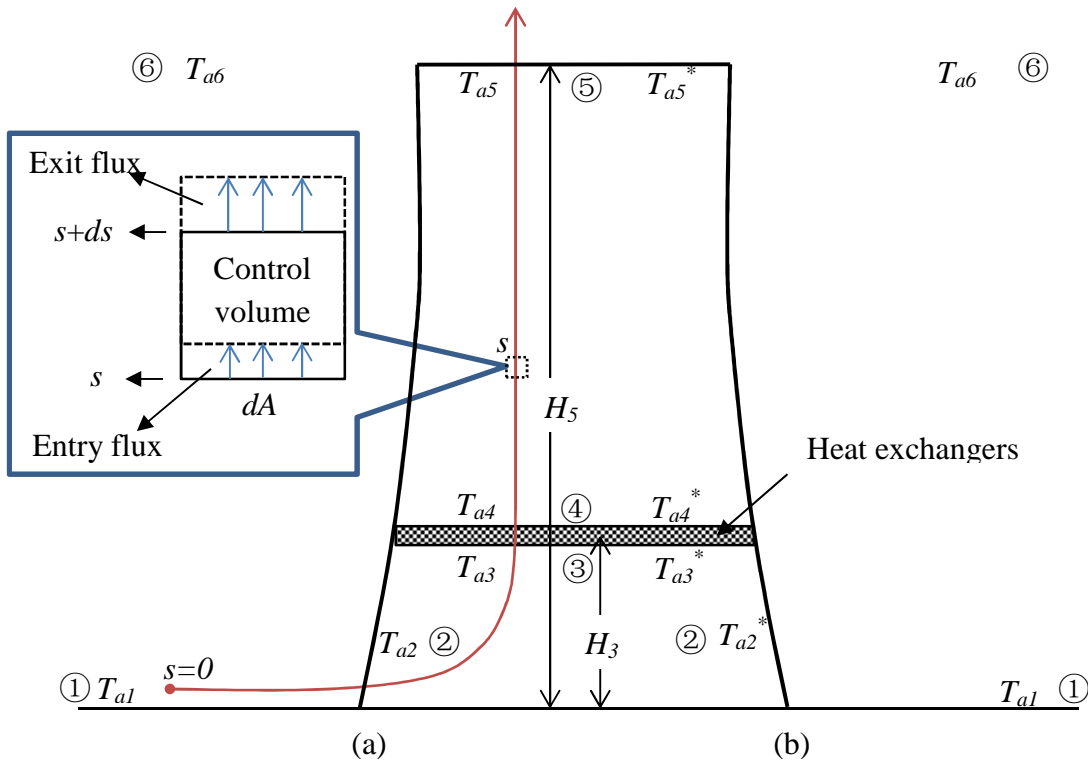
Figure 3.1. The temperature variations in a NDDCT with horizontal heat exchangers

3.2.1 Conventional NDDCT

The air initially located between position 3 and 4 is heated by heat exchangers. Hot air is less dense so that it moves upward driven by the net buoyancy force. Cool air underneath position 3 is sucked in to replace it, so a continuous air flow forms in the cooling tower. The air flow is approximately a steady-state, one dimensional flow. Therefore if B denotes any physical quantity in the air flow, B is the function of only coordinate s, i.e. $B = B(s)$, where the coordinate axis is along with the streamline, and $s = 0$ is located where the air is still stagnant.

In the analysis of air dynamics and thermal properties in the cooling tower, B particularly represents the energy E, namely i.e. $E = E(s)$. By choosing an arbitrary elemental fixed control volume of air in any streamline of air flow as a closed system, the system has only one entry and exit energy flux. The Reynolds transport theorem is thus applied that change of total energy of the system ΔE equals to the entry energy flux minus the exit one. Meanwhile, according to the first law of thermodynamics, ΔE equals to the total heat added into it W_Q minus the work done by external force on this system W_M. The equation then can be expressed in the form of the differential for t [44]:

Chapter 3

$$\frac{dE(s)}{dt} = \frac{dW_M}{dt} + \frac{dW_Q}{dt} =$$

$$-\frac{dm_{in}}{dt}[\hat{h}(s) + \frac{\alpha v(s)^2}{2} + gz(s)] + \frac{dm_{out}}{dt}[\hat{h}(s+ds) + \frac{av(s+ds)^2}{2} + gz(s+ds)]$$

(3.1)

where W_Q and W_M are the total heat added in and the external mechanical work done onto the system, respectively. The summation $\hat{h} + v^2/2 + gz$ in right side of the equation comprises E, where $\hat{h}$ is the enthalpy of the air. z is the elevation above ground. m_{in} and m_{out} are the mass entering and exiting the control volume respectively. And $m_{in} = m_{out} = m_a$, where m_a is the mass of air, as mass is always conserved. The velocity distribution factor $a \approx 1$ for turbulence flow. The control volume located at an arbitrary s has height and bottom area of ds and dA, respectively.

The total mechanical work consists of two parts:

$$W_M = W_b - W_{loss}$$

(3.2)

Where W_b accounts for the work done by buoyancy force, which is essentially the difference of external pressures between the entry and exit face of the control volume. But it excludes the pressure caused expansion/contraction work as this part is already included by enthalpy h. Thus W_b done within period dt is expressed as:

$$dW_b = P(s)v(s) \cdot dAdt - P(s+ds)v(s+ds) \cdot dAdt$$

(3.3)

It is followed by its differential form expressed as:

$$dW_b = [\frac{P(s)}{\rho(s)} - \frac{P(s+ds)}{\rho(s+ds)}]dm_a$$

(3.4)

Where P and ρ are pressure and density, respectively.

The total "loss" work W_{loss} counted in Eq. (3.2) includes the negative work done by drag, friction, expansion/contraction and redirection in ds. Its differential form is expressed by:

$$dW_{loss} = \Delta P_{lossds} \cdot \bar{v} \cdot dAdt = \frac{1}{2}\sum K_{lossds}\overline{\rho v}^3 \cdot dAdt = \frac{1}{2}\sum K_{lossds}\bar{v}^2 dm_a$$

(3.5)

Where the summation $\sum K_{lossds}$ represents the total loss coefficient within the control volume. The terms $\bar{\rho}$ and $\bar{v}$ are the mean density and velocity in the control volume, respectively. dA is the cross-section area of the control volume.

The heat transferred W_Q is equal to the change of the enthalpy of the control volume system:

$$\frac{dW_Q}{dt} = \dot{Q} = \dot{m}_a[\hat{h}(s+ds) - \hat{h}(s)] \tag{3.6}$$

where $\dot{Q}$ is the heat transfer rate.

Substitute Eq. (3.4) and Eq. (3.5) into Eq. (3.1), yielding the following equation using the dot notation to denote the derivatives with respect to time t:

$$\frac{\dot{Q}}{\dot{m}_a} + [\frac{P(s)}{\rho(s)} - \frac{P(s+ds)}{\rho(s+ds)}] - \frac{1}{2}\sum K_{lossds}\overline{v}^2 =$$
$$[\hat{h}(s+ds) + \frac{v(s+ds)^2}{2} + gz(s+ds)] - [\hat{h}(s) + \frac{v(s)^2}{2} + gz(s)] \tag{3.7}$$

Eq. (3.7) is independent of dA, which means this is a general expression of the energy conservation used for any cross-section of the air flow in a NDDCT. The air moving along the stream path from position 1 to 5 actually experiences three changing processes: the isentropic process from 1 to 3, the process with nearly unchanged absolute air pressure from 3 to 4, and the isentropic process again from 4 to 5.

In first and third processes, no heat added in to the system. According to Eq. (3.6), the heat related terms can be extracted from Eq. (3.7) if ignore the heat exchanged with surrounding air. Therefore, integrate Eq. (3.7) for ds along the coordinate axis position 1 to 3 and position 4 to 5, respectively, yielding followings:

$$\dot{Q} = \hat{h}_1 - \hat{h}_3 = 0 \tag{3.8a}$$

$$(P_1 + \frac{\rho_1 v_1^2}{2} + g\rho_1 z_1) - (P_3 + \frac{\rho_3 v_3^2}{2} + g\rho_3 z_3) \cong \frac{1}{2}\sum K_{loss13}\overline{\rho v}_{13}^2 \tag{3.8b}$$

and

$$\dot{Q} = \hat{h}_4 - \hat{h}_5 = 0 \tag{3.9a}$$

$$(P_4 + \frac{\rho_4 v_4^2}{2} + g\rho_4 z_4) - (P_5 + \frac{\rho_5 v_5^2}{2} + g\rho_5 z_5) \cong \frac{1}{2}\sum K_{loss45}\overline{\rho v}_{45}^2 \tag{3.9b}$$

On the other hand, in the second process heat transferred from water to the air. Since the elevation difference between position 3 and 4 is very small, i.e. $z_3 \approx z_4$, this stage can be considered the isobaric process. Thus Eq. (3.7) is integrated from 3 to 4 and flowed by:

$$\dot{Q} = \hat{h}_4 - \hat{h}_3 = \dot{m}_a c_{pa}(T_{a4} - T_{a3}) \tag{3.10a}$$

$$(P_3 + \frac{\rho_3 v_3^2}{2}) - (P_4 + \frac{\rho_4 v_4^2}{2}) \cong \frac{1}{2} \sum K_{loss34} \overline{\rho v}_{34}^2 \tag{3.10b}$$

By combining Eqs. (3.8b), (3.9b), and (3.10b), and re-expressing all the pressure loss coefficient K_{loss13}, K_{loss34} and K_{loss45} in right sides of equations referring to the heat exchangers frontal area A_{fr}, one gets:

$$(P_1 - P_5) + (\frac{1}{2}\rho_1 v_1^2 - \frac{1}{2}\rho_5 v_5^2) + g(\rho_1 z_1 - \rho_3 z_3) + g(\rho_4 z_4 - \rho_5 z_5) = \frac{1}{2} \sum K_{losshx} \overline{\rho}_{34} \overline{v}_{34}^2 \tag{3.11}$$

And from Eqs. (3.8a), (3.9a), and (3.10a), the total heat transfer rate in all the processes between position 1 and 5 can be combined as $\Sigma \dot{Q}$. According to the heat transfer principle of the surface heat exchangers $\Sigma \dot{Q}$ can be expressed by following equation:

$$\Sigma \dot{Q} = \dot{m}_a c_{pa}(T_{a4} - T_{a3}) = \dot{m}_w c_{pw}(T_{wi} - T_{wo}) = UA_a \frac{(T_{wo} - T_{a3}) - (T_{wi} - T_{a4})}{\ln[(T_{wo} - T_{a3})/(T_{wi} - T_{a4})]} F_T \tag{3.12}$$

where T_a, T_{wi} and T_{wo} are air, inlet water and outlet water temperatures respectively. The numbers in subscripts represent the positions. U and A_a are the total heat transfer coefficient and air side area of the heat exchangers, respectively. $\overline{\rho}_{34}$ and $\overline{v}_{34}$ are the mean density and velocity between positions 3 and 4. F_T is the temperature correction factor. The last three terms in Eq. (3.12) state that the heat transferred into the air is equal to the heat extracted from the cooling water or the heat transferred through the heat exchangers.

It has been found pressure at position 5 P_5 in Eq. (3.11) is slightly smaller than that of the ambient air at same height far away from the cooling tower outlet—position 6, resulting in Eq. (3.13) [4] where the K_{to} is the loss coefficient in tower outlet:

$$P_5 = P_6 - \frac{1}{2} K_{to} \rho_5 v_5^2 \tag{3.13}$$

where K_{to} is the pressure loss coefficient at tower outlet.

As position 1 is a stagnation point, $v_1 = 0$. The following approximations can be made: $\rho_1 \approx \rho_3$, $\rho_5 \approx \rho_4$, $P_1 - P_6 \approx \rho_1 g(z_6 - z_1) = \rho_1 g H_5$, and $z_3 \approx z_4 = H_3$, where H_3 and H_5 are the tower inlet height and tower height, respectively. Eq. (3.11) then can be simplified and rearranged as:

$$(\rho_3 - \rho_4)g(H_5 - H_3) \approx \frac{1}{2} \sum K_{losshx} \overline{\rho}_{34} \overline{v}_{34}^2 + \frac{(1 - K_{to})\rho_5 v_5^2}{2} \tag{3.14}$$

Eq. (3.14) is well known as the draft equation of natural draft dry cooling towers [45], which states that the draft provided by the tower is balanced by the total pressure loss the airflow experiences. In practices, ρ_3 often refers to the ambient air density outside the cooling tower at the same height H_3, though there is a tiny difference between the exterior and interior of the tower. The summation of all the loss coefficient K_{losshx} in right hand side consists of the losses due to the heat exchanger bundles, flow contraction and expansion, tower support and shell, *etc.* and the subscript *hx* means the quantity is recalculated based on heat exchanger frontal area, and the heat exchanger loss accounts for largest part of the total loss [3].

Eq. (3.14) has a more precise version if one considers the fact that the actual pressure or density in Eq. (3.11) is not linear to the elevation but is given by:

$$\frac{dP_z}{dz} = -\rho_z g \tag{3.15}$$

where P_z and ρ_z are all functions of z.

For an isentropic process of the idea gas, it has:

$$P_z / \rho_z{}^{\psi} = C \text{ and } P_z = \rho_z R T_z \tag{3.16}$$

where $\psi = c_p / c_v$. The dry adiabatic lapse rate is expressed as:

$$T_z = T_1 - \frac{g(\psi - 1)z}{\psi R} \tag{3.17}$$

Combine Eqs. (3.15), (3.16), and (3.17) and integrate, the pressure at any elevation z can be expressed by:

$$P_z = P_1 [1 - \frac{g(\psi - 1)z}{\psi R T_1}]^{\psi/(\psi-1)} \tag{3.18}$$

Therefore it is obviously to get the following expressions by applying Eq. (3.18):

$$P_4 - P_5 = P_4 \{ 1 - [1 - \frac{g(\psi - 1)(H_5 - H_4)}{\psi R T_4}]^{\psi/(\psi-1)} \} \tag{3.19a}$$

$$P_1 - P_6 = P_1 \{ 1 - [1 - \frac{g(\psi - 1)H_5}{\psi R T_1}]^{\psi/(\psi-1)} \} \tag{3.19b}$$

Based on this correlations, D.G Kröger [3] had derived a more practical draft equation which has been widely used in the design works of NDDCT:

$$P_1 \left[\left\{ 1 - \frac{0.00975(H_3 + H_4)}{2T_{a1}} \right\}^{3.5} \cdot \left\{ 1 - \frac{0.00975(2H_5 - H_3 - H_4)}{2T_{a4}} \right\}^{3.5} - \left(1 - \frac{0.00975H_5}{T_{a1}} \right)^{3.5} \right]$$

$$= \sum K_{losshx} \frac{m_a^2}{2\rho_{34}A_{fr}^2} \cdot \left[1 - \frac{0.00975(2H_5 - H_3 - H_4)}{2T_{a4}} \right]^{3.5} + (1 - K_{to}) \frac{m_a^2}{2\rho_5 A_5^2} \qquad (3.20)$$

where A_{fr} is the frontal area of heat exchanger bundles. Eqs. (3.12) and (3.14) are the fundamentals in the designs of natural draft dry cooling towers. These two equations are usually solved through numerical iterations.

3.2.2 NDDCT with inlet air pre-cooling

For power plants built in arid regions, evaporative cooling of the inlet air has been proposed to cool inlet air so as to be able to maintain the power plant performance on even very hot days [16, 17, 46]. In this section, the precooling equations will be incorporated with the natural draft dry cooling tower governing equations introduced in the preceding section. The existence of evaporative cooling prior to the tower inlet will significantly reduce the air temperature underneath the heat exchanger and may also result in lower temperatures above the heat exchangers compared to the application without inlet precooling. The cooling tower equations need to be examined under these conditions to make sure that the advantages of cooler inlet air are not cancelled by reduced buoyancy due to the smaller difference between the tower interior and exterior temperatures.
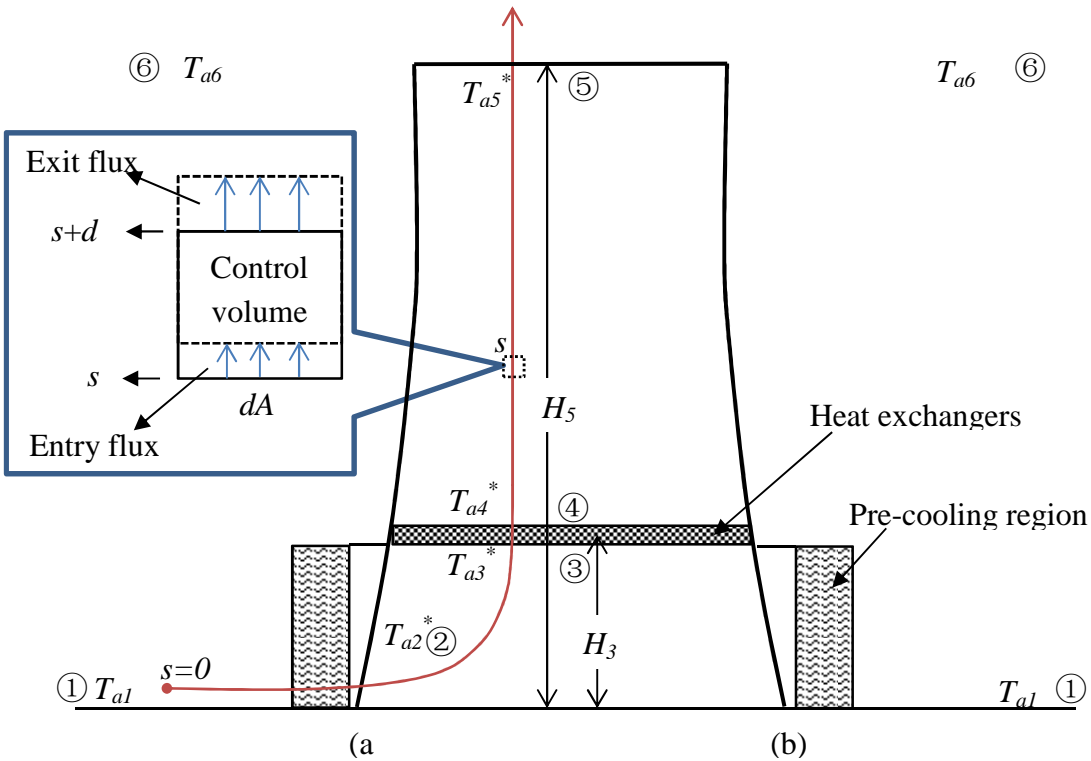
Figure 3.2. NDDCT with pre-cooling

Referring to Figure 3.2, if the control volume is selected in the pre-cooling region, it has

$\dot{m}_{in} = \dot{m}_a^* + \dot{m}_v = \dot{m}_{out}$. Where $\dot{m}_v$ is the mass flow rate of water vapour, and the superscript *

indicates the quantity has changed because of inlet pre-cooling. The energy is still conserved so that

Eq. (3.7) is still valid. By re-integrating both sides of this equation for ds in domain (1, 5), it follows:

$$\dot{Q}^* = \dot{m}_a^* c_{pa}(T_{a4}^* - T_{a3}^*) - \dot{m}_v \ell \tag{3.21a}$$

$$(P_1 - P_5^*) + (\frac{1}{2}\rho_1 v_1^{\,2} - \frac{1}{2}\rho_5^* v_5^{*2}) + g(\rho_1 z_1 - \rho_3^* z_3) + g(\rho_4^* z_4 - \rho_5^* z_5) = \frac{1}{2}\sum K_{losshx}^* \overline{\rho}_{34}^* \overline{v}_{34}^{*\,2} \tag{3.21b}$$

where ℓ is the latent heat of water. The pressure loss within the pre-cooling region is assumed to be

very small so that the total pressure drop remains nearly unchanged, i.e. $\sum K_{losshx}^* \approx \sum K_{losshx}$. The

aforementioned approximations are still valid with $\rho_5^* \approx \rho_4^*$, $P_1 - P_6 \approx \rho_1 g(z_6 - z_1) = \rho_1 g H_5$, and

$z_3 \approx z_4 = H_3$, however $\rho_1 \approx \rho_3 < \rho_3^*$. Substituting the updated Eq. (3.13) into Eq. (3.21b) yields:

$$(\rho_3 - \rho_4^*)g(H_5 - H_3) + (\rho_3 - \rho_3^*)gH_3 \approx \frac{1}{2}\sum K_{losshx}\overline{\rho}_{34}^* \overline{v}_{34}^{*\,2} + \frac{(1 - K_{to})\rho_5^* v_5^{*2}}{2} \tag{3.22}$$

Where ρ_3 is the ambient air density which is the same one as used in Eq. (3.14).

Eq. (3.19) is the draft equation for an NDDCT with inlet air pre-cooling. It has the same terms as Eq.

(3.14) except that an addition term $(\rho_3 - \rho_3^*)gH_3$ with negative value occurs on left side of the

equation. The physical meaning of this new term is that the cooled air between the pre-cooling

region and the heat exchangers causes a negative buoyancy force to the air flow. This force

decreases the total draft of the cooling tower. On the other hand, the balance in heat transfer in heat

exchangers is still valid, so that:

$$\dot{m}_a^* c_{pa}(T_{a4}^* - T_{a3}^*) = \dot{m}_w c_{pw}(T_{wi} - T_{wo}^*) = UA_a \frac{(T_{wo} - T_{a3}^*) - (T_{wi} - T_{a4}^*)}{\ln[(T_{wo} - T_{a3}^*)/(T_{wi} - T_{a4}^*)]} \tag{3.23}$$

The density ρ_3^* in Eq. (3.22) can be calculated treating the humid air as an ideal gas,

$$\rho_3^* = \frac{P_3^*}{R^* T_{a3}^*} \approx \frac{P_3}{R^* T_{a3}^*} \tag{3.24}$$

Eq. (3.24) applies a basic assumption in this calculation that the pressure loss in the pre-cooling

region is negligible. Since the air flow between position 2 and 3 is in an isentropic process, T_{a3}^* can

be calculated by T_{a2}^{*}, the dry-bulb temperature of the moist air just exiting the pre-cooling region, using the following correlation [3]:

$$T_{a3}^{*} = T_{a2}^{*} - 0.00975\, H_3 \tag{3.25}$$

The cooled moist air is not necessarily saturated, so T_{a2}^{*} might be any value between the dry bulb temperature T_{a1} and the wet-bulb temperature T_{wb} of the ambient air, depending on the humidity of the air. To determine the T_{a2}^{*}, another assumption is made that any property change in the pre-cooling region is an adiabatic process. Figure 3.3 illustrates the path of determination of T_{a2}^{*} in the psychrometric chart. This path is equivalent to the calculations below.
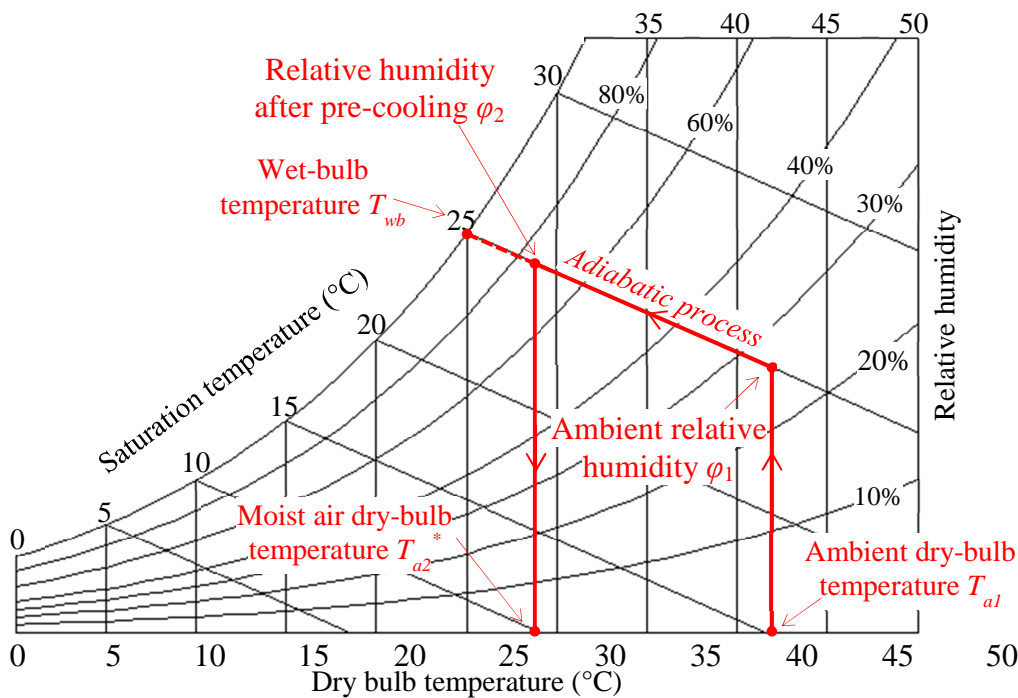
Figure 3.3. The path of determination of T_{a2}^{*} in the psychrometric chart

The ambient air with initially relative humidity φ_1 keeps the constant dry-bulb temperature at T_{a1}. The humidity ratio χ at any position can be obtained through Eq. (3.26):

$$\chi = \left. \frac{P_v}{P - P_v} \right|_{Ta} \tag{3.26}$$

where P is the total pressure of the moist air, and P_v is the partial pressure of water vapour and can be defined by:

$$P_v = \left. \varphi \cdot P_{vs} \right|_{T,P} \tag{3.27}$$

where P_{vs}, the water vapour saturation pressure is the function of only the dry-bulb temperature T_a, i.e. $P_{vs} = P_{vs}(T_a)$.

Here, all the variables in Eqs. (3.26) and (3.27) refer to the quantities in position 1, namely χ_1, P_{v1}, P_{vs1}, φ_1, P_1 and T_{a1}.

With a known χ_1, the thermodynamics wet-bulb temperature T_{wb} of ambient air at pressure P_1 can be calculated using the correlation showed in Eq. (3.25) [47].

$$\chi = \frac{[2501 - 2.326(T_{wb} - 273.15)]\chi_{swb} - 1.006(T_a - T_{wb})}{2501 + 1.86(T_a - 273.15) - 4.186(T_{wb} - 273.15)} \tag{3.28}$$

where χ_{swb} refers to the saturation humidity ratio at wet-bulb temperature, which is a function of only T_{wb} at a fixed pressure.

Assuming an adiabatic process, the wet-bulb temperature, T_{wb}, remains constant in the pre-cooling region, although the dry-bulb temperature changes. In position 2, after the water droplets are fully evaporated, the relative humidity of the air flow increases and is known as φ_2. But the humidity ratio χ_2, water vapour pressure P_{v2}, and dry-bulb temperature T_{a2}^* in this position need to be solved. By rearranging Eq. (3.27) and combining Eqs. (3.13) and (3.28) to eliminate one unknown χ_2, a set of equations with only two unknowns T_{a2}^* and P_{v2} is obtained:

$$\begin{cases} \varphi_2 = \dfrac{P_{v2}}{P_{vs2}(T_{a2}^*)} \\[3mm] \dfrac{P_{v2}}{P_2^* - P_{v2}} = \dfrac{(3136.3469 - 2.326T_{wb})\chi_{swb} - 1.006(T_{a2}^* - T_{wb})}{3136.3469 + 1.86T_{a2}^* - 4.186T_{wb}} \end{cases} \tag{3.29}$$

where the first equation is directly the definition of relative humidity φ [47]. And $P_2^* \approx P_2 \approx P_1$.

The solutions of this equation set include the desired T_{a2}^*, therefore T_{a3}^* is obtained. Meanwhile, using the new quantities after pre-cooling region to replace the original ones in Eq. (3.17), one can get:

$$P_1\left[\left\{1 - \frac{0.00975(H_3 + H_4)}{2T_{a1}}\right\}^{3.5} \cdot \left\{1 - \frac{0.00975(2H_5 - H_3 - H_4)}{2T_{a4}^*}\right\}^{3.5} - \left(1 - \frac{0.00975H_5}{T_{a1}}\right)^{3.5}\right]$$

$$= \sum K_{losshx} \frac{m_a^{*2}}{2\rho_{34}^* A_{fr}^2} \cdot \left[1 - \frac{0.00975(2H_5 - H_3 - H_4)}{2T_{a4}^*}\right]^{3.5} + (1 - K_{to})\frac{m_a^{*2}}{2\rho_5^* A_5^2} \tag{3.30}$$

Eqs. (3.23) and (3.30) are the key equations to estimate the cooling tower performance in presence of inlet air pre-cooling treatment. The computation of the two equations follows the similar way as that used in Eqs. (3.12) and (3.14).

3.3. Tower size design for small renewable power plants

Mathematically, there exists a range of geometry sizes for NDDCT which can achieve both the draft-pressure loss and the thermal balances, namely the establishment of Eqs. (3.12) and (3.14). Therefore for a desired cooling capacity (or heat rejection rate Q) , one can always find a smallest tower size, provided that the design conditions is specified including water inlet temperature and ambient air temperature at a fixed Initial Temperature Difference (ITD). During the design process, an iteration procedure is applied to calculate the smallest NDDCT size under given conditions and theoretically predict its thermal performance. The procedure starts with the two balances.

3.3.1. The thermal balancing

Eq. (3.12) states that in a cooling tower operation, the total heat transferred into the cooling air is equal to the heat extracted from the cooling water through the heat exchangers. The overall heat transfer coefficient h_u of heat exchangers based on air side area A_a is a function of air side heat transfer coefficient h_a and water side coefficient h_w and tube wall conductivity k:

$$h_u = \frac{1}{A_a/(A_w h_a) + A_a \ln(r_o/r_i)/(2\pi kL) + 1/(h_w)}$$
(3.31)

The heat transfer rate through the heat exchanger surface is calculated using the logarithm mean temperature difference LMTD, namely the term $\frac{(T_{wo} - T_{a3}) - (T_{wi} - T_{a4})}{\ln[(T_{wo} - T_{a3})/(T_{wi} - T_{a4})]}$, with the LMTD correction factor F_T which is defined as [3]:

$$F_T = 1 - \sum_{i=1}^{4}\sum_{k=1}^{4} a_{i,k} (1 - \varphi_{cf})^k \sin\left(2i \arctan\frac{\varphi_h}{\varphi_c}\right)$$
(3.32)

where $\varphi_h = \frac{T_{wi} - T_{wo}}{T_{wi} - T_{a3}}$, $\varphi_c = \frac{T_{a4} - T_{a3}}{T_{wi} - T_{a3}}$, $\varphi_{cf} = \frac{\varphi_h - \varphi_c}{\ln[(1 - \varphi_c)/(1 - \varphi_h)]}$. $a_{i,k}$ are the sixteen values of the empirical constant which depends on the heat exchanger tube configurations [3].

The air side and water side heat transfer coefficients have complex correlations with the Reynolds number for air and water, respectively. These correlations are highly dependent on the geometric characteristics of the heat exchangers. Therefore, it is not possible to size a natural draft dry cooling tower without selecting a particular heat exchanger configuration.

In this chapter, a typical layout of heat exchanger bundles is used for the size selection of heat exchangers and NDDCT: cross-flow, 4-rows, 2-passes, air-cooling heat exchangers with extruded bi-metallic finned tubes (as shown in Figure 3.4). This is representative of heat exchangers used in industrial installations but does not correspond to a specific brand. The heat exchanger bundles are arranged horizontally in A-frame to cover around 75% of the base area of cooling tower with the rest of 25% are sealed/blocked. The details of the selected heat exchangers can be found in reference [3] and reproduced in Tables 3.1 to 3.2.

Aluminiu m ASTM

Mild steel ASTM A214

(a)

(b)
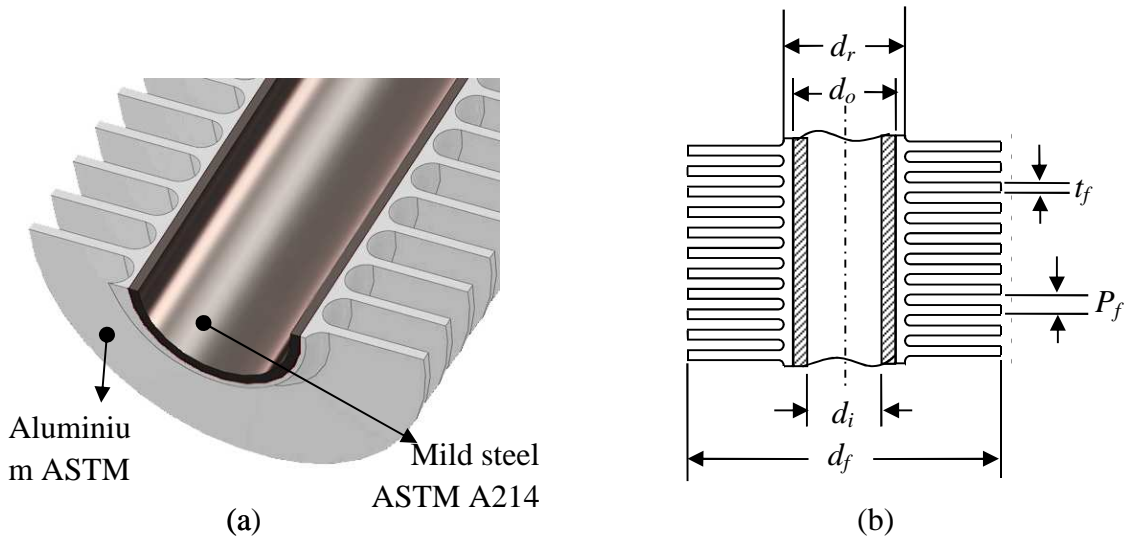
Figure 3.4. The extruded bi-metallic finned tube (a); the geometry parameters of finned tube (b)

Table 3.1 Finned tube specifications

parameters	dimensions
Hydraulic diameter (inside) of tube	d_i=9 mm
Outside diameter of tube	d_o=0.0254
Relative surface roughness:	ε/d_i=5.24 X 10-4
Thermal conductivity of tube (ASTM A214 mild steel)	k_t=50 w/mk
Full Length of finned tube	L_t=5.0 m
Effective Length of finned tube	L_{te}= 4.7 m
Mean thermal contact resistance	R_c=4*10^{-5} m^2k/w
Fin diameter	d_f=57.2 mm
Fin root diameter	d_r=27.6 mm

Fin cross-section shape	Isosceles trapezium
Thickness of fin (mean)	$t_f = 0.5$ mm
-Thickness of fin tip	$t_{ft} = 0.25$ mm
-Thickness of fin root	$t_{fr} = 0.75$ mm
Fin pitch	p_f=2.80 mm
Thermal conductivity of fin (ASTM 6063 Aluminium)	k_t=204 w/mk

Table 3.2 Heat exchanger bundles specifications

parameters	dimensions
Number of tube rows per bundle	N_r=4
Number of bundles	N_b to be determined
Number of effective tubes per bundle	N_{tb}=154
-Number of actual tubes per row	N_{tra}=39
Number of water passes	N_{wp}=2
Transversal tube pitch	P_t=58 mm
Longitudinal tube pitch	P_l=50.22 mm
Apex angle of A-frame	2θ=61.5°
Inlet contraction loss coefficient	K_{ci}=0.05

The air side and water side heat transfer coefficients are therefore calculated by the following empirical equations [3]:

$$h_a = 383.6173 k Pr^{0.333} \left(\frac{\dot{m}_a}{\mu A_{fr}}\right)^{0.5237} \left(\frac{A_{fr}}{A_a}\right) \tag{3.33}$$

$$h_w = \frac{(f_d/8)\,(\text{Re}-1000)\,\text{Pr}\left[1+(d/L)^{0.67}\right]k}{\left[1+12.7\,(f_d/8)^{0.5}\,(\text{Pr}^{0.67}-1)\right]d_e} \tag{3.34}$$

3.3.2. Pressure loss balancing

The draft equation Eq. (3.14) establishes the equality between the draft pressure provided by the tower (left hand side) and the total pressure drop the airflow experiences (right hand side). The total pressure loss coefficient $\sum K_{losshx}$ in Eq. (3.14) in a NDDCT mainly consists of the losses caused by tower supports (K_{ts}), tower inlet (K_{ct}), air contraction in front of heat exchanger (K_{ctc}), air diffusion after heat exchanger (K_{cte}) and the main part heat exchanger (K_{he}), namely [4]:

$$\sum K_{losshx} = (K_{ts} + K_{ct} + K_{ctc} + K_{he} + K_{cte})_{hx} \tag{3.35}$$

where the subscript hx represents that all loss coefficients are referred to the heat exchanger frontal area [3]. All the pressure loss coefficients in right hand of Eq. (3.35) are calculated by the following correlations [3, 4]:

$$K_{ts} = \frac{C_{Dts}L_{ts}d_{ts}n_{ts}A_{fr}^2}{(\pi d_3 H_3)^3}\left(\frac{\rho_{a34}}{\rho_{a1}}\right) \tag{3.36}$$

$$K_{ct} = \left[0.072(d_3/H_3)^2 - 0.34(d_3/H_3) + 1.7\right]\frac{\rho_{a34}}{\rho_{a3}}\left(\frac{A_{fr}}{A_3}\right)^2 \tag{3.37}$$

$$K_{ctc} = (1 - 2/\sigma_c + 1/\sigma_c^2)\frac{\rho_{a34}}{\rho_{a3}}\left(\frac{A_{fr}}{A_{e3}}\right)^2 \tag{3.38}$$

$$K_{cte} = (1 - A_{e3}/A_3)\frac{\rho_{a34}}{\rho_{a4}}\left(\frac{A_{fr}}{A_{e3}}\right)^2 \tag{3.39}$$

where the drag coefficient of tower support $C_{Dts}=2.0$; L_{ts} and d_{ts} are the tower support length and diameter, respectively; N_{ts} is the number of tower support. σ_c is the contraction ratio of heat exchanger bundles. A_{e3} is the total projection area of the heat exchanger bundles.

For this particular type of heat exchanger bundle, the pressure loss coefficient is a function of normal air velocity, which is expressed as [3]:

$$K_{hx} = 1383.9475(\frac{\overline{\rho_a v_a}}{\mu})^{-0.332458} \tag{3.40}$$

The tower outlet pressure loss coefficient K_{to} in Eqs. (3.14) and (3.20) is calculated by [3]

$$K_{to} = -0.28Fr_D^{-1} + 0.04Fr_D^{-1.5} \tag{3.41}$$

where Fr_D is the densimetric Froude number based on tower outlet diameter, and

$Fr_D = (m_a / A_5)^2 / \left[\rho_{a5}(\rho_{a6} - \rho_{a5}) g d_5 \right]$ is valid for $0.5 \leq d_5 / d_3 \leq 0.85$.

3.3.3. Iteration strategy

In the design process, the thermal balance equation Eq. (3.12) as well as draft equation Eq. (3.14) must be satisfied simultaneously. Since these equations are also coupled, the solution must follow an iterative procedure.

Some basic assumptions are necessary for the iteration process. The ratio of the heat exchanger bundles project area to the entire tower base area is assumed constant, and the ratio of tower inlet height to base diameter is also fixed. This indicates the total heat exchanger bundles change proportionally with the change of cooling tower size.

The computation process consists of three levels of loops. The outer and middle loop levels are the determination of dimension parameters of heat exchangers and cooling tower. Theoretically the total heat dumped is approximately proportional to the air mass flow rate m_a, whereas m_a is again proportional to the tower height H_5 and heat exchanger area A_{fr}. Therefore H_5 and A_{fr}, as two key variables in outer loop, have been iterated throughout all their feasible values to get all the solutions to be compared.

The key iterative variables in the inner loop are air-side and water-side outlet temperatures, T_{a4} and T_{wo}. Based on them, the mean values of air and water properties are obtained, followed by the air mass flow rate m_a and the three separated heat transfer rates in Eq. (3.12). By comparing the differences of these heat transfer rates, a decision on ending the inner loop can be made. The whole computation process is briefly illustrated in Figure 3.5, upon which the computation codes are based.
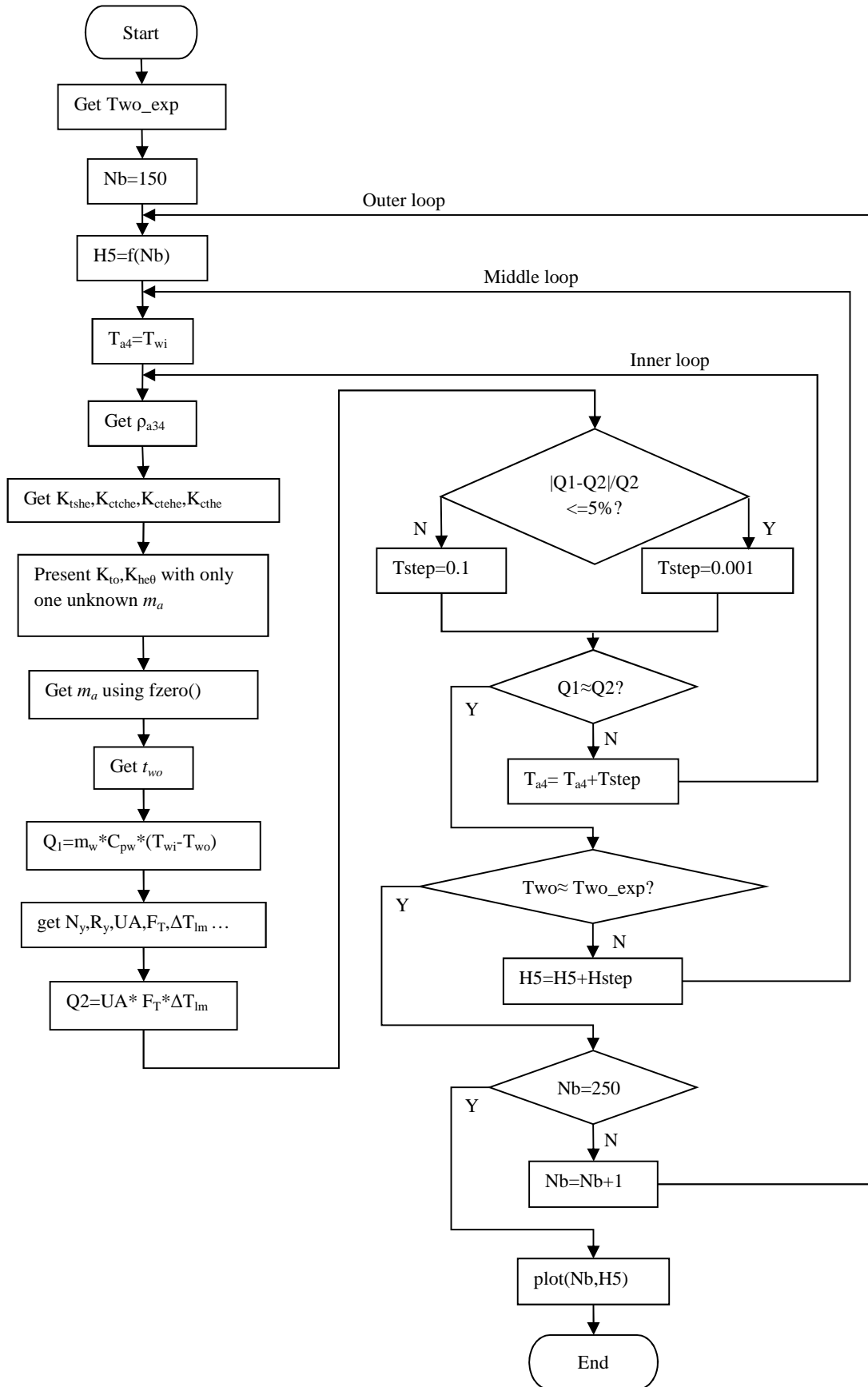
Figure 3.5. The flow chart of the iterative computation code.

3.3.4. Example result

For a fixed amount of heat, decreasing the cooling tower draft height requires more heat exchanger areas, and *vice versa*. As a result of the calculation, the negative correlation between height of cooling tower required and the total frontal area of heat exchanger bundles is depicted in Figure 3.6 for a constant heat rejection capacity of 25 MW and two ITD values. The tower diameter here is determined by the heat exchanger areas on the basis of the assumption that the ratio of the heat exchanger bundles project area to the entire tower base area is 60%. Obviously, the selection of tower height and heat exchanger area requires a trade-off decision in design work of NDDCTs.
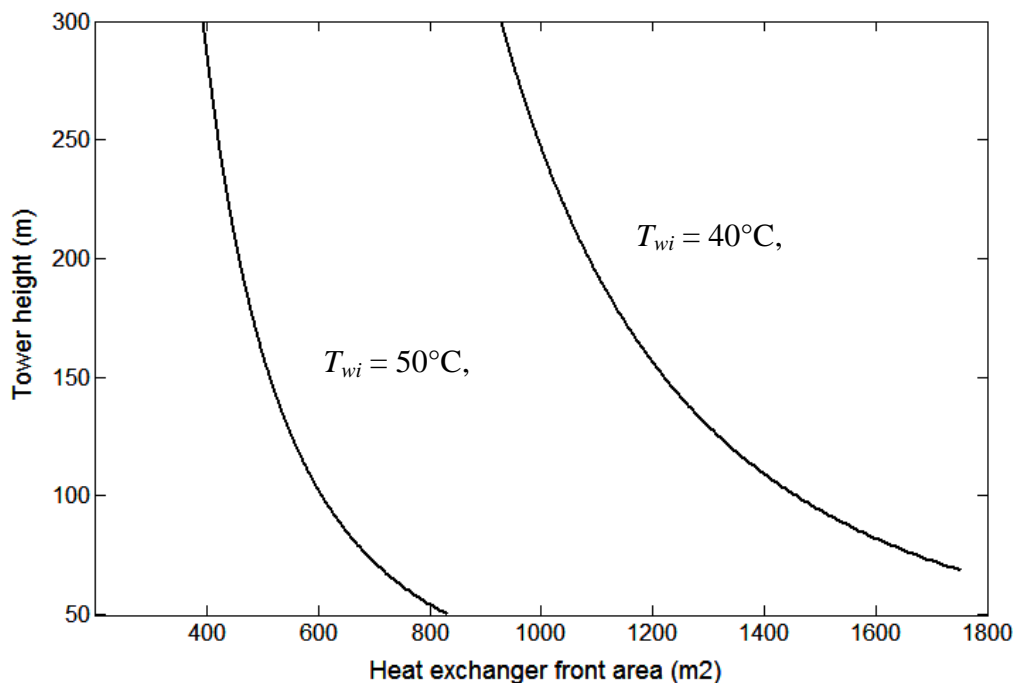
Figure 3.6. Correlation of the tower height required vs heat exchanger total area for a constant heat rejection capacity of 25 MW

On the other hand, if fix the aspect ratio of cooling tower (i.e. the ratio of tower height to the tower base diameter), the heat exchanger frontal area is limited to certain range for a particular tower height. Therefore in order to dump the certain amount of heat for a particular power generation rate, there exists a minimum tower height required by the design conditions. Figure 3.7 plots the correlation of the minimum tower height with the net power generation capacity at two different ITD values when the tower aspect ratio is fixed at 1.25. Here the energy conversion efficiency of the power plant is assumed as 15%. As seen in the figure, the cooling tower height increases more rapidly in the low power generation rate than that in high rate, which means that in small scale thermal power plants, the cooling tower height is a very sensitive parameter. The ITD also

influences the cooling tower performance. Increasing the ITD will improve the heat dump rate significantly. Figure 3.7 suggests that for small scale power cycle of net power generation less than 1 MW, the cooling tower can be decreased to less than 30 m for both ITDs.
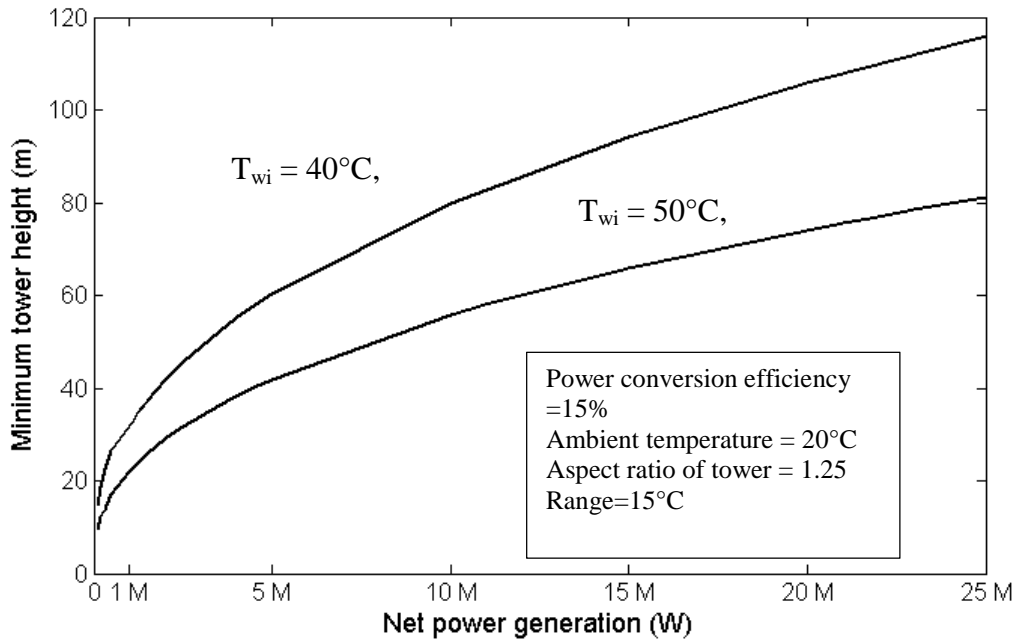
Figure 3.7. Minimum tower height as a function of the net power generation rate under conditions indicated

Small capacity geothermal power plants are more likely to use small cooling towers. As a calculation example, for a portable 100kW renewable power test plant proposed by the Queensland Geothermal Energy Centre for Excellence (QGECE), the minimum sizes of the NDDCT are shown in Table 3.4, while the design conditions for this proposal are specified in Table 3.3.

Table 3.3 The design conditions and constraints of natural draft dry cooling system

Design conditions/ constraints	Values
Total thermal efficiency, %	15
Ambient air temperature T_{ai} (°C)	20
Ambient air relative humidity	20 %
Air static pressure (Pa)	100,688
Water inlet temperature T_{wi} (°C)	40, 50
ITD $T_{wi} - T_{ai}$ (°C)	20, 30

Heat need to be dump (KW)	567
Aspect ratio	1.25
Ratio of heat exchanger projection area to tower base area	≤60%
Approach $T_{wo} - T_{ai}$ (°C)	10, 15

Table 3.4 Tower sizing for 100KW power plant

Parameter	Case 1	Case 2
Water inlet temperature (°C)	50	40
Ambient air temperature (°C)	20	20
Heat dumped (W)	568325.11	567562.37
Smallest tower height (m)	9.5	14.6
Total frontal area (m^2)	55.12	128.62
Water mass flow rate (kg/s)	12	13.5
Water outlet temperature (°C)	38.66	29.93
Air mass flow rate (kg/s)	24.02	53.21
Air outlet temperature (°C)	43.47	30.56
Mean Reynolds number of air based on base area of tower	206646.8	302703.9

3.4 A case study on a conventional NDDCT with air inlet pre-cooling

In this case study, the performance of water-evaporative inlet air pre-cooling applied in a conventional NDDCT for the above EGS plant is analysed and modelled. The heat exchangers are arranged horizontally on top of the tower base, and the inlet ambient air is cooled in a pre-cooling region in periphery of the tower base through water evaporation. The region is treated as a "black box". So no matter what methods are used to achieve the water evaporation inside the box, it simply turns the "input"—the ambient hot air into the "output"—the cooled moist air at certain humidity. The moist air is not necessarily saturated, but the water droplets are assumed either fully evaporated

or eliminated by drift eliminators. Since the moist air as the mixture of pure air and water vapour generally obeys the ideal gas law, the working principle in the rest part of the cooling tower system is the same as a conventional NDDCT.

A cooling tower for a 5 MW geothermal power plant has been proposed and is used as the study case. A thermal conversion efficiency of 17% is assumed with a brine temperature of 250 °C, which means about 25 MW redundant heat has to be dumped through air cooled heat exchangers in a small scale hyperbolic NDDCT. The design points of such a cooling system are shown in Table 3.5. The selection of the ambient air temperature, humidity and static pressure is based on the statistics of the meteorologic data [48] of a potential EGS plant construction site.

Table 3.5 The precooling design conditions and constraints

Design conditions/ constraints	Values
Ambient air temperature T_{a1} (°C)	25
Ambient air relative humidity	20 %
Air static pressure (Pa)	100,688
Water inlet temperature T_{wi} (°C)	50
ITD $T_{wi} - T_{a3}$ (°C)	30
Heat need to be dump (MW)	25

Because of its relatively lower efficiency compared with coal fire power plants at the same net capacity [2], an EGS plant generally requires rejecting more heat for its cooling system and therefore more heat exchanger area and a larger cooling tower are normally required to handle the cooling load. Optimising the selection of tower size and heat exchanger area is one of the goals in the design work. In this case study, the same type heat exchanger bundles with the geometric parameters listed in [3] was selected for the low temperature geothermal power generation. The correlations of air side heat transfer coefficient h_a with air flow mass rate m_a are given in Eq. (3.33) and pressure drop coefficient K_{hx} is calculated by Eq. (3.40) [4]. The parameters of heat exchangers are therefore fixed except the total heat exchanger area and the length of each bundle which depend on the dimension of tower base. Furthermore, the constraint conditions, as shown in Table 3.5, have been set to simplify the calculations.

The resultant minimum size of cooling tower based on the design points and the constraints is listed in Table 3.6.

Table 3.6 The construction parameters for the minimum size of the cooling tower

Parameters	Value
Tower height	38.0 m
Tower base diameter	33.0 m
Tower outlet diameter	26.0 m
Tower inlet height	5.0 m
Length of finned tube	12.0 m
Numbers of tubes per bundle	124
Numbers of bundles	61
Total air side area	136, 288.1 m^2
Percentage of tower base area covered by heat exchanger bundles	78.68%

With above heat exchanger bundle and cooling tower dimensions, the 25MW heat cooling capacity can be achieved under the design environmental conditions. The result at design point is shown in the first column of Table 3.7 below.

Table 3.7 The comparison of the cooling performance in different cases

variables	Under design condition (25 °C)	Pure dry cooling in hot period (37 °C)	With pre-cooling in hot period (37 °C)
T_{a3} (°C)	25	37	37
T_{a3}* (°C)	N/A	N/A	22.58
Relative humidity of inlet air	20%	20%	20%
Relative humidity after pre-cooling	N/A	N/A	80%
ma (kg/s)	1288.48	904.43	838.44

Air flow velocity based on the minimum cross-section area of tower (m/s)	1.33	0.96	0.87
T_{a4} (or T^*_{a4})(°C)	44.41	48.19	46.44
T_{wo} (or T^*_{wo})(°C)	39.92	45.91	41.85
Q(or Q^*) in air side (KW)	25,257.62	10,240.88	20,434.76
Q(or Q^*) through heat exchangers (KW)	25,256.09	10,239.78	20,434.68
Draft provided by cooling tower (Pa)	22.66	12.38	10.64
Total pressure loss of air flow (Pa)	22.78	12.49	10.59

When the ambient air temperature varies, the air flow and heat transfer rates vary accordingly. The results calculated for an ambient temperature of 37 °C are presented in the second column of Table 3.7. As predicted, the heat transfer rate of the cooling system Q^* drops by 41% compared with the design point. The heat is removed at such low rate because the ITD is much smaller in 37 °C case compared to that in 25 °C case. Meanwhile less buoyancy force is produced by the hot air, so that the draft of the cooling tower drops, leading to the significant decrease in the air flow rate.

The situation is different if inlet pre-cooling is added. The third column in Table 3.7 shows one scenario where the relative humidity of the inlet air is increased to 80% by evaporating water in the entry region. It is found that the draft and the air mass flow rate are even less, because of the negative buoyancy force in Eq. (3.22). However, with a much lower inlet temperature (T_{a3}^*), the ITD is much larger and the heat transfer rate is almost doubled. Although it is still not as high as the design-point value, the off-design cooling performance of the entire cooling tower in hot environment is significantly improved compared with the case without pre-cooling.

Cases with different ambient air temperatures under the same design condition for with and without inlet pre-cooling have been calculated. To compare the results, two new parameters are introduced as the relative performance η and the benefit of pre-cooling β:

$$\eta = \frac{X}{X_{design}} \tag{3.42}$$

$$\beta = \frac{X_{pre-cooling}}{X_{nopre-cooling}}\bigg|_{Ta1} \qquad (3.43)$$

In Eq. (3.42), the quantity X without a subscript can be either the off-design total heat transfer rate Q (or Q^*), or the off-design air mass flow rate m_a (or m_a^*), and the η is then denoted as η_Q or η_{ma} accordingly, while X_{design} is the quantity at design point. Eq. (3.43) defines the performance ratio between the cooling system with inlet air pre-cooling ($X_{pre-cooling}$) and without pre-cooling ($X_{nopre-cooling}$) at the same ambient temperature. Here the $X_{pre-cooling}$ represents either Q^* or m_a^*, while $X_{pre-cooling}$ can be Q or m_a, corresponding to β_Q and β_{ma} respectively.

Figure 3.8 shows how the relative performance η_Q (solid lines) and the benefit of pre-cooling β_Q (dashed lines) vary with the ambient dry-bulb temperature under different target relative humidity (RH) of the moist air after pre-cooling. The atmospheric static pressure is not varied. Figure 3.9 illustrates the same points for the air flow rate by plotting the changes in η_{ma} and β_{ma} under the same conditions as in Figure 3.8.
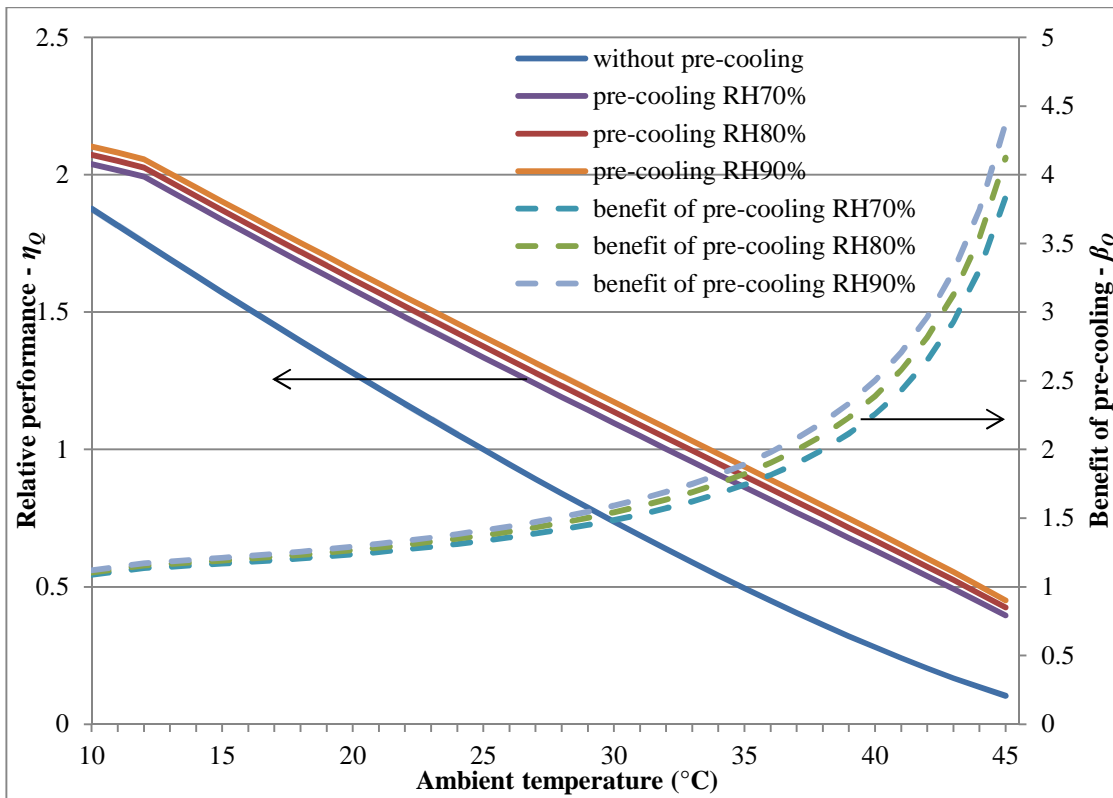
Figure 3.8. The relative heat transfer rate η_Q and the benefit of that in pre-cooling β_Q as the functions of ambient dry-bulb temperatures
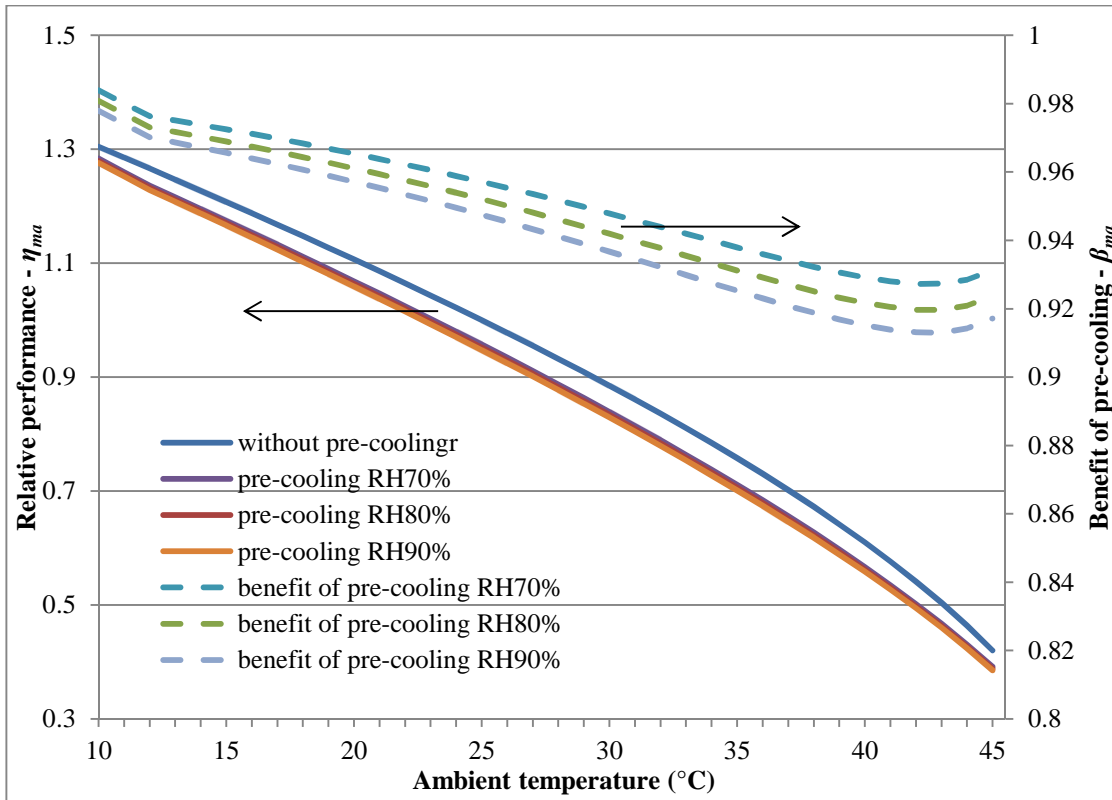
Figure 3.9. The relative air mass flow rate η_{ma} and the benefit of that in pre-cooling β_{ma} as the functions of ambient dry-bulb temperatures

It is clear that NDDCT with the inlet air pre-cooling always has an enhanced heat rejection ability compared to a conventional dry cooling tower at the same ambient dry-bulb temperature and humidity, despite the air mass flow rate decreases. The higher the ambient temperature, the more is the benefit from the added pre-cooling system. The higher the relative humidity φ_2 achieved by evaporation, the better is the cooling performance of the cooling tower. As more heat of the inlet dry air is absorbed by the evaporation, a larger ITD for the heat exchangers can be achieved.

3.4. Summary

Natural draft dry cooling tower is a device working based on the stack effect: the air entering the tower is heated by the heat exchangers causing the air density difference between the inside and outside. Less dense air is lifted by the buoyancy force while denser, cool ambient air is drawn in through the tower inlet, which causes continuous air flow passing through the heat exchanger. The airflow is stabilized when two balances are satisfied in the tower: the aerodynamic balance and the energy balance. The former states that the buoyancy force caused by the air density difference is equal to all the resistance forces when the air flows through the tower. The latter means that heat

transferred into the air is equal to the heat extracted from the cooling water through the heat exchanger surface.

A 1D mathematical model for the NDDCT performance prediction has been introduced based on the aerodynamics and energy balance principle. And the model has then been used to determine the minimum size of NDDCTs for small-scale geothermal power plants. The advantage of inlet pre-cooling has been investigated. As a calculation example, for a 100kW low-temperature renewable power test plant proposed by the Queensland Geothermal Energy Centre for Excellence (QGECE), the minimum NDDCT can be as high as around 15 m with the diameter of 12 m when the ITD is assumed as 30 °C, based on a heat exchanger lay-out with horizontally-arranged 4-rows, 2-passes, air-cooling heat exchangers. This configuration would be able to dump around 567 KW heat.

Chapter 4 Numerical study of crosswind influence on the small NDDCT performance

4.1. Introduction

Geothermal and solar thermal power plants in Australia are more likely located in arid remote inner lands. Although natural draft dry cooling towers (NDDCTs) are more expensive to build compared with other types of cooling towers, they feature no water loss and no parasitic power consumption during operation. In long perspective, NDDCTs are more economic and perhaps the only alternative in these areas. In a natural draft dry cooling tower, no fans are required. The flow of air through the bundles of heat exchangers is by means of buoyancy effects. Buoyancy occurs due to a difference in air density between the inside and outside of the tower resulting from the temperature difference. The greater the temperature difference and the height of the tower structure, the greater the buoyancy force. In natural draft cooling tower design, both the aerodynamic balance and thermodynamic balance should be satisfied at the same time which can be expressed as follows[3]:

$$\Delta P \approx (\rho_{ao} - \rho_{ai}) g (H - H_{hx}) = (\sum K_{resist}) \frac{\overline{\rho}_a v^2}{2} \qquad (4.1)$$

$$Q = m_a c_{pa} (T_{ao} - T_{ai}) = m_w C_{pw} (T_{wi} - T_{wo}) = h_u A F_T \Delta T_{lm} \qquad (4.2)$$

The first equation means the total pressure drop over various components of the tower must be balanced by the buoyancy force. The Eq. (4.2) states that the heat transferred into the air is equal to the heat extracted from the cooling liquid (water) and this heat is transferred through the heat exchangers.

The above equations for NDDCT design and selection do not include the crosswind effects. The negative effect of the crosswind is common and seen during operations of both wet and dry cooling towers in power plants. Early studies on the crosswind influence on natural draft cooling towers were focused on either experimental methods such as full scale tower measurements [33] or laboratory tests [8, 9, 34]. However, numerical analysis (CFD) became the preferred method since the last decade [11, 49].

Both the experimental and the numerical studies in the past have discovered that crosswind has a negative influence on the NDDCT cooling performance. For instance, a study showed that the heat transfer rate decreased by more than 30% at crosswind velocities above 10m/s [11]. Wind break walls, by using either experimental [50] or numerical method [37, 51], were found to improve the thermal performance of natural draft cooling towers under windy conditions. However, all the

studies above focused on either Heller-type or surface-condenser-type indirect large natural draft cooling towers with heights above 100m.

The Queensland Geothermal Energy Centre of Excellence (QGECE) has been developing small natural draft cooling towers (NDDCT) with the height less than 30 m for geothermal and solar thermal power plants [52]. No previous study has been reported on such scale natural draft cooling towers. It is expected that crosswind will have significant negative effect on the performance of small NDDCTs as the draft force in them is much lower than large ones. In this chapter, CFD modelling will be carried out first to numerically investigate the heat transfer performance of a 15m-high small NDDCT under different crosswind speeds. The mechanisms of wind effects will be analysed in detail. Then a simple correlation of cooling tower heat transfer with the crosswind speed is proposed based on the CFD results.

4.2. CFD Modelling methodology

4.2.1. Governing equations and solvers

Unlike the analytical method used in Chapter 3, numerical (CFD) method describes the heat transfer and airflow dynamics in the cooling tower using a set of governing equations of the material–the air. Since the air velocity in this study is far below 0.3 Mach, the incompressible air model with constant density is assumed. A buoyancy generating term is introduced in vertical component of the momentum equation using the Boussinesq's approximation to reflect the buoyancy effect caused by the density difference. The model is simulated by solving a series of conservation equations of physical quantities, whose general term is expressed as:

$$div(\rho \vec{v} \phi) = div(\Gamma_\phi grad\phi) + S_\phi \tag{4.3}$$

The expressions of ϕ, Γ_ϕ and S_ϕ for the above equation are shown in Table 4.1.

Table 4.1 Summary of governing equations

Equation	ϕ	Γ_ϕ	S_ϕ
continuity	1	0	0
x momentum	U	μ_e	$-\dfrac{\partial P}{\partial x} + \nabla \cdot \left(\mu_e \dfrac{\partial}{\partial x} \cdot \vec{v} \right) + F_x$

y momentum	V	μ_e	$-\dfrac{\partial P}{\partial y}+\nabla\cdot\left(\mu_e\dfrac{\partial}{\partial y}\cdot\vec{v}\right)-\rho_0\beta(T-T_0)g+F_y$
z momentum	W	μ_e	$-\dfrac{\partial P}{\partial z}+\nabla\cdot\left(\mu_e\dfrac{\partial}{\partial z}\cdot\vec{v}\right)+F_z$
energy	T	$\dfrac{K_e}{C_p}$	$\dfrac{1}{C_p}\left(\dfrac{qA_{cell}}{V_{cell}}\right)$
k	k	$\mu+\dfrac{\mu_t}{\sigma_k}$	$G_k+G_{kb}-\rho\varepsilon$
ε *	ε	$\mu+\dfrac{\mu_t}{\sigma_\varepsilon}$	$\rho C_1 S\varepsilon-\rho C_2\dfrac{\varepsilon^2}{k+\sqrt{v\varepsilon}}+C_{1\varepsilon}C_{3\varepsilon}G_{kb}\dfrac{\varepsilon}{k}$

Where

$$\mu_e=\mu+\mu_t,\ \mu_t=\rho C_\mu\frac{k^2}{\varepsilon},\ K_e=K+K_t,\ K_t=\frac{C_p\mu_t}{Pr_t}$$

$$G_k=\mu_t S^2,\ G_{kb}=\beta g\frac{\mu_t}{Pr_t}\frac{\partial T}{\partial y},\ \beta=\frac{1}{T_0}\Big|_{P_0}$$

$$C_1=\max\left[0.43,\frac{S\dfrac{k}{\varepsilon}}{S\dfrac{k}{\varepsilon}+5}\right],\ C_{1\varepsilon}=1.44,\ C_{3\varepsilon}=\tanh(V/U),\ C_2=1.92,\ \sigma_k=1.0,\ \sigma_\varepsilon=1.44,$$

$$Pr=0.74,\ Pr_t=0.85,\ T_0=293.15$$

---

* the realizable k-ε turbulence model is used in this modelling.

The source terms F_x, F_y, F_z in each momentum equation refer to porous media resistance defined as

Eq. (4.7), while $\dfrac{qA_{cell}}{V_{cell}}$ in energy source represents heat transfer of heat exchangers with q calculated

by Eq. (4.6).

The implicit partial differential governing equations are discretised with the second order of upwind discretization scheme and are decoupled using pressure-based segregated algorithms: SIMPLE [53]. The convergence criterion is that the scaled residuals for all variables (except energy) drop to the order of 10^{-5} and the monitored variables remain stable when iterating. The calculation process is iterated for more than 15,000 steps and converged results can be obtained.

4.2.2. Model geometry

The first stage of the study was a theoretical analysis to find the possible smallest size of NDDCT for a particular small renewable power generator under given conditions using a one-dimensional (1D) mathematical model based on Eq. (4.1) and Eq. (4.2) [54]. The geometry of tower is assumed to have cylinder rather than hyperbolic shape. While hyperbolic shape provides better structure strength for reinforced concrete towers and has slightly lower air flow resistance, it increases the building costs especially if the tower is built with steel structure as appropriate for small towers in remote areas. Cylindrical shapes have been widely used in steel structure natural draft cooling towers of power plants. A steel tower offers more economic for remote area installations since the air flow resistance caused by the shape is insignificant comparing the building cost involved. According to the above two equations Eq. (4.1) and Eq. (4.2), the wall profile has insignificant influence on the heat transfer and the air pressure drop inside the tower. The contracting and diffusing the air flow area can cause a difference in the pressure loss but this change is negligible compared to the total resistance, the largest part of which comes from heat exchangers. The heat transfer and flow characteristics of the heat exchangers are based on the empirical correlations developed for 4-rows finned tube heat exchanger bundles described in Section 3.3. the air-side heat transfer correlation and pressure drop correlation can be expressed by Eq. (4.4) [55] and Eq. (4.5) [56], respectively.

$$h_a = 0.38 Re_c^{0.6} Pr^{0.333} (A_a / A_r)^{-0.15} K / d_r \qquad (4.4)$$

$$K_{resist} = 18.93 n_r Re_c^{-0.316} \left(\frac{p_t}{d_r} \right)^{-0.927} \left(\frac{p_t}{p_d} \right)^{0.515} \qquad (4.5)$$

It was found that an NDDCT with an internal horizontal heat exchanger placement could be as small as 15m in height and 12m in base diameter for a plant with net power generation of 100 kW under the proposed design conditions in Table 4.2.

Table 4.2 Proposed design conditions

Design point	Value
Tower aspect ratio *	1.25
Total thermal efficiency, %	15
Water inlet temperature, °C	40

Ambient air dry bulb temperature, °C	20
Water mass flow rate, kg/s	16
Heat exchanger tube diameter, mm	21
Tube length, m	8
Fin diameter, mm	51
Transversal tube pitch, mm	60.6
Total heat exchanger frontal area, m^2	73.7
Heat exchanger tubes	3 rows, 3 passes
Bundle arrangement	Horizontal inside the tower

[*] defined as the ratio of total height to base diameter

At the design point as defined in Table 4.1, the heat exchangers can reject around 578 kW heat at no crosswind condition. However, with crosswind, the heat rejected by the heat exchangers will be different. CFD models of the NDDCT of Table 4.1 have been built in the commercial CFD software ANSYS FLUENT to study its heat rejection performance at different crosswind speeds, with and without a windbreak.

The geometry of tower in the CFD model, including tower support, is a cylinder with the size given in Figure 4.1. The cylinder shape selected to reflect the practicality of steel construction of small towers. The computational domain (to simulate outside ambient air) is also of cylindrical shape with 90m in height and 72m in radius. Past CFD studies show that the distances from tower to domain boundaries affect the numerical results to a certain extent [57]. So this CFD model uses 12 times the tower diameter for the domain diameter and 6 times the tower height for the domain height.
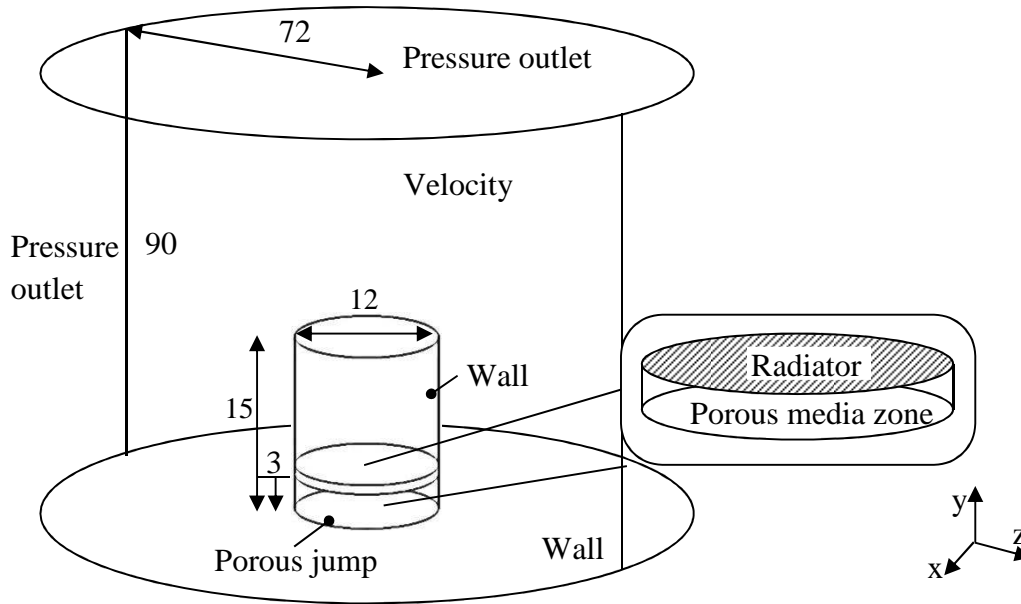
Figure 4.1. Geometry of 3D models with or without walls

4.2.3. Boundary conditions and initial conditions

As shown in Figure 4.1, the wall boundaries are set as slip walls because the boundary layers are sufficiently thin so cannot influence flow separations at tower inlet and outlet [58]. The velocity inlet boundary is defined at the windward side of the domain. The velocity profile is applied in this boundary defined by Eq. (4.6), where a is recommended as 0.2 [59].

$$\frac{v_{cw}}{v_{ref}} = \left(\frac{y}{y_{ref}}\right)^a \tag{4.6}$$

The pressure outlet boundary condition is applied in leeward side as well as on the top of domain. The temperatures on both the inlet and outlet boundaries are set equal to the ambient temperature, i.e. the air inlet temperature of heat exchanger.

Several ways of modelling heat exchangers in CFD can be found in open literature. The radiator model in FLUENT was used in this study to represent the heat exchanger bundles as a lumped face without thickness, whose heat transfer rate is calculated by Eq. (4.7) [53].

$$q = h(T_r - T_{ao}) \tag{4.7}$$

where the heat transfer coefficient, h, is a function of the heat exchanger characteristic parameters and the air inlet velocity, v_{ai}, normal to radiator. T_r is the radiator temperature and T_{ao} is the air temperature downstream of the radiator [59].

For air flow pressure drop, the radiator model can simulate resistance to air flow in the direction normal to radiator face. However, it does not provide resistance in other two directions, i.e. velocity components parallel to radiator face. This will cause overestimation of the possibility of vertices occurring near the radiator, since real structure of fin tube heat exchanger bundles can prevent horizontal air flow, allowing air flow through heat exchanger only vertically. Therefore a porous media model is added to represent the pressure loss within the heat exchanger, leaving the radiator model to represent heat transfer only. Porous media model offers an ideal approximation for modelling the heat exchangers in this context where the internal structure detail is not of concern but a distributed resistance is important. A porous media zone introduces an additional source term in momentum equation of each i- axis [53]:

$$F_i = -\left(\frac{\mu_e}{\alpha} v_i + C \frac{1}{2} \rho v_i^2 \right) \qquad (4.8)$$

Where α and C are determined by the friction factor of heat exchangers in the 1D model.

By this modelling strategy, the vertical air flow can be guaranteed by setting the resistances in other two directions much larger than that in vertical direction (y axis).

The tower support is set to the porous jump boundary which is simplified as a cylinder face with same pressure resistance coefficients corresponding to those of supporting pillars in real towers.

4.2.4. Meshing and convergence improvement

The whole computational domain is discretised by structured prism meshes. The cells in high-gradient regions such as near the walls and the heat exchangers were refined through the inflation method so that the minimum thickness of cell layers dropped to 5 cm with the aspect ratio in 4-6 in these areas. An average cell size of 12 cm was used inside the cooling tower while the cells in outer space grew from 0.12 m to 0.8 m.

Grid-independence has been tested by analysing the no-crosswind cases at different mesh sizes. When the cell quantity is over 3 million, the conserved variables monitored change by less than 0.5% compared with results in mathematics model. Final model uses about 3,750,000 structured prism cells. The thickness of first cell layer near tower walls is 0.08 m while the maximum cell size inside the tower is 0.15m. And a finer mesh is used in the regions of heat exchanger and tower outlet: cell size is less than 0.1m. Figure 4.2 shows the final mesh used in the CFD model. The final mesh size allowed capturing most features of eddies at those length scales that the two-equation RANS model could resolve in this study.
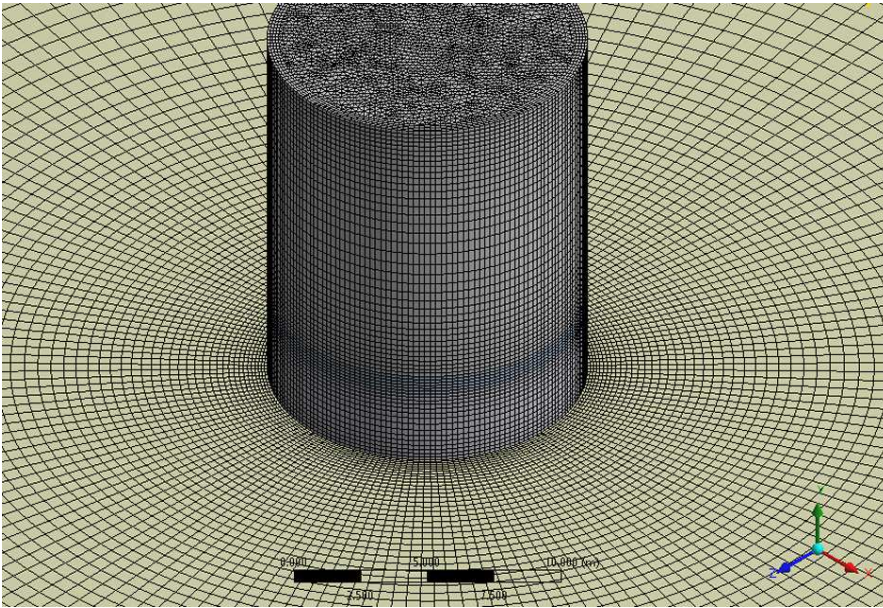
Figure 4.2. Structured meshes in tower body and ground

4.3 Validations of the CFD model

The simulation outcomes under the normal condition without the windbreak walls are compared with the results obtained by using the analytical NDDCT design methods and this is a preliminary validation of the CFD model. There is no research data on such a small-size NDDCT to be compared with in open publications. All reported data refer to larger cooling towers serving relatively large thermal power plants. However, to offer more supports for the validity of above CFD modelling methodology, i.e. settings of boundary conditions, turbulence model, solver, *etc.*, a 120m-high 3D NDDCT model has been specially built using the exactly same aforementioned methodology for the validation purpose. The predicted heat dumping capacity of this big cooling tower is around 327 MW [3]. The comparison is done in the form of approach temperature as shown in Figure 4.3, which compares the approach difference with those obtained in the previous studies on three large natural draft dry cooling tower sizes.
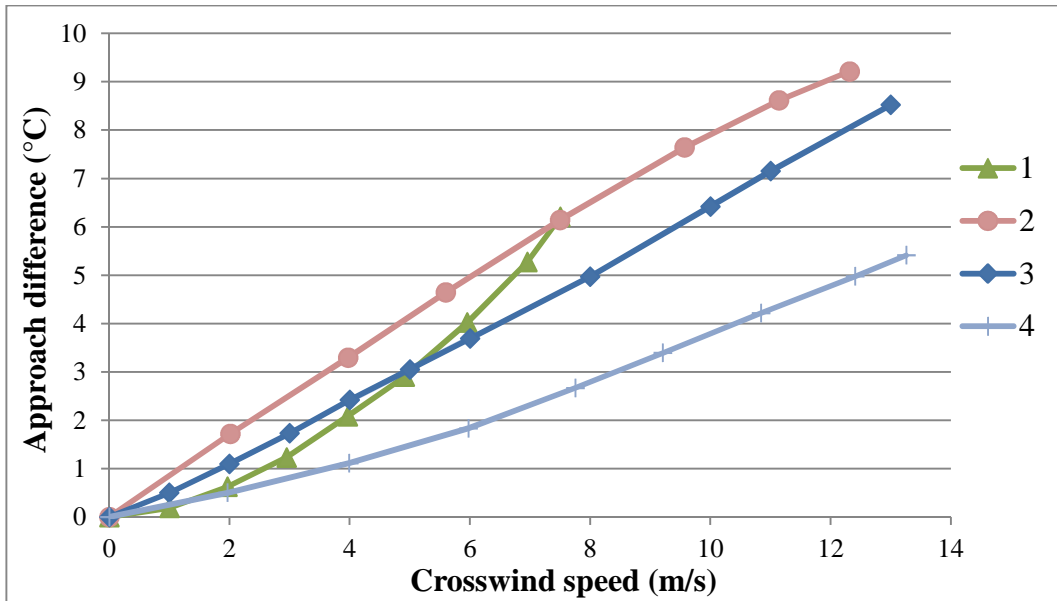
Figure 4.3. The effect of crosswind on the approach difference of four large NDDCTs: (1) 125m high, 200MW heat dumping [38]; (2) 129m high, 285MW heat dumping [11]; (3) 120m high 3D NDDCT model (built for model validation only); (4) 165m high, 650MW heat dumping [33].

The curves 1 and 2 in Figure 4.3 are numerical simulation results reported in the literature for large cooling towers and the curve 4 is generated based on field measurements on a real NDDCT. The numerical results generated in this study are plotted as the curve 3. Curve 1 presents a slightly different trend in these three curves as the cooling tower has a vertical heat exchanger arrangement [38]. It is noticed that the result of current large cooling tower model (curve 3) is closer to curves 1 and 2 than curve 4. This is because all the cooling towers have different heat dump rates and the wind effect tends to be increasingly less important along with the increase of heat dumping rates of the cooling tower [33]. Despite of this, all four study results show a same change trend of the cooling performance, which implies that current modelling methods are consistent.

4.4 The crosswind effects on the cooling performance of the small NDDCT

The comparison of the large tower CFD model results against modelled and measured data in the literature confirms that the methodology of the present project is accurate. The results for a small cooling tower for a small renewable thermal power plant are generated using the same methodology. The small tower cooling performance was first simulated under no-wind conditions. The three dimensional streamlines and the temperature contours at the central vertical cross section of the NDDCT are shown in Figure. 4.4. Both temperature and velocity distributions displays an axisymmetric pattern, which indicates the heat transfer is uniform throughout the whole heat exchanger area. The 3D CFD results are then compared against the 1D analytical ones with ITD of

20°C (Table 4.3), and the relative error in heat flux is about 3.02%. This comparison is useful to verify the internal consistency of our modelling approach.

Table 4.3 The comparison between the calculation results of 3D model and 1D model

Parameters	3D model	1D model
Mean air outlet temperature (°C)	30.1	30.6
Mean air velocity inside tower (m/s)	0.38	0.35
heat flux of heat exchanger (W/m^2)	8997	8732
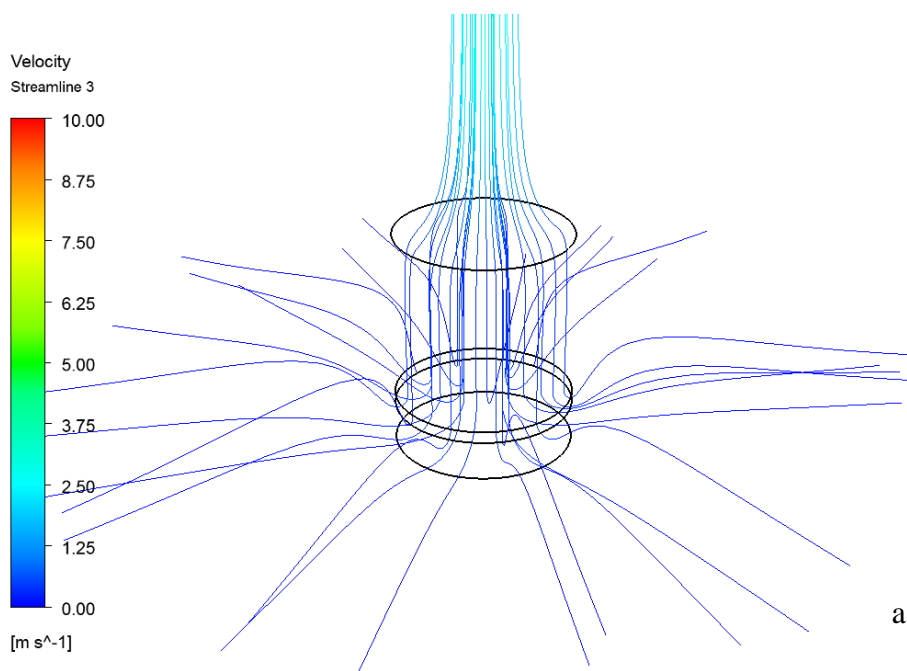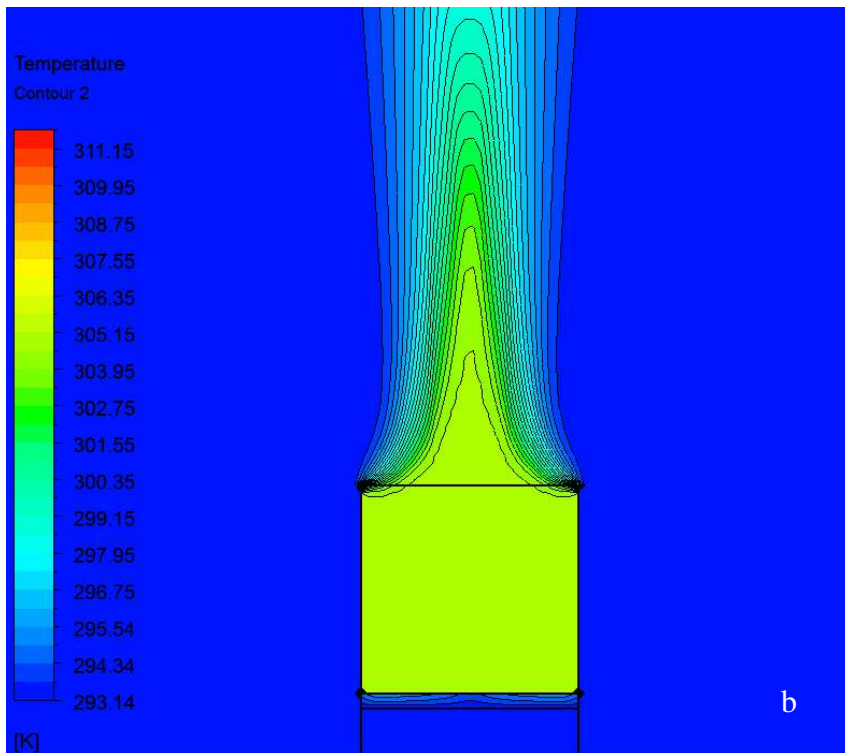
Figure 4.4. The 3D streamlines (a) and temperature contours at the central vertical cross section (b) of the NDDCT

This 1D-verified CFD model is then used for modelling at various crosswinds, which is not possible to do using the 1D model. The crosswind speed was varied from zero (no wind) to maximum of 18 m/s at the reference elevation of 10m as defined in Eq. (4.5).

With horizontally-blowing wind, the airflow inside the cooling tower is not only driven by the buoyancy force created by the difference of air density between inside and outside of the tower, but also influenced by the outside crosswind. Figure 4.5 shows the airflow 3D streamlines inside the tower as well as at the bottom of the cooling tower while Figure 4.6 is the air temperature contours at the central vertical cross section of the tower at various crosswind speeds. At low wind speeds such as 0.5m/s, the air flow inside the tower is near uniform, and the ambient air enters into the tower bottom only through the windward side. As the speed of crosswind increases, two vertices form due to the different mechanisms applying in each region and penetration or downwash [60] of hot air in the downstream of the tower outlet is observed.
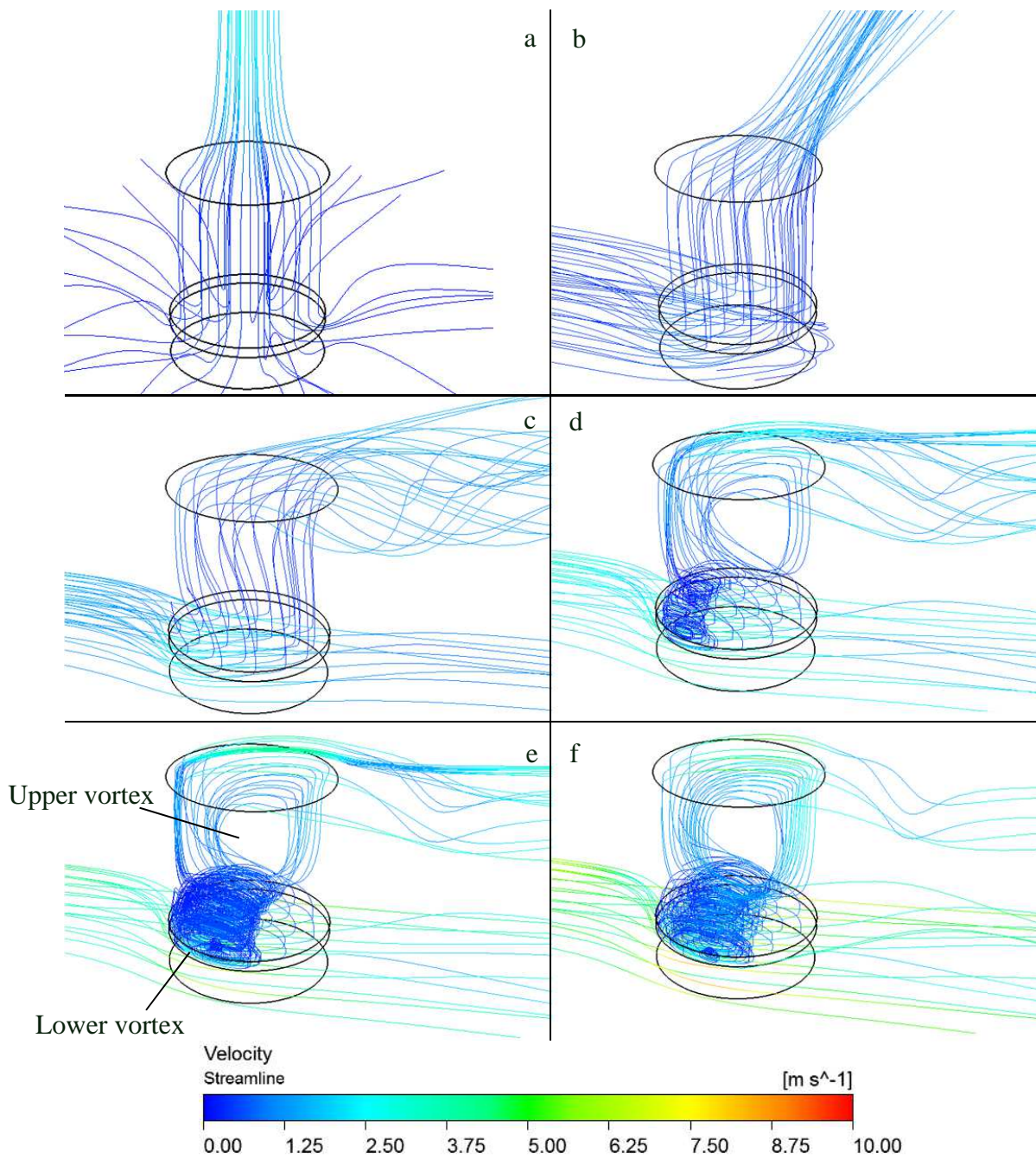
Figure 4.5. 3D streamlines inside and under cooling tower when crosswind speed is (a) 0m/s, (b) 0.5m/s, (c) 2m/s, (d) 4m/s, (e) 6m/s and (f) 8m/s.
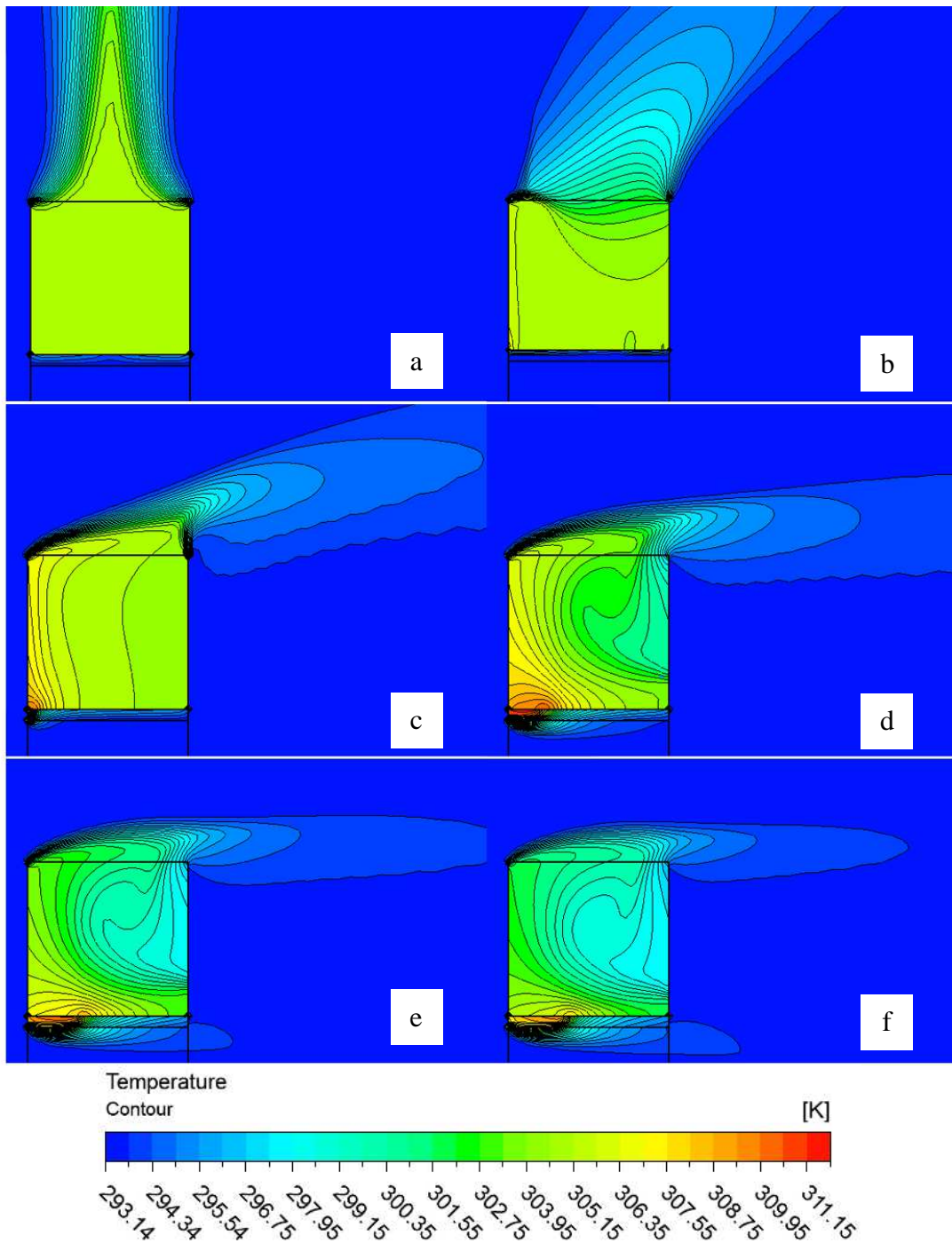
Figure 4.6. The temperature contour at the mid-xy plane when wind speed is (a) 0m/s, (b) 0.5m/s, (c) 2m/s, (d) 4m/s, (e) 6m/s and (f) 8m/s.

The upper vortex is caused by the crosswind forming a high speed zone acting like a lid above the tower outlet to resist the air inside the tower flowing. Therefore, the hot air exiting from the tower flows at a much slower speed (around 0.4 m/s) and cannot break through the "wind lid". In fact, the upward-flowing hot air is quickly cooled near the tower exit by the cross wind and some of the air sinks back into the cooling tower (Figure 4.7). This phenomenon is referred to in the literature as

the cold inflow in large industrial towers , which can be usually assessed with the value of the Froude number [32]. The result is the reduction of the effective draft height of the cooling tower. While at the tower bottom, hot air inside the tower at the windward side is sucked down because of the negative pressure underneath the heat exchangers caused by the crosswind speed. Figure 4.8 shows this negative pressure getting lower and lower along with the increasing of crosswind speed. This air re-enters into the heat exchanger bundles at leeward side, forming another hot air circulation. The lower vortex largely decreases effective transfer area of heat exchanger bundles and makes heat transfer in this region rather complicated.
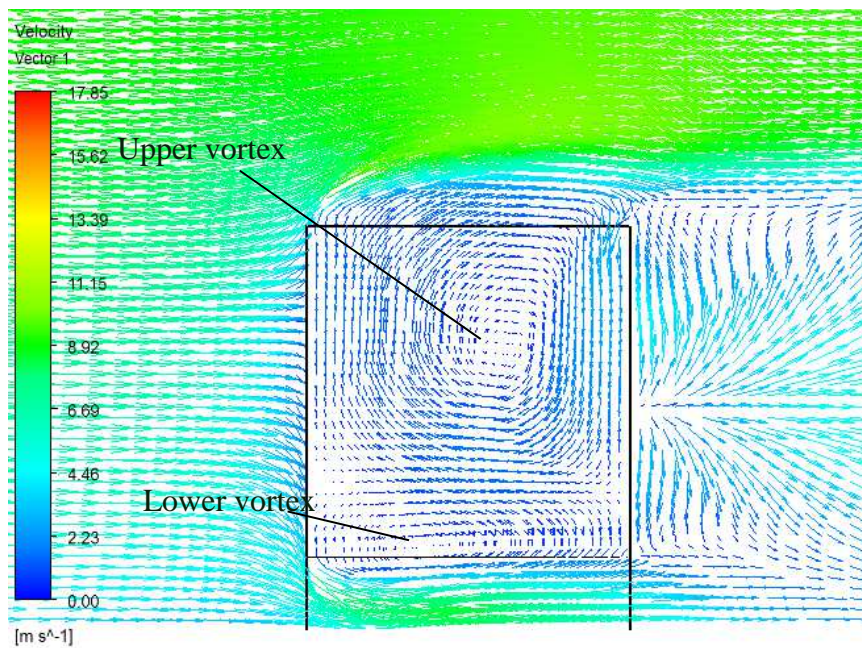
Figure 4.7. Velocity vectors at mid-xy plane when crosswind speed = 6m/s.
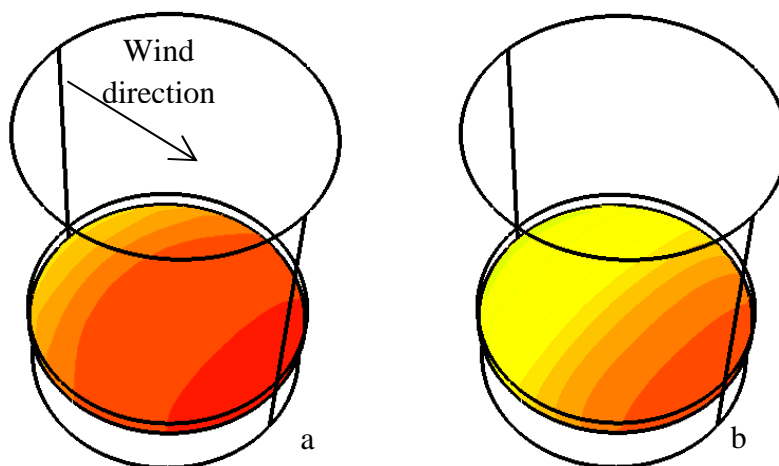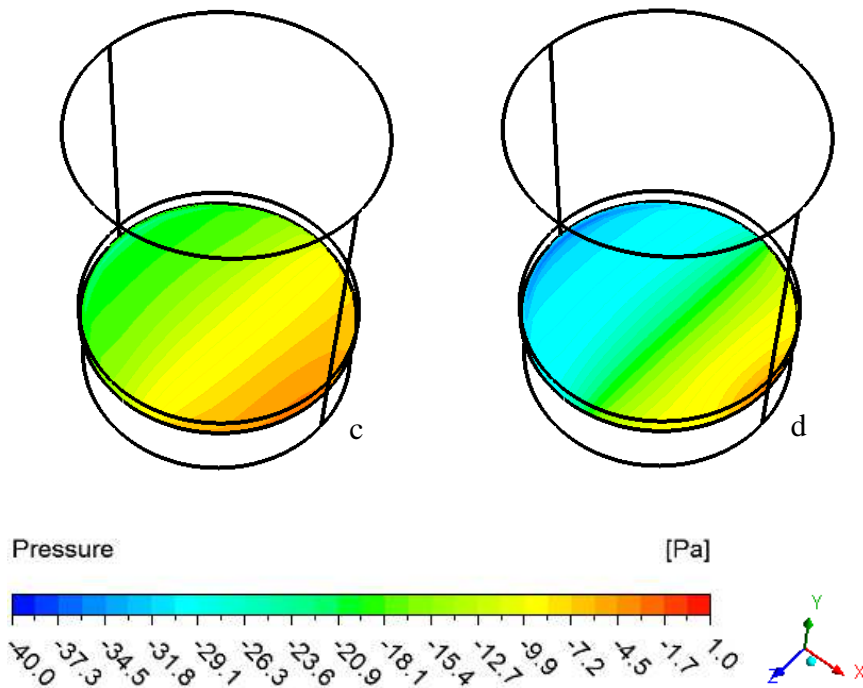
Figure 4.8. Pressure contours at the heat exchanger inlet face when crosswind speed is (a) 2m/s, (b) 4m/s, (c) 6m/s, and (d) 8m/s showing the negative pressure zone.

Although the emergence of these two air vertices inside tower is attributed to different mechanisms, the suction effect under the heat exchangers is believed to play a dominant role. This has been proven by a complementary case study where the crosswind effects on the tower exit and tower inlet are examined separately. In this case study, the space outside the tower is divided into two parts by virtual horizontal faces. And in each simulation, crosswind flow is applied in either upper or lower part of computational domain to study their effect separately. The velocity vectors at the cross section of the central plan (Figure 4.9a) show that in the case when crosswind is applied on the tower outlet (upper part) only, the inside tower air flow field does not change much compared with no-crosswind case. However, when the crosswind is applied only at the tower inlet (lower part), air flow reverses its direction (Figure 4.9b), for the zone below the heat exchangers now has lower pressure.
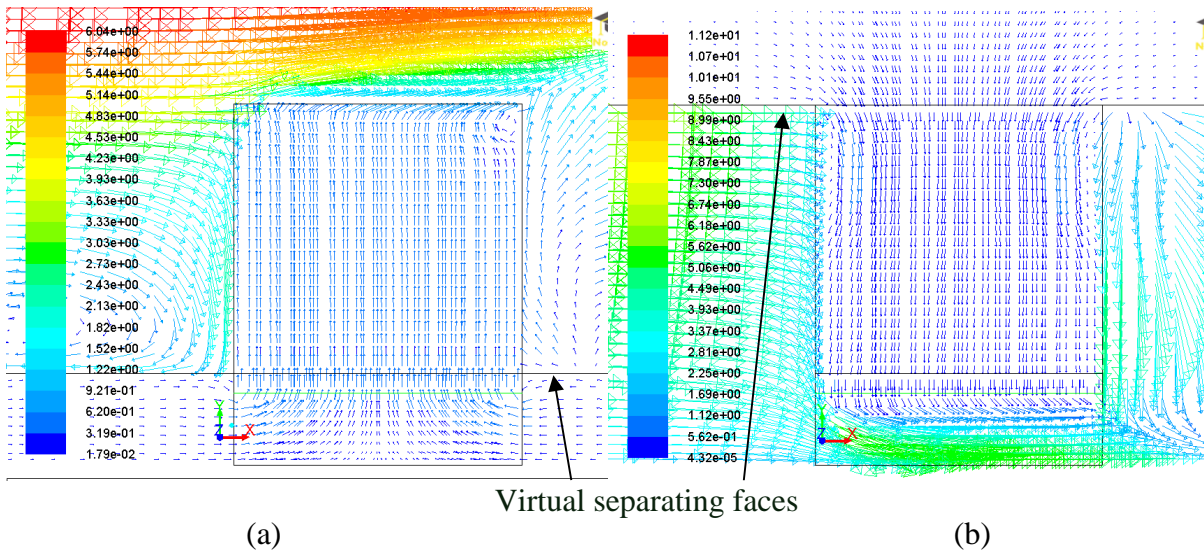
Figure 4.9. Velocity vectors at mid-*xy* plane for case study with the virtural separating faces at the levels of (a) heat exchanger and (b) tower exit.

To quantitatively assess the effect of the crosswind on the NDDCT cooling performance, the air mass flow rate m_a and total heat transferred Q at the radiator are computed. Here air mass flow rate m_a accounts for the net flow across the radiator face, which is extracted from the numerical results as the net difference between the upward and downward mass flow, the latter representing the inverse air flow at the heat exchangers.

Figure 4.10 plots the m_a and Q against the crosswind speed v_{cw}. The mass flow rate m_a decreases first along with rising crosswind speed and remains nearly constant after 10 m/s. The variation of the heat dump rate with crosswind is more interesting. In this small tower, the crosswind does not always exert a negative effect on the cooling tower performance in terms of total heat transfer rate at the radiator Q. Q reaches its lowest point at a crosswind speed around 5 m/s and then increases with increasing crosswind speed.

Figure 4.11 compares the variation of the heat flux (defined as Q/A, where A is the area of radiator) at the radiator surface at different crosswind speeds. It can be seen that there are more low heat transfer areas covering the surface at wind speeds of 4 m/s and 5 m/s, as predicted by the curve in Figure 4.10.
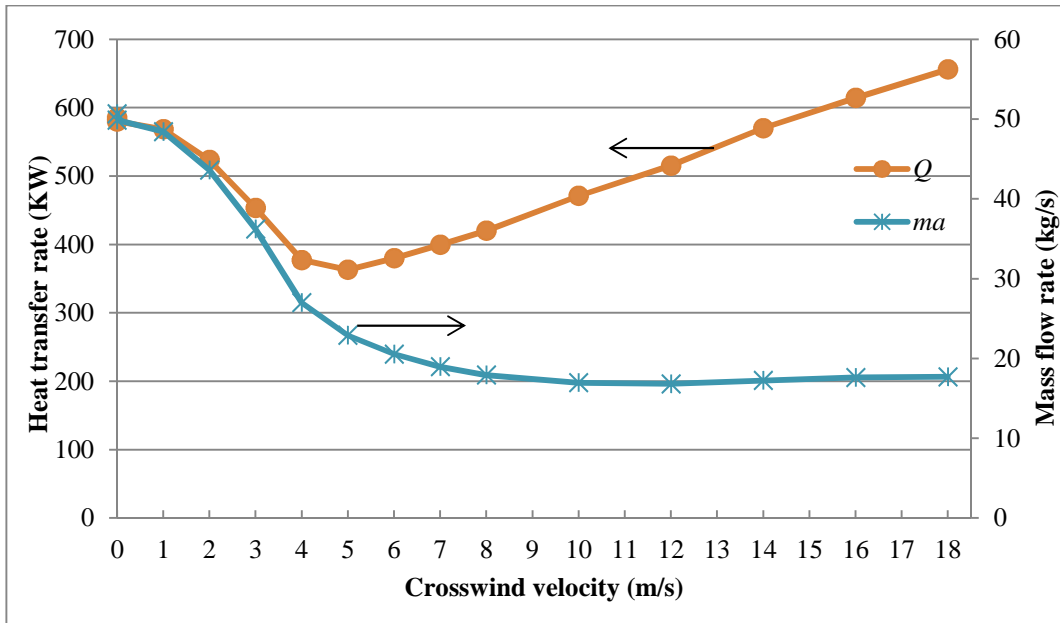
Figure 4.10. The performances (m_a, Q) of the NDDCT under different crosswinds speeds

The trend of the NDDCT cooling rate is better understood by separately examining the two cooling components: the heat taken away by the air updraft leaving through the tower outlet at the top, and the heat carried away by the air that leaves through the bottom part of the. The total heat taken away from the heat exchangers (radiator), Q is equal to the sum of these two components. When there is no crosswind, the second component is zero and all heat is dissipated through tower top.

The turn-around of Q shown in Figure 4.10 indicates that under high-speed (> 5m/s) crosswind conditions, the second component, i.e. the heat transfer rate through the tower bottom, becomes influential in the overall heat transfer rate. This phenomenon is seldom seen in large NDDCT installations since a tall tower provides a relatively large draft force for hot air and normal crosswind speeds are not high enough to cause inverse flow at heat exchangers against this relatively large updraft. This effect is further explored in the next section.

It is seen from Figure 4.10 that with the existence of crosswind at certain speed levels, the total transferred heat Q could decrease by 37% compared with no-crosswind condition, which leads to a significant drop in net power generation at certain cross wind speeds. At some high speed levels, the total heat rejected Q have been increased. It is very hard to design a small cooling tower under unpredictable crosswind without some controllable means to be introduced.
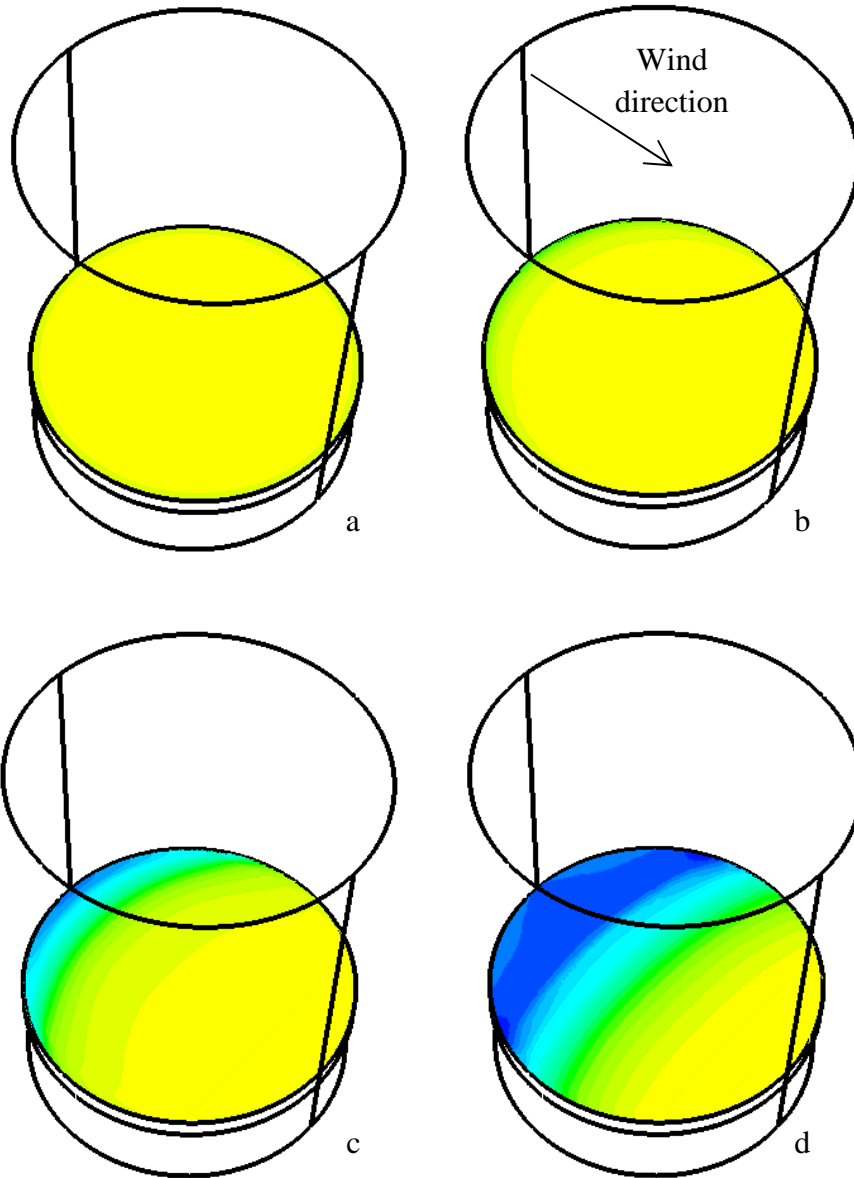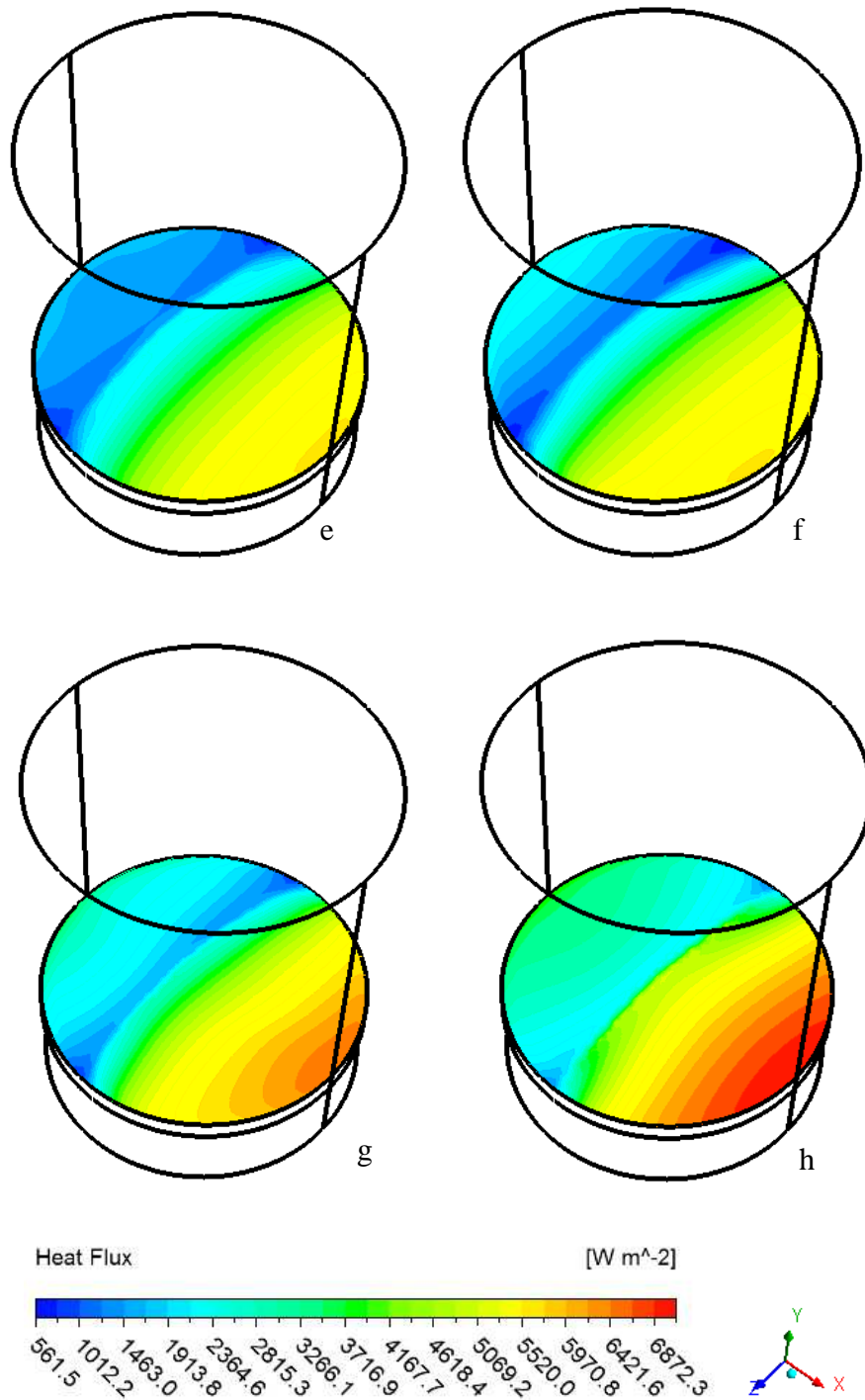
Figure 4.11. Heat flux contours at the radiator surface when no crosswind (a) and when crosswind speed is 0.5 m/s (b), 2m/s (c), 4m/s (d), 5m/s (e), 6m/s (f), 8m/s (g), and 10m/s (h).

The CFD results imply that the crosswind has the potential for improving the heat rejection if its flow direction is controlled. Some sorts of barriers can be deployed inside or near cooling tower base to prevent the negative crosswind effect near ground. When there is no crosswind, the cooling air enters into the tower freely without any obstruction from the walls. If crosswind exists, the barriers stop the crosswind flowing across the bottom, change the direction of the crosswind, and

force it flow through heat exchanger. Since more air flows through the heat exchanger, it improves the performance of the tower. This idea will be discussed in next chapter in detail.

4.5 A simple heat transfer model

This interesting turn-around trend of the total heat transfer rate was only explained qualitatively in Section 4.4 through the way that heat dissipation methods. Further analysis has been made and a simple mathematical model can be proposed.
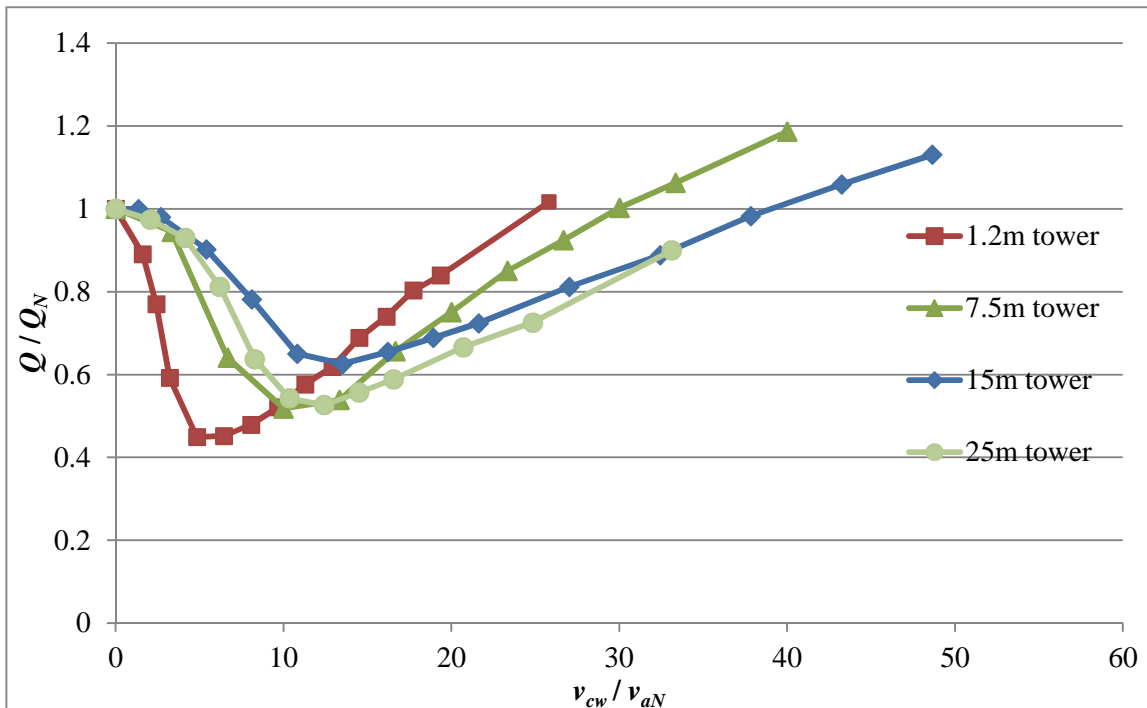
Figure 4.12. The dimensionless heat transfer rate as functions of crosswind velocity ratio NDDCTs of different sizes

The results plotted in Figure 4.12 are firstly nondimensionalized using the corresponding quantities in pure natural convection case without the crosswind. In other words, the dimensionless heat transfer rate is defined as Q/Q_N , and the dimensionless mass flow rate is m_a/m_{aN}, where Q_N and m_{aN} represent the heat transfer rate and air mass flow rate without the crosswind affecting, respectively. The crosswind speed is nondimensionalized by the pure natural convection air speed v_{aN}, i.e. v_{cw}/v_{aN}, which is of the physical meaning that the heat transfer in cooling tower is due to a common effort of these two airflows. It is therefore true that:

$$\frac{Q}{Q_N} = f(\frac{v_{cw}}{v_{aN}}) \tag{4.9}$$

The dimensionless heat transfer rates as predicted by Eq. (4.9) are plotted in Figure 4.12 for four small tower sizes: the 15-m tall tower as in the previous sections, a 1.2 m-high, a 7.5 m-high, and a

25 m-high cooling tower models. All these curves are obtained from the results of 3D CFD models. These tower models are built using the same modelling method as mentioned above, i.e. boundary conditions, solver, turbulence model, mesh, etc. And they are all geometrically proportional to others while they have different tower heights, diameters and other dimensions. The aspect ratio (ratio of height to diameter) for all three tower models is 1.25.

The heat exchangers on these CFD cooling tower models follow the same thermal and aerodynamic characteristics rather than being scaled at the geometric ratio, which means the Rayleigh number and Reynolds number are not the same for them. So the flow conditions in these models do not satisfy the full similarity conditions. But similar functional relation of Eq. (4.9) for the three is still expected. In fact, in Figure 4.12, all curves show a same turn-around trend although their slopes are different.

As explained above, with the presence of crosswind, the heat from water side is taken away by not only the upward air stream through the tower outlet but also the horizontal airflow through the tower inlet. The latter enhances significantly as the wind speed increases resulting in a rise of the total heat transfer rate. In fact, the two ways of heat transfer between heat exchanger surface and air correspond to the natural convection in upward direction and the forced convection horizontally on the lower heat exchanger surface, respectively. So heat transfer in the cooling tower under crosswind is a combined convection problem. If $Q_{natural}$ and Q_{forced} denote the heat transfer rates due to pure natural convection and pure forced convection respectively, and $Nu_{natural}$ and Nu_{forced} are their respective heat transfer coefficients, the combined heat transfer rate of the cooling tower is a sum of both, namely: $Q = Q_{Natural} + Q_{Forced}$. For the combined heat transfer coefficient, there is an empirical correlation of the form as [61]

$$Nu = \left(Nu_{natural}^n + Nu_{forced}^n\right)^{1/n} \tag{4.10}$$

where Nu is the combined overall heat transfer coefficient of the entire cooling tower under crosswind conditions. Exponent n is a constant and is suggested to be 3 or 4 [61]. $Nu_{natural}$ and Nu_{forced} are all based on the tube diameter of the heat exchangers.

The natural convection heat transfer coefficient $Nu_{natural}$ is positive-related to the buoyancy-induced upward airflow rate. In windless condition, the mean airflow rate maintains at a constant value, v_{aN}, which only depends on the density difference and cooling tower draft height. The heat exchangers used in NDDCTs are essentially the cross-flow tube banks, for which numerous empirical

correlations have been proposed between the overall heat transfer coefficient and the airflow speed. Their general term [3] is similar to:

$$Nu_N = a_1 Re_d^b Pr^c = a_2 v_{aN}^b Pr^c \tag{4.11}$$

where the subscript N stands for normal case or no-wind case which is certainly a pure natural convection case. Re_d is based on the diameter of the finned tube of the heat exchangers d and the air velocity at the minimum free flow area–v_c [3]. Pr is Prandtl number of air. The exponents b and c generally vary slightly case to case around 0.6 and 1/3, respectively for $10^3 < Re_d < 2 \times 10^5$ [3, 61]. Obviously v_c is always proportional to v_{aN}, therefore by rearranging Re_d, one can obtain $Re_d^b = a_3 v_{aN}^b$ where a_3 is merged into a_1 resulting in a_2 in Eq. (4.11).

When the crosswind exists, the vertical hot airflow gets deflected when just leaving the tower exit, resulting in the reduction of v_a. In an earlier study, Hooman [62] has defined a deflection angle between the normal airflow direction and the actual inclined flow direction at the tower outlet, and concluded the heat transfer coefficients ratio between crosswind case and no wind case $Nu_{natural}/Nu_N$ can be roughly expressed using wind velocity ratio v_{cw}/v_{aN} as:

$$\frac{Nu_{natural}}{Nu_N} \sim \sqrt{\frac{1}{\sqrt{1+(v_{cw}/v_{aN})^2}}} \tag{4.12}$$

On the other hand, the forced convection heat transfer happens mainly when the airflow caused by the crosswind passing parallel to the heat exchanger bundles. If one assumes the bundle to be a hot square plane, the convective heat transfer coefficient over the plane is approximately in the term of [63]:

$$Nu_{forced} = a_4 Re_x^{0.8} Pr^{1/3} \tag{4.13}$$

where Re_x is based on the distance x from the leading edge of the bundle and the parallel forced airflow which is the function of the crosswind speed v_{cw}. Here x is relevant to the length or width of a heat exchanger bundle. Similar to Eq. (4.12), one can define a ratio of the forced convection heat transfer coefficient to the heat transfer coefficient in normal case Nu_N. This ratio has a similar functional relation with v_{cw}/v_{aN}, i.e.:

$$\frac{Nu_{forced}}{Nu_N} = \frac{a_4 Re_x^{0.8} Pr^{1/3}}{a_2 v_{aN}^{0.6} Pr^{1/3}} = a_6 \left(\frac{v_{cw}}{v_{aN}}\right)^{0.8} \tag{4.14}$$

where coefficient a_6 is a function of the many parameters including the Re_d and/or Grashof number of the cooling tower in still air, heat exchanger characteristics, and the cooling tower geometry–the aspect ratio in this paper. Based on Eqs. (4.10), (4.12), and (4.14), it can be finally proposed that:

$$\frac{Nu}{Nu_N} = \left[\left(\frac{Nu_{natural}}{Nu_N}\right)^n + \left(\frac{Nu_{forced}}{Nu_N}\right)^n\right]^{1/n} = \left\{\left[1 + a_5\left(\frac{v_{cw}}{v_{aN}}\right)^2\right]^{-0.25n} + \left[a_6\left(\frac{v_{cw}}{v_{aN}}\right)^{0.8}\right]^n\right\}^{1/n} \quad (4.15)$$

where a_5 is a speed ratio correction factor to the proposal of Hooman [62], which is similar to a_6.

Eq. (4.15) gives a rough function relationship between heat transfer coefficient ratio Nu/Nu_N and the wind velocity ratio v_{cw}/v_{aN} for horizontal heat exchanger NDDCTs subject to crosswind. In particular NDDCTs, the temperature changes from windless case to crosswind case only in numbers but not in order, therefore it always has:

$$\frac{Nu}{Nu_N} \sim \frac{Q}{Q_N} \quad (4.16)$$

So the heat transfer ratio for pure natural convection $(Q/Q_N)_{natural}$ and for pure forced convection $(Q/Q_N)_{forced}$ can be plotted against v_{cw}/v_{aN} using the correlations in Eq. (4.12) and Eq. (4.14), respectively. For the horizontal heat exchangers and cylindrical NDDCTs with the aspect ratio $H/D = 1.25$ in this study, the standard nonlinear regression analysis has been made based on the data of all aforementioned cooling towers of different heights. a_5 and a_6 in Eq. (4.15) can be presented as following:

$$a_5 = 21.211\left(\frac{Gr}{Re_D^2}\right)^{-1.341} \text{ and } a_6 = 0.123\left(\frac{Gr}{Re_D^2}\right)^{-0.174} \quad (4.17)$$

The squared residual of the regression–R^2 is 0.922 for $n=3$. Here the Grashof number is defined as $Gr = \frac{g\beta(T_{hx}-T_a)\rho_a^2 H^3}{\mu^2}$ and Reynolds number is $Re_D = \frac{\rho_a D v_{aN}}{\mu}$. T_{hx} is the mean heat exchanger surface temperature, and T_a is the mean temperature of inlet and outlet air. ρ_a is the mean air density across the heat exchangers. H and D are the tower height and base diameter, respectively.
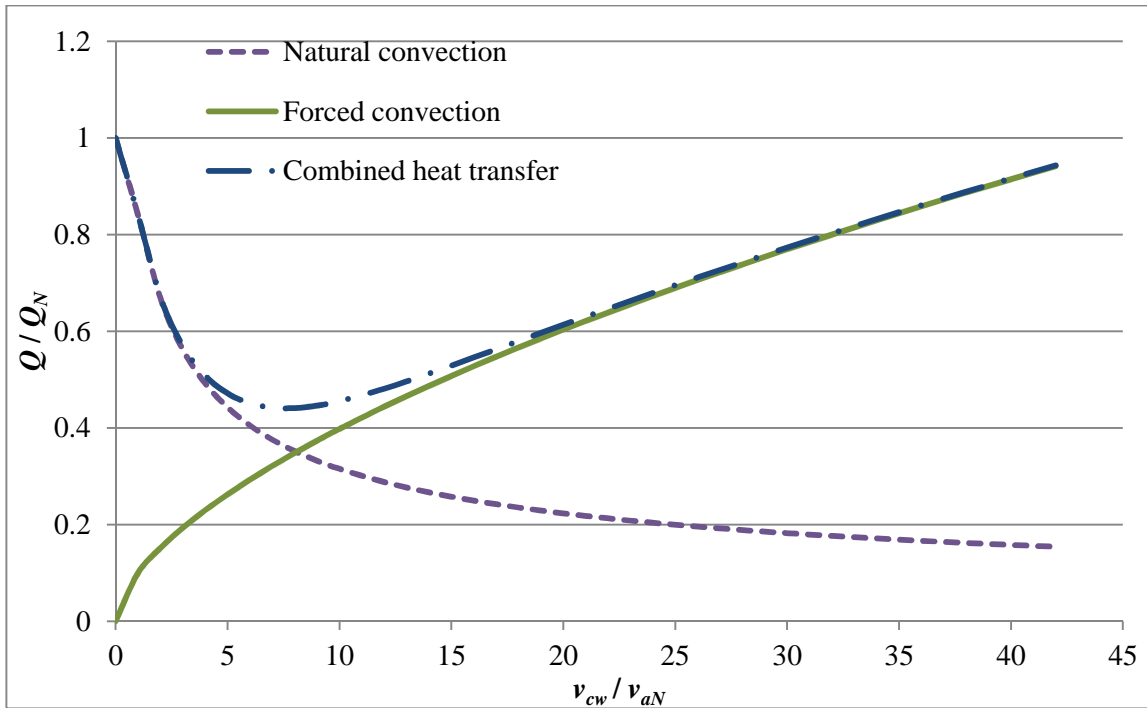
Figure 4.13. The general trends of Q/Q_N vs v_{cw}/v_{aN} curves for both heat transfers and their combination in a natural draft dry cooling tower.

According to Eqs. (4.12) and (4.14), the ratio Q/Q_N for the natural convection persistently reduces along with the crosswind speed, while the one for forced convection keeps continuously increasing. Figure 4.13 demonstrates the general trends of both correlations expressed in Eqs. (4.12) and (4.14) and their combined values as per Eq. (4.15) as well. In small NDDCTs, the natural convection effect is not much stronger than the forced one so that Gr/Re^2 is small [64]. Consequently the coefficient of the forced convection term in Eq. (4.15)–a_6 is considerable. On the other hand, the crosswind velocity ratio v_{cw}/v_{aN} in small cooling towers can reach a very high number under normal environmental wind speeds, e.g. far over 30. Therefore the forced convection term in Eq. (4.15) plays an important role in the combined heat transfer ratio Q/Q_N which must follow the V-shaped turn-around trend. By contrast, Gr/Re^2 in large cooling towers is a large number leading to a much smaller a_6 in Eq. (4.15). Plus, the v_{cw}/v_{aN} on large towers is usually less than 20. As the result, the forced convection term in the combined Q/Q_N is negligible. This explains why in most previous studies, all the conclusions are similar to the dashed line (natural convection) in Figure 4.13.

4.6 Conclusions

Crosswind would stop small natural draft cooling tower functioning properly in certain crosswind conditions. In this chapter, CFD modelling has been done to quantify the crosswind effects on

cooling performance of small size NDDCT with horizontally-arranged heat exchangers. A new approach has been introduced to simulate the heat transfer and pressure drop of the heat exchanger in the cooling tower model: a combination of a FLUENT "radiator" element to represent the convective heat transfer term and a porous media zone to represent the heat exchanger pressure drop.

Simulations under different crosswind speeds indicate that the heat transfer is significantly affected by crosswind. The total transferred heat Q could decrease by 37% compared with no-crosswind condition. The air flow field inside the tower is disturbed by the horizontally-flowing wind and forms two major vortices leading to inverse flow through the heat exchangers. The main reason for the formation of vortices is the suction effect of the wind passing underneath the heat exchangers.

With the inverse air flow, the total heat transfer between the heat exchangers and the air is no longer uni-directional and the heat can be dissipated through both the tower top and the tower bottom simultaneously. And at certain wind speed, larger part of heat is dissipated underneath the heat exchangers, which unexpectedly increases the total cooling performance of heat exchangers.

The total heat transfer rate can be expressed as a sum of natural convective heat transfer and forced convective heat transfer. In small cooling towers, because of the low buoyancy-induced airflow, natural convection term is comparable with forced convection term. Therefore a turn-around trend in total heat transfer exists and the critical point occurs when the sum of the two terms is minimum.

The numerical results are internally consistent and the numerical predictions under no crosswind conditions are in agreement with the correlations developed using industrial data. Later chapters will report the results of experiments carried out to test the fundamental assumptions of the representation used in this model so as to produce a more rigorous experimental validation of the numerical method.

Chapter 5 Mitigation of the crosswind effects

5.1. Introduction

In Chapter 4, a 15 m-high cooling tower design was introduced as a natural draft dry cooling tower suitable to serve a small 100-kWe geothermal power plant. This tower was equipped with horizontally arranged finned-tube heat exchangers and had a heat rejection capacity around 578 kW with the free convection air speed of 0.38 m/s (i.e. the mean velocity of the hot air in the tower) in still ambient air.

It was found that crosswind could reduce the total transferred heat Q by 37% from Figure 4.10, leading to a significant drop in net power generation at certain cross wind speeds. The analysis in the last chapter showed that this decrease was due to a lower vertical hot air speed inside the cooling tower, which was mainly caused by the negative pressure underneath the heat exchangers.

It is therefore necessary to deploy some barriers inside or near the cooling tower base to prevent the negative crosswind effect near the ground. When there is no crosswind, the cooling air should enter into the tower freely without any obstruction. If crosswind exists, the barriers should stop the crosswind flowing across the tower bottom, change the direction of the crosswind, and force it through the heat exchanger plane. More air flowing through the heat exchangers would improve the tower performance.

Crosswind mitigation methods have been proposed using windbreak walls or wind shells. A cross-shaped windbreak wall installed under horizontally arranged heat exchangers in a 165m-high NDDCT was proposed and investigated by Du Preez and Kröger [12, 65]. The wall was porous and as high as the tower inlet and was able to decrease the approach by up to 8 ˚C at wind speeds below 18 m/s. This conclusion was verified by Al-Waked *et al*. [37], who numerically studied the effect of this type of windbreak wall on the thermal performance of NDDCTs. Al-Waked *et al*. [37] also found that the walls did not have to be solid. Either porous or solid windbreak walls would have similar favourable effects on cooling tower performance. Chen *et al*. [50] ran experiments on a scaled wet cooling tower model installed with the same windbreak walls and found that improvement in the cooling performance of the tower due to the windbreak walls depended on the setting angles of the walls. As an alternative option, wind shells placed on the periphery of the tower base were investigated by Wang *et al*. [66] using a scaled model tower in the laboratory. They found that the air flow rate and the cooling efficiency increased remarkably after the inlet air was directed by the wind shells with various installation angles. Zhai *et al*. [51] proposed a similar

but much simpler version of outer shells—the placement of two walls at two opposite lateral sides of towers, which was found to improve the cooling efficiency by about 50% by hindering the cross-airflow and forcing the air flowing into the towers.

All these past studies focused on natural draft cooling towers or their prototypes with heights usually over 100 m and with crosswind speeds up to 20 m/s. Compared to these tall towers employed in conventional power plants, the effect of crosswind on the cooling performance of short towers is much more complicated. The sensitivity of short towers to ambient wind conditions can be explained by comparing the ratio between the crosswind speed and the speed of the tower exit air in still air for short and tall towers [8] as Eq. (5.1)

$$\delta = \frac{v_{cw}}{v_{aN}} \tag{5.1}$$

In Eq. (5.1), v_{cw} is the crosswind speed at the reference height and v_{aN} stands for the upward pure natural convective air speed inside the cooling tower in windless condition.

Since tall towers provide high air draft speeds, the velocity ratios used in past studies were generally limited to below 10. This ratio, δ, can easily exceed 10 for short towers. In a previous study, the present authors considered crosswind effects on a short NDDCT at velocity ratios up to 47 (corresponding to a wind speed of 18 m/s) [67]. They found that the heat rejection performance of the short tower kept declining with increasing velocity ratio until reaching a maximum reduction of 37% at a velocity ratio of around 13. This corresponded to an actual crosswind speed of 5 m/s, only a slightly annoying speed on most large NDDCTs. It was proposed in [67] that, by introducing tri-blade-like windbreak walls in small NDDCTs, the negative effect of the crosswind in a wide range of velocity ratios (up to 40) could be effectively arrested and even converted into a significant performance boost.

In this chapter, the proposed deployment of a tri-blade-like windbreak wall underneath the heat exchanger bundles and the effect of the crosswind angle of attack are examined. The variation of the heat transfer rates at different velocity ratios are examined and explained by considering the vortices in the air flow. The results should provide guidance for designers who need to design relatively short natural draft dry cooling towers for renewable power plants.

5.2. Methodology of numerical simulations

5.2.1. Governing equations and solver

The physical flow problem in NDDCTs can be expressed as a series of unsteady, three-dimensional Navier-Stokes equations supplemented with some simplified mathematical component models. These equations are solved to obtain the conserved solutions using a general-purpose CFD code, Fluent. The governing equations can be expressed in the form of the following transport equation Eq. (5.2):

$$\frac{\partial \rho \phi}{\partial t} + \nabla(\rho \vec{v} \phi) = \nabla(\Gamma_\phi \nabla \phi) + S_\phi \tag{5.2}$$

The generalized scalar ϕ, diffusion coefficient Γ_ϕ and source term S_ϕ for each governing equation are defined in Table 5.1.

Table 5.1 Summary of governing equations

Equation	ϕ	Γ_ϕ	S_ϕ
continuity	1	0	0
x momentum	U	μ_e	$-\frac{\partial P}{\partial x} + \nabla \cdot \left(\mu_e \frac{\partial}{\partial x} \cdot \vec{v} \right) + F_x$
y momentum	V	μ_e	$-\frac{\partial P}{\partial y} + \nabla \cdot \left(\mu_e \frac{\partial}{\partial y} \cdot \vec{v} \right) - \rho_0 \beta (T - T_0)g + F_y$
z momentum	W	μ_e	$-\frac{\partial P}{\partial z} + \nabla \cdot \left(\mu_e \frac{\partial}{\partial z} \cdot \vec{v} \right) + F_z$
energy	T	$\frac{K_e}{C_p}$	$\frac{1}{C_p}\left(\frac{qA_{cell}}{V_{cell}} \right)$
k	k	$\mu + \frac{\mu_t}{\sigma_k}$	$G_k - \gamma^* \rho k \omega + G_{kb}$
ω	ω	$\mu + \frac{\mu_t}{\sigma_\omega}$	$G_\omega - \gamma \rho \omega^2 + G_{\omega b}$

Where

$$\mu_e = \mu + \mu_t, \ \mu_t = \xi^* \frac{\rho k}{\omega}, \ K_e = K + K_t, \ K_t = \frac{c_p \mu_t}{Pr_t},$$

$$G_k = \mu_t S^2, \ S = \sqrt{2 S_{ij} S_{ij}}, \ S_{ij} = \frac{1}{2}\left(\frac{\partial U_j}{\partial x_i} + \frac{\partial U_i}{\partial x_j} \right), \ G_{kb} = \beta g \frac{\mu_t}{\sigma_\rho} \frac{\partial T}{\partial y}, \ G_\omega = \xi \frac{\omega}{k} G_k,$$

$$G_{\omega b} = \frac{\omega}{k}\left[(\xi + 1)\max(G_{kb}, 0) - G_{kb} \right],$$

$$\xi = \frac{0.52}{\xi^*}\left(\frac{0.111 + Re_t / 2.95}{1 + Re_t / 2.95} \right), \ \xi^* = \left(\frac{0.024 + Re_t / 6}{1 + Re_t / 6} \right), Re_t = \frac{\rho k}{\mu \omega}, \ \beta = -\frac{1}{T_0},$$

$$\gamma = 0.075, \gamma^* = 0.09, \ \sigma_k = 2.0, \ \sigma_\rho = 0.9, \sigma_\omega = 2.0, \ Pr_t = 0.85, \ T_0 = 293.15$$

The air was assumed to be incompressible, and the Boussinesq's approximation was applied so that the air density was a function of temperature only. The turbulent air flow was simulated by the two-equation RANS model SST k-ω in the comprehensive consideration of accuracy, computing time and robustness [68].

All numerical calculations were run first using the pressure-based steady-state solver with SIMPLE segregated algorithms and second-order discretization [53]. The convergence criterion in each calculation was for all scaled residuals of the dependent variables to drop to the order of 10^{-4} [69] and remain invariable afterwards. In addition, the integral variables monitored also remained stable when iterating. Based on these converged results, the transient solver was used to solve the conservation equations in a time-dependent manner. Then we compared the steady-state solutions and the time-averaged transient results carefully, finding that the difference between them was sufficiently small.

5.2.2. Model geometry and meshes

The natural draft dry cooling tower and the computational domain are both modelled as regular cylinders, as shown in Figure 5.1. The windbreak walls consist of three solid radial walls arranged symmetrically with separating angles of 120°. The walls are located under the heat exchangers at the same height as the tower inlet and divide the tower base into three identical sectors, denoted sector A, B, and C respectively. The walls themselves are named after the sectors they separate, for example, wall A-B is the wall between sectors A and B. The wind angle of attack refers to the angle between the incoming crosswind direction and the axis of the leeward wall, as shown in Figure 5.1.
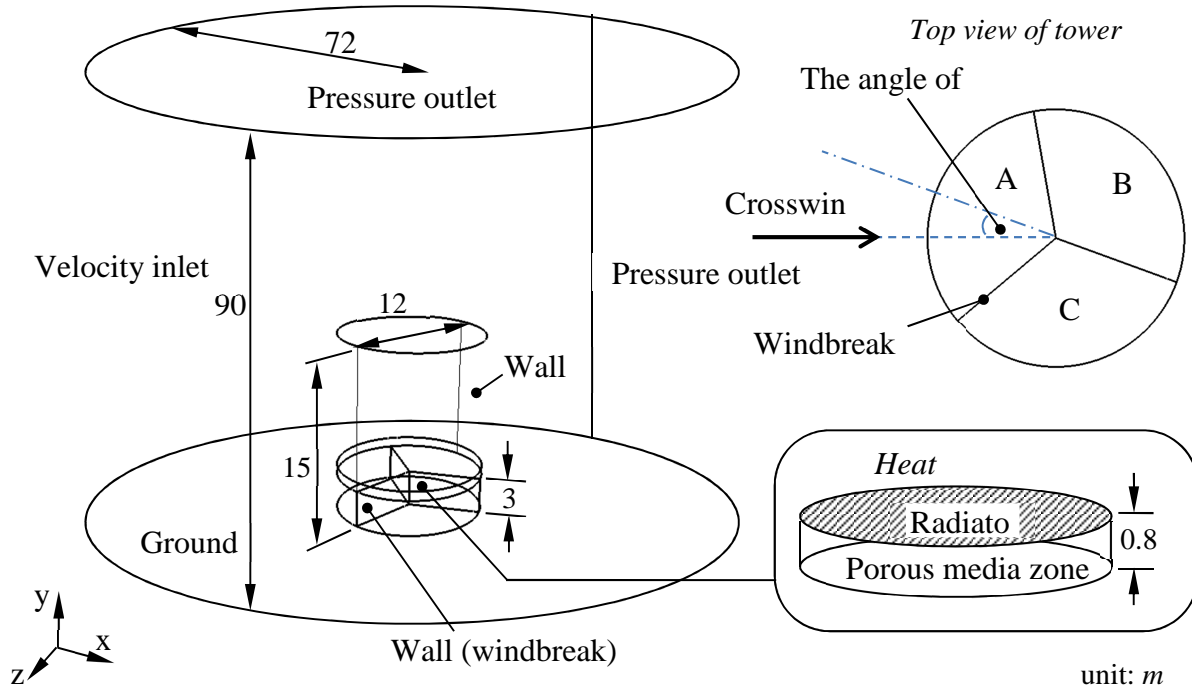
Figure 5.1. The dimensions of the CFD model and the boundary conditions.

The whole computational domain is discretised by structured prism meshes. A series of grid-independence tests have been done in the case without windbreaks at a crosswind speed of 4 m/s using different mesh sizes until the integral heat transfer rate over the whole radiator (i.e. Q_r, as discussed below) is nearly independent of the mesh refinement. Figure 5.2 indicates that three million mesh cells would be fine enough. The final model of the cooling tower contains over 3.7 million cells in total. Cells near the walls and the heat exchangers are further refined through the inflation method so that the minimum thickness of the cell layers drops to 5 cm with the aspect ratios of 4-6 in these areas. An average cell size of 12 cm is used inside the cooling tower. Figure 5.3 shows the final mesh of the tower. Testing shows that the final mesh size allows the capturing of most features of the turbulence structures at the length scales that the two-equation RANS model could resolve.
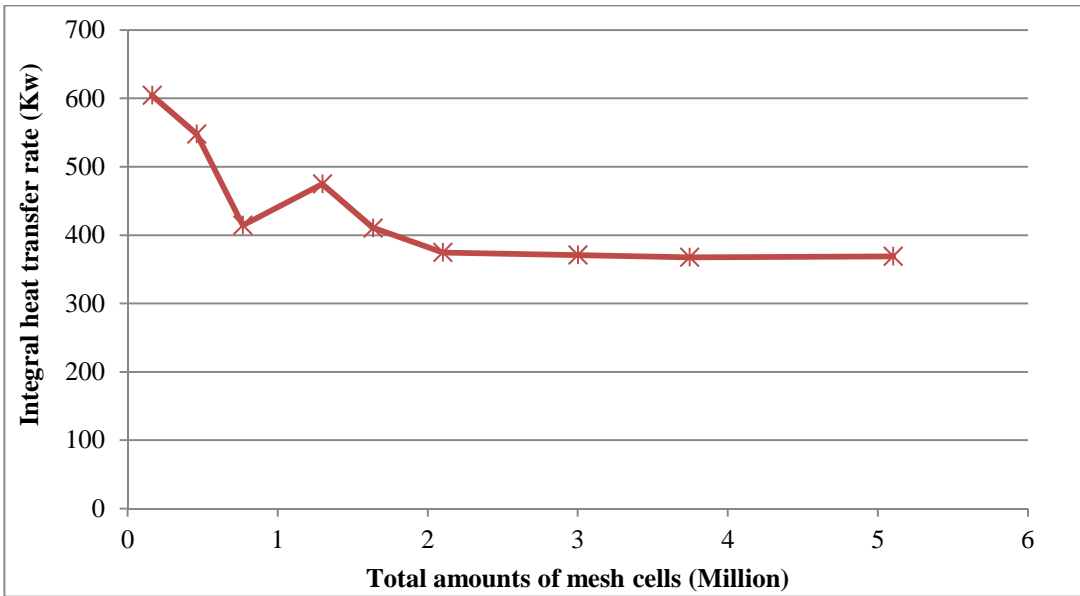
Figure 5.2. The variation in the integral heat transfer rate of a radiator with cell numbers of the CFD model without windbreak walls at a wind speed of 4 m/s.
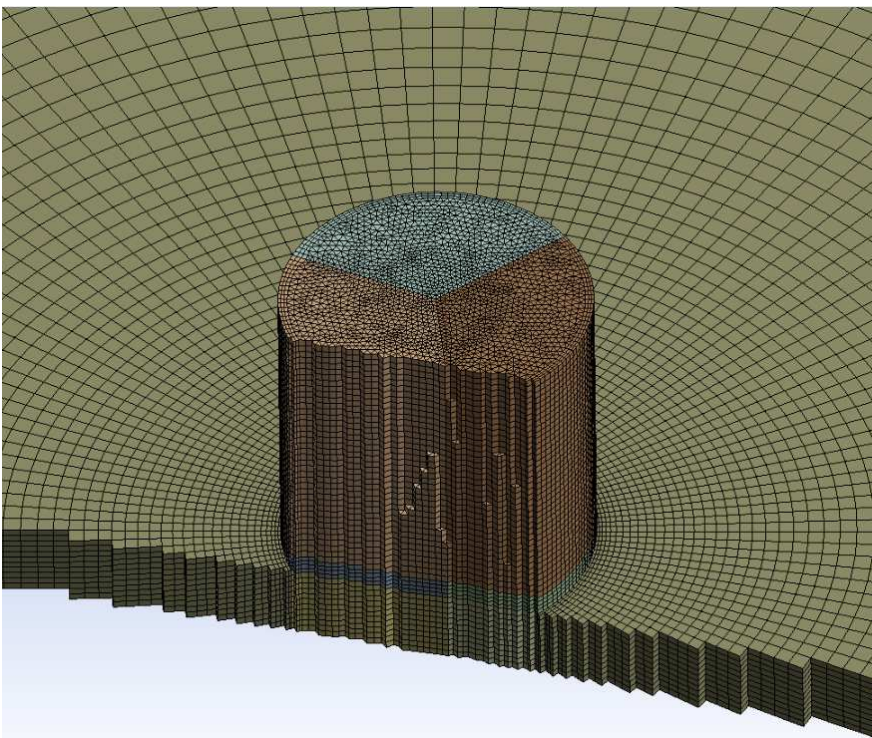
Figure 5.3. Refined meshes inside and outside of cooling towers.

5.2.3. Boundary conditions

The velocity inlet boundary condition is used on the windward half surface of the domain. The profile of the inlet x-velocity U obeys the power law defined by Eq. (5.3) while the other two

velocity components V and W equal to 0. A constant ambient temperature is applied, and the turbulence quantities k and ω at the boundary are determined using Eqs. (5.4) and (5.5).

$$U = v_{cw} = \left(\frac{y}{y_{ref}}\right)^a v_{ref} \tag{5.3}$$

$$k = \frac{3}{2}(v_{cw}I)^2 \tag{5.4}$$

$$\omega = \frac{0.09k}{\mu_t} \tag{5.5}$$

where y is the height and v_{ref} is the reference velocity at the reference height y_{ref} [70]. The term "*crosswind speed*" refers to the reference velocity at the reference height of $y_{ref} = 10$ m. The turbulence intensity I and the turbulent viscosity μ_t are determined according to a preliminary CFD simulation for the same cylindrical domain without any object inside.

At the leeward half surface and the top surface of the domain, the pressure outlet boundary is applied, where the air static pressure is set to 0. The velocity, temperature and turbulence quantities are computed by CFD codes.

The heat exchangers are modelled by a cylindrical porous media zone associated with the radiator boundary condition on its upper surface. The porous media represent the pressure loss within the heat exchanger by adding an additional source term (as defined in Eq. (5.6)) in each momentum equation [71] in Table 5.1. The radiator boundary condition only reflects the heat transfer between heat exchangers and the air, calculating the heat flux q_r using Eq. (5.7) [72]:

$$F_i = -\left(\frac{\mu_e}{\alpha}v_i + C\frac{1}{2}\rho v_i^2\right) \tag{5.6}$$

$$q_r = h_r(T_r - T_{ao}) \tag{5.7}$$

where F_i and v_i are the source term and velocity for the ith (x, y, or z) momentum equation. $1/\alpha$ and C are resistance factors; T_r and T_{ao} are the radiator reference and air outlet temperatures respectively. The resistance factors $1/\varphi$ and C and the convective heat transfer coefficient h_r are all functions of air velocity and the heat exchanger specifications, which are derived from correlations shown in Eq. (5.8) [56] and Eq. (5.9) [55], respectively.

$$K_r = 37.86 n_r Re_c^{-0.316} \left(\frac{p_t}{d_r}\right)^{-0.927} \left(\frac{p_t}{p_d}\right)^{0.515} \tag{5.8}$$

$$h_r = 0.38 Re_c^{0.6} Pr^{0.333} (A_a / A_r)^{-0.15} K / d_r \tag{5.9}$$

where K_r is the pressure loss coefficient of heat exchangers and R_{ec} is the air-side Reynolds number based on the minimum free flow area of the finned tubes. Parameters d_r, n_r, P_t, P_d, A_a, and A_r are all the specifications of the heat exchangers. K is the molecular thermal conductivity of air. For the horizontal directions, i.e. the x- and z- axis, the source F_i is set significantly larger than that in vertical direction y- axis so that the horizontal air flow inside the heat exchanger zone is prevented.

Non-slip and adiabatic conditions are applied to the tower wall and the windbreaks as well [73]. The pressure drop due to the tower support structures is also simulated by a cylinder face with pressure resistance coefficients in the tower model.

5.2.4. Model validations

Using the same method in Chapter 4, validations have been made in above CFD modelling methodology, i.e. the settings of boundary conditions, turbulence model, solver, *etc.* The same 120 m-high 3D NDDCT model has been built using the same aforementioned methodology. The analytical heat-dumping capacity of this big cooling tower is around 327 MW [3]. The crosswind effects on this cooling tower with and without are assessed in the form of approach temperature differences, where the approach temperature is defined as the water outlet temperature minus the air inlet temperature: T_{wo} - T_{ai}. Figure 5.4 compares the approach temperature difference in this result with those obtained in previous studies. In addition, a cross-shape windbreak wall with the same porosity as that in [12] was used underneath the heat exchangers inside the tower base, as indicated in Fig. 5.4.
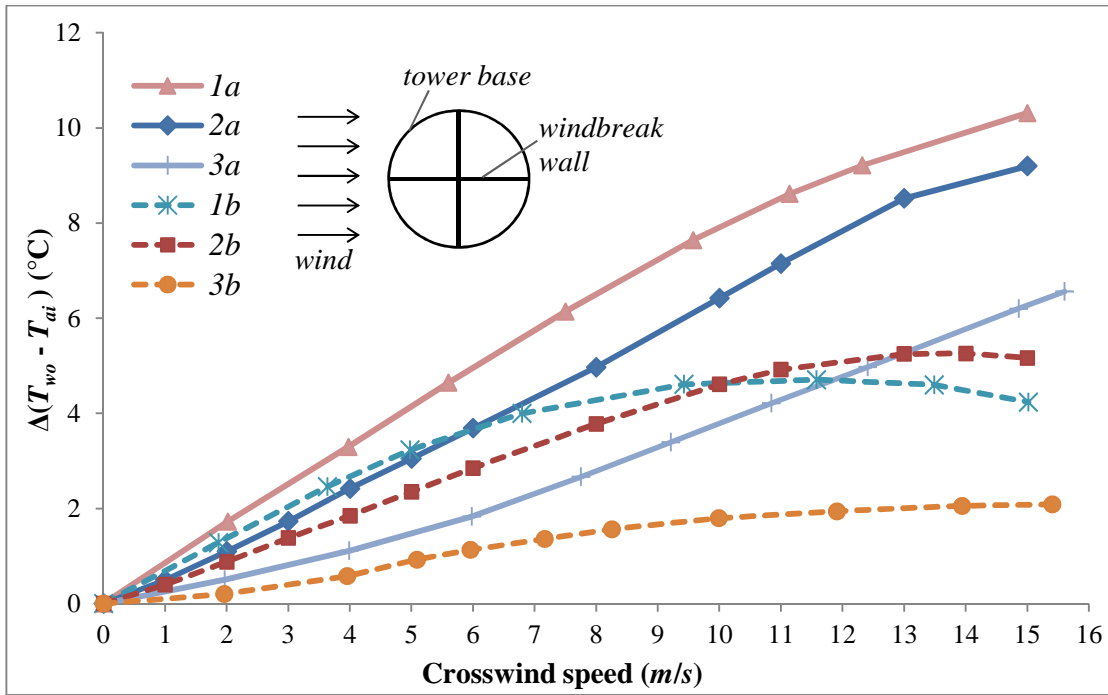
Figure 5.4. The effect of crosswind on the approach difference of large NDDCTs (1) 129 m high, 285 MW heat dumping [11]; (2) current 120 m high 327 MW (built for model validation only); (3) 165 m high, 650 MW heat dumping [33], where *a* and *b* denote the cases without and with the windbreak wall, respectively.

In Fig. 5.4, the solid lines (curves 1a, 2a, and 3a) represent the results without the windbreak wall while the dashed lines (curves 1b, 2b, and 3b) for windbreak wall cases. Particularly, curves 3a and 3b are obtained in a field measurement [33] and a scale model test [12], respectively. It is noticed that the result of our current large cooling tower model (curves 2a and 2b) is very close to that of Al-Waked *et al*. [11] (curves 1a and 1b). The other two curves (curves 3a and 3b) are moderately different. The differences are partly due to the fact that the cooling towers included in the comparison all have different heat dumping rates, and the magnitude of the wind effect tends to decrease with the increase of heat dumping rates of the cooling tower [33]. In spite of this qualification, all four studies concluded the same change trend in the cooling performance, which supports the consistency of the current modelling method.

5.3. Results and discussion

Using the above three-dimensional CFD model of the 15m-high small NDDCT, the air flow and the heat transfer within the computational domain have been calculated. The simulations are carried out at different wind speeds (0, 1, 2, 3, 4, 6, 8, 10, 12, 14, and16 m/s) and different wind attack angles (0°, 10°, 20°, 30°, 40°, 50°, and 60°).

The installation of windbreak walls in the 15m-high tower are found to have a strong effect on the air flow behaviour in the tower base, and this results in a large change in the heat dissipation capacity of the heat exchangers. The parameters of the integral net upward mass flow rate m_a and the convective heat transfer rate Q_r at the radiator are introduced here to assess quantitatively the overall thermal performance of the heat exchangers and the cooling tower. In this model, m_a and Q_r are computed using Eqs. (5.10) and (5.11) respectively.

$$m_a = \int_A \rho v_{ao} dA \tag{5.10}$$

$$Q_r = \int_A h_r (T_r - T_{ao}) dA = \int_A q_r dA \tag{5.11}$$

All variables on the right-hand sides of both equations are solved and conserved in the numerical iterations to enable reporting of the quantities on the left side after the computations are completed. When both m_a and Q_r are divided by their corresponding values under no-crosswind condition m_{aN} and Q_{rN}, respectively, they become dimensionless quantities. These two dimensionless quantities are plotted against the velocity ratio δ for different angles of attack using solid lines, as shown in Figures 5.5 and 5.6, respectively. For comparison purposes, the simulated results without the windbreak walls [67] are plotted in dashes in Figures 5.5 and 5.6 as well.
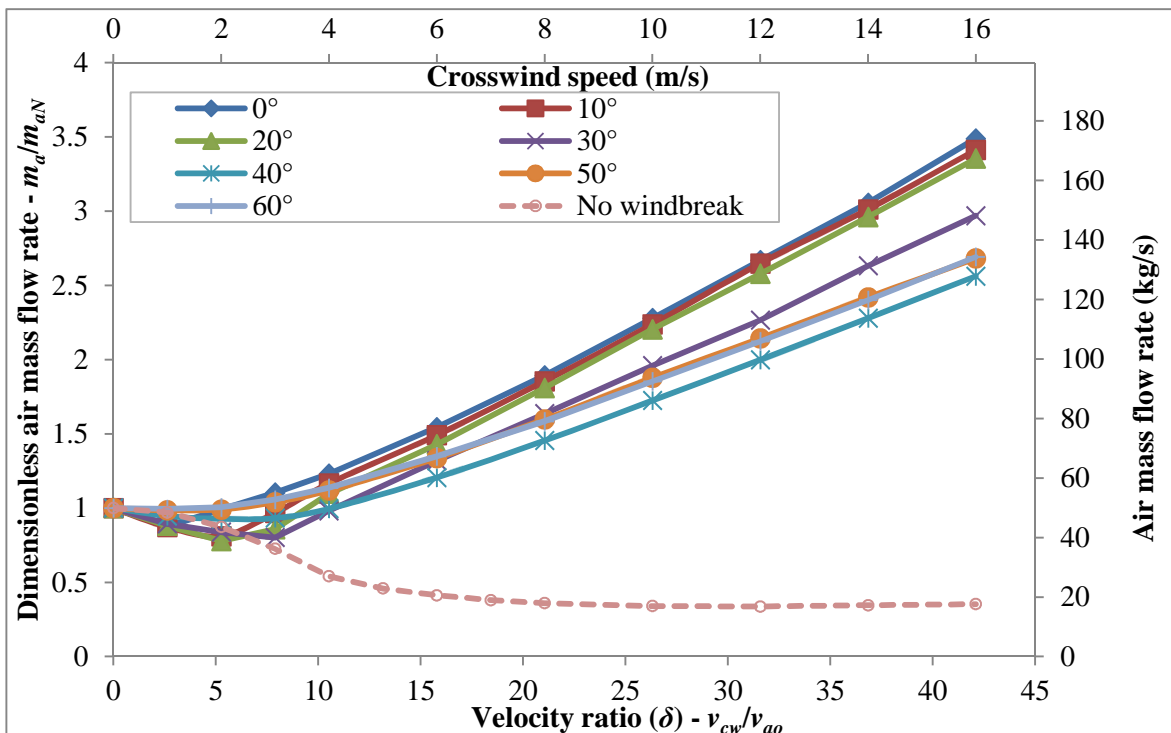
Figure 5.5. The dimensionless air mass flow rate m_a/m_{aN} as a function of the velocity ratio δ in all cases of angles of attack. The legend refers to the wind attack angle. The secondary x-axis and y-axis show the corresponding dimensional values of wind speed and air mass flow rate, respectively.
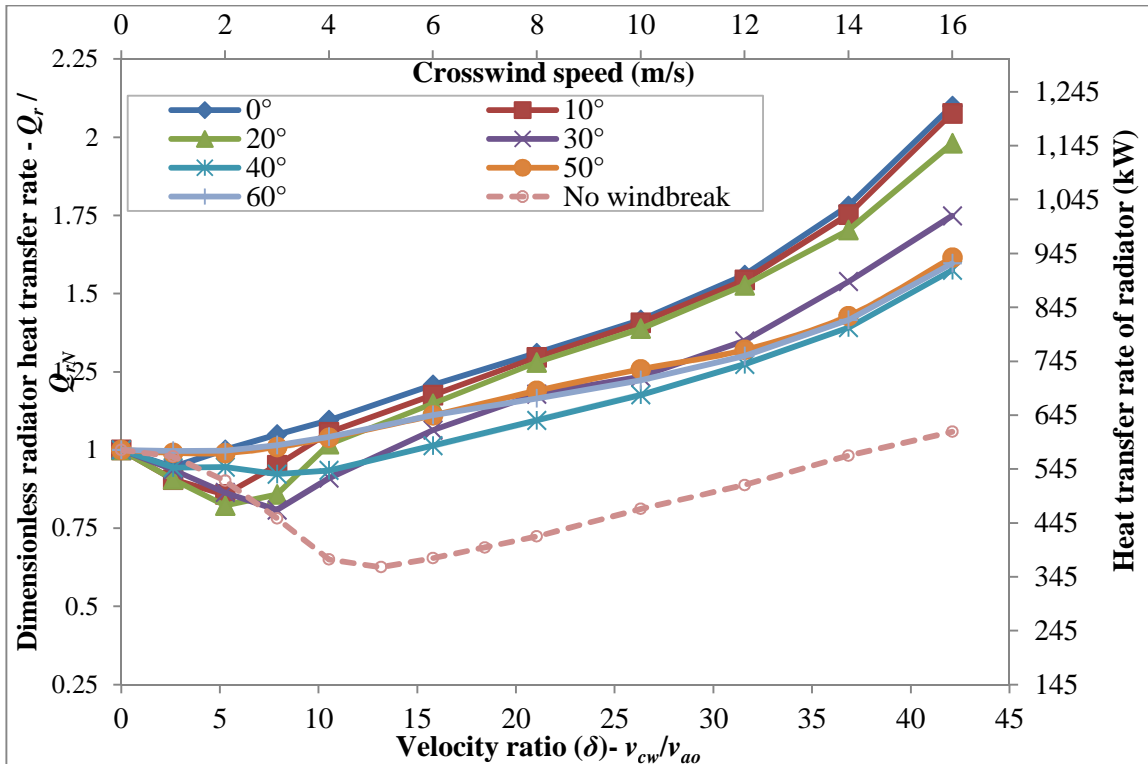
Figure 5.6. The dimensionless radiator heat transfer rate Q_r/Q_{rN} as a function of the velocity ratio δ in all cases of angles of attack. The legend refers to the wind attack angle. The secondary x-axis and y-axis show the corresponding dimensional values of the wind speed and the heat transfer rate, respectively.

For wind attack angles from 0° to 40°, the ratios of both air mass flow and the heat transfer rate start to decline at low velocity ratios until the velocity ratio reaches a critical value. Different attack angles show different declinations. Above the critical value, the trend is reversed, which indicates the benefits of the windbreak walls. The troughs of these curves, depending on the wind attack angle, occur in the velocity ratio range of 2.5–10. In this 15 m-high NDDCT, an air velocity ratio of 10 corresponds to a crosswind speed of approximately 4 m/s. A comparison between the solid lines and the dashed lines shows the significant effectiveness of the windbreak walls at high velocity ratio ($\delta > 10$).

It is interesting to note the turn-around of heat transfer rate without windbreaks (i.e. the dashed curve in Figure 5.6) at velocity ratios above 13, which cannot be found in previous open published results. Most of the research studies on natural draft cooling towers involved air velocity ratios of below 10. A previous study [67] of the current authors found that the turn-around feature in the dashed curve could be attributed to the reverse airflow in the windward part of the heat exchanger area caused by the suction effect of crosswind underneath the heat exchanger. The inverse flow occurs only at certain crosswind speeds. With this inverse flow, the total heat transfer Q_r between

the heat exchangers and the air can be dissipated in two paths at the same time—one through the tower top whose mass flow rate is described by m_a, and the other via the tower bottom. Increasing wind speed depresses the former but boosts the latter. The change in the total Q_r of the entire cooling tower is thus the result of both the negative and positive effects of crosswind.

While similar trends have been observed at the curves for all wind attack angles, Figures 5.5 and 5.6 show that the critical crosswind speed corresponding to the troughs of m_a/m_{aN} or Q_r/Q_{rN} curve for attack angles from 0° to 40° are different at different angles of attack. It is noted that at the attack angles of 50° and 60°, the cooling performance is almost unaffected at low velocity ratios ($\delta <10$) region, which implies a great advantage compared with other wind attack angles. Once the wind velocity ratio exceeds $\delta >10$ ($v_{cw} >4$ m/s), a significant advantage is observed for the attack angles of 0°, 10°, and 20°, where the wind direction is closer to one of the walls.

The underlying reasons for the interesting trends of the numerical results presented in Figures 5.5 and 5.6 are investigated by detailed examination of the air flow patterns around the heat exchangers under two sets of conditions: the same crosswind speed at different angles of attack; and the same angle of attack at different crosswind speeds.

5.3.1. Effect of angles of attack

The air flow patterns in the tower interior and around the tower base are visualized by the time-averaged 3D streamlines at different attack angles at the wind speed of 4m/s, as shown in Figures 5.7 and 5.8.
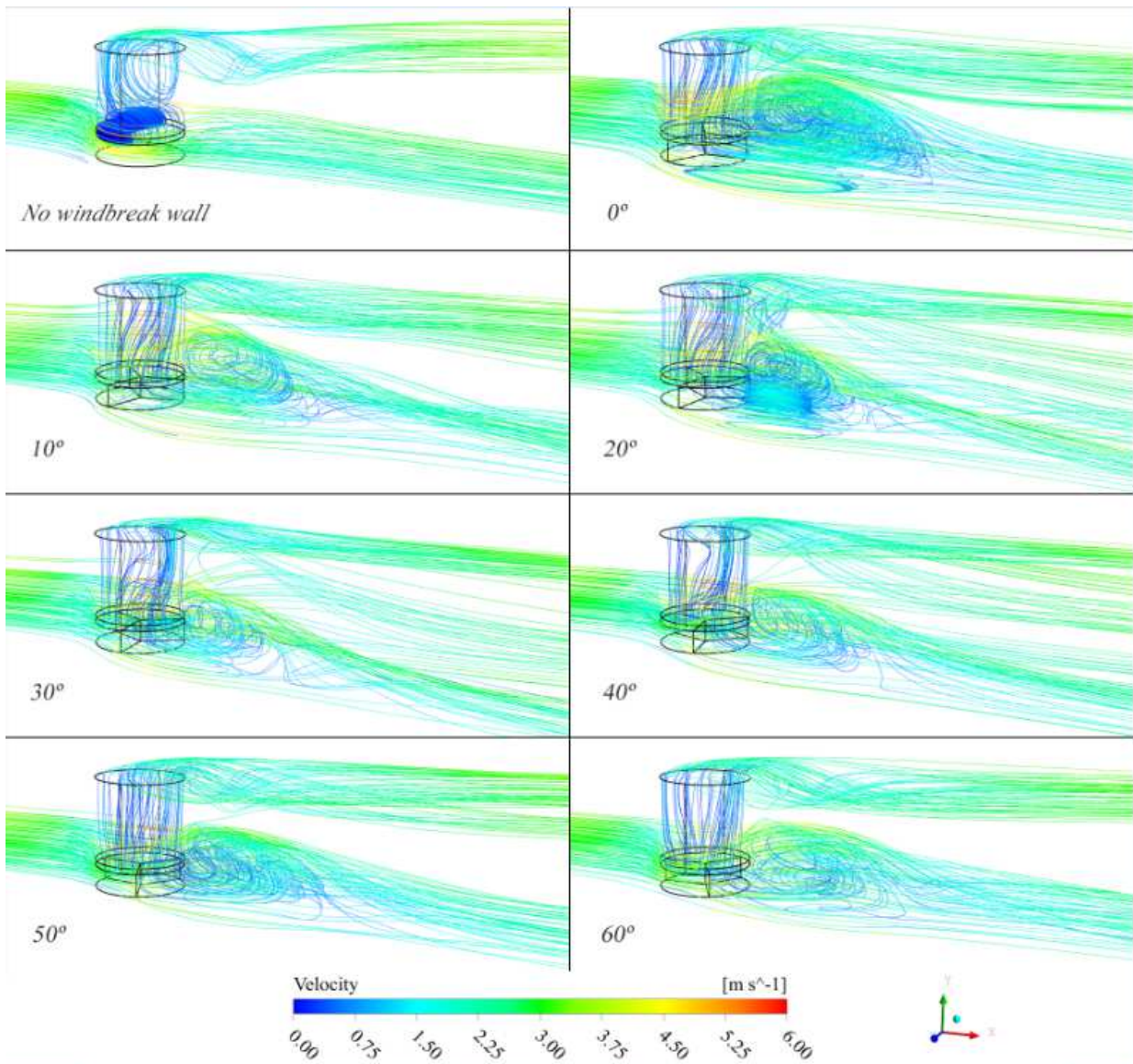
Figure 5.7. Side views of the time-averaged 3D streamlines passing through the tower bottom at a crosswind speed of 4 m/s and at different wind attack angles as indicated.
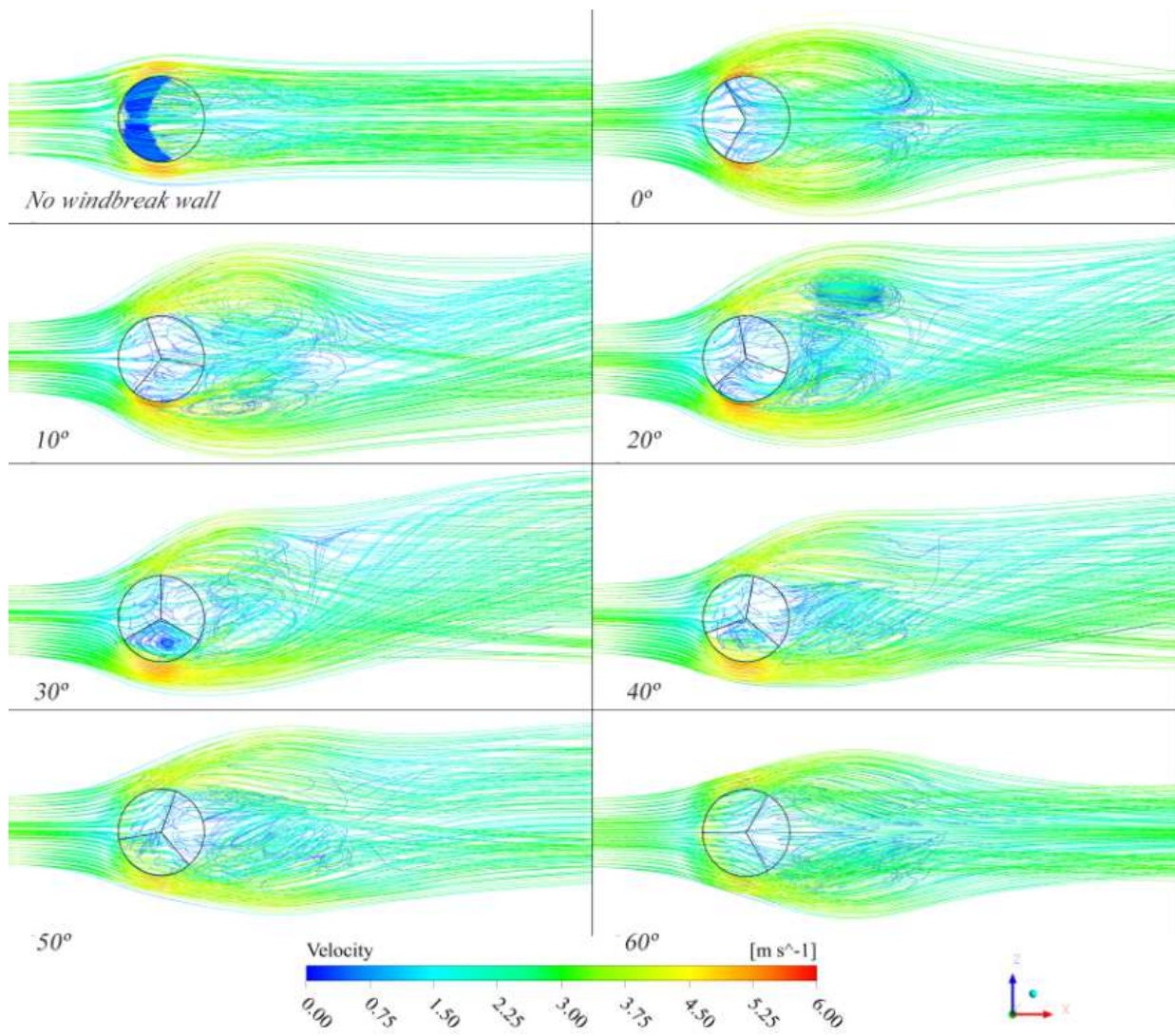
Figure 5.8. Top views of the time-averaged 3D streamlines passing through the tower bottom at a crosswind speed of 4 m/s and at different wind attack angles as indicated.
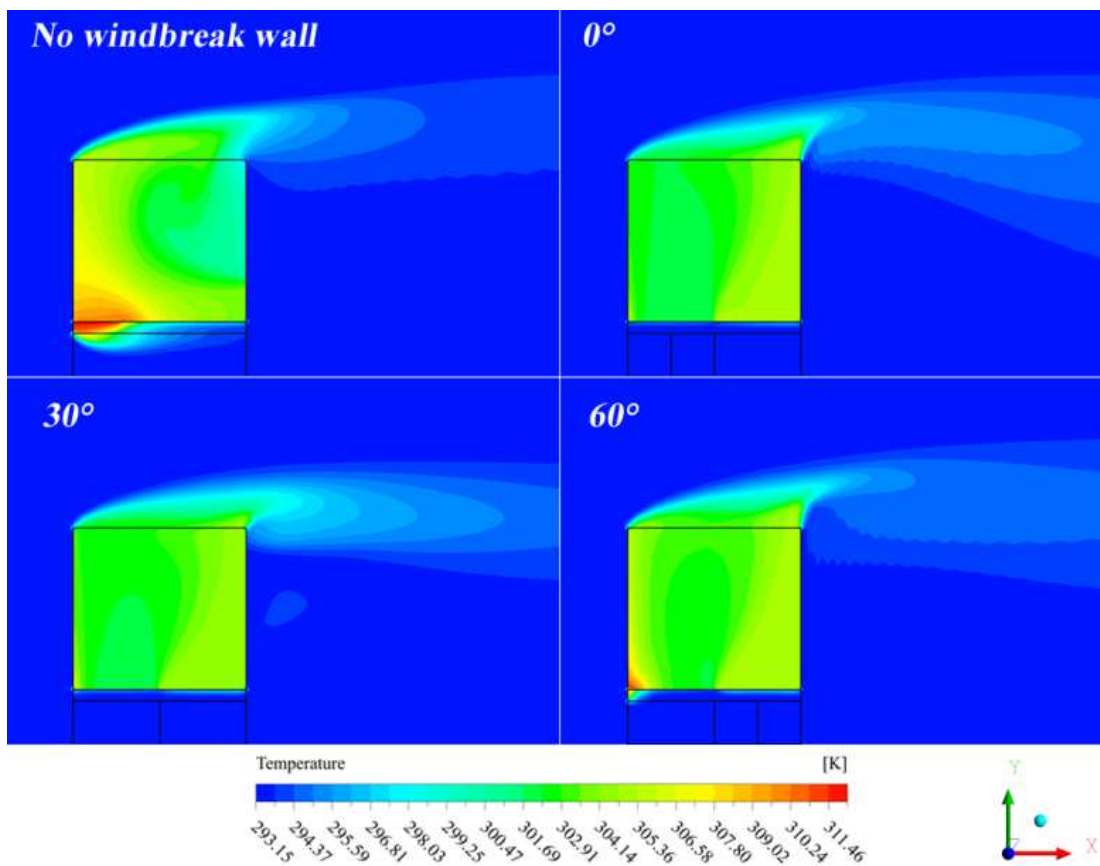
Figure 5.9. Temperature contours at mid-*xy* plane for different wind attack angles as indicated when crosswind speed is 4 m/s.

With no windbreak walls, the air flows directly across the tower base with significant vortex activity being observed inside the tower. By contrast, towers with windbreak walls experience a smoother and more uniform air flow inside the tower. This improvement leads to a difference in the air temperature profiles. Figure 5.9 compares the temperature contours at mid-*xy* plane of the cooling tower for different wind attack angles at the same crosswind speed. No hot air region is seen underneath the heat exchanger from the contours when the windbreaks exist. The windbreak walls enhance the convective heat transfer from the heat exchangers by improving the airflow above the heat exchangers.

However vortices are generated in the wake of the tower base caused by the separation of the air flow at the tips of windbreak walls. At a wind speed of 4 m/s (δ=10.5), the Reynolds number based on the tower base diameter is around 3.2×10^6. The wake structures are complex at such a high Reynolds number and sensitive to windbreak wall orientations as well. At attack angles of 0° and 60°, where the walls are arranged symmetrically about the wind direction, the time-averaged streamlines of air flow vortices are symmetrical as expected. For other attack angles, the tips of the

windbreak walls where flow is separated are not symmetrically positioned about the wind direction, resulting in the different vortex distributions on the two sides. This causes an asymmetric and biased streamline pattern behind the walls as seen in Figure 5.8 at attack angles in the range of 10°–50°.

The air flow through the tower base in one of the cases is presented in greater detail in Figure 5.10, which shows the horizontal components of the time-averaged velocity vectors in the plane of y=2.5 m at a non-symmetric attack angle of 30°. This height corresponds to the layer just underneath the plane of the heat exchangers, which are placed at a height of 3 m. Figure 5.10 shows that the air flow is separated at the tips of the windbreak walls forming the wake. An imaginary boundary between the free stream zone and the wake zone (free-wake boundary) can be seen as shown in shaded lines. The flow regimes are distinctly different at the two sides of this boundary.
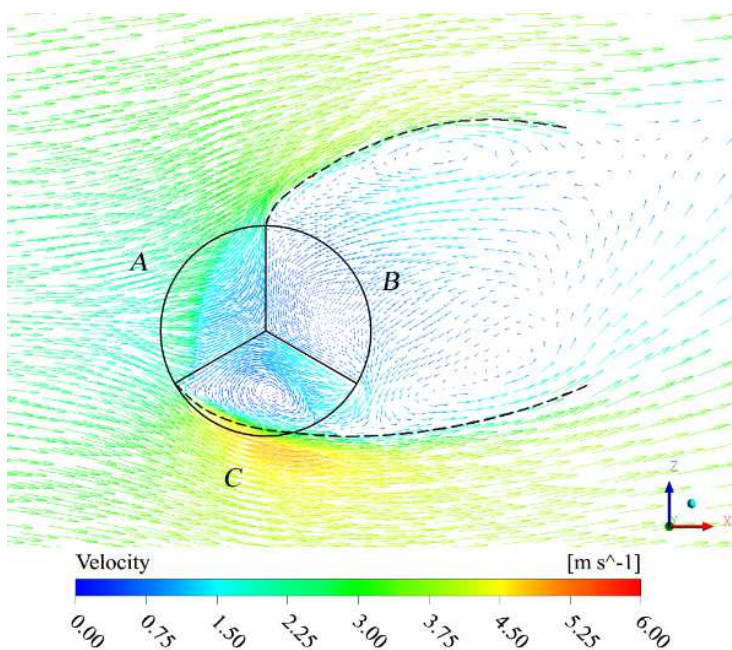
Figure 5.10. The time-averaged horizontal velocity components at y=2.5 m, an attack angle of 30° and a crosswind speed of 4 m/s.

The magnitude of vorticity, which is a measure of the local spinning motions of air, is introduced to help in understanding the distribution of the vortices and the wake flow structure. Figure 5.11 shows the vorticity contours at the horizontal plane of y=2.5 m at different angles of attack under a crosswind speed of 4m/s. The vorticity in the wakes of windbreak walls is generally higher than those in the ambient air, and it is especially strong along the free-wake boundaries and closer to the wall tips. In these areas, the velocity gradients are much higher, causing the shear stress to increase dramatically. If the free-wake boundaries are located inside a sector, the strong shear force near the

boundaries substantially dominate the air flow field in this sector by inducing a large-scale circulation of air movement in the wake of this leading wall. In Figure 5.11, this phenomenon is clearly visible in sector C in cases of attack angles of 30° to 50°.

The air flow underneath the heat exchangers at y=2.5 m is influenced by not only the separation but also the lifting effect of buoyance force. Unlike the shear stress, the lifting force tends to regulate the air flow by drafting air moving upward through the heat exchanger. Sectors without significant shear stresses experience relatively low vorticity despite the sectors falling into the wake zones, such as sector B in Figure 5.11. The vortices in the leading edge of windward sector A relate to a reverse suction effect of the heat exchangers, as discussed in Chapter 4.
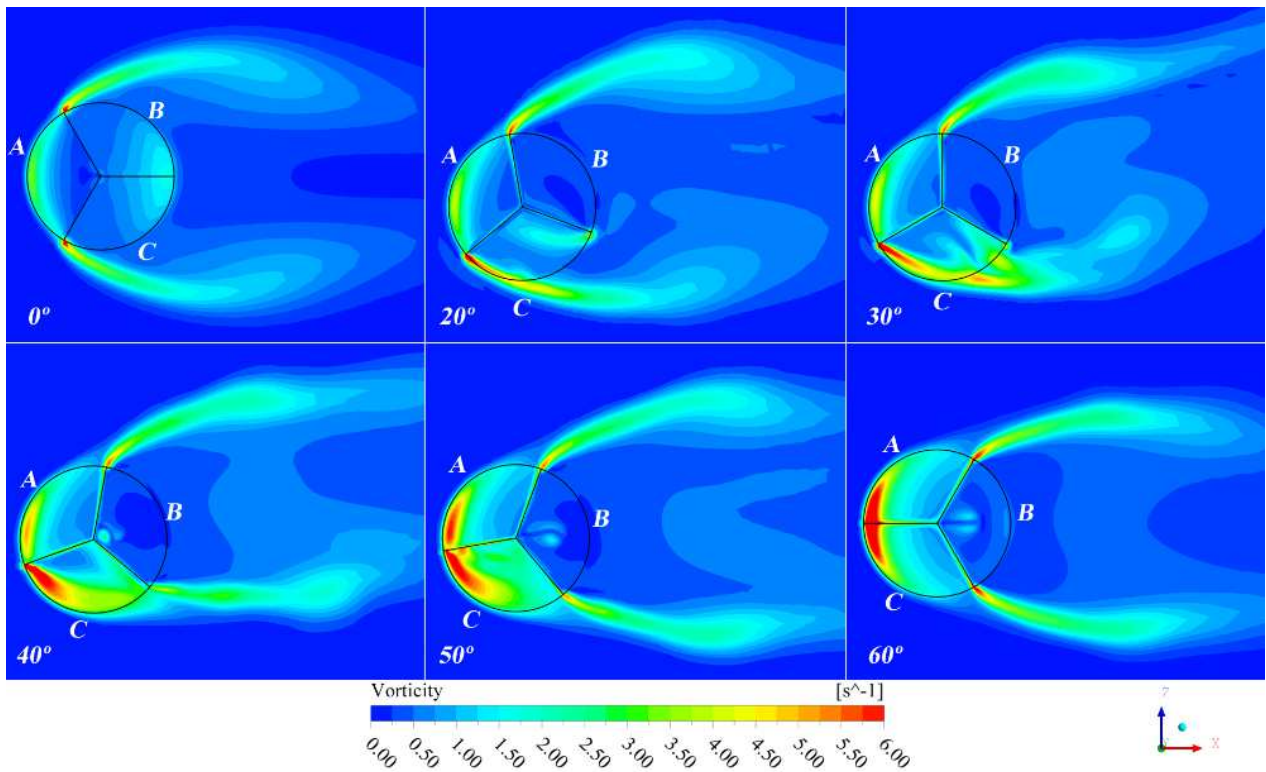
Figure 5.11. The vorticity contour at plane y=2.5 m for a crosswind speed of 4 m/s and at different wind attack angles as indicated.

The larger magnitude of local vorticity indicates a more severe spinning of the air nearby which consequently implies that lower air pressure occurs and vice versa. According to the working principles of a cooling tower with horizontally arranged heat exchangers [3], the variation of the inlet pressure in a given zone of heat exchangers directly influences the air flow rate through the heat exchanger bundles and consequently the heat transfer rate in that zone. Figure 5.12 plots the contours of the air pressure, P, in the surface under the heat exchangers at different angles of attack, while Figure 5.13 shows the corresponding locally averaged heat flux, q_r, in the upper surface of the

heat exchangers. The distributions of the net heat transfer rate Q_r can then be calculated by applying Eq. (5.11).
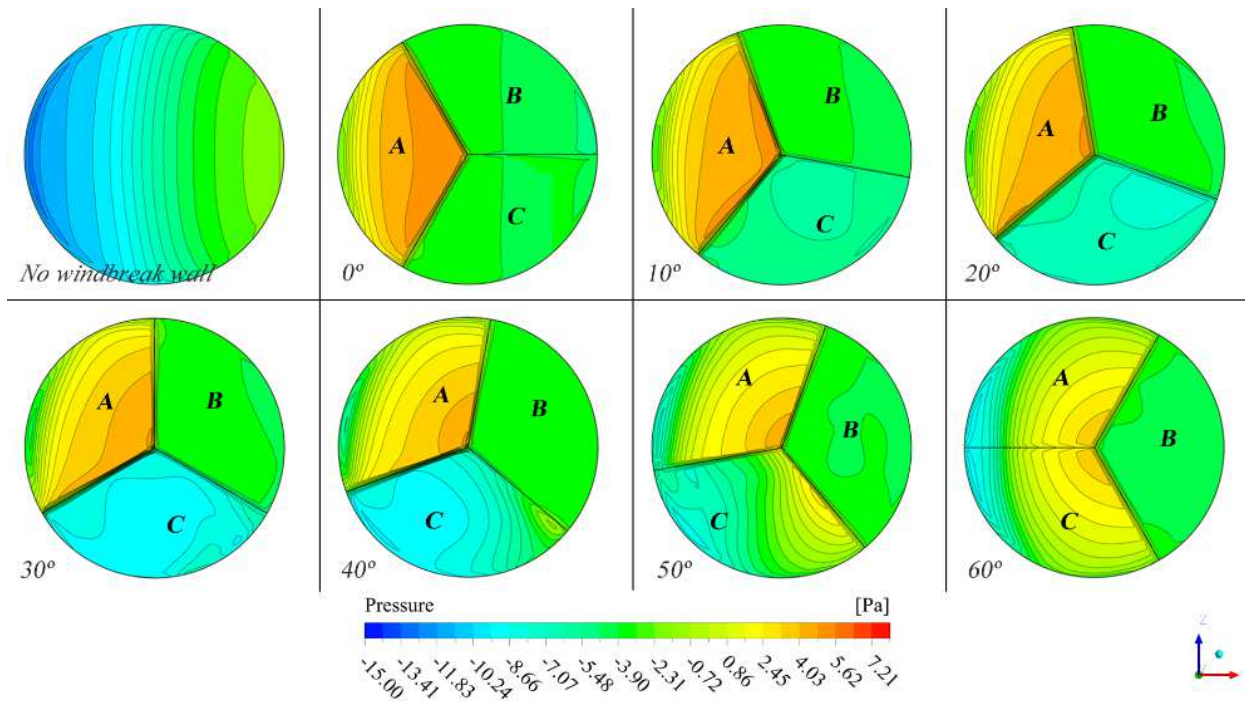
Figure 5.12. Pressure P contours at a surface 1 cm under heat exchangers at a crosswind speed of 4 m/s and at different wind attack angles as indicated.
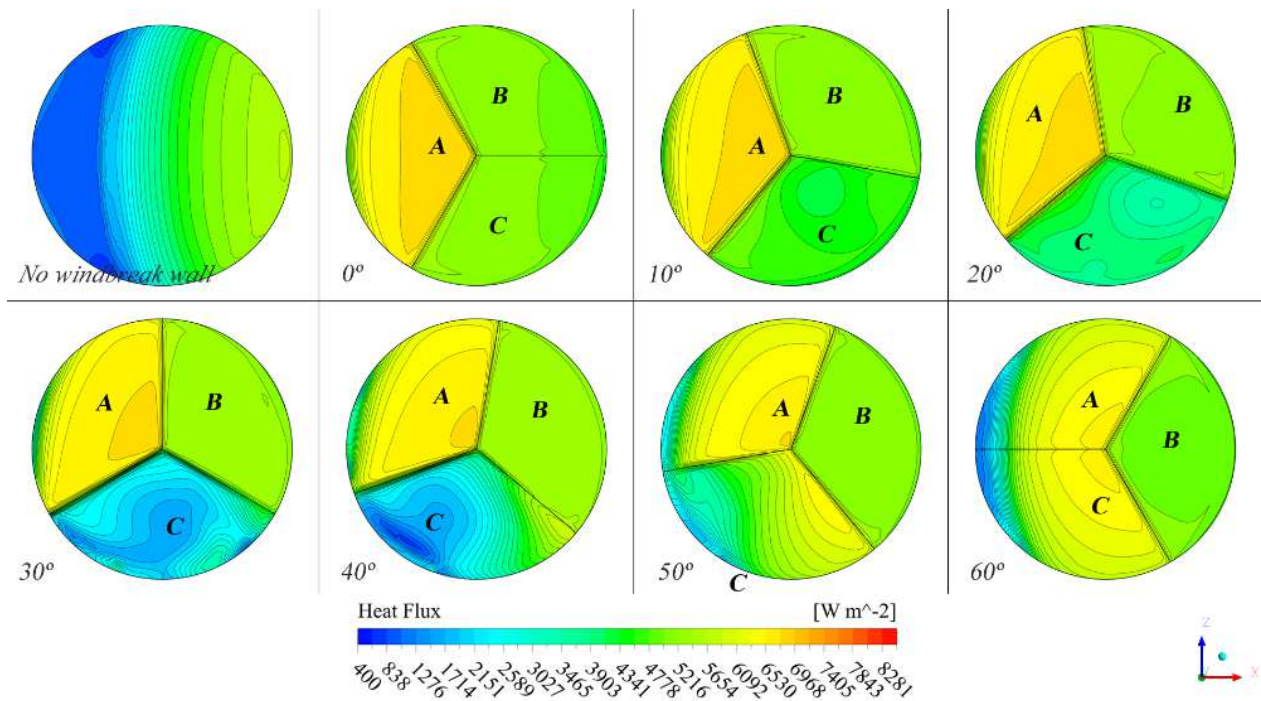
Figure 5.13. Heat flux q_r contours at heat exchanger upper face at a crosswind speed of 4 m/s and at different wind attack angles as indicated.

Clearly, low-value zones for P and q_r are observed at positions of high vorticity. The heat transfer performance in sectors facing or mainly facing toward the oncoming wind (e.g. sector A in all cases) has been significantly enhanced compared to the same areas with no windbreak walls since both the air flow rate and pressure in this area are increased, which can be understood from the streamlines (Figure 5.7) and pressure distributions (Figure 5.12). By contrast, the laterally facing sectors (sector C in cases 20°, 30°, and 40°) suffer reduced P and the q_r for the opposite reason, causing a lower overall heat transfer rate of the entire cooling tower.

5.3.2. Effect of wind speeds

For different crosswind speeds at the same wind attack angle, the vortices at y=2.5 m are shown in Figure 5.14 for the attack angle of 30°. With the existence of wall B-C, the wake of wall A-C is confined within sector C at a wind speed of 1m/s. As a result, the shedding vortices accumulate in this region rather than dissipate downstream, forming a great local circulation of air flow. The circulation reduces the local air pressure and therefore yields less air flow through the heat exchangers. As the crosswind speed increases, the air circulation expands gradually until it covers the whole area of sector C when the crosswind speed is 3m/s. However, a further increase in the wind speed causes the wake of the wall A-C to extend out of sector C so that vortices can dissipate far downstream of the cooling tower and the large local circulation shrinks. As a result, the air flow rate through the heat exchangers recovers.

Concerning the local heat flux distributions (Figure 5.15), increasing crosswind speeds boost the heat transfer rate in sector A, where the upward air flow rate and pressure underneath the heat exchangers are both enhanced. Meanwhile, the cooling performance is also improved slightly in sector B, benefiting from the extension of the separated flow areas of both walls A-B and A-C. Because the low-velocity zone is enlarged, providing more intake air for this sector. However, a low heat flux zone appears in sector C because of the large local air circulation. The q_r in this sector experiences a turn-around process along with increasing crosswind speed.
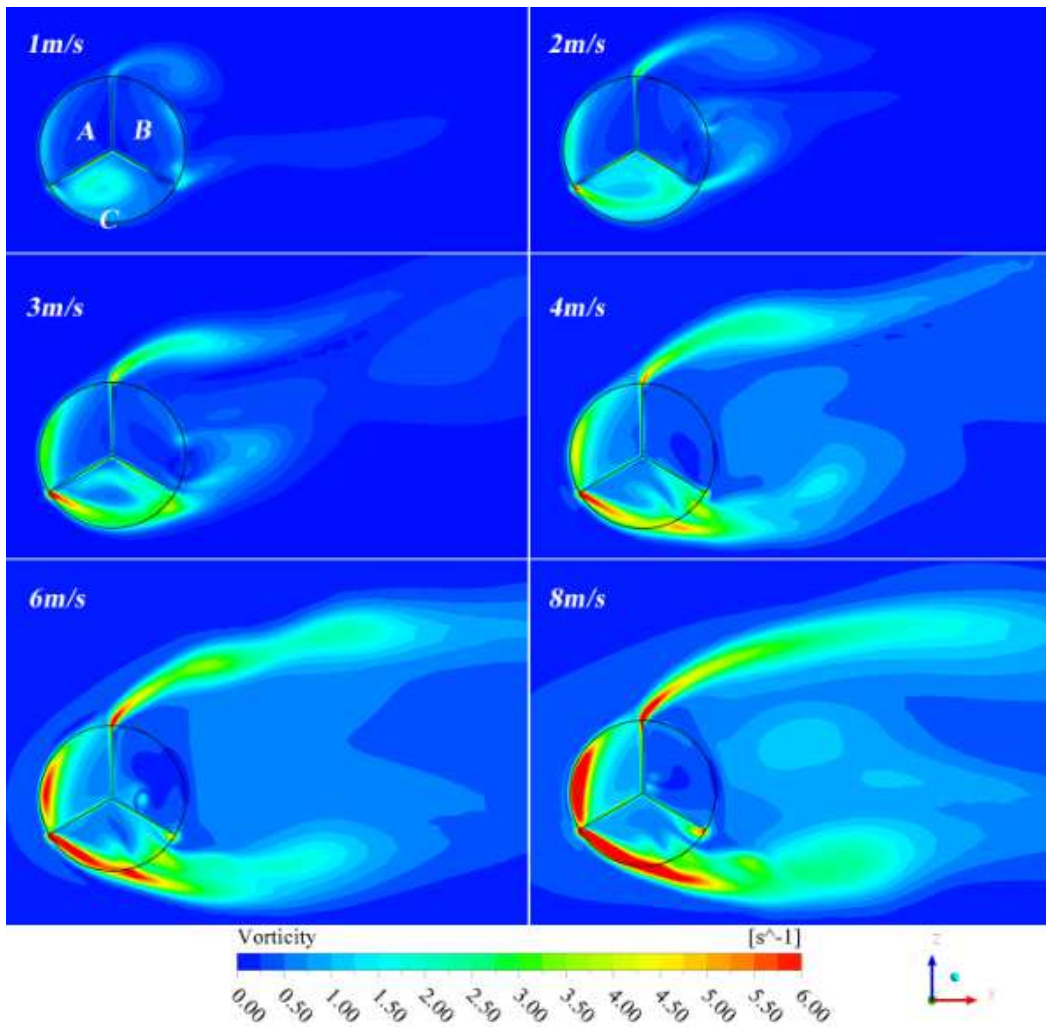
Figure 5.14. The vorticity contour at plane y=2.5 m for a wind attack angle of 30° at different crosswind speeds as indicated.
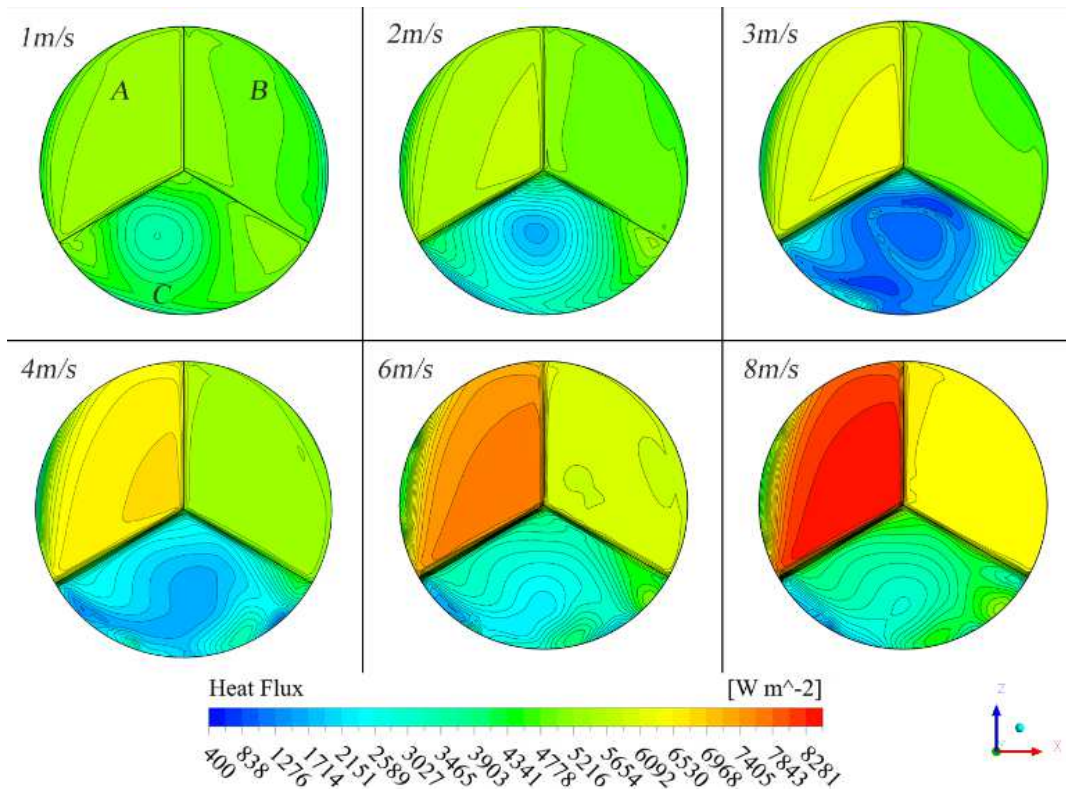
Figure 5.15. Heat flux q_r contours at the heat exchanger upper face for a wind attack angle of 30° at different crosswind speeds as indicated.

The variation of the overall heat transfer rate of the cooling tower Q_r at different crosswind speeds is therefore subject not only to increased heat transfer in sectors A and B but also the decrease in sector C. By integrating the local heat flux q_r over the entire heat exchanger area using Eq. (5.11), it is found that the minimum Q_r occurs at the wind velocity ratio of 8 with a arrangement of the windbreaks at the attack angle of 30°. For $\delta >8$, the total air flow rate, m_a, across the heat exchanger surface starts to increase, resulting in the enhancement of cooling performance. In fact, the results at other attack angles follow the same trend, which explains the existence of critical wind speeds for both the m_a and Q_r curves in Figures 5.5 and 5.6.

5.4. Conclusions

The influence of crosswind speed on the heat transfer performance of a small NDDCT equipped with tri-blade-like windbreak walls in the bottom has been studied using CFD numerical modelling. The overall heat rate Q_r of the tower was found to be significantly enhanced compared to that of the same tower without a windbreak wall when the velocity ratio of air δ was over 10. For the short tower examined in this study, this velocity ratio corresponds to crosswind speeds larger than 4 m/s. The results confirm the benefits of using windbreak walls for cooling performance in small NDDCTs with horizontally arranged heat exchangers. The variation of this benefit depends on the

structure of the turbulent airflow in the tower bottom, which in turn is sensitive to the orientations of the windbreak walls with respect to the crosswind velocity vector. The study also finds that:

1. The flow separation causes the forming of vortices in the wake of the windbreak walls. The vortices with high magnitude of vorticities waste the majority of the kinetic energy of the air flow, resulting in reductions in the air pressure and the heat transfer rate of heat exchangers in these regions.

2. The increase of crosswind speed could consistently enhance the air flow and the cooling performance in the windward and leeward sectors of the cooling tower heat exchangers.

3. When the windbreak walls are arranged with wind attack angles of 0° and 10° with respect to the crosswind direction, the heat-dumping rate of the cooling tower is significantly higher than other angles at air velocity ratios of over 10. At the lower velocity ratios, the performance is slightly better for the attack angle of 50° or 60° and then 0°.

In general, the windbreak walls give the most beneficial performance at wind attack angles of 0° and 60° as they enhance the cooling rate of the heat exchanger over the entire range of crosswind speed. This implies that the tri-blade-like walls should be placed with one wall, i.e. one symmetry axis, always aligned with the dominant direction of the crosswind. The most practical implication of this result is that the findings can be used to determine the windbreak installation angles with respect to the most frequent direction(s) of the environmental crosswind in a given district. If there is no dominant crosswind direction, the results can be used to quantify the benefits of designing a rotatable windbreak wall fitted at the tower bottom under the heat exchangers.

Chapter 6 Experimental study of NDDCT performance with and without the windbreaks

6.1. Experimental objectives

The full size 3D CFD NDDCT models of the previous chapters predicted both the air flow field and the heat transfer in cooling towers subject to crosswinds. Comparisons with the data from the previous studies confirmed the validity of the approach. There is still an uncertainty on the how well the model will apply under conditions where no published data exist, for instance short towers subject to significant cross wind. The present chapter reports on an experimental study of a lab-scale tower under crosswind conditions. The objective of the experiment was to validate the crosswind performance modelling used in the previous chapters. A scaled natural draft dry cooling tower model was tested in a wind tunnel. An experimental schedule was designed to accomplish the following steps:

1. Measure the quantities (temperature, velocity, pressure and heating power) of the model cooling tower under various crosswind conditions.
2. Process the experimental data and compare them with the CFD results.
3. Visualize the air flow in and around the model tower with smoke.

6.2. Experimental design

6.2.1. Design of the Lab-Scale cooling tower

By using dimensional analysis, one can investigate similarity laws by which the results for lab-scale cooling tower models can be translated to corresponding results for full-size towers. It is possible to develop such similarity laws but it has been found that it was impractical to design an experimental set-up that would fully satisfy these similarity laws. This is explained in the following section.

6.2.1.1. Dimensional analysis

As seen in above chapters, the most interesting quantities in the performance quantification of natural draft dry cooling towers are the air mass flow rate m_a and the heat transfer rate Q. In practical testings, the air velocity v_a is measured so that m_a can be calculated.

In an investigation of appropriate scaling laws, the correlations of v_a and Q with their parameters are analysed first.

1. Kinetic correlation

Chapter 6

It is proposed that the air flow velocity v_a under crosswind condition is a function of the hot air velocity in pure natural convection condition (no crosswind) v_{aN}, cross wind velocity v_{cw}, inlet and outlet air densities, tower height, tower diameter, gravitational acceleration, and viscosity,

$$v_a = f(v_{aN}, v_{cw}, \rho_{ai}, \rho_{ao}, H, D, g, \mu) \tag{6.1}$$

The number of the variables in Eq. (6.1) can be reduced through the dimensional analysis so that the equation can be nondimensionalized because:

- A simpler experimental design would suffice because there would be fewer independent variables to investigate; and

- Data from tests with small towers can be converted to expectations for large towers by using the dimensionless number definitions.

All the dimensions appearing in the variables in Eq. (6.1) are listed in Table 6.1:

Table 6.1 List of dimensions in Eq. (6.1)

Variables	v_a	v_{aN}	v_{cw}	ρ_{ai}	ρ_{ao}	H	D	g	μ
Dimensions	LT^{-1}	LT^{-1}	LT^{-1}	ML^{-3}	ML^{-3}	L	L	LT^{-2}	$ML^{-1}T^{-1}$

There are totally three independent dimensions $\{M, T, L\}$ in Eq. (6.1). According to the Buckingham pi theorem, the nine variables can be reduced to six dimensionless variables (Πs) by three independent variables which do not form a dimensionless variable among themselves– v_{aN}, ρ_{ai}, and H [74]. The six Πs are constructed following the theorem and some engineering judgment:

$\Pi_1 = \frac{v_a}{v_{aN}}$, $\Pi_2 = \frac{v_{cw}}{v_{aN}}$, $\Pi_3 = \frac{\rho_{ao}}{\rho_{ai}}$, $\Pi_4 = \frac{H}{D}$, $\Pi_5 = \frac{gH}{v_{aN}^2}$, and $\Pi_6 = \frac{\rho_{ao}Dv_{aN}}{\mu}$. Here Π_5 is actually the Froude number Fr based on tower height H, and Π_6 is Reynolds number Re of hot airflow based on the tower diameter D.

The above 5 dimensionless variables (Πs) form the dimensionless function that can replace Eq. (6.1):

$$\frac{v_a}{v_{aN}} = F(\frac{v_{cw}}{v_{aN}}, \frac{\rho_{ao}}{\rho_{ai}}, \frac{H}{D}, \frac{gH}{v_{aN}^2}, \frac{\rho_{ao}Dv_{aN}}{\mu}) \tag{6.2}$$

It is noted that v_{aN} is different from v_a in Eq. (6.2). The former is the upward air velocity inside the cooling tower in purely natural convection without crosswind, while the latter is the same air velocity under the crosswind conditions.

2. Thermal correlation

The total heat transferred in the cooling tower under crosswind conditions is subject to many parameters and essentially can be calculated using Eq. (3.12) in Chapter 3. However, in order to reveal its relation with crosswind and the tower size, a new correlation is proposed:

$$Q = f(Q_N, H, A, v_{cw}, v_{aN}, \mu) \tag{6.3}$$

where Q, and Q_N are the total heat dumped by heat exchangers in the presence of crosswind and without crosswind, respectively. A is the total frontal area of heat exchangers.

Eq. (6.3) implies that without knowing the actual temperature difference or the convective heat transfer coefficient, the heat dumping rate of the cooling tower under crosswind conditions can be expressed based on the heat rate and buoyancy-induced velocity in windless condition, i.e. Q_N and v_{aN}, tower dimensions and crosswind speed. Following a procedure similar to that above, Eq. (6.3) has been nondimensionalized. There are 3 dimensions in Eq. (6.3) which indicates the 7 variables can be reduced to 4 dimensionless parameters. By analysis, the four Πs are $\Pi_1 = \frac{Q}{Q_N}$, $\Pi_2 = \frac{H^2}{A}$, $\Pi_3 = \frac{v_{cw}}{v_{aN}}$, and $\Pi_4 = \frac{\rho_{ao} D v_{aN}}{\mu}$. Therefore, Eq. (6.3) is equivalent to the following dimensionless function:

$$\frac{Q}{Q_N} = F(\frac{H^2}{A}, \frac{v_{cw}}{v_{aN}}, \frac{\rho_{ao} D v_{aN}}{\mu}) \tag{6.4}$$

Eqs. (6.2) and (6.4) are two basic equations in dimensionless form which describe the behaviour of a NDDCT of any size under crosswind conditions. According to the scaling law, the scaled cooling tower model is completely similar to a full scale prototype tower if and only if all the dimensionless parameters in these equations have the same values for both [74]. The experimental model and the testing conditions are therefore designed and set up to ensure the similarity with a full-scale as much as possible. If the similarity is satisfied, the experiment results could be used to validate the CFD simulation results for the full-size prototype cooling tower. Next section describes whether and how this is achieved

6.2.1.2. Similarity/scaling laws

As discussed, the scaled model of the NDDCT in the wind tunnel testing should be designed obeying the scaling laws in order to achieve the complete similarity to the prototype CFD model. So, ideally, all the dimensionless parameters describing the physical behaviours of the problem in the scaled model tower need to be same as the corresponding ones in the prototype. These parameters

include not only the ones in Eqs. (6.2) and (6.4), but also others in all the governing equations. Therefore, the similarity criteria between the scaled cooling tower model and the prototype are determined as followings.

1. Geometric similarity

Both the Eqs. (6.2) and (6.4) involve the dimensionless parameters related to the geometric size: $\frac{H}{D}$, and $\frac{H^2}{A}$, which implies that the geometric similarity is crucial. The criteria are thus that all the corresponding parameters between the scaled tower and the prototype have the same scale ratio, namely:

$$\tau = \frac{(H)_m}{(H)_p} = \frac{(D)_m}{(D)_p} = \frac{(H_i)_m}{(H_i)_p} = const \qquad (6.5)$$

where τ is the scale ratio of the experimental model. The subscripts m and p denote "model" and "prototype", respectively.

With the correlation defined in Eq. (6.5), it automatically exists that $\left(\frac{H}{D}\right)_m = \left(\frac{H}{D}\right)_p$, and $\left(\frac{H^2}{A}\right)_m = \left(\frac{H^2}{A}\right)_p$.

2. Kinematic similarity

The velocity ratio, $\frac{v_{cw}}{v_a}$, in Eq. (6.2) requires the tower model to be kinematically similar to its prototype. The criterion is that the corresponding velocities in model and prototype follow the scaling law:

$$\left(\frac{v_{cw}}{v_a}\right)_m = \left(\frac{v_{cw}}{v_a}\right)_p \qquad (6.6)$$

$$\left(\frac{v_{cw}}{v_{aN}}\right)_m = \left(\frac{v_{cw}}{v_{aN}}\right)_p \qquad (6.7)$$

3. Dynamic similarity

The dimensionless velocity correction in crosswind condition (Eq. (6.2)) involves Froude number Fr and Reynolds number Re. Therefore these two parameters should be considered in the dynamic similarity criteria.

Since the heat transfer in a NDDCT is essentially a natural convection problem, the momentum equation describing the air motion in the airflow can be rearranged specifically as following:

Chapter 6

$$\rho_0 \frac{dV}{dt} = \rho_0 g\beta(T - T_0)\widehat{k} - \nabla P + \mu\nabla^2 V \tag{6.8}$$

where $\widehat{k}$ is the unit vector in z direction. ρ_0 is the ambient air density. The term $\rho_0 g\beta(T - T_0)\widehat{k}$, which applies the Boussinesq's approximation, is the net buoyancy force only in z direction

Eq. (6.8) has 4 basic dimensions $\{M, T, L, \Theta\}$ all together. It can be nondimensionalized through the 4 reference constants–the characteristic velocity V, characteristic length L, characteristic temperature T_r, and characteristic pressure ΔP_r. And let $V = v_{cw}$, $L = H$, and $T = T_r$ and $P = \Delta P_r$. Therefore each of the variables in the equation has its dimensionless form denoted by a superscript *:

$$V^* = \frac{V}{V}, \nabla^* = L\nabla, \nabla^{2\,*} = L^2\nabla, t^* = \frac{tV}{L}, T^* = \frac{T-T_0}{T_r-T_0}, P^* = \frac{P}{\Delta P_r} \tag{6.9}$$

Rearrange these equations and then substitute them into Eq. (6.8), yielding:

$$\frac{dV^*}{dt^*} = \frac{g\beta(T_r-T_0)L}{V^2}T^*\widehat{k} - \frac{\Delta P_r}{\rho V^2}\nabla^* P^* + \frac{\mu}{\rho VL}\nabla^{2*}V^* \tag{6.10}$$

Eq. (6.10) can be simplified as following equation:

$$\frac{dV^*}{dt} = \frac{Gr}{Re^2}T^*\widehat{k} - Eu\nabla^* P^* + \frac{1}{Re}\nabla^{2*}V^* \tag{6.11}$$

where $Gr = \frac{g\beta(T_r-T_0)\rho^2 L^3}{\mu^2}$ is the Grashof number and $Eu = \frac{\Delta P_r}{\rho V^2}$ is the Euler number. Eq. (6.10) is the dimensionless momentum equation.

The dynamic similarity forms when the dimensionless momentum equations are same for both the model tower and the prototype. So all the dimensionless parameters should obey the relations below:

$$(Re)_P = (Re)_m, (Gr)_P = (Gr)_m, (Fr)_P = (Fr)_m, (Eu)_P = (Eu)_m \tag{6.12}$$

However, it is nearly impractical to satisfy all of these constraints at the same time. For example, $(Re)_m$ decreases with the geometrical size H. In order to get the same $(Re)_m$ as $(Re)_p$ for the case when the hot air velocity is $(v_{aN})_p$ in the prototype cooling tower, the $(v_{aN})_m$ in the wind tunnel should be $\frac{1}{\tau}(v_{aN})_p$. The scale ratio τ in this experiment is 1/12.5, and $(v_{aN})_p$ is around 0.38 m/s according to the CFD result. So $\frac{1}{\tau}(v_{aN})_p$ could be 4.75 m/s, which far exceeds the possible natural draft speed of current lab-scale cooling tower model.

Approximations and compromises can be made in this experiment. In fact, the Reynolds numbers based on the crosswind speed and tower height are in the order of magnitude of 10^5 and 10^6 in the tower model and the prototype, respectively. Referring to Eq. (6.10), such large Reynolds numbers

make the viscous term negligibly small. And the air motion is thus dominantly driven by the inertial force and buoyancy force (in z-direction). Therefore, it is not necessary to have strict equality between the model and prototype Reynolds numbers but it is only required to maintain a large tower-model Reynolds number in above order of magnitude so that some approximate similarity in the momentum equations can be achieved. This statement matches the findings of the study in [75] which reported that the airflow in a NDDCT becomes independent of Reynolds number when the Reynolds number inside the tower is larger than 3×10^4.

The Grashof numbers do not have to be identical either because of the difference in Reynolds numbers. On the other hand, the equality in Grashof numbers requires the completely similarity in the convective heat transfer of the heat exchanger. However, the natural convective heat transfer cannot be scaled only using the parameters that used in geometric and kinetic similarity. It is thus not considered in this experiment. In addition, in order to reflect the effect of air density difference, the densimetric Froude number Fr_D is considered in the similarity criteria instead of the normal Froude number Fr.

Consequently, the dynamic similarity criteria are as followings. And for convenience, the characteristic velocity in these criteria is replaced by the pure natural convection air speed inside the tower–v_{aN} so that the physical meanings of the equations are much clearer.

$$(Eu)_P = (Eu)_m = (\frac{\Delta P}{\rho v_{aN}^2})_m = (\frac{\Delta P}{\rho v_{aN}^2})_p \tag{6.13}$$

$$(Fr_D)_m = (Fr_D)_p = \left(\frac{v_{aN}^2}{\frac{\rho_0-\rho}{\rho}gH}\right)_m = \left(\frac{v_{aN}^2}{\frac{\rho_0-\rho}{\rho}gH}\right)_p \tag{6.14}$$

The equality in Euler number in Eq. (6.13) requires the total air pressure drop in the scaled tower model remaining at certain value. So the pressure drop through the heat exchanger model needs to be calculated and a mesh screen is used to provide extra resistance to the airflow, while pressure loss in other model parts is very small thus can be ignored.

The equalities of the dimensionless parameters in Eqs. (6.5), (6.6), (6.13), and (6.14) are the criteria for scaling the experimental cooling tower model, which are summarized in table below. A compromised similarity then will be satisfied between the experiment model and the prototype in CFD simulations.

The test rig has been designed to achieve similar dimensionless numbers when it is practically possible. However, the inability to achieve equality between the two Reynolds numbers and some others as described above means that the test model results cannot be directly used to validate the

CFD model for the full-scale prototype tower. Therefore, it has been decided to validate the CFD modelling approach by building a CFD model with the identical dimensions as the test rig. This will be discussed in Section 6.5, after the test model and the testing conditions are defined.

Table 6.2 List of the key scaling parameters

Scaling parameter	Physical meaning	Note
H/D	Ratio of tower height to base diameter	i.e. Aspect ratio of tower
v_{cw}/v_{aN}	Ratio of crosswind speed to upward air velocity inside the tower	i.e. Crosswind speed ratio
v_a/v_{aN}	Ratio between hot air velocities with and without crosswind	
$\dfrac{v_{aN}^2}{\dfrac{\rho_0 - \rho}{\rho} gH}$	Ratio of kinetic energy to potential energy of the upward airflow inside the tower	i.e. densimetric Froude number Fr_D
$\dfrac{\Delta P}{\rho v_{aN}^2}$	Ratio of pressure drop to kinetic energy of the upward airflow inside the tower	i.e. Euler number

6.2.2. Measuring techniques and error analysis

The key scaling parameters in Table 6.2 require the measurement of two basic quantities in the experiments: the air speed and temperature. The uncertainties involved in the scaled tower model experiments are caused by systematic and random reasons [76, 77].

Systematic uncertainties are related to the nature of physical problem being studied and the conditions of the test rig. Since the airflow in a NDDCT is driven by the natural convection effect, the distribution of quantities in the flow field is highly non-uniform and time dependent. This is especially true when testing a small tower. Moreover, the wind flow in the wind tunnel is not perfectly stable and uniform in spite of the filtering screens and straighteners preceding the test section. To reduce the effect of these systematic uncertainties, the following methods might be helpful:

- More measuring points in the region where airflow field is not uniform;

- Longer recording time to capture steady-state parameters while the experimental conditions are kept constant; and

- Avoiding sensor placement in regions such as wall boundary layers, heat exchanger tube wakes *etc*.

The random uncertainties in current experiment are primarily due to the noises in the data acquisition system and the unexpected problems in the sensors. Using the filter circuits in the system is an effective way to reduce the random uncertainties. The sensors with problems can be identified by a "cross check" that swap sensors in different points and run the measurements in same conditions and then compare the results.

Nevertheless, the uncertainties can only be reduced but not eliminated completely. So the error analysis is needed to estimate the uncertainties in the testings. Suppose X represents any quantity of temperature, velocity, pressure, or electric power measured in the scaled cooling tower testings, X has n recording data (X_1, X_2, X_3, … X_n) over a period of time in a measurement in which the flow condition is nearly constant. The extent of scatter in X can be quantified by the sample standard deviation s [77]:

$$s_X = \sqrt{\frac{\sum_{i=1}^{n}(X_i - \bar{X})^2}{n(n-1)}} \tag{6.15}$$

Therefore the uncertainty of the quantity X in this measurement is defined as [77]:

$$\sigma_X = \frac{s}{\sqrt{n}} \tag{6.16a}$$

or

$$\varepsilon_X = \frac{s}{\bar{X}\sqrt{n}} \tag{6.16b}$$

where σ_X and ε_X are the uncertainty and percent uncertainty of the quantity X.

The uncertainties of directly measured quantities will be propagated in the following calculations of the parameters which are functions of these quantities. For instance, if the calculated parameter $F = f(X, Y, Z)$, the uncertainty of F is estimated by following equation [77]:

$$\sigma_F = \sqrt{\sigma_X^2 \left(\frac{\partial f}{\partial X}\right)^2 + \sigma_Y^2 \left(\frac{\partial f}{\partial Y}\right)^2 + \sigma_Z^2 \left(\frac{\partial f}{\partial Z}\right)^2} \tag{6.17}$$

where σ_X, σ_Y, and σ_Z are uncertainties for X, Y, and Z, respectively. And the partial derivatives are all calculated using the arithmetic means of the relevant quantities.

6.3. Testing apparatus and instrument

6.3.1 Cooling tower model

The scaled model of the 15 m-high NDDCT in Chapter 4 is designed following the similarity criteria in Section 6.2.1. The tower model consists of three major components: the cylindrical tube as the cooling tower body, the circular finned-tube electric heater as the heat exchangers and the stand as the tower base supports, as shown in Figure 6.1.
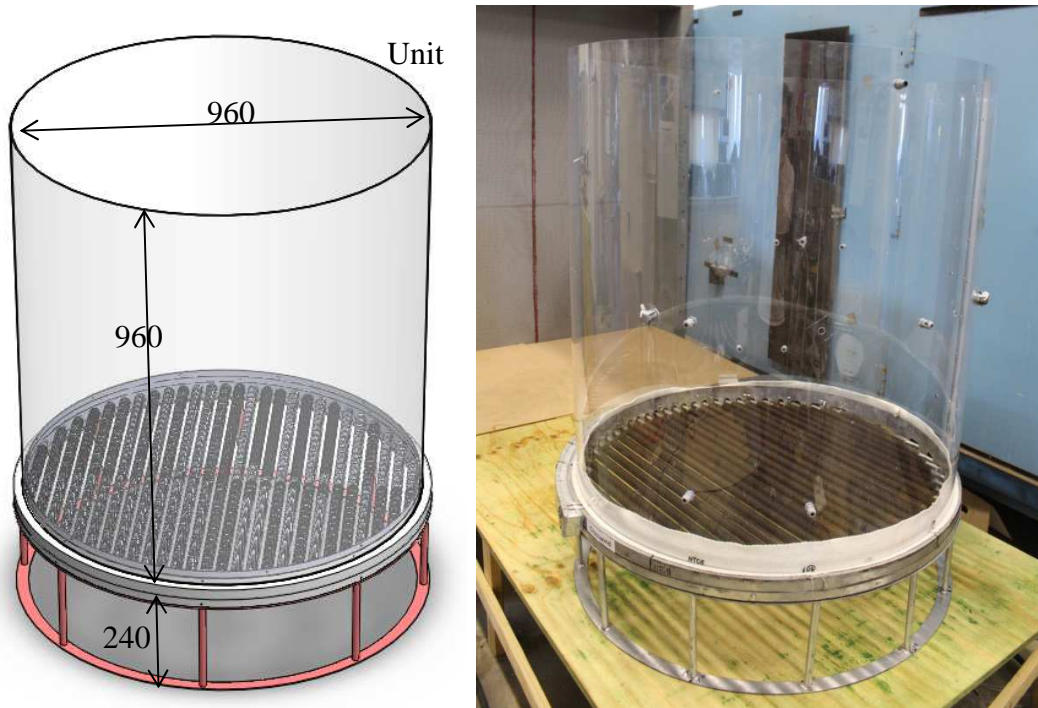
Figure 6.1. The dimensions of the scaled cooling tower model

The scale ratio τ defined in Eq. (6.5) is therefore calculated in Eq. (6.18) and the geometrical dimensions of the tower model excluding the heater are listed in Table 6.3 below:

$$\varphi = \frac{(H)_m}{(H)_p} = \frac{(D)_m}{(D)_p} = \frac{1.2m}{15m} = \frac{0.96m}{12m} = \frac{1}{12.5} \tag{6.18}$$

Table 6.3 Specifications of the model tower body excluding the heater

Parameter	Size	Note
Total tower height (m)	1.2 ± 0.01	Satisfy the scale ratio τ
Tower diameter (m)	0.96 ± 0.03	Satisfy the scale ratio τ
Tower inlet height (m)	0.24 ± 0.002	Stand height. Satisfy the scale ratio

Support diameter (mm)	12 ± 0.01	Satisfy the scale ratio τ
Tower shell thickness (mm)	3	Thickness of the transparent sheet which makes the cylinder. Not satisfy τ. Material: clear polycarbonate.

It is noted that all parameters are in the ratio of 1/12.5 expect the tower shell thickness, since the influence of tower shell thickness on the inlet pressure loss of the cooling tower is negligible [71]. The aspect ratio H/D is equal to 1.25 which should be exactly same as the one in prototype tower.

6.3.2. Heater and its control

A round electric heater is applied as the model of horizontally arranged flat heat exchangers in the prototype cooling tower of the CFD simulations. The heater contains 27 heating spiral-fin tubes of different lengths. All of the heating tubes are arranged in a plane with a constant spacing between any two tubes, as seen in Figure 6.2.

Figure 6.2. The round electric heater

The key manufacturing parameters of the heater are shown in table below:

Table 6.4 The specifications of the electric heater

Parameters (mm)	Size	Note
Tube diameter d_o	13 ± 0.2	Same as fin root diameter d_r

Tube length L_t	-	Varies depending on the position of the tube
Fin thickness t_f	0.65 ± 0.05	
Fin pitch p_f	2.4 ± 0.2	
Fin diameter d_f	24.8 ± 0.2	
Heater diameter d_{hx}	950 ± 4	Inner diameter
Tube pitch p_t	35 ± 2	Transversal pitch
Heater height H_{hx}	80 ± 1	
Frame width	6 ± 2	

The geometric dimensions of the heater do not satisfy the scale ratio τ with its prototype because the heat transfer and pressure loss cannot be scaled up simultaneously while the velocity ratio v_{cw}/v_{aN} is already in scale. In fact, the dimensions of the heater are designed with the purpose that the pressure drop coefficient through the finned tube elements K_h can be calculated by following correlation [78]:

$$K_h = 2.271 Re_c^{-0.325} \left(\frac{P_t}{d_o}\right)^{-1.849} \frac{A_a}{A_c} \tag{6.19}$$

where Re_c is the Reynolds number based on the minimum flow area of the heater A_c. A_a is the total air surface area of the heater.

Apparently the single tube row heater cannot provide the entire pressure drop which is required by the similarity of Euler number in Eq. (6.13), as the heater exchanger in the prototype cooling tower has 4 rows of tubes. The extra pressure loss is introduced by a mesh screen placed above the heater as discussed below.

6.3.3. Mesh screen

A mesh screen is used just above the heater to provide more resistance to the airflow in the scaled tower model. The screen is a round plate with an outer diameter of 960 mm and a total thickness of 4.62 mm, as shown in Figure 6.3.
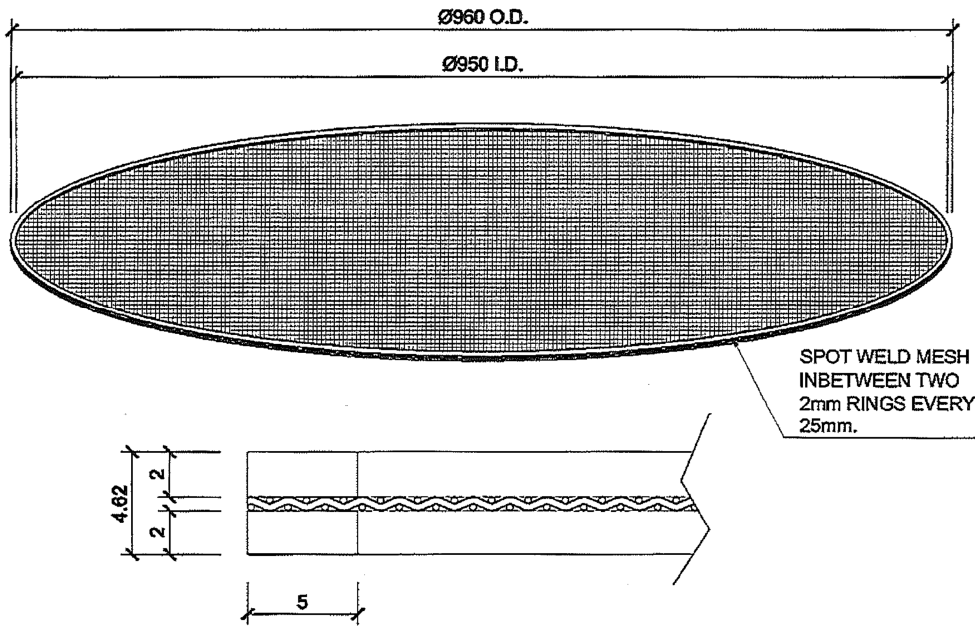
Figure 6.3. The dimensions of the mesh screen

The mesh is woven using stainless wires of 0.31 mm diameter with the aperture of 0.53 mm (30 mesh / 30 swg). The pressure loss coefficient K_m through the mesh can be estimated by the following correlation [79]:

$$K_m = \left(\frac{1}{C^2}\right)\left(\frac{1-\alpha^2}{\alpha^2}\right) \tag{6.20}$$

Where α is the permeability of the mesh screen, and C is discharge coefficient, which is given as a function of Reynolds number Re_D, namely: $C = 0.1\sqrt{Re_D}$. Here Re_D is based on the aperture of the mesh.

6.3.4. Wind tunnel

An open circuit blower type wind tunnel is used in the experiment. The tunnel consists of seven main parts: air intake fan, diffusing section, setting section, working section, exit diffusing section, and exhaust fan, as seen in Figure 6.4. The intake fan is a centrifugal blower driven by a 75 kW motor with the capacity to deliver up to 20 m^3 air per second [80]. The diffusing section and the setting chamber altogether contain eight screens and one honeycomb. The former are able to prevent the separation of the boundary layer and produce a uniform wind in the tunnel profile while the latter eliminates the swirl and lateral velocity from the air flow [80]. The air flow is thus ensured to uniformly spread out in the whole cross-section of the working section.
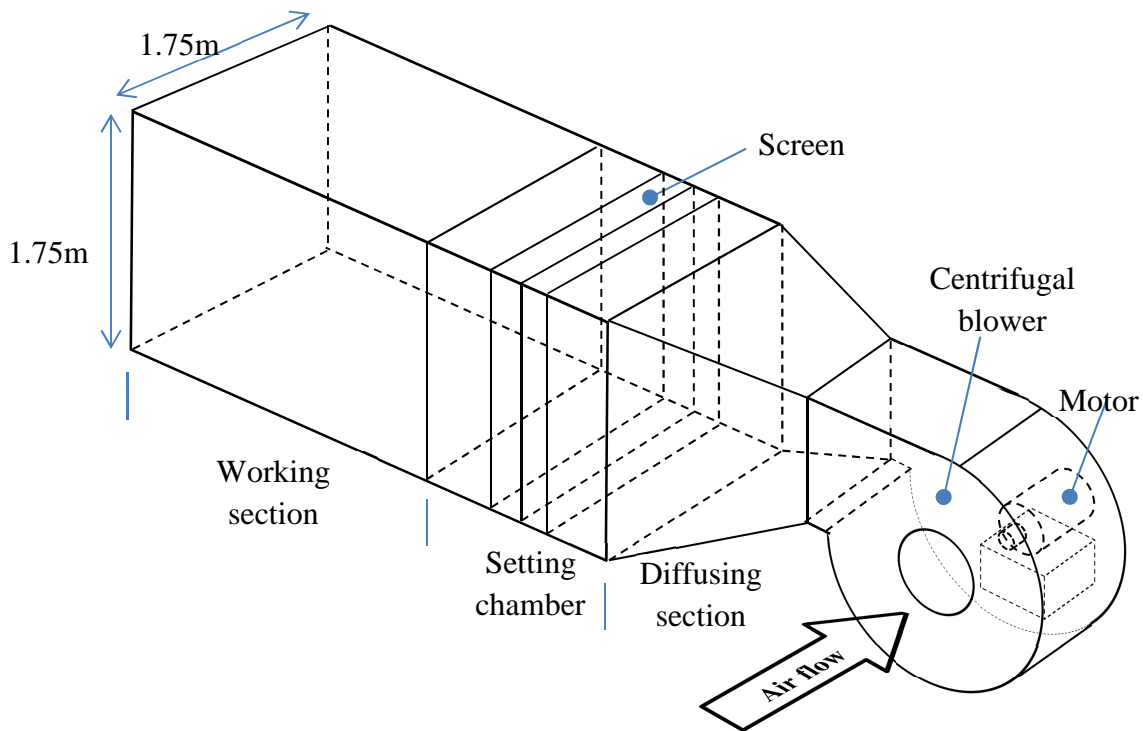
Figure 6.4. A schematic drawing of the wind tunnel (the exit diffusing section and exit section are not shown in this figure)

The working section where the cooling tower model is placed has a length of 8 m and the cross-section of 1.75m by 1.75m. The air speed in this section can reach up to 6.9 m/s theoretically when both the intake and exhaust fans operate at their maximum speeds. Figure 6.5 illustrates the position of the scaled cooling tower model.
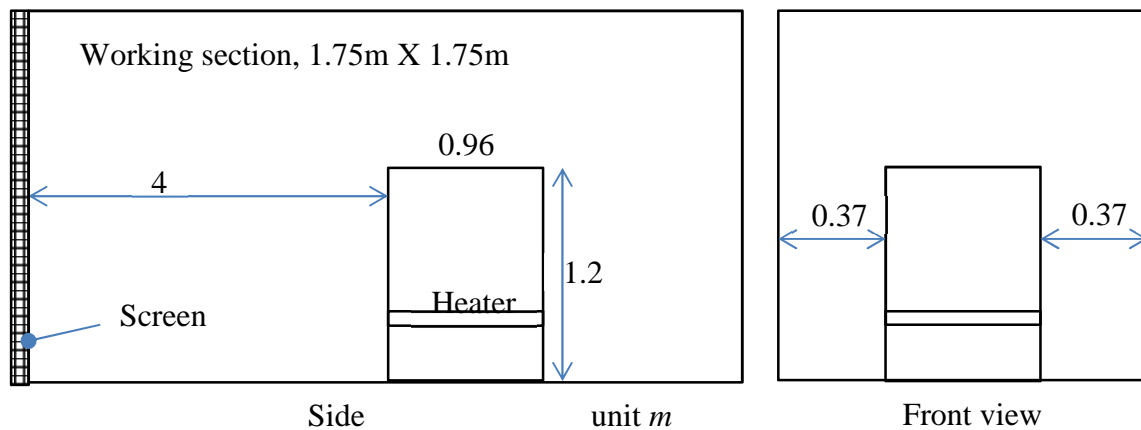
Figure 6.5. The position of the scaled cooling tower model in the wind tunnel.

The clearance between tower top and the ceiling of tunnel is around 0.55 m, while the distances to each tunnel side wall are 0.37 m. The tower model is placed 4 m away from the last screen which

well exceeds the 0.5 hydraulic diameter of the section so that the non-uniformities of the air flow are reduced below an acceptable level [81].

It is noted that the clearance above the tower top is less than one tower height, which may influence the dissipation the hot air under windless or low wind speed condition. Therefore, tests without the working section are also be implemented in order to give the comparisons. This will be discussed in Section 6.4.4 in detail.

6.3.5. Sensors and data acquisition system

According to the experiment design, physical quantities which are needed to be measured in the scaled cooling tower testing are air temperature, velocity, pressure, and the electrical power of the heater. These quantities are tested by the sensors in below table:

Table 6.5 The list of sensors

Quantities measured	Sensors/apparatus	Measuring range	Uncertainty/ Accuracy	Response time (s)
Air temperature	thermistor	0-150 $°C$	±0.2 $°C$	
	RTD	0-150 $°C$	±0.2 $°C$	
Air velocity	Hot-wire anemometer (OMEGA)	0-5.08 m/s	±1.5%	0.25-2
	Hot-wire anemometer (TSI)	0-30 m/s	±3%	
Static pressure	transducer	0-50 Pa	±0.1 Pa	0.1
current	Digital voltage/ampere meter	0-90 A	±0.5%	1.2 s (Refresh time)
voltage	Digital voltage/ampere meter	0-500 V	±0.5%	As above

All the sensors are integrated in a data acquisition/ control system, the schematic diagram of which is shown in Figure 6. The temperature sensors are arranged in five different levels inside the cooling tower, while the velocity and pressure sensors are mainly in the middle level of the tower body.

The electric heater is controlled by the computer generating a micro current signal through the signal generating module. This current ranges in 4-20 mA. Then this signal is transmitted into the power regulator in the heater control panel which converts the current signal to the corresponding voltage output. Therefore the working voltage of the heater is a function of the control signal. The real time voltage and current of the heater is independently monitored and logged by a digital power meter, to calculate the actual real time electric power. Figure 6.7 shows the correlation between the input control signal and the heater electric power.

The data acquisition (DAQ) comprises of an UIE (United Electronic Instruments) Power DNA serials gigabit-class Ethernet I/O module, one 8-ports analogue voltage input board, and two 8-ports analogue current input boards. The hardware co-works with a software user interface developed on the Labview system as seen in Figure 6.8. The temperature, velocity, and pressure data is acquired through analogue input boards, while the communication between the computer and the power meter is conducted through the RS-485 serial ports under the MODBUS® protocol [82].
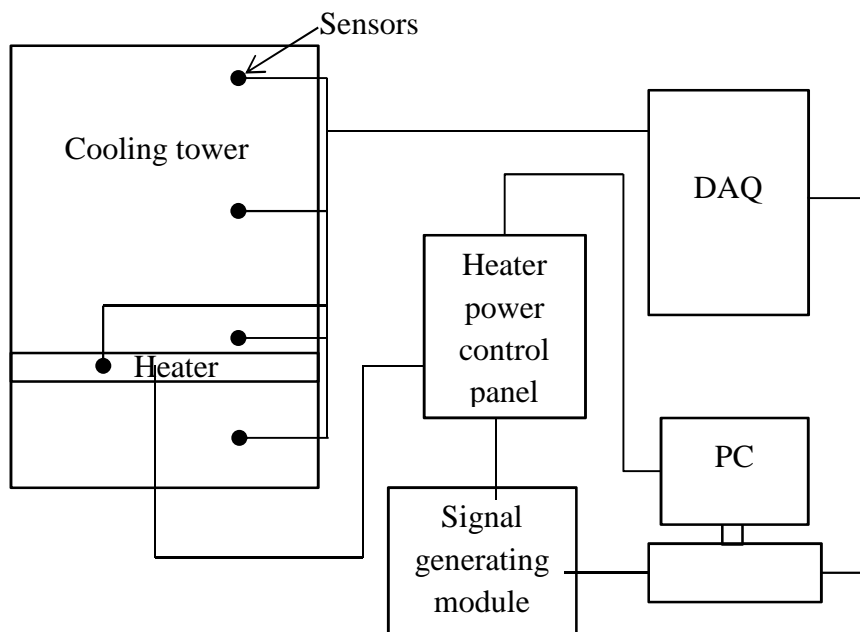
Figure 6.6. The sketch of the data acquisition and control system
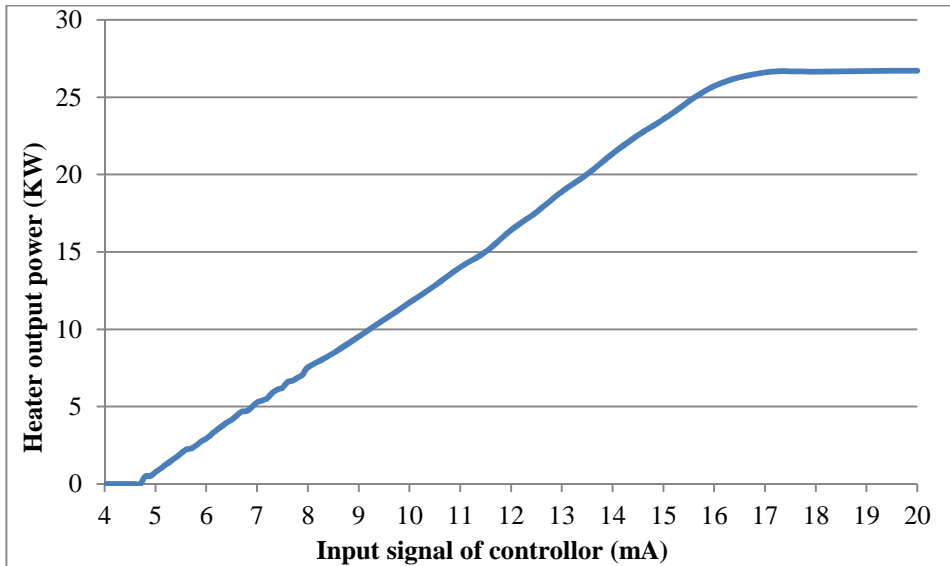
Figure 6.7. The actual correlation of heater power with the input control signal
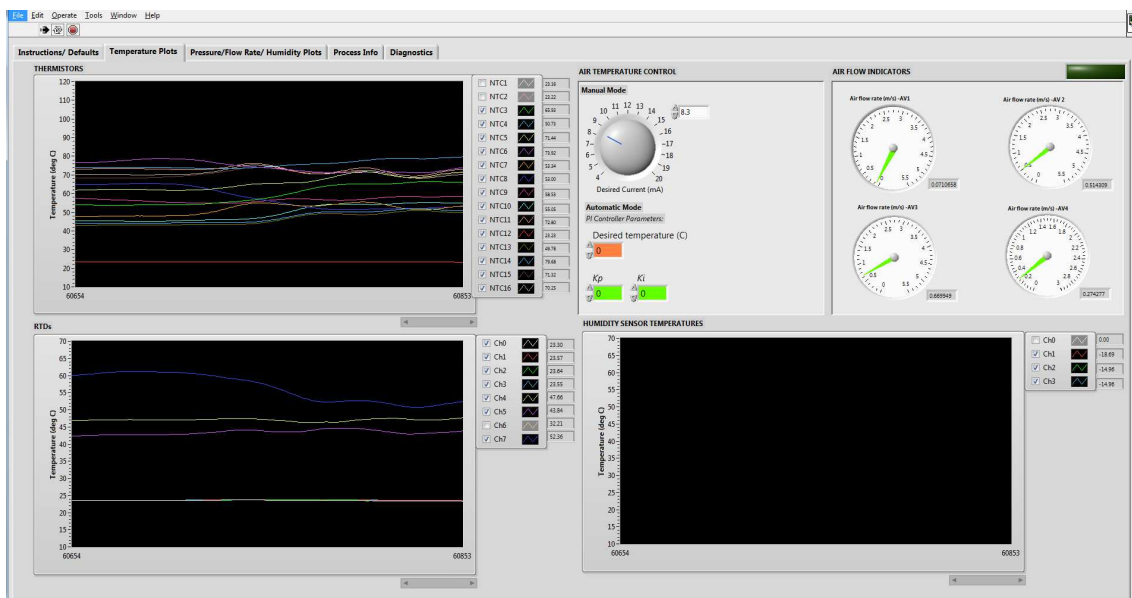
Figure 6.8. The user interface of the data acquisition system

6.4. Testing methods

6.4.1 Sensor position

The sensors are positioned at five different levels in the tower model: top, middle, bottom, heater level, and underneath the heater. Figure 6.9 shows their locations.
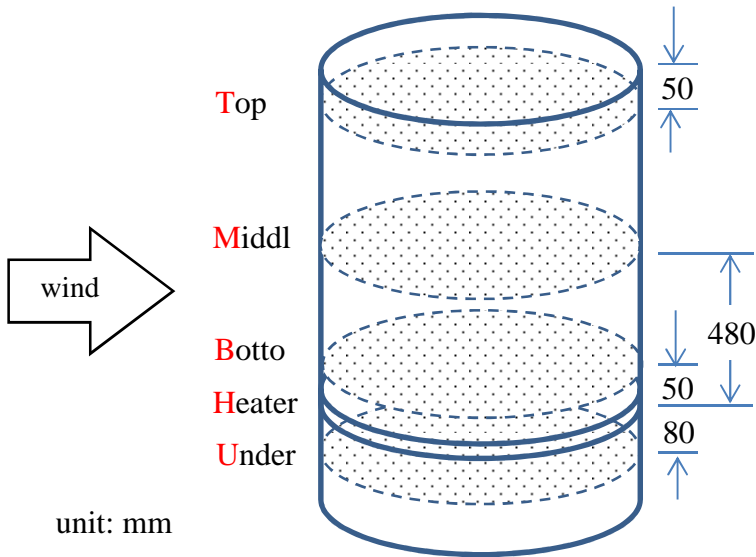
Figure 6.9. Five levels for sensor position
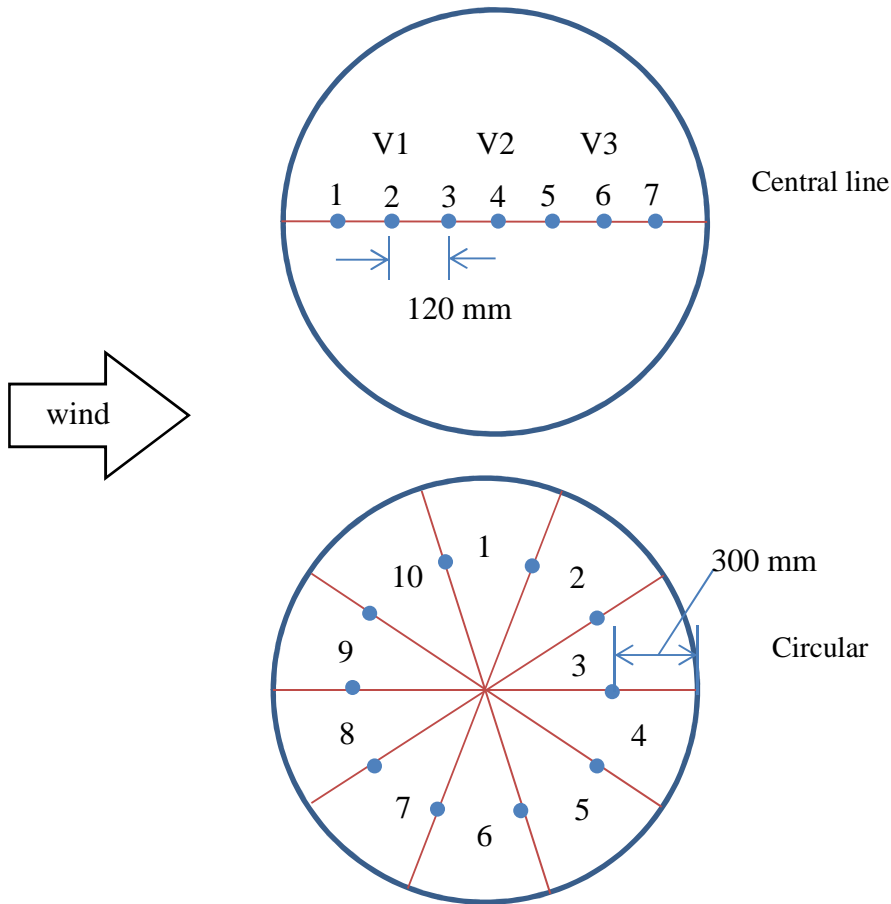
Figure 6.10. The sensors layout at levels except for the heater level

In any level except the heater level, the sensors can be arranged in two different layouts, as shown in Figure 6.10. The central line layout positions all sensors in a straight line with the pitch of 120

mm. In the circular layout, all the sensors are arrangement at every 36° around the tower. In the heater level, the sensors are attached to the surfaces of finned tubes directly. Multiple measurements are required at a same condition and in each measurement sensors are placed at one of the levels with only one layout so that the influence of sensors on the airflow can be minimised.

It is noted that with current sensor arrangement, it is hard to detect local effects of the airflow in detail throughout the cooling tower, as the number of measure points is such small. However, a rough variation of the measured quantities at a particular position, like the temperature distribution in the central lines of three different levels, can be still obtained.

6.4.2 Measurement procedure

The air temperature is measured using thermistors and RTDs in the aforementioned four levels of the cooling tower model, while the air velocity is measured at bottom and middle levels. Because of the limit in number of sensors, the only one level is measured at each testing. The air static pressure drop across the heater is measure using a transducer, which reads the absolute pressures of two sides of the heater and then calculates the difference of them.

Before the experiments, all these sensors have been tested for their repeatability. In this test, sensors are placed and the recording of data starts before the heater is switched on. Once the heater is on and its surface temperature turns to be stable, the crosswind speed varies from 0 to 4m/s with the increment of 0.5 m/s each time and reverses the changing back to 0 m/s again. Finally the heater is power off, and the recording lasts until the heater is completely cooled down. This process is repeated three times. It is found that the quantities measured in these three tests are repeatable.

During experiment, the flow conditions at each crosswind speed remain stable for at least 10 min before starting measurement window. And the measurements are done at a sampling rate of 1 Hz lasting for another 10 minutes.

6.4.3 Heater control mode

The whole experiment is run based on two basic modes: constant heating power and constant heater surface temperature. In the first mode, the electric power of the heater is fixed. During the measurements, the surface temperature of the heater finned tubes is monitored by the temperature sensors attached on them.

In the second mode, the finned tube surface temperature is controlled and maintained at a constant value [83]. The controlling is achieved by a loop system: the real-time temperatures in different positions are measured by the attached sensors and then the control system in the computer

calculated a mean value based these data and get a corresponding change in the heating power through a PID module; finally the signal is transmitted to the heater controller so that the heating power can be changed. In spite of a constant temperature at heater surface, the air temperature changes with the crosswind speed. And there is no significant difference the measured quantities compared to those in the case of fixed heating power.

6.4.4 Working section and open channel

As mentioned above, the limitation in the height of the wind tunnel working section may affect the performance of the cooling tower model. Therefore, further tests have been done with part of the working section replaced by an open channel without the ceiling. The channel simply consists of three rectangular timber boards which form the channel floor (with some short legs supporting underneath) and two vertical walls on two sides, respectively. The channel has a height and a span of 1.75 m so that it can join up with the remaining part of wind tunnel working section perfectly. The function of this channel is equivalent to the original working section except for the open top. The scaled cooling tower model is placed inside the open channel. In spite of the absence of ceiling, the airflow attacking on the tower model is generally uniform as the channel top is still 0.55 m higher than the tower outlet.

The measurement results are then compared with those obtained in the original working section. It is found that both results at a crosswind speed of 1.5 m/s or higher are close enough, which accords with the numerical predictions. The CFD results indicate that the hot plume leaving the cooling tower reach up to further 23% of the tower height when wind velocity ratio is above certain value (around 9). But at low crosswind speed (<1.5 m/s) there are some moderate differences between the two results, and the one measured in open channel is more trustable because these tests are relatively closer to a real situation.

Therefore, the final results for low crosswind speeds (<1.5 m/s) discussed in this chapter are all obtained in the open channel tests.

6.5. Identical-dimension CFD model for direct comparison

As discussed in Section 6.2, the similarity between the scaled tower model and the CFD prototype cannot be satisfied completely as certain dimensionless parameters are not the same for both. Therefore, an extra CFD model has been built up to simulate the scaled cooling tower and the conditions in the wind tunnel. The CFD tower model has the same geometric dimensions as those of

the experimental rigs: the tower is 1.2 m high and 0.96 m in diameter while the computational domain has the same size of the wind tunnel working section, as shown in Figure 11.
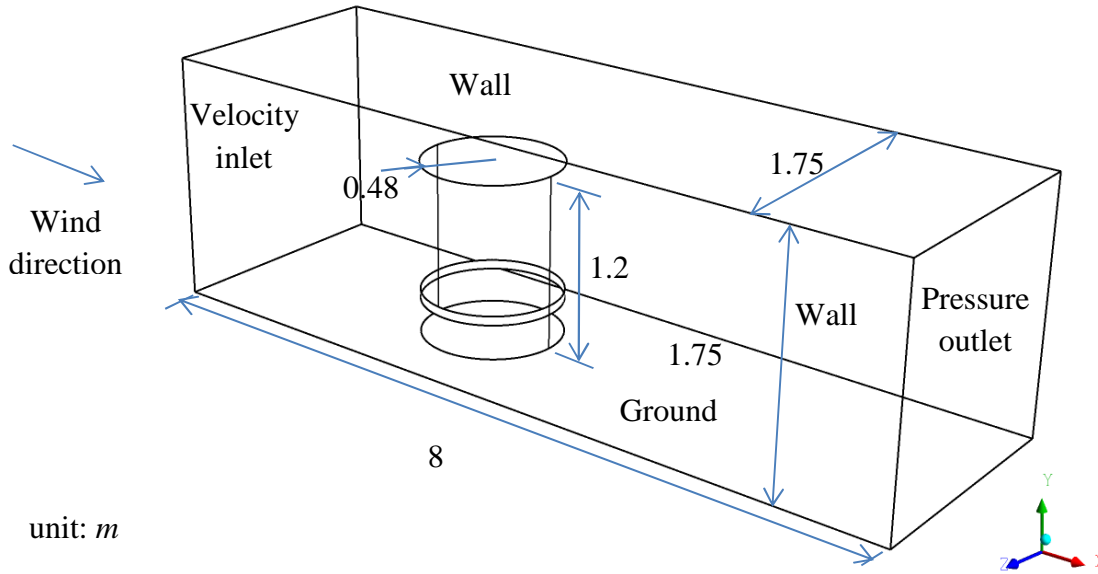
Figure 6.11. The geometry of the CFD model and the computational domain

The boundary conditions are set the same as the conditions in the wind tunnel. The velocity inlet uses a uniform velocity profile with the turbulence intensity I is calculated by:

$$I = 0.16Re_D^{-1/8} \tag{6.21}$$

where Re_D is the Reynolds number based on hydraulic diameter D which is 1.7 m here. The wall boundary is applied on two lateral sides and the top, and the downstream face of the tunnel is set as pressure outlet boundary where only the static pressure is specified.

This CFD model uses the same porous media associated with the radiator boundary introduced in Chapters 4 and 5 for the heater. The coefficients in momentum source term, i.e. Eq. (4.8), and the heat transfer coefficient h of the radiator in Eq. (4.7) are all derived from the wind tunnel testings rather than the correlations in Chapter 3.

More precisely, for Eq. (4.8), a is the permeability of mesh screen and C is recalculated by k_h and in Eq. (6.19) and k_m in Eq. (6.20). Meanwhile, T_r in Eq. (4.7) is the heater surface temperature, and the total convective heat transfer coefficient h can be roughly estimated by the heat transfer correlation proposed in [78] which is also valid for this heater, i.e.:

$$Nu = \frac{hd_o}{k} = 0.495Re_c^{0.509}\left(\frac{P_t}{d_o}\right)^{-0.209} \tag{6.22}$$

The CFD model uses the same meshing methods in Chapter 4. The cell size near the walls is 20 *mm*.

The CFD model is constructed to have all the dimensionless parameters introduced in section 6.2 to be identical to those for the experimental cooling tower model. Therefore, the simulation results of the CFD model can be directly compared to the experiment results. Since many of the dimensionless numbers (except Grashof and Reynolds number) for the test rig are also similar to those for the full-height CFD model, the comparison with the full-size prototype will also be reported in terms of dimensionless numbers, although the agreement with the experimental results is expected to be weaker for the full-scale cooling tower.

6.6. Cooling tower performance in natural convection case

The cooling tower operates in a pure natural convection manner when there is no crosswind. Thus the scaled NDDCT model is tested first outside the wind tunnel. The heater works at the first mode– at a constant power of approximately $P_{heater} = 5.216$ KW. Even though the tests are conducted indoors, to prevent any ambient air flow disturbance, barriers are installed 3 meters away surrounding the tower model.

The natural convective air flow rate due to the buoyancy is measured by three hotwires in the middle level of the tower model. A mean velocity is then calculated by averaging the three measurements. Figure 6.12 plots the real time mean air velocity recorded in a period of 700 seconds. The data sampling rate in the figure was 1 *Hz*.
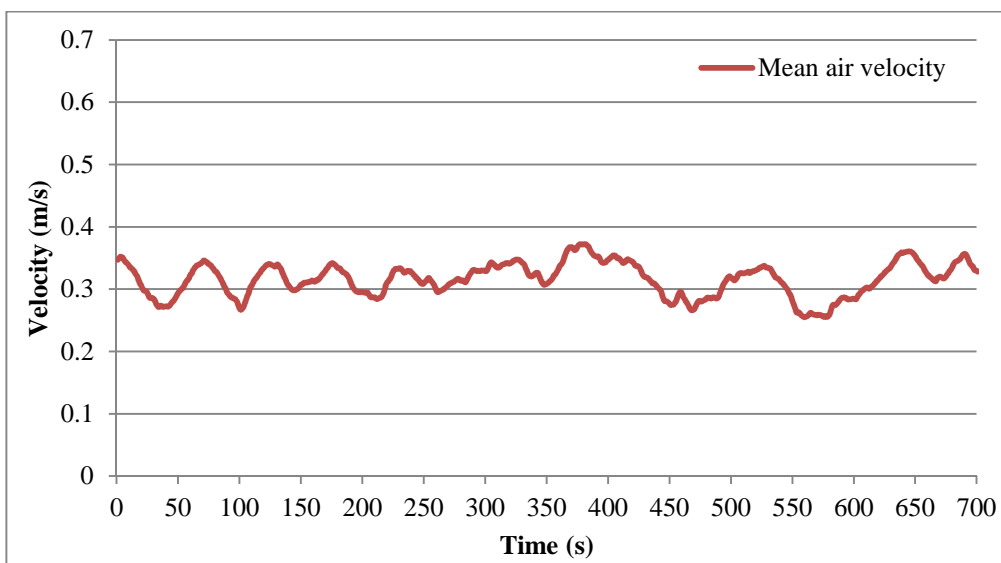

Figure 6.12. The spatial averaged real time air velocity at the constant heating power mode

The uncertainty analysis on the results shows that air velocity over the given period of time has an average value of 0.316 m/s with the standard deviation of 0.027 m/s. The fluctuation of instantaneous velocity indicates that certain level of instability occurs in the air flow. In fact, the free convection air flow in such scale tower is a high Reynolds number turbulent flow, and can be disturbed by any tiny external influence which is inevitable in current laboratory condition. Therefore, the measurement is taken in several points over a sufficiently long period of time (>10 min).

The air temperature is measured at different levels inside the tower model, and each level has 6 or 10 measuring points. Figure 6.13 shows the averaged real time temperatures in each level: bottom, middle, top,underneath, and tower inlet (ambient air) in the same period of 700 seconds as above.
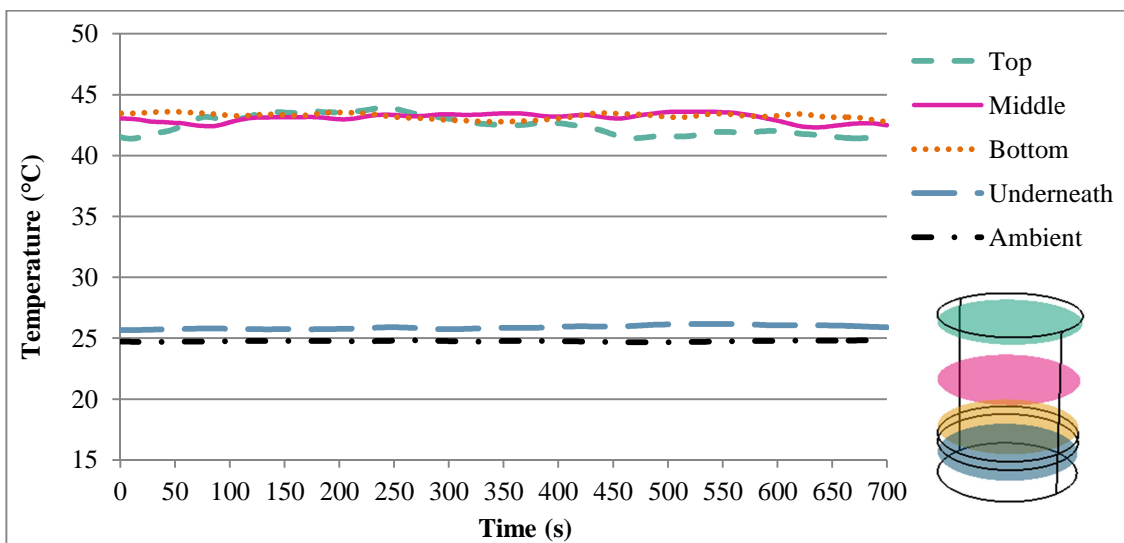
Figure 6.13. The spatial averaged real time temperature in four levels as indicated at the constant heating power mode

The result of the uncertainty analysis on these measurements is shown in table below.

Table 6.6 The uncertainties of the real time temperature

Measured quantity	Arithmetic mean over all sensors	Standard deviation
Velocity at middle level	0.32 m/s	0.03 m/s
Top level temperature	42.5 °C	0.8 °C
Middle level temperature	43.1 °C	0.4 °C
Bottom level temperature	43.3 °C	0.2 °C
Underneath level temperature	25.9 °C	0.2 °C

Ambient (inlet) temperature	$24.7\ °C$	$0.04\ °C$

These measurement results have verified that the target similarity has been achieved between the experimental model and the 15 m-high tower prototype in CFD as discussed above. For example, with the average air velocity in pure natural convection case, the similarity defined in Eq. (6.14) can be verified, namely:

$$(Fr_D)_p = \left(\frac{v_{aN}^2}{\frac{\rho_0-\rho}{\rho}gH}\right)_p = \left(\frac{0.47^2}{\frac{1.19-1.173}{1.173}\cdot g \cdot 15}\right) = 0.1037 \tag{6.23a}$$

$$(Fr_D)_m = \left(\frac{v_{aN}^2}{\frac{\rho_0-\rho}{\rho}gH}\right)_m = \left(\frac{0.31^2}{\frac{1.195-1.112}{1.112}\cdot g \cdot 1.2}\right) = 0.1095 \tag{6.23b}$$

Therefore:

$$(Fr_D)_m \approx (Fr_D)_p \tag{6.23c}$$

All the values in Eq. (6.23a) are extracted from the CFD results. $(\rho_0)_m$ and $(\rho)_m$ in Eq. (6.23b) are calculated using Eq. (3.16) where the barometric pressure in laboratory $(P_0)_m \approx 101100$ Pa, and the air temperatures are based on the measurements. The Froude number for model is slightly larger than that in prototype which indicates the actual convective air speed is slightly larger than what expected. This is due to a relatively smaller pressure loss in the heater than designed value.

Additionally, a direct comparison of the results between the measurement and the identical CFD model (1.2 m-high) is made in table below, which indicates there is a very good agreement for them:

Table 6.7 A comparison between the experiment and CFD results for pure natural convection case

parameters	measurements	identical CFD model (1.2 m-high)
Mean air velocity (v_{aN})	0.316 m/s	0.315 m/s
Mean air outlet temperature (Bottom level)	42.5 °C	43.2 °C

With the spatial averaged temperature and air velocity at each time step, the total heat absorbed by the air flow from the heater is calculated by Eq. (6.24a). It is then plotted against the time in Figure 6.14 for the same period of 700 seconds as above.

$$Q_a = m_a C_{pa}(T_{ao} - T_{ai}) = \bar{\rho}_a v_{a0} A C_{pa}(T_{bottom} - T_{ground}) \qquad (6.24a)$$
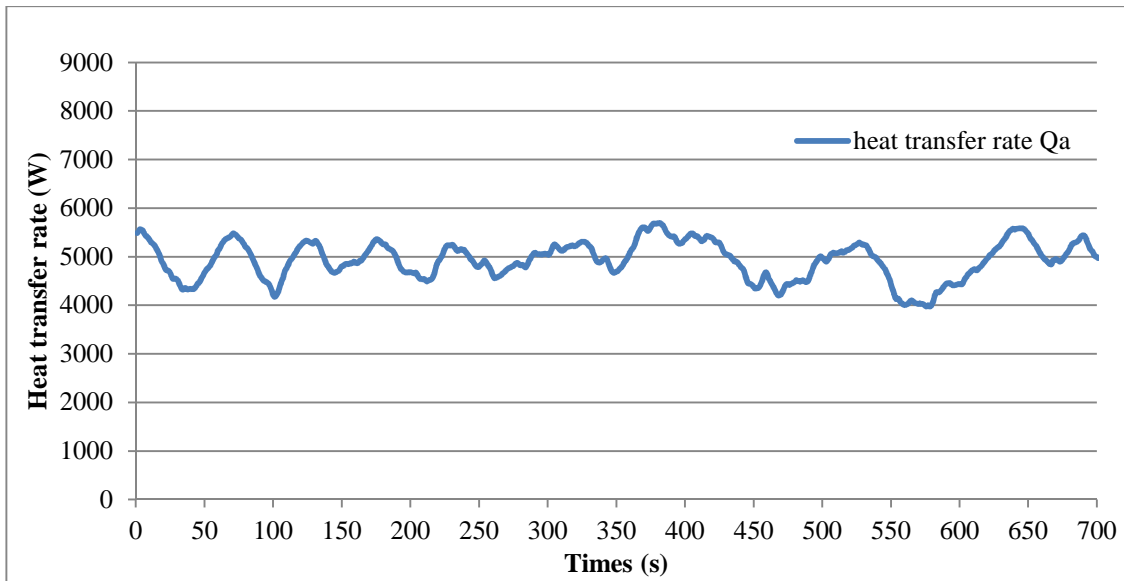

Figure 6.14. The real time total heat transfer rate between the heater and air, at the constant heating power mode

The time average value of the heat transfer rate $\bar{Q}_a$ in the tower model over this measurement window is 4925.5 W with the standard deviation accounting for 7.9%. $\bar{Q}_a$ matches the actual working power of the heater P_{he} quite well, and the heat transfer efficiency η between air and the heater surface is therefore:

$$\eta = \frac{Q_a}{P_{heater}} = \frac{4.925}{5.216} = 94.4\% \qquad (6.24b)$$

There shows around 5.6% of heat mismatch in the heat transfer, which mainly due to the heat dissipation to the surrounding air of cooling tower through heater frame, support, cable *etc*. The imprecision of the measurements could be another reason.

It is noted that the air temperature drops slightly along with the air flow above the heater. The temperature differences between bottom and middle and between middle and top are 1.15 °C and 2.37 °C. The decrease shows that the heat loss through the tower wall (cylinder shell) is not negligible in this model. An approximate estimation of the heat loss on the tower body surface can be calculated by following mathematics model.

The air temperature inside the tower T_i keeps changing from T_{ao} between tower bottom and top as the heat is continuously lost. Therefore the T_i is expected as a function of the distance above the heater h, namely: $T_i = f(h)$. To obtain the correction between T_i and h, consider a random

infinitesimal height dh in which the air temperature decreased by dT_i, as shown in the Figure 6.15 below.
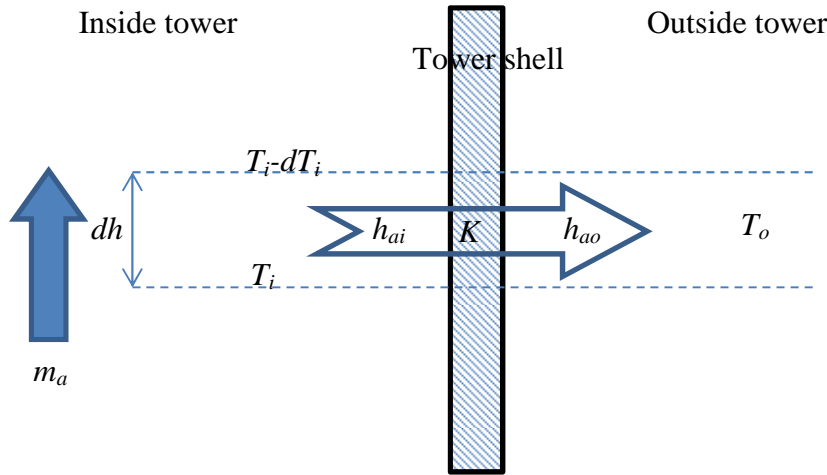

Figure 6.15. Heat loss model at the tower wall

Suppose the ambient temperature outside the tower is a constant T_o, the energy of hot air lost in this infinitesimal height dQ_{loss} is expressed as:

$$dQ_{loss} = m_a C_{pa} dT_i = h_u \pi D (T_i - T_o) dh \qquad (6.25)$$

where U is the overall heat transfer coefficient between internal hot air and the ambient air calculated by:

$$h_u = \frac{1}{\frac{1}{h_{ai}} + \frac{L}{K} + \frac{1}{h_{ao}}} \qquad (6.26)$$

By rearranging the last two term of Eq. (6.25) and integrating from 0 to H, yielding:

$$T_i = (T_{ao} - T_o) e^{\frac{\pi U D}{m_a \cdot C_{pa}} H} + T_o \qquad (6.27)$$

It is calculated that the convective heat transfer on a vertical wall of surface temperature 43 °C is around 9 W/Km^2, therefore the theoretical temperature decrease by calculation is $\Delta T = T_{ao} - T_i = 43.25 - 42.57 = 0.62$ °C. The result is close to the actual temperature difference measured which is 0.77 °C.

6.7. Crosswind effects on the cooling tower without windbreaks

The scaled tower model is then tested in the wind tunnel under different crosswind speeds: 0.5, 0.75, 1, 1.5, 2, 2.5, 3, 3.5, 4, 4.5, 5 and 5.5 m/s when the heater works at the constant heating power mode first and then the constant surface temperature mode. At each wind speed, the data are logged only after all the quantities monitored remains stable, and the recording is done over 10 minutes.

6.7.1. The mean velocity

According to Eq. (6.2), the velocity of the air flow inside the tower under crosswind conditions v_a is nondimensionalized by the pure natural convection air speed without crosswind– v_{aN} as a divider. This ratio represents the variation of air flow in the tower with external wind. Since for the scaled NDDCT model, the variables other than v_{cw}/v_{aN} in Eq. (6.2) remain unchangeable, v_a/v_{aN} can expressed as a function of only wind velocity ratio v_{cw}/v_{aN}:

$$\frac{v_a}{v_{aN}} = f\left(\frac{v_{cw}}{v_{aN}}\right) \tag{6.28}$$

The uncertainty of this function is calculated as following equation:

$$\sigma_{va/vaN} = \sqrt{\left(\frac{1}{\bar{v}_{aN}}\right)^2 \sigma_{va}^2 + \left(-\frac{\bar{v}_a}{\bar{v}_{aN}^2}\right)^2 \sigma_{vaN}^2} \tag{6.29}$$

where σ_{va} and σ_{vaN} are the uncertainties of v_a and v_{aN} respectively

Figure 6.16 shows the dimensionless air velocity v_a/v_{aN} varies with the crosswind speed ratio in measurement and the two CFD models. The electric power of the heater in the experiment is fixed at approximately $P_{heater} = 5.216$ KW while in the two CFD models, the heat transfer rates of the heat exchanger model are constants. So, all the curves in Figure 6.16 are for the results from the constant heat dumping rate mode. The uncertainties in the measurement are shown on experimental results. In the experiment, air velocity v_a is the mean value at the middle level of the cooling tower. All three curves show a similar turn-around trend. However, the slope of the curve for the 15 m-high prototype CFD model is different from the other two. This is because the similarity between the model and the prototype in CFD simulations is not completely satisfied, for instance the Reynolds numbers do not satisfy the similarity. On the other hand, the comparison of the experimental result with that in the identical CFD model (1.2 m-high tower) shows a good agreement with slight difference for the velocity ratio v_{cw}/v_{aN} more than 12.
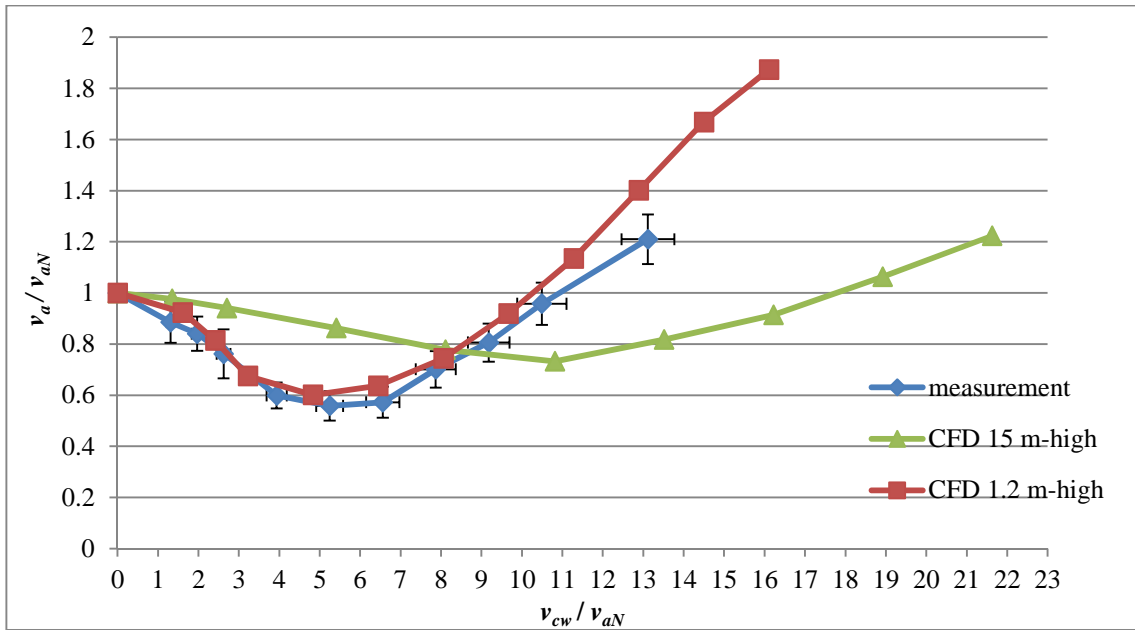
Figure 6.16. Air velocity v_a/v_{aN} changes with the crosswind at constant heat dumping rates, both experimental and numerical results. The error bars are shown on experimental results.

The turn-around trend of the natural convection-induced hot air speed implies that airflow pattern is complex and the air circulations may exist. In this wind tunnel experiment, the speed sensors can measure the air flow in directions normal to the sensor probes which are placed horizontally inside the tower but cannot determine the exact direction. On the other hand, the vertical airflow speed in the tower is inevitably decreased by the horizontal wind which causes the inclined exiting airflow at cooling tower outlet [62]. Therefore, the increase of air speed post the critical wind speed in the measurement is attributed to no reason other than the redirection of the actual airflow. This argument can be further proved by the CFD results from the 1.2 m-high cooling tower model. Figure 6.17 shows the velocity vectors at mid-*xy* plane of the cooling tower under no-wind condition and at crosswind speed of 4 m/s, respectively. The speed 4 m/s corresponds to wind velocity ratio v_{cw}/v_{aN} of around 12.7 at which v_a/v_{aN} is larger than 1. In Figure 6.17, a large vortex is seen in the middle and upper part of the cooling tower when crosswind speed is 4 m/s, and it is clear that the mean absolute air speed at the middle level in (b) is larger than that in (a) which is no-wind case.
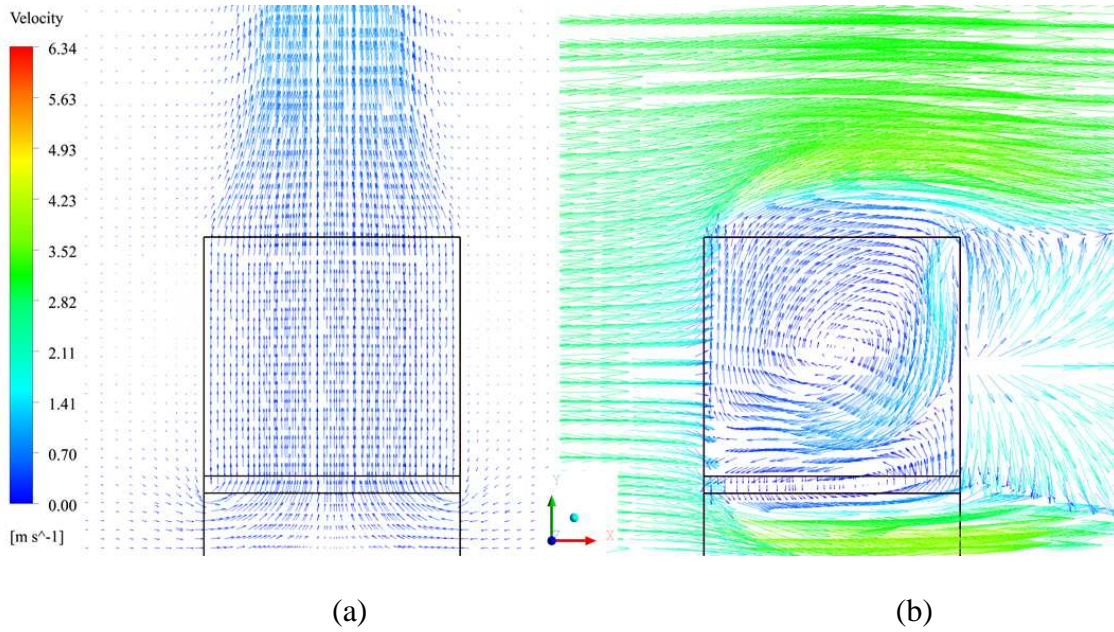
(a)   (b)

Figure 6.17. Velocity vectors at mid-*xy* plane under no-wind condition (a) and when crosswind speed = 4 m/s (b).

6.7.2. The mean air temperature

The temperature sensors are arranged in the layouts introduced in Section 6.4.1 at each testing level so that the level mean temperature T_a can be calculated. It is found that at any level the mean air temperature changes with the air velocity. According to the scaling analysis, the non-dimensional parameter is defined for the temperature, i.e.:

$$T^* = \frac{T_a - T_0}{T_{aN} - T_0} \tag{6.30}$$

where T_0 is the ambient constant air temperature and T_a is the mean air temperature. The divider $T_{aN} - T_0$ stands for the temperature difference between the inlet and outlet air of heat exchangers when there is no crosswind. T^* at every time step varies with the time and Figure 6.18 shows the real time T^* measured at the bottom level of the tower model for a stable 10-minute time window, when v_{cw}/v_{aN} is around 5.2.
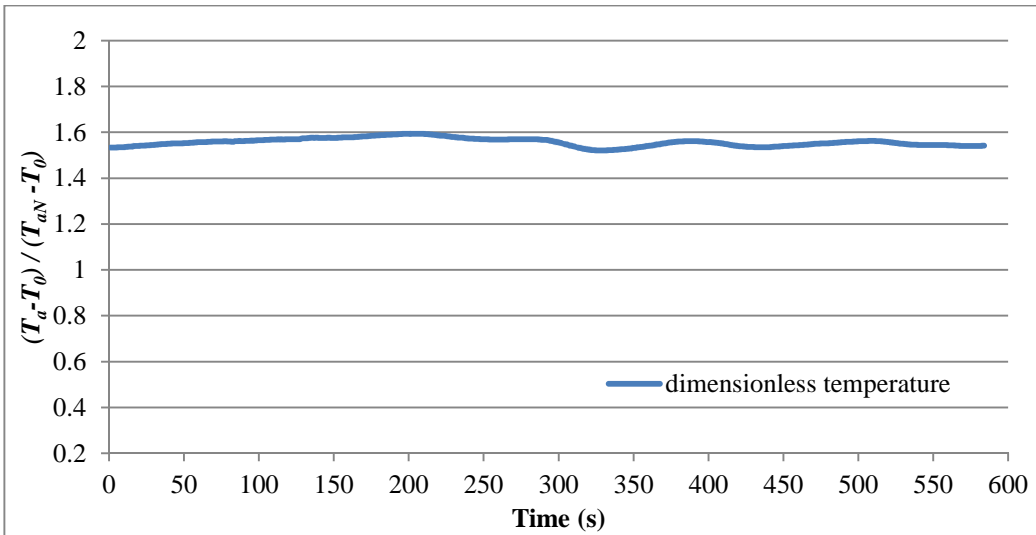
Figure 6.18. The real time T^* at the bottom level for a stable 10-minute period at the crosswind speed ratio of 5.2.
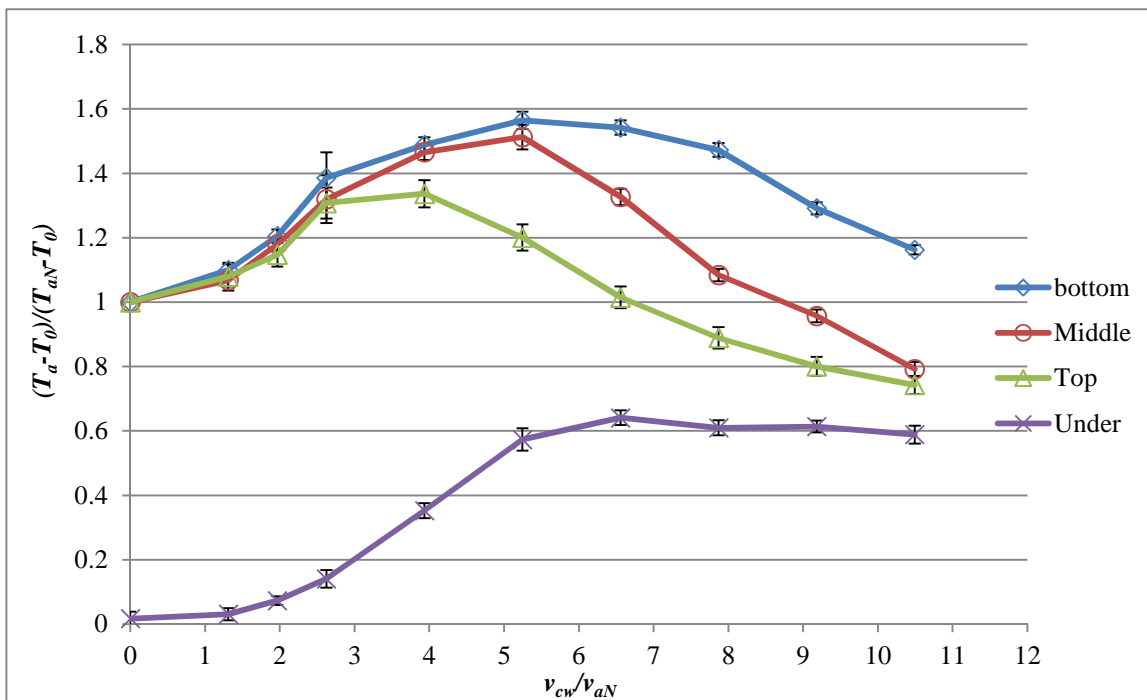
Figure 6.19. The experimental air temperature at different testing levels changes with the crosswind at constant heating power mode

The dimensionless air temperature T^* is plotted against the crosswind speed ratio. Figure 6.19 shows the dimensionless air temperature at different levels as the functions of crosswind velocity ratio v_{cw}/v_{aN} when the heater works the same constant heating power mode as that in Section 6.7.1. The overall temperature above the heater, i.e. inside the tower, generally follows the opposite trend to the air velocity. Air temperature at the tower top tends to be much cooler than that in the bottom when the wind velocity ratio is larger than 3. This difference also implies that the air flow is not

130

unidirectional above the heat exchangers, but there are vortices in tower upper part causing the cool ambient air penetrated into the tower from the outlet. This supports the CFD observations presented in earlier chapters.

On the other hand, temperature underneath the heater is 0 as expected since $T_a = T_0$ in Eq. (6.30). As the crosswind speed increases, it shows a generally increasing trend and tends to converge to be the value of the middle and top temperatures. This is evidence for the existence of the air circulation around the heater exchanger as predicted by the CFD simulations. As seen in Figure 6.17, part of the hot air above the exchangers is sucked down by the negative pressure in the tower bottom caused by the crosswind, as the result, the air is heated again. Therefore, the temperature in the reverse flow region increases significantly.

The measured temperatures are then compared with the numerical results of the identical 1.2 m-high CFD model at each level at the approximately same heat dumping rate 5.216 KW, as shown in Figure 6.20.
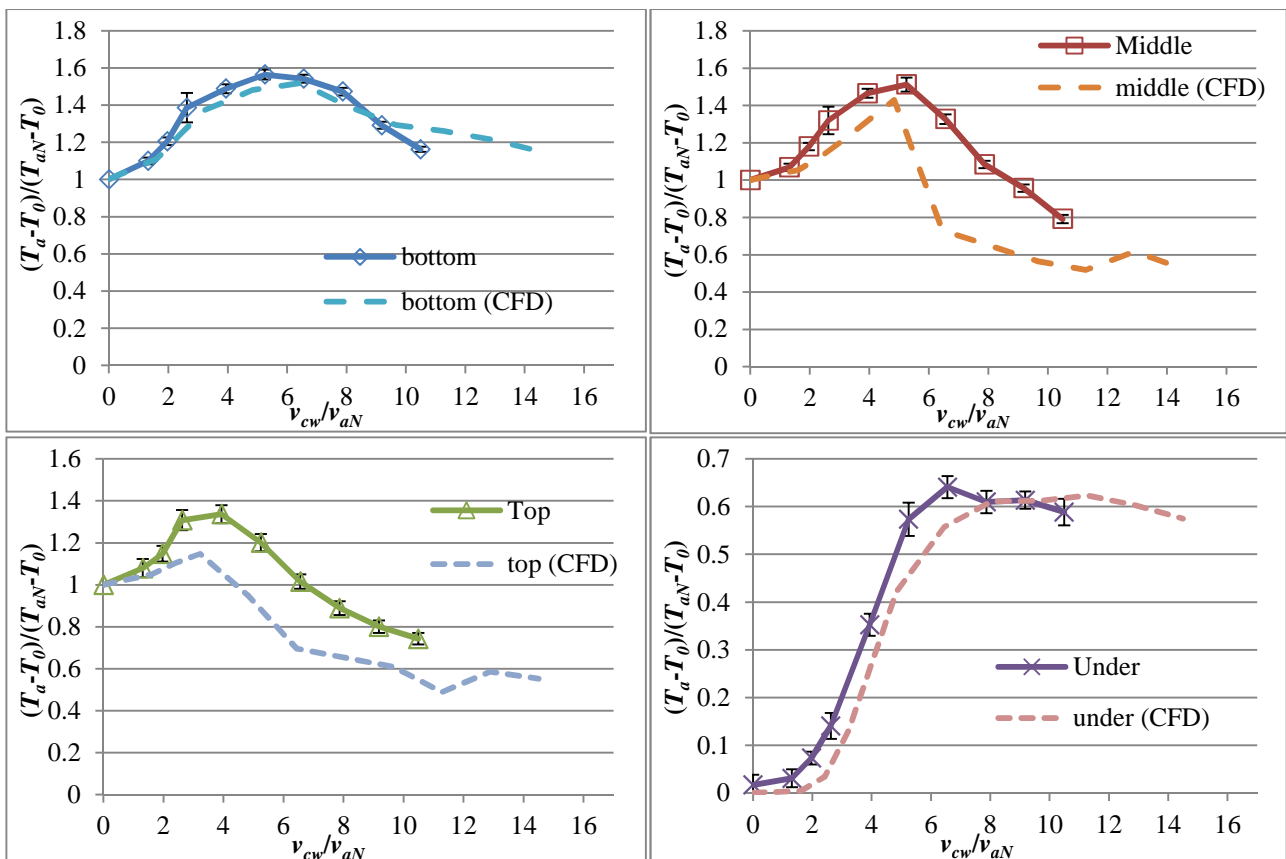

Figure 6.20. Comparisons of dimensionless temperature variation at different measurement levels between the experiment and CFD results at the same heat dumping rate 5.216 KW.

The experiment and CFD results for temperature at both tower bottom level (above the heater) and the heater underneath level agree generally well, but at the tower middle and top levels there are differences between both results, especially in high wind velocity ratio range. Further investigation indicates that the air flow field at tower base and lower part predicted by CFD simulations are very close to that in the wind tunnel measurement. However in tower upper part, air temperature is lower in CFD results because more cool ambient air penetrates through tower outlet, which points out that the airflow vortices are overestimated by numerical simulations. This may be due to the limitations of the two-equation RANS turbulence model used in this study [84]. Despite of this, all curves verify that air temperature obtained in either experiment or CFD have very similar change trends with respect to the variation of crosswind speed.

6.7.3. Temperature distributions

The air temperature distribution in particular positions is investigated in order to estimate the variation of the flow field pattern of the cooling tower when there is crosswind.

The temperature distribution is implemented by measuring the increased air temperature along the central lines of four different levels of the cooling tower shown in Figure 6.21. The heater in the measurements is controlled at the constant heating power mode. The increased temperature means the difference between the temperature of testing point and the inlet ambient temperature of the tower, as defined in Eq. (6.31).This parameter is introduced to eliminate the influence of the environmental temperature on the experiment results.

$$\Delta T_a = T_a - T_{ai} = T_a - T_0 \tag{6.31}$$
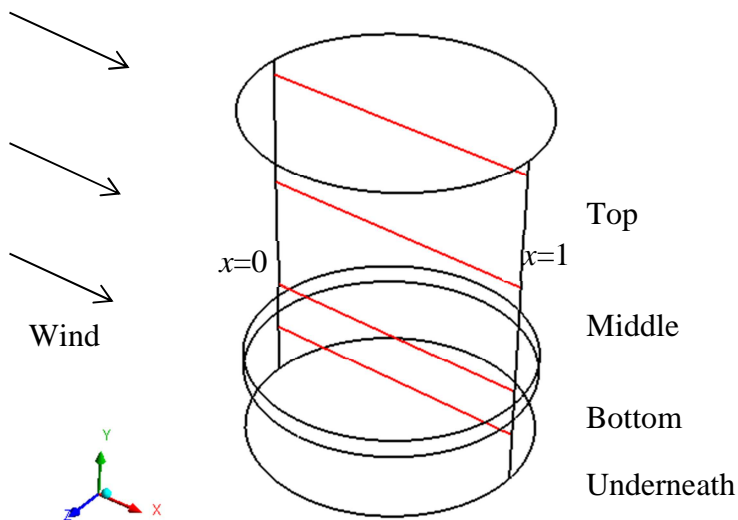
Figure 6.21. Positions in the cooling tower (red lines) where the increased temperature is measured

Figures 6.22-6.25 plot the distributions of the increased air temperature in the central lines at different levels when crosswind speed changes from 0 m/s to 4 m/s and the electric power of the heater, i.e. heat dumping rate, is same as that in Section 6.7.1. The *x-axis* in these figures is ratio of *x* to tower diameter *D*, where *x* is the *x*-coordinate of the position of a temperature sensor. And the crosswind direction is same as the *x-axis*, namely, *x* = 0 is windward side while *x* = 1 is leeward side.

Figure 6.22. Measured temperature distributions in the central line of bottom level at different crosswind speed (constant heat dumping rate)
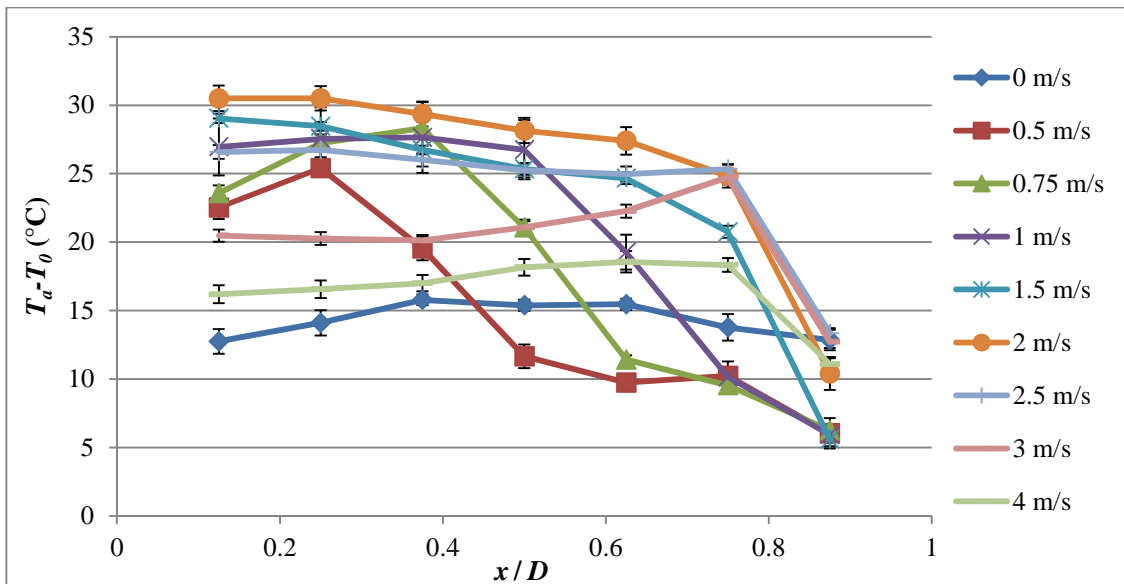
Figure 6.23. Measured temperature distributions in the central line of middle level at different crosswind speeds (constant heat dumping rate)

133
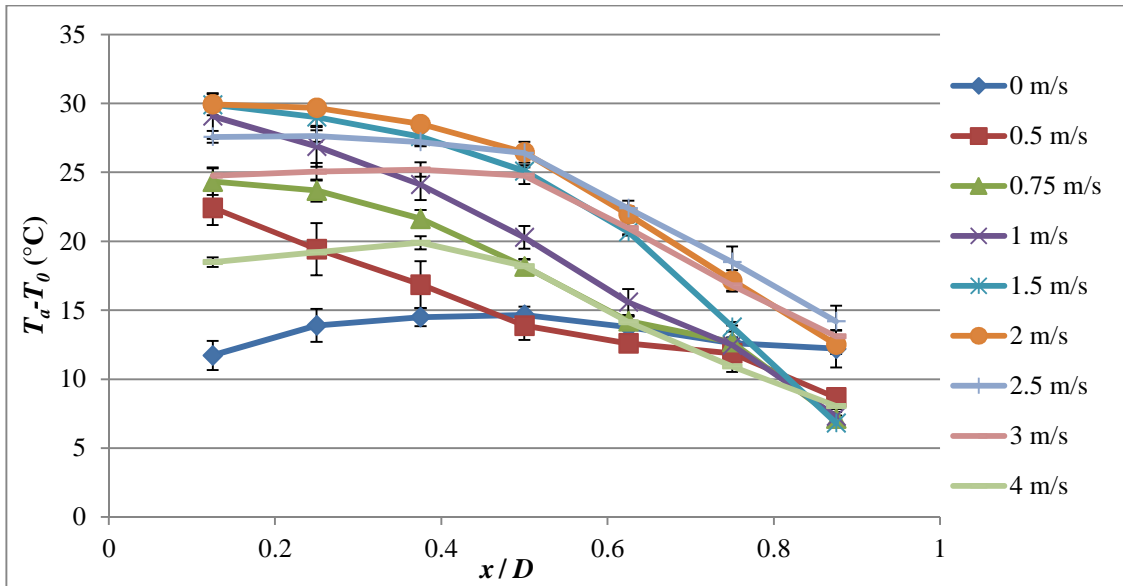
Figure 6.24. Measured temperature distributions in the central line of top level at different crosswind speeds (constant heat dumping rate)

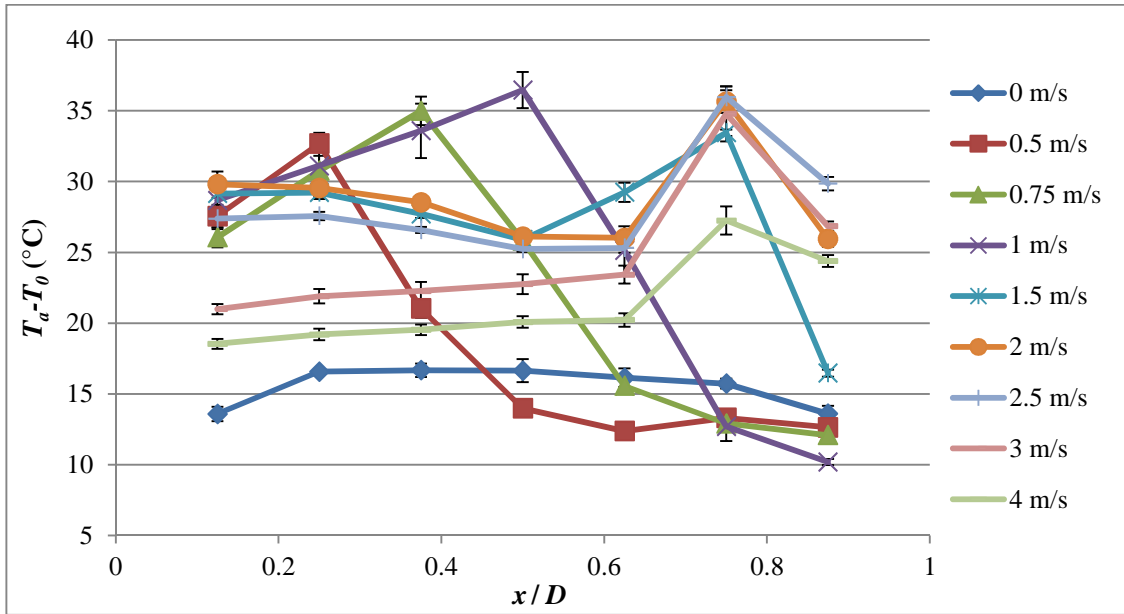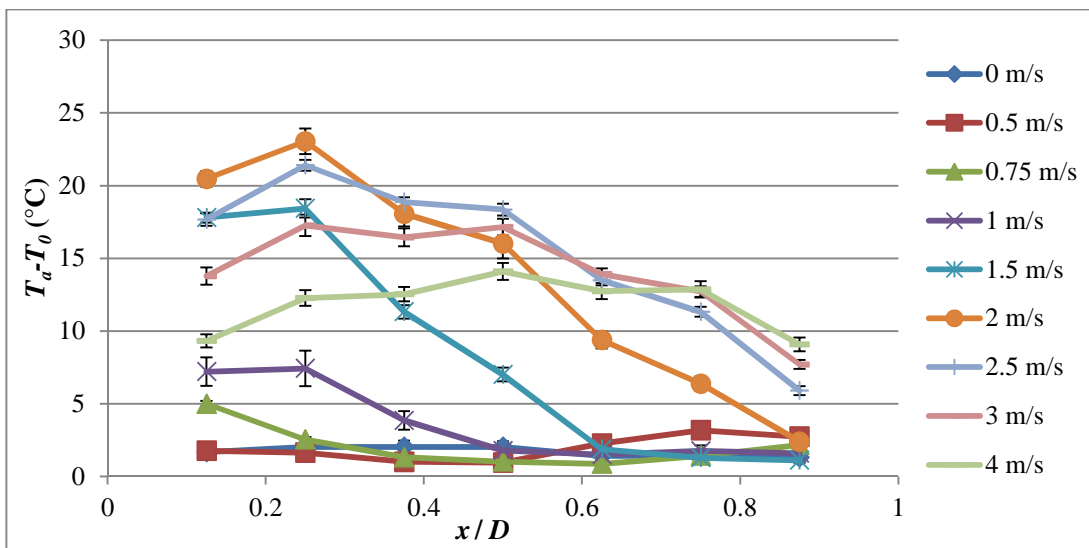Figure 6.25. Measured temperature distributions in central line underneath the heater at different crosswind speeds (constant heat dumping rate)

The temperature distributes nearly symmetric along with the central line at any level of the tower in free convection case. The crosswind tends to increase the temperature much more on windward side than on leeward side. This is quite clear shown in top and underneath levels. Situations at bottom and middle levels seem a little complicated. In fact the maximum temperature position changes with the crosswind speed: this position generally moves towards the leeward side as the wind speed increases. According to the analysis in Chapter 4, the highest temperature in a horizontal line occurs where the air velocity is lowest. This is exactly the position of airflow circulation centre. When the

crosswind speed is increasing, this centre is pushed towards the leeward because the negative pressure zone under the heat exchanger in windward side is expanding. The experiment results therefore verify the prediction of the CFD simulations in previous chapters.

Generally speaking, the profile of temperature distribution at each measuring levels provides strong evidence that the crosswind causes air circulations inside the tower as discussed above. In the region near tower outlet, temperature in leeward side declines as cool air penetrates. Consequently, the natural convection air speed decreases, leading to the rise of temperature in the region out of the air vortices. While underneath the heat exchangers, reverse airflow exists at windward part especially at high crosswind speeds. Reverse flow decreases the net air flow rate passing through the heat exchangers, but it is not always harmful to the overall heat transfer which is unlike the vortices near tower outlet. As discussed in Chapter 4, in certain high crosswind speed range, the heat can dissipate through the reverse air flow.

The temperature distribution obtained in experiment is then compared against the results of the 1.2 m-high CFD model computed at the same heat dumping rate. Figures 6.26–6.28 compare the temperature distributions in the central lines of tower bottom, top, and base (under the heat exchangers) from both the experiment and CFD results at crosswind speeds as indicated.
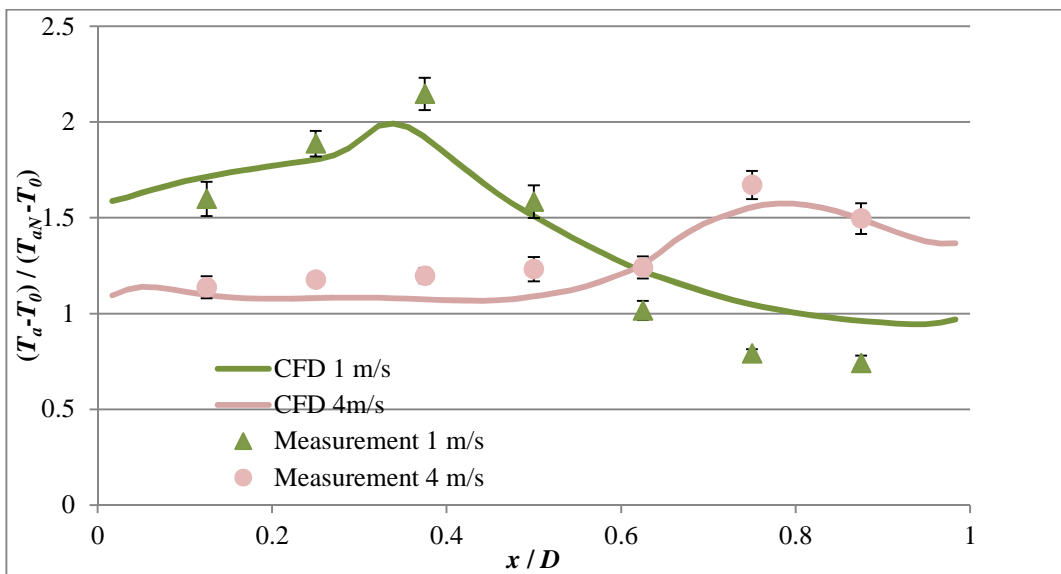
Figure 6.26. A comparison of temperature distributions in central line of bottom level when crosswind speed is 1 m/s and 4m/s between the experiment and CFD results (same constant heat dumping rate).
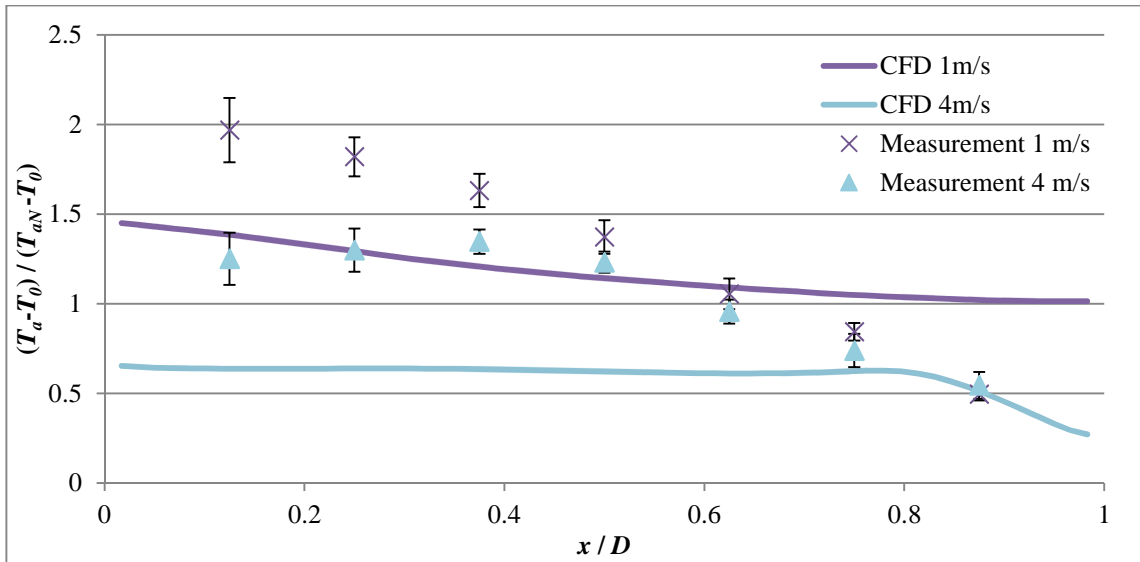
Figure 6.27. A comparison of temperature distributions in central line of top level when crosswind speed is 1 m/s and 4m/s between the experiment and CFD results (same constant heat dumping rate).
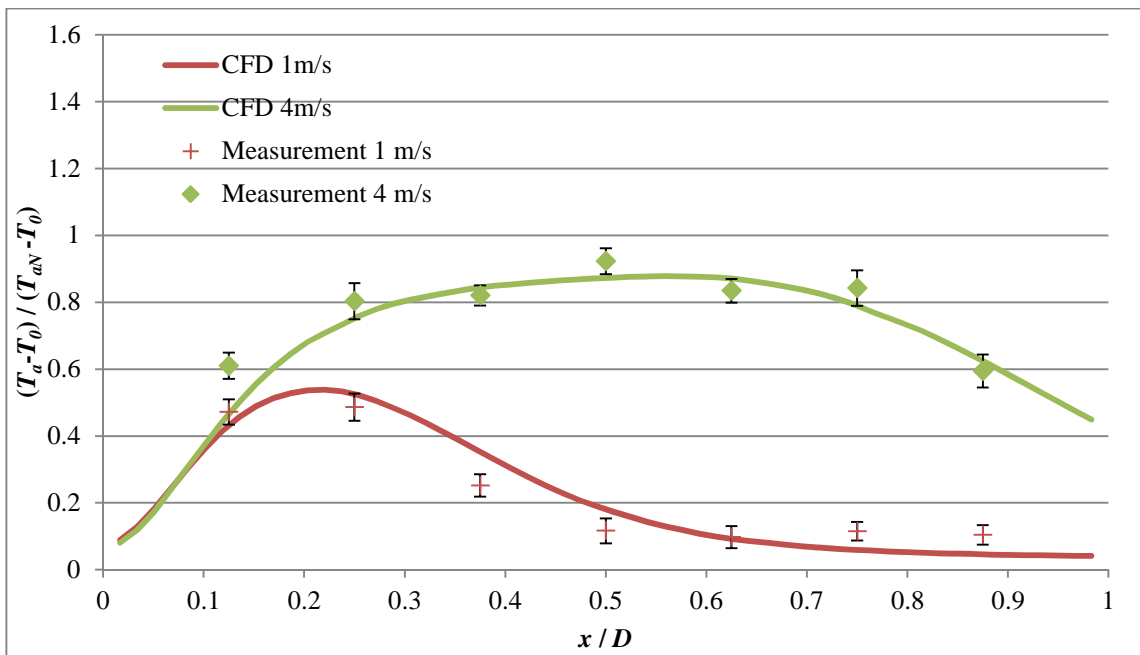
Figure 6.28. A comparison of temperature distributions in central line underneath the heat exchangers when crosswind speed is 1 m/s and 4m/s between the experiment and CFD results (same constant heat dumping rate).

These comparisons show a satisfied agreement between the experiment and CFD results for bottom and underneath levels. However, the consistency is not made at tower top. It is believed that the air flow field in this part is very complicated. The CFD results suggest there exists air vortices in this

region, but its scale is probably exaggerated in numerical simulations, leading to that the airflow field in upper part of tower predicted by the CFD model is not same as that in the experiment results.

However, these temperature distributions reflect only a rough estimation of the temperature variation in the aforementioned locations rather than the complete state of the airflow in the cooling tower. Because with such small number of measuring points, many very detailed local effects might be missed out.

6.7.4. The total heat transfer rate

To examine the crosswind effect on total heat transfer rate Q of the heater, the measurements at variable heating power mode is conducted. In this testing mode, the surface temperature of the heater is maintained at a constant value which is the heater temperature in free convection case when there is no crosswind. While crosswind changes, regulate the input electric power depending on the real time temperature monitored and the stabilized power is then recorded. As the discussion in 5.1, more than 94% of the electric power is transferred to the air which is emitted through the outlet of the cooling tower. So the variation of heat transfer can be reflected by electric power changing measured.

The scaling analysis defines the ratio of total heat transfer rates between the cases of crosswind and no crosswind Q/Q_N. According to Eq. (6.4), this ratio can be expressed as a function of the crosswind speed ratio v_{cw}/v_{aN} while the others are constant for a certain tower model, namely,

$$\frac{Q}{Q_N} = f\left(\frac{v_{cw}}{v_{aN}}\right) \tag{6.32}$$

The correlation obtained from the experiment data is displayed in Figure 6.29 where a comparison with the two CFD results is given as well. In these two CFD models, the surface temperatures of the heat exchanger models are fixed instead of the heat dumping rate.
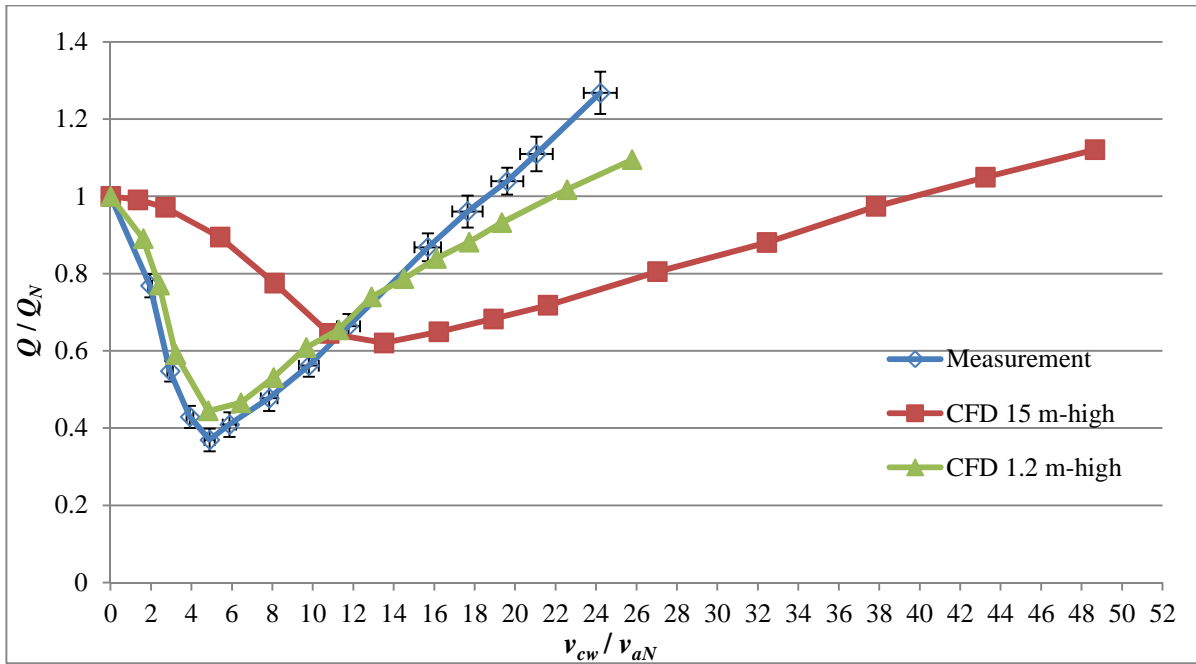
Figure 6.29. The total heat dumped by the cooling tower at different crosswind speeds when the heater/heat exchanger surface temperatures are constants.

In Section 4.5, the correlation of Nu/Nu_N and v_{cw}/v_{aN} proposed in Eq. (4.13) indicates that the turn-around trend of the heat transfer rate exists because of a combination of natural and forced convection. Figure 6.29 shows that the experiment curve has matched up with the curve of 1.2 m-high CFD model quite well. The curve for 15 m-high CFD model appears different slopes from the other two. Again, the difference is mainly because of the incomplete similarity of the scaled tower model.

It is noted in Figure 6.29 that in the range of wind velocity ratio between 0 and 13, the measurements, either the air velocity or the heat transfer rate, agree quite well with the predictions of its identical 1.2 m-high CFD model. But at higher velocity ratios (i.e. >13) the experiment obtains a smaller air velocity or a larger heat transfer rate than the CFD simulation. This fact is still due to that in high wind velocity ratios CFD calculation overestimates the airflow circulations inside the cooling tower, so that it underestimates the cooling performance of the heat exchangers. However, the CFD modelling methods are still considered valid because its prediction of the critical points for both the airflow velocity and heat transfer rate is accurate according to the comparisons with the scaled model measurement results in the wind tunnel.

6.9. Crosswind effects on the cooling tower with windbreak walls

According to the CFD results in Chapter 5, the existence of the windbreak stops the crosswind flowing across the bottom, change the direction of the crosswind, and force it flow through the heat exchanger. Since more air flows through the heat exchanger, it improves the performance of the tower. When there is no crosswind, the cooling air enters into the tower freely without any obstruction from the walls. The benefit of the windbreak wall is clear seen in the numerical results.

This experiment uses the same shape of windbreak wall underneath the heater in the tower base. Three cases of the wall installing angles have been investigated: 0°, 30°, and 60° at the constant heating power mode first. Figure 6.30 shows the dimensionless air velocity v_a/v_{aN} averaged at the tower middle level changing with the crosswind speed ratio in these three cases of angles (solid lines), while the corresponding results from the 15 m-high CFD prototype and the identical 1.2 m-high CFD model are presented in the figures as well for comparisons. All the experimental and CFD results are obtained in the case that the heat dumping rates are constants.
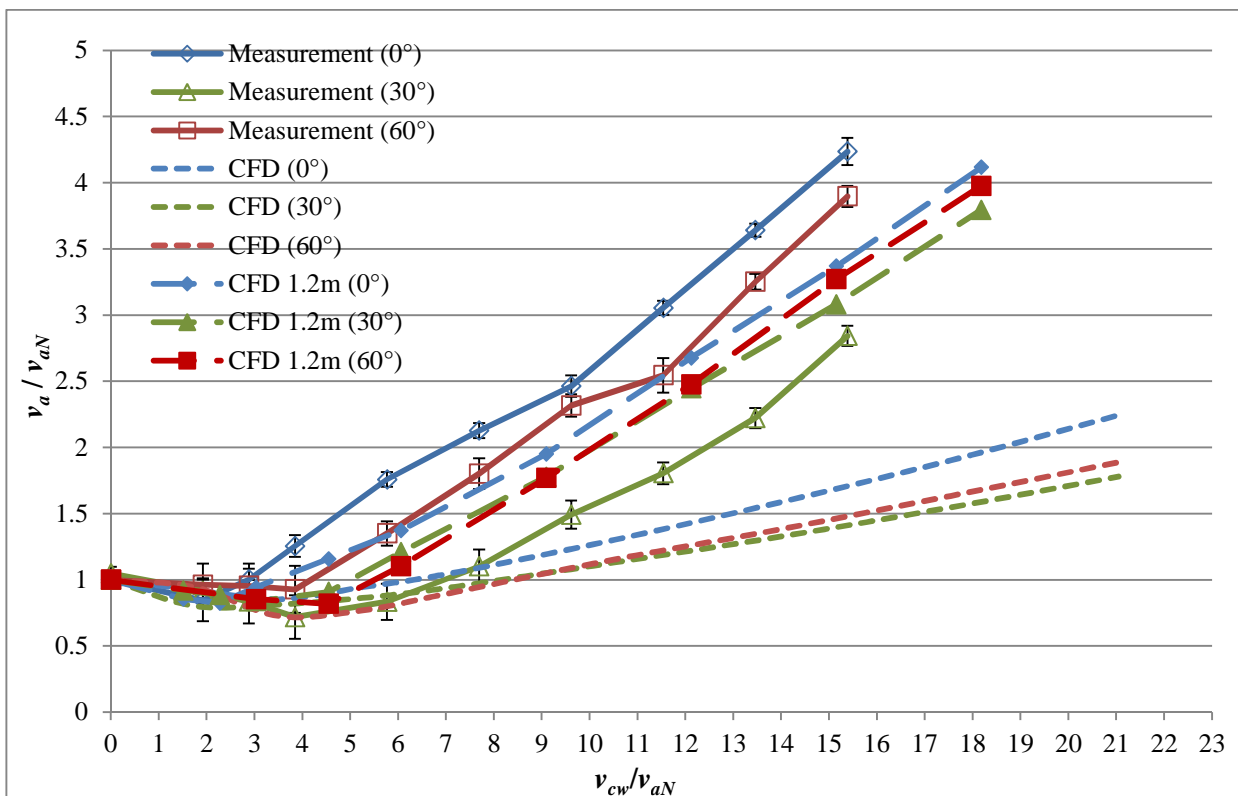

Figure 6.30. Air velocity as a function of crosswind speed ratio for different attack angles at constant heat dumping rates

It is found the windbreak wall generally enhances the air velocity inside the cooling tower as crosswind speed increases for the attack angle of 0° and 60°. The air velocity for 30° attack angle

139

experiences a temporary decrease in low crosswind speeds followed by a turnaround at the wind speed ratio around 4. All the experiment and CFD results show the similar trend as the crosswind speed varies, although the gradients of the curves for the 15 m-high cooling tower are much smaller the other ones.

On the other hand, the dimensionless temperature difference at the same level changes in the opposite trend as the velocity, which is shown in Figure 6.31 using solid lines. The results of the 15 m-high and 1.2 m-high CFD model are compared in Figure 6.31 too.
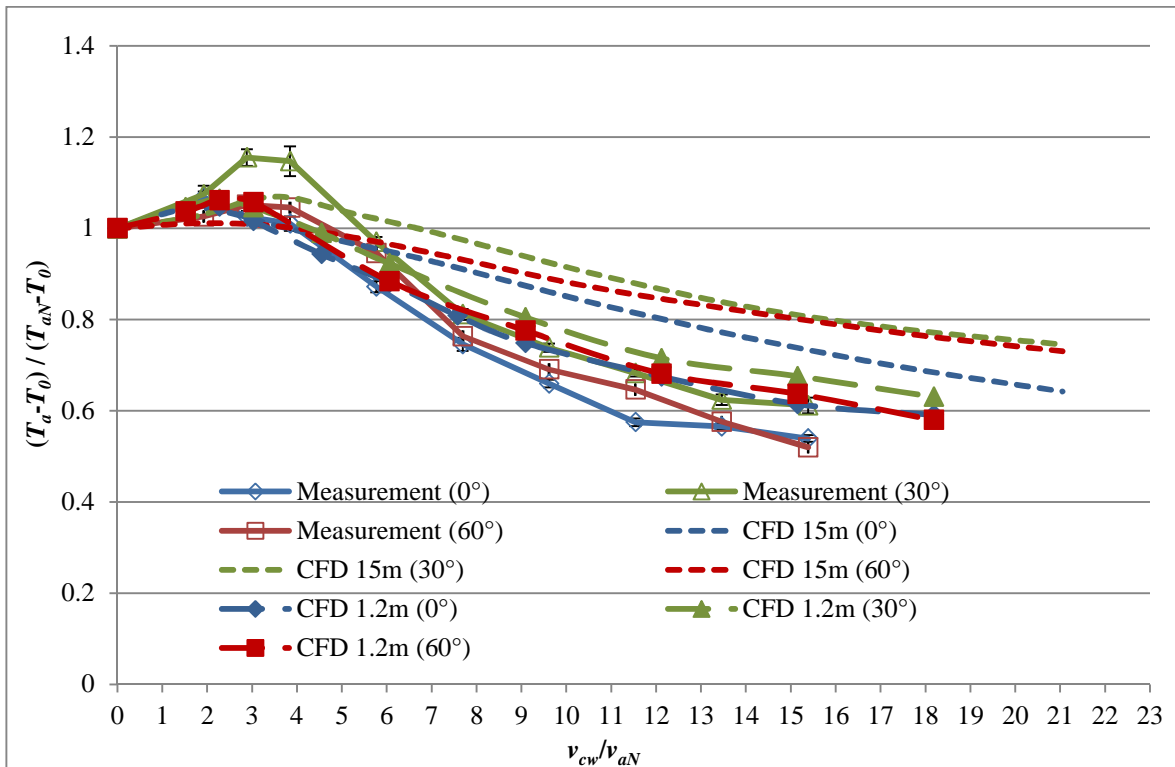
Figure 6.31. Temperature difference as a function of crosswind speed ratio for different attack angles at constant heat dumping rates

The measurement at the variable heating power mode is conducted to examine the crosswind effect on total heat transfer rate Q of the heater. The surface temperature of the heater elements is maintained at a constant value which is the heater temperature in free convection case when there is no crosswind. The electric power recorded is approximately equal to the total heat the "heater exchanger" dumps. Figures 6.32-6.34 show the dimensionless heat transfer rate Q/Q_N as the functions of crosswind speed ratio v_{cw}/v_{aN} for different attack angles, obtained from experiment and CFD results. As seen in the figures, the experiment and CFD results for 1.2 m-high CFD tower model agree with each other generally well for all the cases of attack angles.
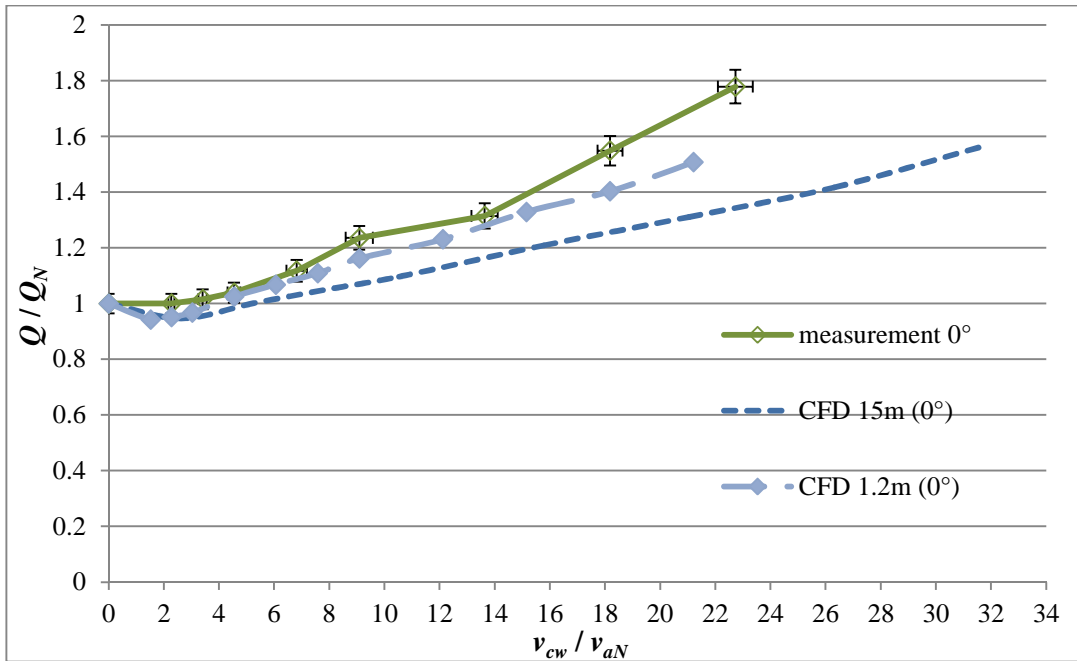
Figure 6.32. Total heat transfer rate varies with the crosswind speed for different attack angle of 0°, both experiment and CFD results, constant heater/heat exchanger surface temperatures
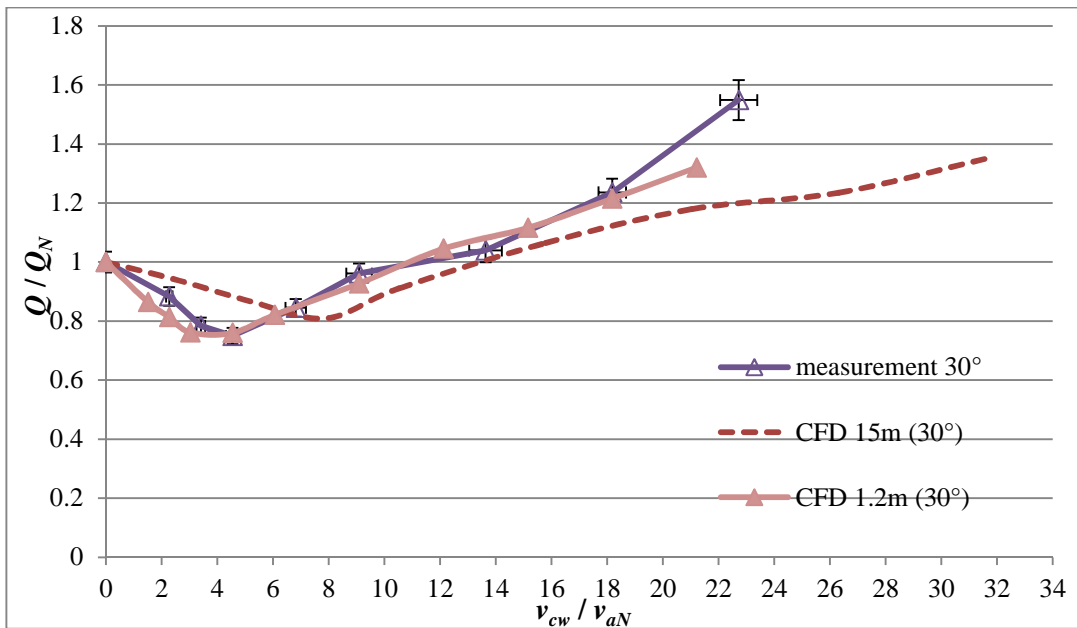
Figure 6.33. Total heat transfer rate varies with the crosswind speed for different attack angle of 30°, both experiment and CFD results, constant heater/heat exchanger surface temperatures
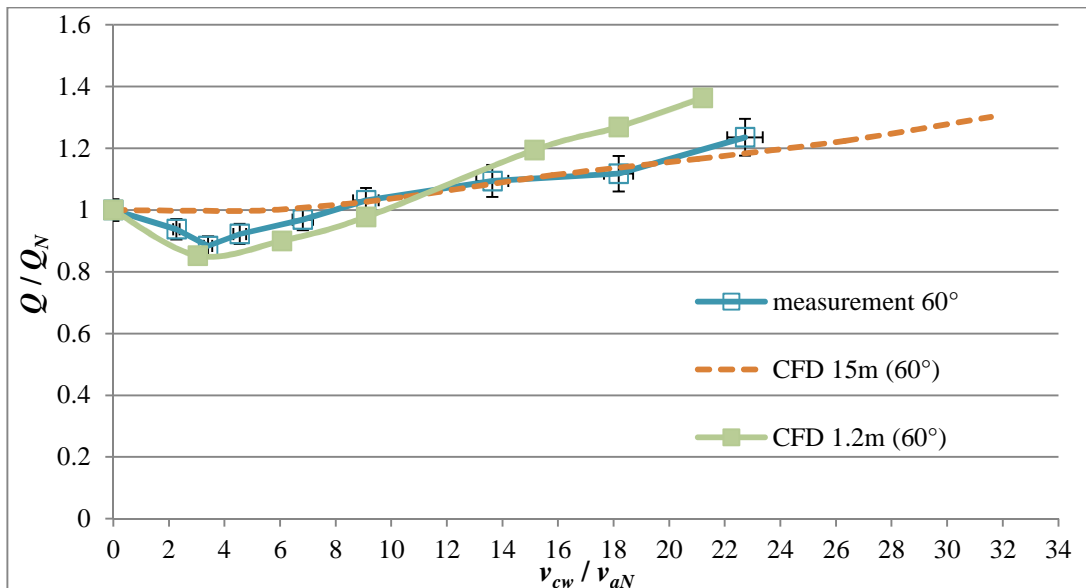
Figure 6.34. Total heat transfer rate varies with the crosswind speed for different attack angle of 60°, both experiment and CFD results, constant heater/heat exchanger surface temperatures

It is noted that despite that the measurement results are comparable with its identical CFD model, there are still some differences between both especially in the air velocity. The most possible reason for this is believed to relate to the complexity of airflow field in the cooling tower base and cannot be modelled in the CFD model. Since the windbreak wall exists under the heat exchangers, the airflow in this region has been changed greatly and the vortices generates, according to the analysis in Chapter 5. As the result, the flow field inside the cooling tower tends to be very irregular and unstable. This is a source of inaccuracy for and the CFD model which causes the discrepancies in the final results.

The benefit of windbreak walls under the heat exchangers has been verified by the experiment. The cooling performance of the tower generally exceeds the value in normal natural convection condition (no wind case) when the walls are arranged at attack angles of 0° and even 60°. This conclusion accords with the findings of CFD study in Chapter 5 [85].

6.10. Flow visualization

The air flow in the scaled cooling tower model is visualized through smoke. The smoke is generated by a smoke machine and guided through a piece of hose to a short chamber underneath the tower model base. The chamber is covered by a perforated sheet so that the smoke can flow out. The smoke has the same temperature and density as ambient air, so it cannot form a constant durable flow by itself unless there is an airflow carrying the smoke.
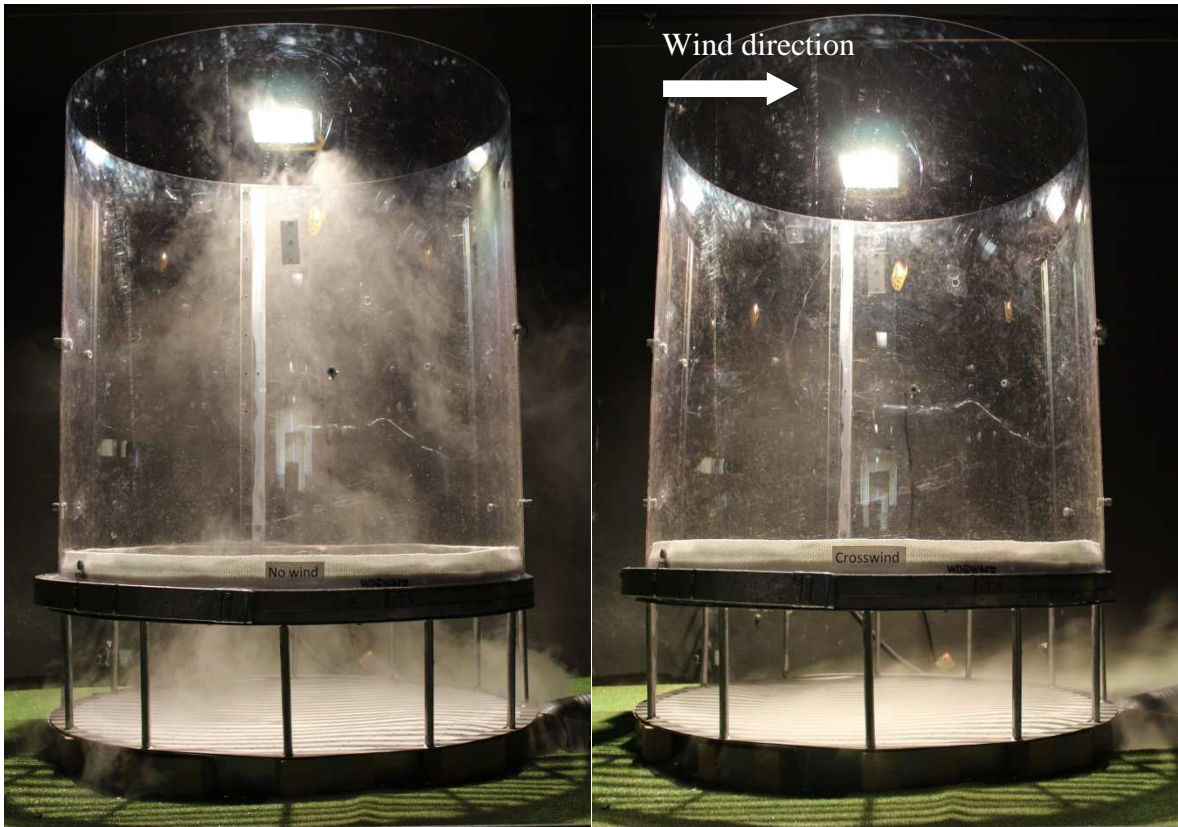
(a)   (b)

Figure 6.35. The airflow in the cooling tower under no wind condition (a) and at crosswind speed of 2 m/s (b).

Figure 6.35 compares the smoke flow in the cooling tower under no wind condition and at crosswind speed of 2 m/s when the heater works at the constant power of 5.216 KW. As seen in the figure, the nearly all the air flows through the heater in free convection case. The contraction of the air flow at heater level indicates that ambient air surrounding the tower base is sucked in at certain speed. When there is crosswind, all the smoke is blown away sideways. This indicates the horizontal airflow dominates the tower base region so that only a part of air flows through the heater.

Figure 6.36. Smoke visualization in the tower base for windbreak wall angle of 0° at wind speed of 2 m/s

Figure 6.37. Smoke visualization in the tower base for windbreak wall angle of 30° at wind speed of 2 m/s
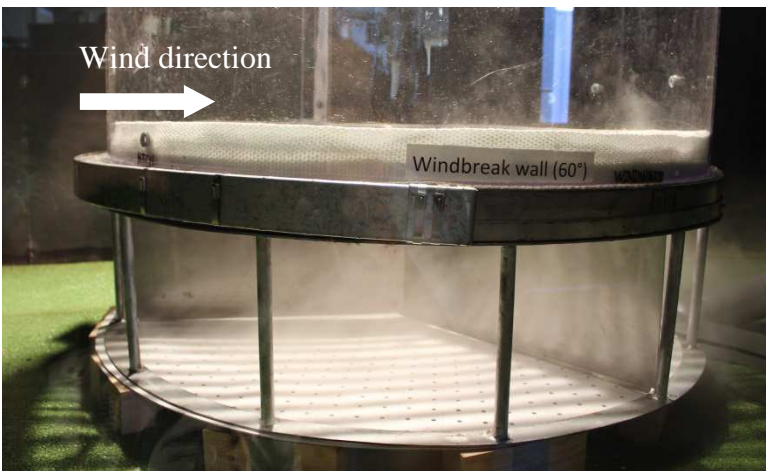
Figure 6.38. Smoke visualization in the tower base for windbreak wall angle of 60° at wind speed of 2 m/s

From Figure 6.35, it is clear that the crosswind reduces the upward air flowing through the heat exchangers which leads to the decrease in the heat transfer rate in the entire cooling tower. Once the windbreak wall is used under the heat exchanger, the horizontal influence of the crosswind can be limited significantly and even can be converted to the beneficial effect. Figures 6.36-6.38 show the air flow in the tower base for the three install angles of the windbreak wall at the same heating power when the crosswind speed is 2 m/s. It has been seen that most part of the smoke is not blown away by the wind, and there is more smoke passing across the heater. This improvement is more remarkable in the wake areas of the windbreak blades. In these areas, much thicker and larger plume of smoke is seen than the sectors directly facing the incoming wind, which means that there exist air vortices in the wall wakes–the smoke circulates locally with airflow.

6.11. Conclusions

The 1:12.5 scaled natural draft dry cooling tower model has been tested in the wind tunnel. The experiment is designed obeying the scaling law as much as possible to model the cooling performance of the proposed cooling tower under crosswind conditions with or without the windbreak walls. Several quantities (temperature, velocity, and electric power) on this tower model have been measured. The final data is then compared to the results of two 3D CFD models: the 15 m-high prototype tower model and a new 1.2 m-high identical numerical tower model. The experiment results generally agree with what the CFD calculations predicted which verify the methodology used in the CFD.

1. The total heat transfer rate and airflow velocity in scaled tower model experience the same decrease-turnaround trend along with the increase of crosswind speed as found in the CFD simulations.

2. The air temperature distributions inside the cooling tower model proves that crosswind causes the local air circulations in the tower. In the region near tower outlet, temperature in leeward side declines as cool air penetrates through the tower outlet. While underneath the heat exchangers, reverse airflow exists at windward part especially at high crosswind speeds, leading to the local air temperature increases significantly.

3. The CFD models slightly overestimate the circulations of the airflow especially near the tower outlet. This is believed due to the limitation of the turbulence model used. As a result, the distribution of the quantities predicted by CFD in upper part of the tower might be not accurate.

4. The heat transfer rate of the proposed NDDCT in dimensionless form is proposed as a function of crosswind velocity ratio v_{cw}/v_{aN}, aspect ratio H^2/A and Reynolds number $\rho_{ao}Dv_{aN}/\mu$.

Chapter 7 Conclusions

7.1 Summary

In thermal power plants using variety of heat sources, the redundant heat needs to be removed through cooling devices such as heat exchangers and cooling towers. Natural draft dry cooling towers (NDDCTs) feature no water loss and virtually no parasitic power consumption during operation. Although they are more expensive to build, the avoidance of parasitic losses help the plant increase its net power generation. The Queensland Geothermal Energy Centre of Excellence (QGECE) is developing small- or medium-scale geothermal and solar thermal power plant technologies for Australian conditions. These renewable power plants are most likely to be located in remote interior where there is limited water supply. If NDDCTs are to be used in the air-cooled condensers of these plants, the towers will be relatively short because the plants are smaller than typical coal-fired power plants. This Thesis project examined a critical operational issue for such short towers, the cross wind effect, proposed mitigation measures and design guidelines for designers of the future renewable thermal power plants using natural draft dry cooling towers. The working principle of NDDCTs is as simple as the stack effect. Air density difference between inside and outside is crucial to the draft force of the tower. In conventional thermal power plant, natural draft dry cooling towers are usually built higher than 100 m to create a large enough draft velocity so that the expected amount of heat can be dumped. However, for small-scale renewable power plants with net power generation of only few megawatts, our 1D mathematical model has proved that the cooling tower size can be decreased by almost an order of magnitude. With this 1D model, the cooling performance of a particular small NDDCT under certain given conditions can be precisely predicted.

The most important factor influencing the NDDCT operation is the crosswind. The 1D cooling tower performance models currently employed by designers of tall cooling towers for large power plants are not capable of predicting the crosswind effect. A number of previous studies have proved that cooling performance of large cooling towers decreases with the rise of crosswind speed as the natural convection is affected by crosswind but this decrease is not very large for tall towers.

However, the situation for short NDDCTs is entirely different. This study carried out numerical and experimental investigations on the unique effect of crosswind in small NDDCTs with the height less than 20 m. It found that, when there is cross wind, the total heat transfer rate Q in a natural draft cooling tower is a combination of the rates due natural convection and forced convection. While the former causes the vertical airflow inside the tower and decreases with the increases of the crosswind

speed, the latter occurs underneath the heat exchangers in the tower bottom as the horizontal wind passes through and has a positive relation with the wind speed. If the tower height is large enough to produce a high draft force, the natural convection heat transfer is orders of magnitude stronger than the forced convection. So, the latter is negligible in such towers even under high crosswind conditions.

In small NDDCTs, the natural convective heat transfer is low enough to become comparable to the forced convection heat transfer. Therefore, the interaction between them needs to be analysed and evaluated with care. As the results in this study have shown, the cooling capacity of small NDDCTs is not always defeated by crosswind effect. Instead, a turn-around trend with increasing crosswind speed has been observed. The increased cooling tower total heat transfer rate above certain crosswind speeds is attributed to the forced natural convection effect. This is a new phenomenon and it is different from the large cooling towers.

The total heat transfer composition of a NDDCT has been shown to follow a simple correlation of heat transfer rate with the crosswind speed, i.e. Eq. (4.15). This mathematical model predicts the reduced heat transfer rate under crosswinds on all sizes natural draft dry cooling towers with horizontal heat exchangers. The coefficients in the correlation are believed to depend on the size and characteristics of the cooling towers. The velocity ratio in the correlation refers to the ratio of the crosswind speed to the air velocity that would be obtained through the tower under pure natural convection (no crosswind). This ratio has been critical to the predicted performance of short NDDCTs.

In the 15 m-high NDDCT studied in this project, the heat dumping rate of the tower has been shown to decrease by up to 37% when the crosswind speed reaches to its critical point–5 m/s or the velocity ratio of approximately 11. A tri-blade-like windbreak wall was therefore introduced under the heat exchangers in tower bottom in order to reduce the horizontal wind speed in the region. The windbreak wall has been shown to increase the vertical air velocity and thus the natural convective heat transfer in the cooling tower. The effect of the windbreak wall has been found to be highly sensitive to its orientation. It has been found that a tri-blade-like windbreak wall gives the most benefit to the cooling tower performance at wind attack angles of 0° and 60°. This suggests that the windbreak walls should be placed with one wall, i.e. one symmetry axis, always aligned with the dominant direction of the crosswind. This finding can be used to determine the windbreak installation angles with respect to the most frequent direction(s) of the environmental crosswind in a given district.

In this study, a 1:12.5 scaled natural draft dry cooling tower model has been constructed and tested in the wind tunnel. The experiment results generally agree with what the CFD predictions, which indicates that the methodology used in numerical modelling is reasonable. It has also been found that the CFD models may be overestimating the air circulation especially near the tower outlet at high crosswind speeds. This is believed mainly due to the limitation of the turbulence model used. This suggests that the actual crosswind effect on the NDDCT is slightly weaker than what has been predicted by CFD model at high crosswind speeds. However current CFD model is still valid when predicting the change trend of the cooling tower performance.

In summary, this study demonstrates the feasibility of utilising relatively short natural draft dry cooling towers in small- to medium-size renewable thermal power generators. Crosswind effects could be fatal to these towers but can be prevented and even can be converted to benefits with proper wind mitigation measures as described in this study. Finally, it has been demonstrated through validation tests in a wind tunnel that the numerical method used in the study is an effective tool to study natural draft cooling tower operating under different conditions.

7.2 Suggestions for future work

Crosswind effect and its mitigation currently investigated have not been tested in full scale real cooling towers. While numerical and scaled models are well designed to be as similar to the real tower as possible, it would still be valuable to conduct studies on the boundary conditions/ wind profile, scaling issues of the convective heat transfer (i.e. *Re*, *Nu*, *Ra*, *Eu*, *etc.*), tower inlet and outlet pressure drop and airflow structure, more seriously the turbulence in the airflow. Some of these issues cannot be analysed in small laboratory scale towers in wind tunnels. Long term field measurements are required for the investigation of crosswind effects in operating plants. Testing on full scale real NDDCTs is needed, and real industrial finned-tube heat exchangers can be used in these cooling towers. It is noted that although different industrial heat exchangers perform differently in terms of the magnitudes of the heat transfer rate and the pressure resistance, the relation between the overall tower performance and crosswinds should be very similar, because generally speaking, any heat exchanger bundle plays the same role, namely provide heat and resistance, to the airflow in cooling towers.

Although a rough correlation of the crosswind effect has been proposed, more studies are required before it is developed into a more precise and practical mathematical model. The form model could be further developed to involve a set of correlations by considering more cooling tower parameters

like the aspect ratio, Reynolds number, Nusselt number, etc. Combined with experimental validation on full-scale cooling towers, this work is expected to lead to predictive design formula to help future power plant designers planning to use relatively short natural draft dry cooling towers under crosswind conditions.

Reference

List of References

[1] W.H. Wiser, Energy Resources: Occurrence, Production, Conversion, Use, 1st ed., Springer Verlag, New York, 2000.

[2] B. Péter, G. Gyula, G. Iván, Efficiency and Cost Modelling of Thermal Power Plants, Thermal Science, 14(3) (2010) 821-834.

[3] D.G. Kröger , Air-cooled heat exchangers and cooling towers, Pennwell Corp, Tulsa, Okl, USA, 2004.

[4] A.E. Conradie, D.G. Kröger, Performance evaluation of dry-cooling systems for power plant applications, Applied Thermal Engineering, 16(3) (1996) 219-232.

[5] Office of Electricity Delivery and Energy Reliability, Electricity Reliability Impacts of a Mandatory Cooling Tower Rule for Existing Steam Generation Units, in: U.S. D. o. Energy, 2008.

[6] K. Tanimizu, K. Hooman, Natural draft dry cooling tower modelling, Heat Mass Transfer, 49(2) (2013) 155-161.

[7] M. F.K, Dry Cooling Towers, in: F.I. Thomas, P.H. James (Eds.) Advances in Heat Transfer, Elsevier, 1976, pp. 1-75.

[8] Q.D. Wei, B.Y. Zhang, K.Q. Liu, X.D. Du, X.Z. Meng, A Study of the Unfavorable Effects of Wind on the Cooling Efficiency of Dry Cooling-towers, Journal of Wind Engineering and Industrial Aerodynamics, 54 (1995) 633-643.

[9] D.D. Derksen, T.J. Bender, D.J. Bergstrom, K.S. Rezkallah, A study on the effects of wind on the air intake flow rate of a cooling tower: Part 1. Wind tunnel study, Journal of Wind Engineering and Industrial Aerodynamics, 64(1) (1996) 47-59.

[10] T.J. Bender, D.J. Bergstrom, K.S. Rezkallah, A study on the effects of wind on the air intake flow rate of a cooling tower: Part 3. Numerical study, Journal of Wind Engineering and Industrial Aerodynamics, 64(1) (1996) 73-88.

[11] R. Al-Waked, M. Behnia, The performance of natural draft dry cooling towers under crosswind: CFD study, International Journal of Energy Research, 28(2) (2004) 147-161.

[12] A.F. Du Preez, D.G. Kröger , The effect of the heat exchanger arrangement and wind-break walls on the performance of natural draft dry-cooling towers subjected to cross-winds, Journal of Wind Engineering and Industrial Aerodynamics, 58(3) (1995) 293-303.

[13] S. Fu, Z.Q. Zhai, Numerical investigation of the adverse effect of wind on the heat transfer performance of two natural draft cooling towers in tandem arrangement, ACTA MECHANICA SINICA, 17(1) (2001) 24-34.

Reference

[14] R. Al-Waked, M. Behnia, CFD simulation of wet cooling towers, Applied Thermal Engineering, 26(4) (2006) 382-395.

[15] Z. Zou, Z. Guan, H. Gurgenci, Y. Lu, Solar enhanced natural draft dry cooling tower for geothermal power applications, Solar Energy, 86(9) (2012) 2686-2694.

[16] S. He, H. Gurgenci, Z. Guan, A.M. Alkhedhair, Pre-cooling with Munters media to improve the performance of Natural Draft Dry Cooling Towers, Applied Thermal Engineering, 53(1) (2013) 67-77.

[17] A. Alkhedhair, H. Gurgenci, I. Jahn, Z. Guan, S. He, Numerical simulation of water spray for pre-cooling of inlet air in natural draft dry cooling towers, Applied Thermal Engineering, 61(2) (2013) 416-424.

[18] E.J. Pring, G.B. Hill, P.D. Osborn, Cooling towers: principles and practice, Butterworth-Heinemann, London ; Boston, 1990.

[19] W.E. Glassley, Geothermal energy: renewable energy and the environment, CRC Press, Boca Raton, 2010.

[20] K. Duvenhage, D.G. Kröger , Plume recirculation in mechanical-draft air-cooled heat exchangers, Heat Transfer Engineering, 16(4) (1995) 42-49.

[21] R.D. Moore, D.E. Wheeler, K.R. Wilber, A.E. Johnson, An evaluation of schemes for the prediction of recirculation on crossflow rectangular mechanical draft cooling towers, in: Cooling Tower Institute Annual Meeting, 1979.

[22] D.G. Kröger , Reduction in Performance Due to Recirculation in Mechanical Draft Cooling Towers, Heat Transfer Engineering, 10(4) (1989) 37-43.

[23] R. DiPippo, Geothermal power plants: principles, applications and case studies, Elsevier, Oxford, 2005.

[24] K. Hooman, natural draft dry cooling tower modelling, in: 17th Australasian Fluid Mechanics Conference, Auckland, New Zealand, 2010.

[25] L. Forgo, Dry Cooling for Power Stations, in, IEEE, pp. 1099-1103.

[26] D.J. Vanaarde, D.G. Kröger , Flow Losses Through An Array of A-frame Heat-exchangers, Heat Transfer Engineering, 14(1) (1993) 43-51.

[27] G. Gan, S.B. Riffat, L. Shao, Performance prediction of a prototype closed-wet cooling tower, Journal of the Institute of Energy, 73(495) (2000) 106-113.

[28] Cooling towers In: Energy Efficiency in Electrical Utilities, in: M.o.P. Bureau of Energy Efficiency (Ed.), India, 2004, pp. 135-151.

Reference

[29] V. Mucic, Possibilities of Improving the Efficiency of Thermal Power-stations, Brennstoff-Warme-Kraft, 40(12) (1988) 490-498.

[30] R. Al-Waked, M. Behnia, J. Madadnia, Numerical Modelling and Validation of Natural Draught Cooling Towers under Crosswind, in: the 12th IAHR Symposium in Cooling Tower and Heat Exchangers, Sydney, Australia, 2001.

[31] C.M.B. Russell, T.V. Jones, D.W. Holder, H.R. McChesney, M. Verlinden, Crosswind and internal flow characteristics of dry cooling towers, 1977.

[32] M. F.K, Cold Inflow and its Implications for Dry Tower Design, in: Second Conference on Waste Heat Management and Utilization, Miami, 1978.

[33] A.F. Du Preez, D.G. Kröger , Effect of Wind on Performance of A Dry-cooling Tower, Heat Recovery Systems & CHP, 13(2) (1993) 139-146.

[34] M. Gao, F.Z.H. Sun, Research on the Effect of Cross-wind to Temperature Difference and Efficiency of Natural Draft Counter flow Wet Cooling Tower, in: International Conference on Power Engineering, Hangzhou, China, 2007, pp. 513-517.

[35] A.O. Demuren, W. Rodi, Three-Dimensional Numerical Calculations of Flow and Plume Spreading Past Cooling Towers, Journal of Heat Transfer, 109(1) (1987) 113-119.

[36] D.B. Spalding, B.E. Launder, Lectures in mathematical models of turbulence, Academic Press, London ; New York, 1972.

[37] R. Al-Waked, M. Behnia, The effect of windbreak walls on the thermal performance of natural draft dry cooling towers, Heat Transfer Engineering, 26(8) (2005) 50-62.

[38] M.D. Su, G.F. Tang, S. Fu, Numerical simulation of fluid flow and thermal performance of a dry-cooling tower under cross wind condition, Journal of Wind Engineering and Industrial Aerodynamics, 79(3) (1999) 289-306.

[39] K. Duvenhage, D.G. Kröger , The influence of wind on the performance of forced draught air-cooled heat exchangers, Journal of Wind Engineering and Industrial Aerodynamics, 62(2-3) (1996) 259-277.

[40] K.K. Robinson, D.E. Briggs, Pressure drop of air flowing across triangular pitch banks of finned tubes Chem. Eng. Symp. Ser., 64(62) (1966) 177-184.

[41] F.K. Moore, K.E. Torrance, Air flow in dry natural-draft cooling towers subject to wind, in: Cornell EneIgy Report, Ithaca, New York, 1977.

[42] D.E. Briggs, E.H. Young, Convective heat transfer and pressure drop of air flowing across triangular pitch banks of finned tubes, Chem. Eng. Symp. Ser., 41(59) (1963) 1-10.

[43] G.S. Sutton, Atmospheric turbulence, Methuen ; New York, London, 1955.

Reference

[44] S.L. Jameson, N.Y. Schenectady, Tube Spacing in Finned-Tube Banks, Trans. ASME, 67 (1945) 633-642.

[45] J.D. Buys, D.G. Kröger, Dimensioning heat exchangers for existing dry cooling towers, Energy Conversion and Management, 29(1) (1989) 63-71.

[46] S. He, Z. Guan, H. Gurgenci, I. Jahn, Y. Lu, A. M. Alkhedhair, Influence of ambient conditions and water flow on the performance of pre-cooled natural draft dry cooling towers, Applied Thermal Engineering, 66(1–2) (2014) 621-631.

[47] ASHRAE, Chapter 1 Psychrometrics, in: ASHRAE Handbook: Fundamentals, American Society of Heating, Refrigerating and Air-Conditioning Engineers, Inc., Atlanta, GA, USA, 2009.

[48] B.o. Meteorology, Climate Data Online, in, 2014.

[49] G. Ge, F. Xiao, S. Wang, L. Pu, Effects of discharge recirculation in cooling towers on energy efficiency and visible plume potential of chilling plants, Applied Thermal Engineering, 39(Journal Article) (2012) 37-44.

[50] Y. Chen, F. Sun, H. Wang, N. Mu, M. Gao, Experimental research of the cross walls effect on the thermal performance of wet cooling towers under crosswind conditions, Applied Thermal Engineering, 31(17) (2011) 4007-4013.

[51] Z. Zhai, S. Fu, Improving cooling efficiency of dry-cooling towers under cross-wind conditions by using wind-break methods, Applied Thermal Engineering, 26(10) (2006) 1008-1017.

[52] Enlarging geothermal power plant, in, Caribbean Update, Inc, 2010.

[53] ANSYS Inc., Fluent User's Guide, in, ANSYS Inc., New Hampshire, USA, 2011.

[54] Y. Lu, Z. Guan, H. Gurgenci, Development of Small Natural Draft Dry Cooling Towers for Geothermal Power Plants, in: The 15th IAHR Cooling Tower and Air-cooled Heat Exchanger Conference, Beijing, China, 2011, pp. 308-316.

[55] A. Ganguli, S.S. Tung, T. J, Parametric Study of Air-cooled Heat Exchanger Finned Tube Geometry, American Institude of Chemical Engineers Symposium Series C, 81(245) (1985) 122-128.

[56] K.K. Robinsion, D.E. Briggs, Pressure Drop of Air Flowing Across Triangular Pitch Banks of Finned Tubes, Chemical Engineering Progress Symposium Series, 62(64) (1966) 177-184.

[57] J. Franke, C. Hirsch, A.G. Jensen, H.W. Krüs, M. Schatzmann, P.S. Westbury, S.D. Miles, J.A. Wisse, N.G. Wright, Recommendations on the use of CFD in wind engineering, in: v.B. JPAJ (Ed.) Proceedings of the International Conference on Urban Wind Engineering and

Building Aerodynamics. In: van Beeck JPAJ (Ed.), COST Action C14, Impact of Wind and Storm on City Life Built Environment, von Karman Institute, Sint-Genesius-Rode, Belgium, 2004.

[58] H.C.R. Reuter, D.G. Kröger , Computational Fluid Dynamics Analysis of Cooling Tower Inlets, in, American Society of Mechanical Engineers, NEW YORK, 2011, pp. 81104.

[59] L.J. Yang, X.Z. Du, Y.P. Yang, Space characteristics of the thermal performance for air-cooled condensers at ambient winds, International Journal of Heat and Mass Transfer, 54(15) (2011) 3109-3119.

[60] P. Arora, A.K. Saha, Three-dimensional numerical study of flow and species transport in an elevated jet in crossflow, International Journal of Heat and Mass Transfer, 54(1–3) (2011) 92-105.

[61] Y.A. Çengel, A.J. Ghajar, M. Kanoglu, Heat and mass transfer: fundamentals and applications, McGraw Hill Higher Education, New York, 2011.

[62] K. Hooman, Theoretical Prediction with Numerical and Experimental Verification to Predict Cross Wind Effects on the Performance of Cooling Towers, Heat Transfer Engineering, 36(5) (2015) 480-487.

[63] ASHRAE, ASHRAE Handbook: Fundamentals, IP Edition ed., American Society of Heating, Refrigerating and Air-Conditioning Engineers, Inc., Atlanta, GA, USA, 2009.

[64] F.P. Incropera, D.P. Dewitt, T.L. Bergman, A.S. Lavine, Fundamentals of heat and mass transfer 6th edition, John Wiley & Sons, Inc., USA, 2007.

[65] A.F. Du Preez, D.G. Kröger , Effect of the Shape of the Tower Supports and Walls on the Performance of a Dry-Cooling Tower Subjected to Cross Winds, Heat Transfer Engineering, 16(2) (1995) 42-49.

[66] K. Wang, F. Sun, Y. Zhao, M. Gao, L. Ruan, Experimental research of the guiding channels effect on the thermal performance of wet cooling towers subjected to crosswinds – Air guiding effect on cooling tower, Applied Thermal Engineering, 30(5) (2010) 533-538.

[67] Y. Lu, Z. Guan, H. Gurgenci, Z. Zou, Windbreak walls reverse the negative effect of crosswind in short natural draft dry cooling towers into a performance enhancement, International Journal of Heat and Mass Transfer, 63(0) (2013) 162-170.

[68] Z. Zhang, Z.Q. Zhai, W. Zhang, Q.Y. Chen, Evaluation of various turbulence models in predicting airflow and turbulence in enclosed environments by CFD: Part 2-comparison with experimental data from literature, HVAC&R Research, 13(6) (2007) 871-886.

Reference

[69]   M. Lucas, P.J. Martinez, J. Ruiz, A.S. Kaiser, A. Viedma, On the influence of psychrometric ambient conditions on cooling tower drift deposition, International Journal of Heat and Mass Transfer, 53(4) (2010) 594-604.

[70]   L.J. Yang, X.Z. Du, Y.P. Yang, Wind effect on the thermo-flow performances and its decay characteristics for air-cooled condensers in a power plant, International Journal of Thermal Sciences, 53(Journal Article) (2012) 175-187.

[71]   H.C.R. Reuter, D.G. Kröger , Computational Fluid Dynamics Analysis of Cooling Tower Inlets, Journal of Fluids Engineering-Transactions of the ASME, 133(8) (2011).

[72]   [72] L.J. Yang, L. Chen, X.Z. Du, Y.P. Yang, Effects of ambient winds on the thermo-flow performances of indirect dry cooling system in a power plant, International Journal of Thermal Sciences, 64(0) (2013) 178-187.

[73]   A.S. Kaiser, M. Lucas, A. Viedma, B. Zamora, Numerical model of evaporative cooling processes in a new type of cooling tower, International Journal of Heat and Mass Transfer, 48(5) (2005) 986-999.

[74]   F.M. White, Fluid Mechanics-4th edition, 4th ed., McGraw-Hill, Boston, MA., USA, 2003.

[75]   A.F.d. Preez, The influence of cross-winds on the performance of natural draft dry-cooling towers, University of Stellenbosch, South Africa, 1992.

[76]   JCGM, Evaluation of measurement data — Guide to the expression of uncertainty in measurement, in, BIPM, France, 2008.

[77]   J.R. Taylor, An Introduction to Error Analysis: The Study of Uncertainties in Physical Measurements, 2nd ed., University Science Books, Sausalito, California, USA, 1997.

[78]   H. Huisseune, C. T'Joen, P. Brodeoux, S. Debaets, M. De Paepe, Thermal Hydraulic Study of a Single Row Heat Exchanger With Helically Finned Tubes, Journal of Heat Transfer-Transactions of the ASME, 132(6) (2010) 61801.

[79]   R.H. Perry, C.H. Chilton, Chemical engineers' handbook, McGraw-Hill, New York, 1973.

[80]   H.M.F. M.P. Foster, A new wind tunnel facility for atomisation studies, in: Conference on Engineering in Agriculture, Albury, NSW, Australia, 1992.

[81]   R.D. Mehta, The aerodynamic design of blower tunnels with wide-angle diffusers, Progress in Aerospace Sciences, 18(0) (1977) 59-120.

[82]   R. Singh, Dynamics and Control of a Closed Carbon-Dioxide Brayton Cycle The University of Queensland Brisbane, Australia, 2013.

Reference

[83] G. CARUSO, M. FATONE, A. NAVIGLIO, An experimental study on natural draft-dry cooling tower as part of the passive system for the residual decay heat removal, in: Proceedings of ICAPP, Nice, France, 2007.

[84] Z.Q. Thai, W. Zhang, Z. Zhang, Q.Y. Chen, Evaluation of various turbulence models in predicting airflow and turbulence in enclosed environments by CFD: part 1 - Summary of prevalent turbulence models, HVAC&R Research, 13(6) (2007) 853-870.

[85] Lu, Y., Guan, Z., Gurgenci, H., He, S., The influence of windbreak wall orientation on the cooling performance of small natural draft dry cooling towers. International Journal of Heat and Mass Transfer, 2014. 79(0): p. 1059-1069.